

NATIONAL ACADEMY OF SCIENCES  
NATIONAL RESEARCH COUNCIL  
of the  
UNITED STATES OF AMERICA

UNITED STATES NATIONAL COMMITTEE  
International Union of Radio Science



1975 Annual Meeting  
October 20-23

Sponsored by USNC/URSI  
in cooperation with  
Institute of Electrical and Electronics Engineers

University of Colorado  
Boulder, Colorado

Price \$3.00

URSI/USNC  
1975 Annual Meeting  
Condensed Technical Program

Sunday, October 19

2000-2400	U.S. National Committee Meeting	Sheraton	
<u>Monday, October 20</u>			
0900-1200	II-1 III-1 IV-1 V-1/I, II, VII VI-1 VI-2 VIII-1/I B-1a/I B-1b/I	Mining Communications Ionospheric Radio Scintillations - I VLF/ELF Active and Passive Probing Extra-Terrestrial Techniques for Measuring Crustal Motions and Satellite Ranging Scattering - I Antennas Noise and Interference Measurements Auditory Effects Microwave Cataractogenesis Combined Session Evening Lecture	UMC 159 UMC 156 UMC 157 UMC W Blrm RB Aud. RB 1107 UMC F.R. UMC E Blrm UMC E Blrm UMC C Blrm UMC C Blrm
1330-1700			
2000-2200			

Tuesday, October 21

0830-1200	II-2 II-3 III-2 IV-2 V-2 VI-3 VI-4 VIII-2/VII B-2a/I B-2b/I B-3/I I-1 IV-3 V-3/III, VIII	Sub-Surface Propagation and Communications Radio Oceanography Seasat "A" Ionospheric Radio Scintillations - II Plasma Instabilities in the Magnetosphere - I Millimeter Wavelength Techniques Numerical Techniques Integrated and Fiber Optics - I Noise and Interference Models and Radio System Planning Therapeutic Applications Diagnostic Applications Field Survey Instruments Measurements and Techniques Plasma Instabilities in the Magnetosphere - II Interference to Radio Astronomy and CCIR Related Topics Integrated and Fiber Optics - II Scattering - II Cellular and Mutagenetic Effects Exposure Systems Radio Meteorology--Observations, Measurements, and Theory Radar Oceanography--Sea Surface Winds and Ocean Waves	UMC 159 UMC F.R. UMC 157 UMC 158 UMC 156 RB 1107 RB Aud. RB 1103 UMC W Blrm UMC W Blrm UMC E Blrm RB 1103 UMC 158
1330-1700	VI-5 VI-6 B-4/I B-5/I II-4	Interference to Radio Astronomy and CCIR Related Topics Integrated and Fiber Optics - II Scattering - II Cellular and Mutagenetic Effects Exposure Systems Radio Meteorology--Observations, Measurements, and Theory Radar Oceanography--Sea Surface Winds and Ocean Waves	UMC 156 RB Aud. RB 1107 UMC W Blrm UMC E Blrm
1330-1630	II-5	Observation of Spatial and Temporal Structure of the Ionosphere - I	UMC 159
1645-1845	III-3	Commission II Business Meeting	UMC F.R.
1800-2000		Commission III Business Meeting Reception	UMC 157 UMC 156 UMC 157 Sheraton

Wednesday, October 22

0830-1200	II-6 II-7 III-4 IV-4 V-4 VI-7/I VI-8/VIII B-6a/I B-6b/I B-7a/I B-7b/I	Satellite Communications Radio Meteorology--Radio Propagation and Wind Measurements in Convective Storms Observation of Spatial and Temporal Structure of the Ionosphere - II Precipitation and Plasmas Galactic and Extragalactic Observations Inverse Scattering Topics in Communication Theory Behavioral Effects (Low Level Exposure) Behavioral Effects (High Level Exposure) Assessment of Power Deposition in Tissues by Mathematical and Phantom Models Dielectric Properties of Tissues	UMC 159 UMC F.R. UMC 157 UMC 158 UMC 156 RB Aud. RB 1107 UMC E Blrm UMC E Blrm UMC W Blrm UMC W Blrm
-----------	---	---	--

Continued on inside back cover

United States National Committee  
INTERNATIONAL UNION OF RADIO SCIENCE

PROGRAM AND ABSTRACTS

1975 Annual Meeting  
October 20-23

Sponsored by USNC/URSI in cooperation  
with IEEE groups and societies:

Antennas and Propagation  
Circuits and Systems  
Communications  
Electromagnetic Compatibility  
Geoscience Electronics  
Information Theory  
Instrumentation and Measurement  
Microwave Theory and Techniques

Hosted by:

The National Oceanic and Atmospheric Administration  
The National Bureau of Standards  
The Institute for Telecommunication Sciences  
Office of Telecommunications  
The University of Colorado  
The Denver Section, IEEE  
and  
The Denver-Boulder Chapter, IEEE/APS

Boulder, Colorado

NOTE:

Programs and Abstracts of the USNC/URSI Meetings are available from:

USNC/URSI  
National Academy of Sciences  
2101 Constitution Avenue, N.W.  
Washington, D.C. 20418

The full papers are not published in any collected format; requests for them should be addressed to the authors who may have them published on their own initiative. Please note that these meetings are national and are not organized by international URSI, nor are these programs available from the international Secretariat.

MEMBERSHIP

United States National Committee  
INTERNATIONAL UNION OF RADIO SCIENCE

Chairman:

F.S. Johnson, University of Texas, Dallas

Vice Chairman:

J.V. Evans, Lincoln Laboratory, M.I.T.

Secretary:

C.G. Little, Environmental Research Labs, NOAA

Editor:

T.B.A. Senior, University of Michigan

Immediate Past Chairman:

A.T. Waterman, Jr., Stanford University

Commission Chairmen:

Commission I: Radio Measurements and Standards

George Birnbaum

National Bureau of Standards

Building 223, Room B 354

Washington, D.C. 20234

Commission II: Radio and Nonionized Media

Isadore Katz

Applied Physics Laboratory

The Johns Hopkins University

8621 Georgia Avenue

Silver Springs, Maryland 20910

Commission III: On the Ionosphere

John M. Kelso

ITT Electro-physics Labs, Inc.

9140 Old Annapolis Road

Columbia, Maryland 21043

Commission IV: On the Magnetosphere

Andrew F. Nagy

Dept. of Electrical Engineering

University of Michigan

Ann Arbor, Michigan 48104

Commission V: Radio and Radar Astronomy

Alan H. Barrett

Research Laboratory of

Electronics (26-457)

Massachusetts Institute of

Technology

Cambridge, Massachusetts 02139

Commission VI: Radio Waves and Transmission of Information

Aharon A. Ksienksi  
ElectroScience Laboratory  
The Ohio State University  
1320 Kinnear Road  
Columbus, Ohio 43212

Commission VIII: Radio Noise and Interference

George H. Hagn  
Stanford Research Institute  
1611 North Kent Street  
Arlington, Virginia 22209

Persons Taking Office, January 1, 1976:

Chairman:

J.V. Evans, Lincoln Laboratory, M.I.T.

Vice Chairman:

C.G. Little, Environmental Research Labs, NOAA

Secretary:

J.R. Wait, U.S. Department of Commerce, Boulder

Editor:

T.B.A. Senior, University of Michigan

Commission Chairmen:

Commission I: George E. Schafer

Commission II: Alfred H. LaGrone

Commission III: Thomas E. VanZandt

Commission IV: Peter M. Banks

Commission V: Kenneth I. Kellerman

Commission VI: Thomas B.A. Senior

Commission VIII: George H. Hagn

Members at Large:

P.M. Banks E.E. Gossard

C.I. Beard A. Ishimaru

W.C. Erickson J.S. Nisbet

L.B. Felsen W.F. Utlaud

Officers of URSI resident in the United States:

Honorary President:

S. Silver

Chairman, Commission I(A): H.M. Altschuler

Chairman, Commission V(J): G. Westerhout

Vice Chairman, Commission IV(H): F.W. Crawford

Vice Chairman, Commission VI(B): L.B. Felsen

Vice Chairman, Commission VIII(E): G.H. Hagn

Vice Chairman, Commission II(F): A.T. Waterman

American Geophysical Union: A.J. Dessler  
IEEE: E. Weber

United States Government:

Department of Commerce: A.H. Shapley  
Department of Defense: E. Paroulek  
    Air Force: D.J. Sletten  
    Army: A.R. Rasmussen  
    Navy: A.H. Schooler  
FCC: H. Fine  
NASA: E.R. Schmerling  
NSF: R.M. Price  
OTP: W. Dean, Jr.

Foreign Secretary, NAS: G.S. Hammond  
Chairman, NRC Office of  
    Physical Sciences: D.A. Bromley

Honorary Members: H.H. Beverage  
                          A.H. Waynick

DESCRIPTION OF  
INTERNATIONAL UNION OF RADIO SCIENCE

The International Union of Radio Science is one of 17 world scientific unions organized under the International Council of Scientific Unions (ICSU). It is commonly designated as URSI (from its French name, Union Radio Scientifique Internationale). Its aims are (1) to promote the scientific study of radio communications, (2) to aid and organize radio research requiring cooperation on an international scale and to encourage the discussion and publication of the results, and (3) to facilitate agreement upon common methods of measurement and the standardization of measuring instruments. The International Union itself is an organizational framework to aid in promoting these objectives. The actual technical work is largely done by the National Committees in the various countries.

The officers of the International Union are:

President: J. Voge (France)

Immediate Past President: W.J.G. Beynon (UK)

Vice Presidents: W.N. Christiansen  
(Australia)  
W.E. Gordon (USA)  
V.V. Migulin (USSR)  
F.L.H.M. Stumpers  
(Netherlands)

Secretary General: C.M. Minnis (Belgium)

Honorary Presidents: B. Decaux (France)  
W. Dieminger (West Germany)  
C. Manneback (Belgium)  
J.A. Ratcliffe (UK)  
S. Silver (USA)  
R.L. Smith-Rose (UK)

The Secretary's office and the headquarters of the organization are located at 7 Place Emile Danco, 1180 Brussels, Belgium. The Union is supported by contributions (dues) from 35 member countries. Additional funds for symposia and other scientific activities of the Union are provided by ICSU from contributions received for this purpose from UNESCO.

The International Union, as of the XVIII General Assembly held in Lima, Peru, August, 1975, has nine bodies called Commissions for centralizing studies in the principal technical fields. The names of the Commissions and the chairmen follow. The roman numerals in parentheses indicate the designations of the most closely corresponding previously existing Commissions. The listing of Commissions and chairmen of the United States National Committee in this digest uses the old designations, but formal consideration of the United States Commissions by the United States National Committee is pending.

- A. Electromagnetic Metrology (I)  
Altschuler (USA)
- B. Fields and Waves (VI)  
van Bladel (Belgium)
- C. Signals and Systems (VI)  
Picinbono (France)
- D. Physical Electronics (VII)  
Smolinski (Poland)
- E. Interference Environment (VIII)  
Likhter (USSR)
- F. Wave Phenomena in Nonionized Media (II)  
Eklund (Sweden)
- G. Ionospheric Radio (III)  
King (United Kingdom)
- H. Waves in Plasmas (IV)  
Gendrin (France)
- J. Radio Astronomy (V)  
Westerhout (USA)

Every three years, the International Union holds a meeting called the General Assembly. The next General Assembly, the XIX, will be held in Helsinki, Finland in August 1978. The Secretariat prepares and distributes the Proceedings of these General Assemblies. The International Union arranges international symposia on specific subjects pertaining to the work of one Commission or to several Commissions. The International Union also cooperates with other Unions in international symposia on subjects of joint interest.

Radio is unique among the fields of scientific work in having a specific adaptability to large-scale international research programs, for many of the phenomena that must be studied are worldwide in extent and yet are in a measure subject to control by experimenters. Exploration of space and the extension of scientific observations to the space environment is dependent on radio for its communication link and at the same time expands the scope of radio research. One of its branches, radio astronomy, involves cosmos-wide phenomena. URSI has in all this a distinct field of usefulness in furnishing a meeting ground for the numerous workers in the manifold aspects of radio research; its meetings and committee activities furnish valuable means of promoting research through exchange of ideas.

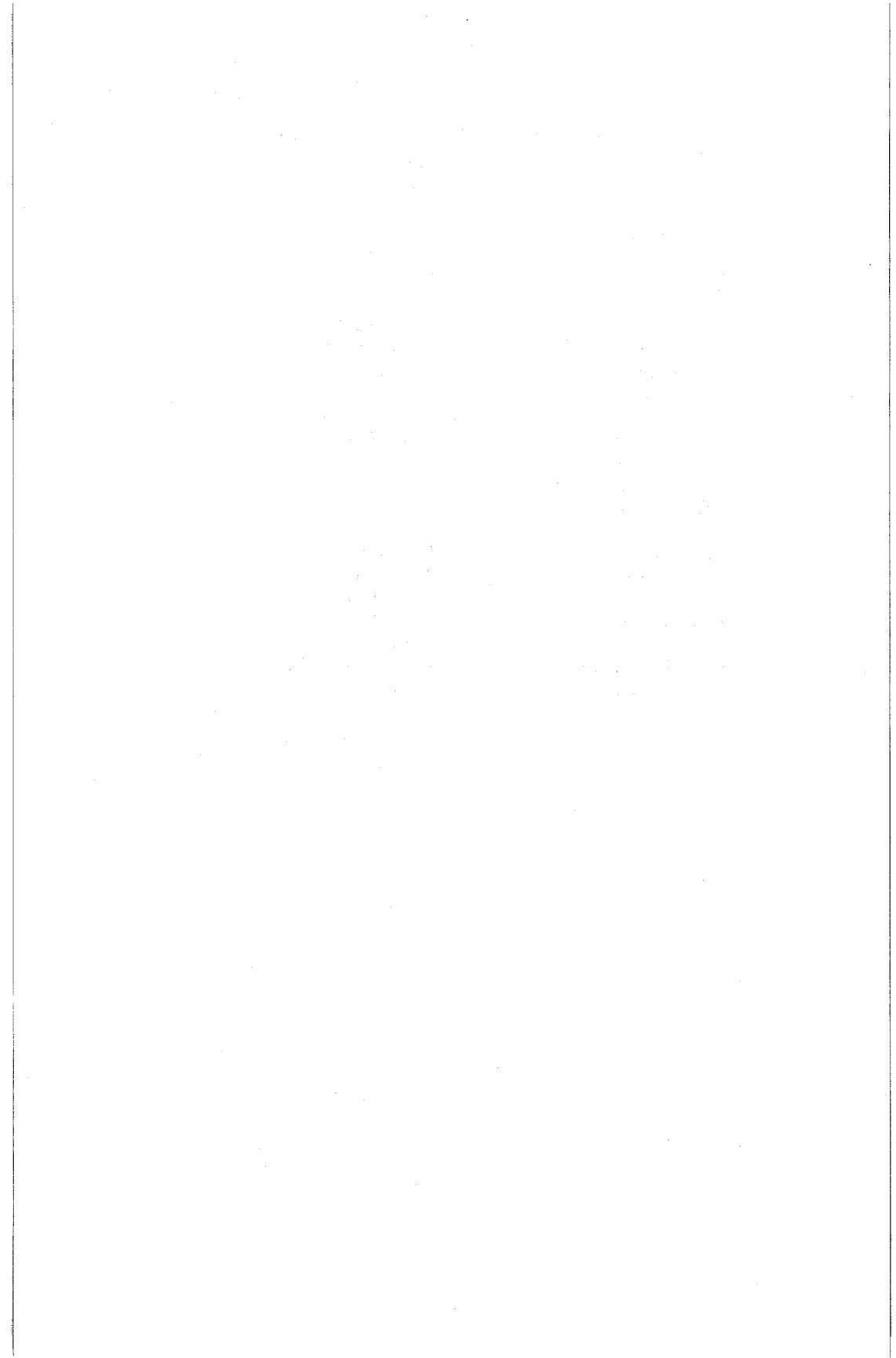
1975 USNC/URSI COMMITTEE MEMBERS:

Steering Committee:

S.W. Maley, Chairman	C.G. Little
M.G. Arthur	K.F. O'Loughlin
F.S. Barnes	R. Ott
D.C. Chang	H. Patterson
R.Y. Dow	E.K. Smith
W. Flock	A.D. Spaulding
R. Gallawa	J. Tary
G. Goulette	W.F. Utlaut
D.A. Hill	P.F. Wacker
C.T. Johnk	J.R. Wait
R.L. Lewis	

Technical Program Committee:

J.R. Wait, Chairman	G. Hagn
H.E. Bussey	A.W. Guy
A.H. LaGrone	D.A. Hill
T.E. VanZandt	S.W. Maley
J. Siren	E.K. Smith
K.I. Kellermann	A.D. Spaulding
T.B.A. Senior	J.W. Wright



---

MONDAY MORNING, OCT. 20 0900-1200

---

MINING COMMUNICATIONS

URSI COMMISSION II

Monday, October 20 0900

USI Session II-1, UMC 159

Organizer: D.A. Hill, OT/ITS

Chairman: J.N. Murphy, U.S. Bureau of Mines

1-1 WHOLE MINE COMMUNICATIONS AND MONITORING  
SYSTEM: Harry Dobroski, Bureau of Mines,  
Pittsburgh Mining & Safety Research Center,  
Pittsburgh, Pennsylvania

An integrated mine communications and monitoring (MCM) system has been developed for underground mines that allows private telephone channels, environmental monitoring, and control of underground equipment, all on a single coaxial cable. System operation is by frequency division multiplex under the direct control of a dedicated minicomputer. Many advanced features are incorporated into the system such as paging to roving personnel, two-way section wireless, through-the-earth emergency communications, and others. This system is presently being installed in U.S. Steel's Robena Mine complex near Uniontown, Pennsylvania.

1-2 WIRELESS COMMUNICATIONS EXPERIMENTS IN DEEP  
MINES: A. J. Farstad, Westinghouse Electric  
Corporation, Boulder, Colorado

Results of experimental work conducted by Westinghouse in 1974 have clearly established the feasibility of achieving effective two-way wireless communications in deep mines. Using communications equipment first developed by Westinghouse in 1971 for the Coal Mine Rescue and Survival System (CMR&SS), tests were conducted at the Sunshine Silver Mine, Kellogg, Idaho, at depths of 2700, 3100, and 4800 feet, and the Pocahontas Coal Mine No. 1, Keen Mountain, Virginia, at a depth of 2200 feet. Prior to conducting these tests, modifications were made to the original CMR&SS Communications System to increase its depth penetration capability. Modifications to the existing voice downlink system were somewhat trivial in that only an extension of the transmitting antenna system was

required to penetrate the deep over-burdens of these mines. Modifications to the Beacon Code Uplink System were more involved; these consisted of adopting a modular transmitter-antenna concept with each transmitter-antenna module being self powered and driven in parallel by a common code generator. In addition, a significant enhancement in uplink signal reception was realized by using a long horizontal wire antenna as a receiving antenna on the surface in place of the more conventional receiving loop. Miscellaneous communications tests were also conducted to determine the performance of a Westinghouse developed FM voice communications system with carrier frequencies from 5 to 115 kHz. Crosslink communications were successfully achieved over a range of greater than 2500 ft. at the 3100 ft. level of the Sunshine Mine.

1-3 THE BI-COAXIAL LEAKY LINE AND ITS APPLICATIONS  
TO UNDERGROUND RADIO COMMUNICATION:  
D. J. R. Martin, National Coal Board,  
Stanhope Bretby, Burton-on-Trent, United  
Kingdom

The bi-coaxial leaky line comprises two separate leaky cables spaced closely parallel so that the two outer braids or conductors form a bifilar transmission line. The type of construction was developed first as a research tool in the study of mode-conversion processes in leaky coaxial cables and to test previously developed theories; the somewhat intangible single-wire modes of the two constituent cables combine to form a bifilar mode which can be more accurately predicted and measured. As well as serving this purpose, the new cable is shown to have particular advantages as a practical leaky cable in underground radio systems, usefully combining the merits of coaxial and bifilar types. The cable construction further lends itself to a new configuration of leaky cable radiocommunication system in which line repeaters are bridged between the constituent coaxial cables in alternate directions instead of being connected simply in series; mid-span filters ensure system stability. Such a system provides duplex communication from a unified base station using simple one-way repeaters, and is particularly adaptable to spurs and branching. The inherent 'tailback' feature also provides a particularly consistent level of coupled signal through the system. The overall system of bi-coaxial cable

and line repeaters will accommodate many separate radio channels simultaneously and thus constitutes a bi-directional 'communications highway' for mining use.

1-4 LEAKY BRAIDED COAXIAL CABLE FOR RADIOPHONIC COMMUNICATION IN TUNNELS: INFLUENCE OF THE POSITION OF THE CABLE: P. Degauque, B. Demoulin, M. Cauterman and R. Gabillard, Lille University, Electronics Department, Villeneuve D'Ascq, France

We have shown in previous papers that a leaky braided coaxial cable could be used to provide communications along mine galleries. The transmission line is made of an insulated coaxial situated at a distance  $h$  of the wall, in a parallel direction with the gallery. Previous theoretical model supposed that  $h$  is a constant. But in the real configuration, the cable could be situated, for example, very near the wall within a short distance. Generally, a change in the position of the cable gives discontinuities of the characteristic impedance for the different modes and then, the propagation constants are modified. In order to see the influence of such discontinuities, we improve the previous theoretical model by studying the propagation along a coaxial cable set at successive distances of the wall:  $h_1, h_2 \dots h_n$ . In a given section, the current propagating on the braid is the result of four propagation modes: coaxial and monofilar, incident and reflected. The amplitude of each mode is given by four coefficients. By applying the non-uniform transmission line theory, we obtain a  $4n$  unknown system to determine the previous coefficients. We have made numerical application in the particular case of three successive distances between the cable and the wall. The results are compared with those experimentally obtained with a coaxial cable situated at different distances above the ground.

1-5 UHF RADIO WAVE PROPAGATION IN THE PRESENCE OF CONDUCTING OBSTACLES IN COAL MINE TUNNELS: Robert L. Lagace and Alfred G. Emslie, Arthur D. Little, Inc., Cambridge, Massachusetts

Approximate formulas for propagation past two classes of obstacles commonly encountered in coal mine tunnels, namely metal haulage vehicles such as trains and the mining machine and metal posts and other obstructions

located in a nearly periodic manner along longwall face tunnels, are derived and evaluated at 450 and 1000 MHz, the UHF frequencies found most favorable in previous mine tunnel work by the authors. The "train obstacle" acts mainly as a rectangular metal plug adjacent to one of the tunnel sidewalls. Noticeable increases in the propagation losses occur only when the unoccupied width is less than half the empty tunnel width, but they increase dramatically whenever the unoccupied tunnel width becomes less than 4-5 feet, and are greatest in low-coal at 450 MHz. The "longwall obstacles" are modelled principally by a tunnel bounded on one side by the coal face, on the other side by a periodic row of vertical metal posts, on the roof and floor by coal and horizontal metal members having a large effective roughness, and a rectangular metal plug "mining machine." An approximate heuristic approach shows that the propagation losses are primarily caused by scattering into higher modes by the obstacles and are significantly increased over those for simple rectangular tunnels, particularly in low-coal and at 450 MHz.

#### 1-6 APPLICABILITY OF VOICE BANDWIDTH COMPRESSION TECHNIQUES TO COAL MINE COMMUNICATIONS:

Richard H. Spencer and Warren G. Bender,  
Arthur D. Little, Inc., Cambridge, Massachusetts

The applicability of voice bandwidth compression techniques for extending the range of mine wireless communication systems is examined. Promise has been attached to such techniques because the lessened bandwidth gave hope for lessened received noise and hence increased operating range or reduced transmitter power requirements. Analog vocoders and digital adaptive predictive coders are examples of real-time techniques examined. For these techniques it is found that as the bandwidth gets narrower, the length to-noise ratio required for these systems to provide adequate voice intelligibility rises, such that the expected benefits of reduced transmitter power are not fully met. What benefits are found are achieved only through the use of sophisticated and costly equipment. In particular, current work on digital systems which produce the largest compression in bit rate is realized only by bringing to bear very significant amounts of computer power to the processing. Non-real-time bandwidth compression can be achieved by stretching out the transmission time for a voice signal to several times its original duration. This

URSI Session II-1

kind of transmission can be achieved with a directly proportional savings in transmitter power. The price paid for this achievement is the necessary time delay that occurs in the transmission because of the time stretch out of the voice message.

# IONOSPHERIC RADIO SCINTILLATIONS - I

URSI COMMISSION III

Monday, October 20 0900

URSI Session III-1, UMC 156

Chairman: R.H. Ott, OT/ITS

1-1 MODEL COMPUTATIONS OF POWER SPECTRA OF GHz SCINTILLATION SIGNALS: C. H. Liu and K. C. Yeh, University of Illinois at Urbana-Champaign, Illinois

Recently, two models of electron density irregularities have been proposed to interpret the GHz scintillation phenomenon. One is an irregularity slab of thickness about 200 km or so around the F-region peak with electron density fluctuations of the order of 20% about its background value. The other assumes an ensemble of field-aligned irregularities throughout the large part of the magnetosphere as the cause for signal fading.

In this paper, we shall investigate the power spectra of the scintillation at GHz frequencies for these two models. The problem will be formulated in such a way that the height variation of the background electron density can be taken into account. Computations are made for the different models. Since observational data of GHz scintillations are beginning to emerge, it is hoped that comparisons between experimental results and model computations on both scintillation levels and power spectra may yield important information about the irregularities.

1-2 SCINTILLATION INDEX OF STRONG PHASE SCREENS: Leonard S. Taylor and Charles J. Infocino, White Oak Laboratory, Naval Surface Weapons Center, Silver Spring, Maryland

Our concern in this paper is to remove certain anomalies in the strong phase-screen theory of ionospheric scattering. The work of Pisareva, Mercier, Salpeter, and Shishov using Gaussian or single scale turbulence models, led, apparently, to the general conclusion that large fluctuations in intensity, characterized by the appearance of random spots of very high intensity near a "mean focal plane" below the screen, will be produced by strong phase screens. The scintillation index  $m^2 = \{\langle I^2 \rangle - \langle I \rangle^2\} / \langle I \rangle^2$  was calculated to reach values

>>1 at the mean focal plane. However, this result is contradicted by observation which shows that  $m \rightarrow 1$  as the strength of turbulence  $\rightarrow \infty$ . Numerical computations using a power-law turbulence model yields results in agreement with this observation, but are dubious on both mathematical and physical grounds. In this paper we base our discussion on the three-dimensional turbulence spectrum for dielectric turbulence,  $\hat{\phi}_\epsilon \sim e^{-\eta^2 r_o^2 / (1+\eta^2 R_o^2)^{a/2}}$ , where  $R_o$  is an outer scale size which produces a lower cutoff in  $\hat{\phi}_\epsilon(\eta)$ . The inner scale,  $r_o$ , is introduced in accordance with the loss of collective behavior of a plasma for a plasma for scales below the Debye length. The appearance of two scale parameters,  $R_o$  and  $r_o$ , shall be shown to produce results for the scintillation index which contrast strongly to those obtained for a single scale model, leading to the conclusion that ordinarily  $m < 1$  for ionospheric observations.

1-3 ANGLE-OF-ARRIVAL FLUCTUATIONS DUE TO IONOSPHERIC SCINTILLATION: R. K. Crane, Lincoln Laboratory, Lexington, Massachusetts

Observations of elevation and traverse angle scintillation were made at the Millstone Hill Radar Facility using 400 MHz transmissions from the U.S. Navy Navigation System Satellites. Angle-of-arrival estimates were constructed from pointing angles recorded for the 84-foot Millstone antenna and simultaneously recorded monopulse error voltages. The angle-of-arrival estimates were processed to yield rms values for the fluctuations and power spectra for the fluctuations. A theoretical analysis based upon weak scatter theory for a thick screen (Rytov Approximation) was performed to predict the angle-of-arrival power spectra. An anisotropic three-dimensional power law power spectrum was used to model the electron density fluctuations. Using this model, the rms fluctuations in elevation and azimuth can be used together with information about the propagation geometry relative to the magnetic field to estimate the axial ratio for the anisotropic irregularities. The observed spectra show good agreement with the predicted spectra. For observations both to the north and south of Millstone (invariant latitudes between  $46^\circ$  and  $66^\circ$  at 300 km height) the estimated axial ratio values ranged from 2 to 5.

## 1-4 AN ITERATIVE METHOD FOR TREATING MULTIPLE SCATTERING: C. L. Rino, Stanford Research Institute, Menlo Park, California

We describe a method for computing the complex space-frequency coherence functions in an extended medium. The technique is based on an iterative application of the Born approximation. The method is valid when a "weak" Markov condition can be assumed. This is essentially the same condition that is used to derive differential equations for the complex field moments from the parabolic wave equation. Indeed, we shall show that when the Fresnel or parabolic approximation is made, our results are in exact agreement with solutions obtained by numerically integrating the moment equations derived by Tatarski. Our method has an advantage in that it admits anisotropic spectra and arbitrary incidence angles. The analysis was performed to analyze ionospheric two-frequency coherence measurements taken from several satellites that have phase-locked VHF and UHF beacons. Some results will be presented and discussed.

## 1-5 NUMERICAL SIMULATION OF SCINTILLATION CAUSING F-REGION IRREGULARITIES: S. L. Ossakow, U.S. Naval Research Laboratory, Washington, D.C.; and A.J. Scannapieco and S. R. Goldman, Science Applications Inc., McLean, Virginia

In an effort to understand the basic physics of scintillation causing F-region irregularities, we have performed a computer simulation which follows the nonlinear evolution (via Perkins' model nighttime F-region equations, valid for middle to high latitudes) of a plasma instability thought to be responsible for some of the observed irregular structures. We do not assume that there are no horizontal gradients in the field line integrated ion number density or Pedersen conductivity. Under these conditions our results show that: (1) an east-west spatially varying F-region ionospheric equilibrium exists; (2) this equilibrium is unstable to the usual gradient drift instability for certain conditions involving the north-south and east-west electric fields, the ionized gradient scale length, and the neutral scale height; (3) the instability evolves nonlinearly to a quasi-final state with sheet-like structures having a preferential east-west orientation; and (4) the power spectrum in this state for the Pedersen conductivity fluctuations goes approximately like  $k^{-2}$ .

VLF/ELF ACTIVE AND PASSIVE PROBING

URSI COMMISSION IV

Monday, October 20 0900

URSI Session IV-1, UMC 157

Chairman: S.D. Shawhan, University of Iowa

1-1 DIFFICULTIES WITH THE USE OF PC 1 PULSATION MEASUREMENTS FOR MAGNETOSPHERIC DIAGNOSTICS:  
A. C. Fraser-Smith, Radioscience Laboratory, Stanford Electronics Laboratories, Stanford University, Stanford, California

Measurements of the dispersion characteristics of naturally-occurring ULF pulsations of class Pc 1 (0.2-5 Hz) have been used over the last decade to derive information about the physical parameters of the magnetosphere. Although these measurements have agreed in a general sense with other independent measurements, there are difficulties of interpretation and in the selection of Pc 1 events. Two major difficulties are introduced by the presence of helium in the magnetosphere and possible ionospheric dispersion of the Pc 1 signals. Perhaps most important, however, is the difficulty in selecting appropriate Pc 1 events for analysis. Purely dispersive Pc 1 events are rare and amplification in the magnetosphere can invalidate the measurements. A particular example will be discussed where a magnetospheric equatorial plasma density can be derived in a seemingly straightforward manner, but where internal inconsistencies suggest that the assumptions on which the measurements are based do not apply.

1-2 SOUNDING THE MAGNETOSPHERE WITH A SATELLITE BORNE VLF TRANSMITTER: B. C. Edgar, The Aerospace Corporation, El Segundo, California

We examine the possible ray paths that a satellite borne VLF transmitter might excite and that would return after transversing a portion of the magnetosphere. The chief advantages of such a system are that transmitter and receiver are contained on one vehicle (or a close mother-daughter pair) and that the spectral and time delay characteristics can be used to measure electron densities and gradient structure. A high altitude satellite (above L=2) can excite a ray path in the MR whistler mode that

travels approximately along the field line at the Gendrin 'constant velocity,' reflects at the LHR, and returns to the satellite. The same satellite could also excite rays which would be trapped by large field aligned density dropoffs. Ducts would probably trap rays, but by the time the signal returns the satellite will have moved out of the duct. However small sized field aligned irregularities such as ducts, troughs, and dropoffs perturb the nonducted returns enough to produce recognizable 'kinks' or signatures into the spectral characteristics.

1-3 A NEW INSTRUMENT FOR REAL-TIME VLF SIGNAL DETECTION AND DIRECTION FINDING: M. Leavitt, Radioscience Laboratory, Stanford University, Stanford, California

A new instrument is described which can automatically detect and track the frequency of VLF signals such as whistlers and artificially stimulated emissions. The improved detection and filtering capability thus provided permits real-time direction finding from a cross-loop and vertical antenna system, as well as providing a record of signal frequency and amplitude as a function of time. The direction finding technique employed displays a number of advantages over the goniometer: unambiguous bearing indication, insensitivity to signal fading and modulation, reduced sensitivity to polarization error, and a continuous real-time output requiring no post-analysis equipment. For the recording of data from the instrument, a technique is described which utilizes a single channel of audio-magnetic tape and which places the data in a form that can be easily correlated with conventional broadband VLF spectrum analysis records. This instrument was installed at Roberval, Canada, in June 1975 as a part of controlled wave-particle interaction experiments using the VLF transmitter at Siple, Antarctica. Preliminary direction finding results on Siple transmitter signals as well as on natural whistlers and chorus will be described.

1-4 PROPERTIES OF THE DUCTED MAGNETOSPHERIC PATHS FOLLOWED BY SIGNALS FROM THE SIPLE, ANTARCTICA VLF TRANSMITTER: D. L. Carpenter and T. R. Miller, Radioscience Laboratory, Stanford University, Stanford, California

A study has been made of the conditions under which

Siple transmitter signals propagate to the conjugate ground station at Roberval, Canada. In 1973 and 1974, transmission periods were typically 8 hours in length. Signals detectable by conventional spectrographic analysis were present on roughly 20% of the days, typically for 3 hours at a time. As expected, the receptions showed evidence of sensitivity to conditions that govern whistler propagation between conjugate hemispheres and also to the presence of energetic electrons in the vicinity of  $L = 4$ . Receptions of transmitter signals at Roberval were most frequent during quieting following geomagnetic disturbances during periods of high whistler rates near  $L = 4$ , and during periods of multi-hop whistler propagation. Signal reception was most frequent near local dawn, and on occasion signal activity varied with whistler and emission intensity when the signal path was near the plasmapause. A detailed study of five months of 1973 and 1974 data showed a concentration of signal path endpoint latitudes within approximately  $\pm 200$  km of the latitude of the Siple-Roberval field line. Multipath propagation was frequently observed, but a single path was usually prominent in terms of received amplitude. The probing signals near  $L = 4$  provided a means of scanning plasmaspheric propagation conditions and density as the position of the plasmapause varied with magnetic activity. At times the paths were well within the plasmapause. Frequently they were in the region of relatively steep plasmapause gradients.

1-5 THE PLASMAPAUSE AS A VLF WAVE GUIDE: U. S. Inan and T. F. Bell, Radioscience Laboratory, Stanford University, Stanford, California

The properties of the plasmapause as a VLF wave guiding structure have been studied and it has been found that in general the plasmapause can guide waves from one hemisphere to the other. Ray paths and wave normal angles for various plasmapause density variations are given with the aim of displaying the effects of plasmapause shape on the ray paths. It is found that only local gradients at the edge of the plasmapause are important in determining the ray paths and that larger local gradients provide stronger and more effective guidance of the waves. For certain plasmapause density distributions, it is found that multi-hop propagation is possible. Waves starting from 100 km altitude with vertical wave normal angles

at latitudes lower than that of the plasmapause converge to the plasmapause field line at about 5000 km altitude and are trapped and guided by the plasmapause gradients to the other hemisphere. As the rays descend to altitudes of 5000-6000 km in the conjugate hemisphere they diverge inward from the plasmapause field line and reach an altitude of 100 km at almost the same latitude as that at which they started and with almost vertical wave normal angles. These rays are quasi-reciprocal and reflected components return to the original hemisphere along the same path. This mode of propagation is shown to be possible for a large latitude (almost 5 degrees) and frequency range (1-5 kHz). Since their wave normal is very nearly vertical, these rays should be able to penetrate the lower boundary of the ionosphere and hence be observed on the ground. The dispersion of such whistlers is similar to that expected for ducted whistlers. Our results have important implications for ground-based whistler studies as well as VLF wave-injection experiments.

EXTRA-TERRESTRIAL TECHNIQUES FOR MEASURING CRUSTAL  
MOTIONS AND SATELLITE RANGING  
URSI COMMISSIONS V, I, II, AND VII  
Monday, October 20 0900  
URSI Session V-1, UMC West Ballroom  
Chairman: C.C. Counselman,  
Massachusetts Institute of Technology

1-1 CRUSTAL MOBILITY AND TECTONIC PROCESSES:  
Carl Kisslinger, Cooperative Institute for Research  
in Environmental Sciences, University of Colorado/  
NOAA, Boulder, Colorado

The hypothesis that the present distribution of surface features of the earth and the major tectonic processes that shape these features are governed by the lateral movements of lithospheric plates is well supported by a variety of independent geological and geophysical data. The techniques now used for determining relative plate motions can only give long-time averages of the motions. Whether the motions occur mainly as episodic events or continuously is not known. The driving mechanism responsible for plate motion is a subject of active investigation now and is imperfectly understood. Relative plate motions are responsible for most earthquakes, and knowledge of strain rates at plate boundaries will be useful input to earthquake prediction efforts. In addition, localized crustal deformations, both horizontal and vertical, may occur prior to earthquakes and detection of anomalous deformation is one of the most promising techniques for identifying the sites of impending major earthquakes, and estimating their probable magnitudes.

1-2 INTER-SITE DISTANCE MEASUREMENT FROM RANGING  
TO ARTIFICIAL SATELLITES: R. Kolenkiewicz and  
D. E. Smith, Geodynamics Branch, Goddard Space  
Flight Center, Greenbelt, Maryland; and  
P. J. Dunn, Wolf Research and Development  
Corporation, Riverdale, Maryland

Laser distance measurements to artificial satellites have been used to determine the chord length between tracking stations. This technique uses quasi-simultaneous laser tracking of a near-earth satellite from two or more sites from which the spacecraft orbit and the relative locations of the tracking sites can be determined. During the last five years experiments

have been conducted that indicate the basic capability of this technique for measuring crustal motion. The first experiment was conducted along the east coast of the United States over a distance of 400 km in 1970, the second between sites 1000 km apart in California in 1972, and the third in 1974 connecting sites on the east and west coasts, 3600 km apart. The results of these experiments show the present capability to measure large chord distances is a few tens of centimeters and that with a higher satellite, improvements in the tracking system, and better knowledge of the forces perturbing the satellite orbit, chord measurements of a few centimeters precision should be possible in the near future.

1-3 EXPECTED CRUSTAL MOVEMENT MEASUREMENTS USING  
LUNAR LASER RANGING: James E. Faller, Joint  
Institute for Laboratory Astrophysics, National  
Bureau of Standards and the University of  
Colorado, Boulder, Colorado

Pulsed laser measurements of the lunar distance have been carried out at the McDonald Observatory in Texas, since 1969. The accuracy for single runs is typically 8 to 15 cm. The data have been used to very much improve our knowledge of the lunar orbit, librations, retroreflector locations, and other quantities. The present theoretical models using BIH values for UTI and polar motion fit the data to 40 cm rms. Single-day values for the earth's angular position with respect to the moon on many days have uncertainties of between 0.2 and 0.4 millisec. The present uncertainty in transforming from the moon to an inertial frame to obtain UTO is estimated to be 0.5 millisec. Additional lunar ranging stations designed for frequent observations are being constructed on Mt. Haleakala in the Hawaiian Islands, in Australia, in France, and in Japan. It is hoped that two additional southern hemisphere stations will be developed in the future and that present measurements in the USSR will continue. The accuracy goal for the Haleakala station is 2 to 3 cm, and upgrading of the other stations to this accuracy is expected. The lunar distance measurements from the international network of fixed stations will give important information on plate tectonics as well as on UTI and polar motion. However, more extensive crustal movement information can be obtained at relatively low cost by means of 3 mobile lunar ranging stations such as the U.S. one proposed by the University of Texas. This station would spend 3 to 6 weeks at a given site, and determine

the station location with respect to the fixed stations with an expected accuracy of 3 cm in each coordinate. Such measurements could monitor the motion of 10 or 15 points per major plate at intervals of 2 or 3 years. These results would clarify the interpretation of the motions measured between the fixed stations on different plates and give valuable information on large scale intra-plate distortions. They would also provide a reference framework for more extensive measurements at many sites per plate using satellite ranging, VLBI, and ground techniques.

1-4     RADIO INTERFEROMETRIC MEASUREMENTS OF EARTH DYNAMICS:  
        A. E. Niell, JPL, Pasadena, California

The radio astronomy technique of Very Long Baseline Interferometry (VLBI) offers promise for the solution of problems of high accuracy three-dimensional measurement of earth crustal movements. The methods of VLBI make it possible for radio receiving stations to be independently operated at arbitrary separations using extragalactic radio sources as a time-invariant frame of reference. Since August 1974, the Project ARIES (Astronomical Radio Interferometric Earth Surveying) 9m transportable antenna has been located at JPL, Pasadena, and has been operated in combination with the 64m Goldstone antenna of the Deep Space Network 180 km away and on the opposite side of the San Andreas Fault. Analyses of several experiments over the past year have yielded baseline determinations with precisions of better than 15 cm in three dimensions. The estimated baseline vector accuracy is also 15 cm. These experiments have incorporated water vapor radiometer calibrations of tropospheric water vapor delay effects above the ARIES station. The length of this baseline was independently measured by the National Geodetic Survey and agrees with the interferometer determination to within 11 cm. Possible earth motions over the 1 year interval will be discussed. Several other activities are currently underway at JPL which will make valuable contributions to the study of earth dynamics. Primary among these are (1) the intercontinental VLBI program of the Deep Space Network which will have an ultimate measurement capability of 10 cm equivalent accuracy for UT1 and polar motion and radio source positions of 0.005 arc sec and (2) development of a simultaneous radio ranging system for establishing a dense grid of geodetic control points at ~20 km intervals with accuracies of 1 to 4 cm.

1-5      VERY LONG BASELINE INTERFEROMETRY FOR GEO-  
PHYSICAL MEASUREMENTS: T. Clark, R. Coates, J.  
Ryan, W. Webster and C. Ma, Goddard Space Flight  
Center, Greenbelt, Maryland; C. Counselman,  
D. Robertson and I. Shapiro, Massachusetts  
Institute of Technology, Cambridge, Massachusetts;  
and H. Hinteregger, C. Knight, A. Rogers, and  
A. Whitney, Haystack Observatory, Westford,  
Massachusetts

Very Long Baseline Interferometry (VLBI) is one of several techniques that show promise of achieving accuracies of a few centimeters for geophysical measurements. This paper will discuss relevant VLBI results obtained by the GSFC/MIT/Haystack Group. These include sub-centimeter level accuracies on the Haystack-Westford (1.2 KM) baseline, decimeter level repeatability on the Haystack-Goldstone (3900 KM) baseline and Haystack-NRAO (845 KM) baseline, and submeter level vector closure on the Haystack-NRAO-Goldstone triangle of baselines. Comparisons of VLBI baseline results and satellite Doppler ("Geoceiver") results on a variety of baselines will also be discussed. The paper will conclude with discussion of future plans for achieving the centimeter-level accuracies required for measurements of tectonic plate motions.

1-6      ADVANCES IN VLBI: GEODETIC AND ASTROMETRIC  
RESULTS: A. E. E. Rogers, H. F. Hinteregger,  
C. A. Knight, and A. R. Whitney, Haystack  
Observatory, Westford, Massachusetts; T. A. Clark,  
Goddard Space Flight Center, Greenbelt, Maryland;  
and C. C. Counselman, D. S. Robertson, and  
I. I. Shapiro, Massachusetts Institute of  
Technology, Cambridge, Massachusetts

A series of experiments has been performed to determine the 1.24 km baseline vector between two antennas of the Haystack Observatory using very-long-baseline interferometry (VLBI) techniques. The results have been repeatable to within a few millimeters, and agree with a conventional survey result within the latter's larger uncertainty. Geodetic and astrometric results from a number of long-baseline experiments involving Haystack, Goldstone, and Greenbank will also be presented, including values for the Love number  $h$ , for the precession constant, and for the positions of two dozen compact radio sources.

1-7 THE ESTIMATION OF TROPOSPHERIC PROPAGATION PATH LENGTH FROM GROUND-BASED MICROWAVE MEASUREMENTS:  
J.M. Moran and B.R. Rosen, Center for Astrophysics,  
Cambridge, Massachusetts

One of the principal limitations to the accuracy of very long baseline interferometry in measuring geometric coordinates is the atmosphere. The water vapor which cannot be accurately predicted from surface measurements causes an excess propagation path length at microwave frequencies of up to about 50 cm. Shaper, et al, (Proc. IEEE 58, 272, 1970) and others have studied the theoretical accuracy to which the path length can be determined from ground-based meteorological data and measurement of the sky brightness temperature using radio sonde data to provide sample atmospheres. We have confirmed their results and extended them by investigating the temporal and spatial change in the regression coefficients relating brightness temperature to path length by using radio sonde data taken at four different locations. To confirm this method, an experiment is being planned to simultaneously measure the sky brightness temperature during radio sonde flights at Haystack Observatory in Westford, Massachusetts.

1-8 A SIMULATION STUDY OF THE DETERMINATION OF TROPOSPHERIC PATH LENGTH FOR VERY LONG BASELINE INTERFEROMETER DATA ANALYSIS:

William J. Webster, Jr., Geophysics Branch,  
Goddard Space Flight Center, Greenbelt,  
Maryland

The several very long baseline interferometer (VLBI) programs use interferometry techniques to make geodetic measurements. At the level of accuracy required, the path length error due to the neutral lower atmosphere makes a significant contribution to the error budget of the interferometer measurements. Current and proposed VLBI systems must correct for this effect. A review of previous work shows that, while very little has been published on the small-scale distribution of the atmospheric water vapor, the large-scale distribution of water vapor is known to vary significantly over time scales as short as 20 minutes. This variation in water vapor content is the main source of the changes in path length error at a particular site. Thus a path length correction system must measure the distribution of atmospheric water vapor. The simulation study shows that, when combined with surface meteorology

data, dual frequency, passive microwave radiometer data permit determination of the path length correction to better than 2 cm of the zenith. By a careful choice of frequencies, a dual frequency system will allow a measurement of the path length correction to better than 4 cm at zenith angles as great as 60°. Because of the wide range of weather conditions to be expected for VLBI sites, it will probably be necessary to use a separate correction algorithm for each site.

1-9 THE EFFECTS OF ATMOSPHERIC TURBULENCE ON THE ACCURACY OF SATELLITE RANGING SYSTEMS: C.S. Gardner and N. Narayana Rao, University of Illinois, Urbana, Illinois

Laser ranging systems have developed to the point where it may now be possible to measure the distance from an orbiting satellite to a point on the earth with uncertainties on the order of only a few centimeters. The precision of satellite ranging systems will be limited in part by atmospheric refraction and scattering. In this paper the effects of atmospheric turbulence on the accuracy of single color and multicolor ranging systems is discussed. The statistical characteristics of the random path length fluctuations induced by turbulence are examined. Correlation and structure functions are derived using several proposed models for the variation of  $C_n^2$  with altitude. For single color systems it is shown that the random path length fluctuations can limit the accuracy of a range measurement to a few centimeters. Two color systems can partially correct for the random path fluctuations so that their accuracy is limited to a few millimeters.

SCATTERING-I  
URSI COMMISSION VI

Monday, October 20 0900

URSI Session VI-1, Radio Building Auditorium

Chairman: R.E. Kleinman, University of Delaware

1-1 WEDGE DIFFRACTION: G. A. Deschamps, Department of Electrical Engineering, University of Illinois, Urbana, Illinois

The problem of diffraction of a high frequency (ray optical) field by a conducting wedge is replaced by similar diffraction problems in a space  $P_2$  made up of two replicas  $P_+$  and  $P_-$  of the physical space  $P$  exterior to the wedge, or in a space  $P_\infty$  where the polar angle is any real number instead of being reduced mod  $2\pi$ . The incident field continued into the extended space  $P_2$ , or  $P_\infty$ , is discontinuous along two shadow boundaries. The solution can be obtained by finding what (diffracted) fields should be added to the incident field to compensate for each discontinuities. Boundaries conditions on the wedge are then satisfied by adding an image field that can be simply constructed in  $P_2$ . This approach readily explains the structure of known exact solutions to the wedge problem. Furthermore, if the wave equation is approximated by a parabolic equation (Ufimtsev, Malyughinetz) each term of the diffracted field (in  $P_\infty$ ) is expressed by  $e^{ikr}V(\tau)$  where  $V$

is a Fresnel integral,  $\tau = \sqrt{2kp} \frac{\psi}{2}$ ,  $\rho$  = distance  $r$  to the edge (for an incident plane wave) or  $\rho = \frac{r - r_0}{r + r_0}$  (for an incident cylindrical wave whose axis is at distance  $r_0$  for the edge), and  $\psi$  is the angle away from the shadow boundary to the observation point. The solution in  $P_2$  is a series obtained by imposing a periodicity in  $\theta$  of twice the wedge exterior angle. When  $\tau$  is large one recovers the exact Keller diffraction coefficients (in spite of the approximation!). By separating in the series the terms for which  $\tau$  is large from the others one obtains a family of uniform solutions continuous across the shadow boundaries and valid near to the edge.

1-2 SCATTERING BY A FINITE WEDGE WITH LINEARLY VARYING SURFACE IMPEDANCE: P. Bhartia and B. Monson, Faculty of Engineering, University of Regina, Regina, Canada

The scattering of electromagnetic waves by a finite

wedge and semicircular cylinder with linearly varying surface impedance is investigated. The method of solution follows the boundary value technique. Using Leontovich impedance boundary conditions and continuity of fields, an infinite set of equations is obtained for the coefficients of the scattered field. Solution of these equations using appropriate truncation and numerical techniques leads to results for the scattered fields. Finally, results are presented for the radar cross section for various cases of surface impedance, wedge dimension  $ka$ , and wedge angle.

1-3 ON DIFFRACTION BY AN IMPERFECT WEDGE: L.B. Dean, Department of Electrical Engineering, The University of Nebraska, Lincoln, Nebraska, and NOAA/ERL, U.S. Department of Commerce, Boulder, Colorado

A formal solution for the diffraction of the fields from an electric line source by an imperfect wedge is obtained by a heuristically reasonable generalization of the Ohm-Rayleigh procedure commonly used for obtaining Green's functions via eigenvalue expansion. In this, "pseudo-eigenfunctions" are developed which are azimuthally periodic in space, with respect to the wedge tip, which satisfy the electromagnetic boundary conditions at both wedge interfaces and which satisfy an eigenvalue wave equation throughout all space that has a different eigenvalue for the interior and exterior of the wedge for the same "pseudo-eigenfunction" (hence the name "pseudo-eigenfunction"). The eigenvalues are thus piecewise constants in space as opposed to being strictly constants for eigenvalues in the usual application of the Ohm-Rayleigh method. A Green's function is then obtained for the geometry by applying the Ohm-Rayleigh method to these "pseudo-eigenfunctions." The "pseudo-eigenfunctions" are obtained only for certain restricted wedge angles and the Green's function is therefore also restricted to these angles. Comments are offered concerning difficulties with the magnetic line source excitation problem.

1-4 DIFFRACTION OF AN ARBITRARY FIELD BY A HALF-PLANE: Y. Rahmat-Samii and R. Mittra, Department of Electrical Engineering, University of Illinois, Urbana, Illinois

The problem of diffraction of an arbitrary incident field by a half-plane is of great interest in many practical problems. As an example, one is often interested in solv-

ing the problem of radiation or scattering from an antenna mounted on a conductive body with sharp edges; or for an antenna with a given pattern function, which is mounted close to the earth and is radiating in the presence of a hill that may be modeled by a knife-edge. It should be mentioned that the principal difference for the case of an arbitrary incident field strongly shows up in the neighborhood of the shadow boundaries, where Keller's representation is not valid because of the infinities in the Keller's coefficient. A search through the literature reveals that there has not been a detailed analysis of the half-plane diffraction of an arbitrary incident field until quite recently. The half-plane diffraction problem of the radiated field by a uniform line source has been discussed by Clemmow, Born, and Wolf and others. A more general case has been analyzed by Khestanov, but his work does not provide any specific results of the behavior of the diffracted field at the shadow boundaries. Recently, a few terms of the asymptotic representation of the diffracted field of a nonuniform line source has been given by Lee and Deschamps using the uniform asymptotic theory (UAT). In this paper, we employ the concept of the spectral theory of diffraction (STD), which has recently been developed by the authors, to construct the field diffracted by a half-plane for an arbitrary incident field in a systematic fashion for any observation angle. The analysis begins by first expressing the incident field in the spectral domain. We then use the spectral diffraction coefficient to find an integral representation for the diffracted field. The integral is evaluated asymptotically using the method of steepest absents. It is found that for observation angles away from the shadow boundaries one recovers the GTD solution. For observation angles near and at the shadow boundaries, we use the complete asymptotic expansion and evaluate an integral in which the first order pole of the kernel coincides with the saddle-point. Results obtained in this paper are compared with those derived via UAT.

1-5 ANALYSIS OF THE RECTANGULAR HORN BY UNIFORM ASYMPTOTIC THEORY OF EDGE DIFFRACTION:  
R.C. Menendez and S.W. Lee, Department of Electrical Engineering, University of Illinois, Urbana, Illinois

The newly-developed uniform asymptotic theory (UAT) (Ahluwalia, Lewis, and Boersma, 1968; Lee and Deschamps, 1974) of high frequency edge diffraction have been applied to the rectangular horn antenna (both sectoral and pyra-

midal) for the calculation of the reflection coefficient and the far field radiation pattern. The present approach resembles past ray-optical analyses of the horn in that the three-dimensional horn is regarded as two two-dimensional horns at right angles to one another. Each two-dimensional horn is then analyzed by considering diffracted rays emanating from the throat wedge due to an incident mode ray. A modified diffraction coefficient (Lee, 1970) has been employed to incorporate the effect of an opposing throat wedge in close proximity. Subsequent interactions between the throat wedge and the flare edge which also contributes to the reflection coefficient and the far field are accounted for by considering multiple images of the throat wedge as multiple sources illuminating the flare edge. These interactions frequently involve evaluating the field in the vicinity of shadow boundaries and, as such, require application of UAT instead of straightforward GTD analysis. Furthermore, exterior to the horn, uniform expressions provide a far field which is free of the discontinuities which arise from the GTD analysis. In addition to the conventional rectangular horns, flanged horns may also be investigated with a trivial extension of this approach. Results for the reflection coefficient and far field patterns will be presented and compared with some experimental values.

1-6 THE INITIAL-VALUE METHOD: A NEW APPROACH TO  
SCATTERING PROBLEMS: Essam A. Marouf, Center  
for Radar Astronomy, Stanford University, Stanford,  
California, and University of Alexandria, Egypt

Dielectric scatterers placed in free-space and excited by external sources can be regarded as dependent-sources. The response of free-space to such sources leads to a self-consistent integral equation for the electric field within the volume of the scatterer. The integral equation, which is a Fredholm integral equation of the second kind, automatically incorporates all of the boundary conditions and is valid for scatterers of any shape and refractive index. Numerical solutions for the internal fields is obtained by transforming the integral equation to an initial-value problem using the "imbedding" technique, that is, a scatterer of a given refractive index  $m$  is imbedded in the larger class of problems in which  $m$  is variable. In such an approach, the inverse kernel of the integral equation is built as a function of  $m$  starting from the initial condition that the inverse kernel is equal to the free-space Green's function at  $m = 1.0$ . The inverse kernel is independent of the exciting field

and hence is a characterization of the shape and material of the scatterer. For any exciting field, the electric field inside the scatterer is obtained by convolving the inverse kernel with the exciting field over the volume of the scatterer. Implementation of the initial-value method is illustrated by the classical example of plane wave scattering from a homogeneous dielectric sphere (scalar case). Eigenfunctions expansion of the internal field in terms of spherical harmonics reduces the three-dimensions problem to a system of one-dimension initial-value problems, each is integrated to obtain the Mie coefficients as a function of the refractive index  $m$ . Solutions obtained are in good agreement with the classical analytical solutions for the Mie coefficients. It is believed, however, that the power of the initial value method actually reveals itself in problems in which the boundary-value solutions are complicated.

1-7 SYMMETRY TECHNIQUES FOR SOLUTION OF MAXWELL'S EQUATIONS: INHOMOGENEOUS ANISOTROPIC LOSSY MEDIA:  
 Paul F. Wacker, National Bureau of Standards,  
 Boulder, Colorado

The theory of group representations is responsible in large part for the practical success of quantum mechanics and is equally applicable to EMT; such a powerful technique can be even more valuable with the added complexities of vector solutions for inhomogeneous anisotropic lossy media. Efficiencies of conventional techniques can be increased by supplying rigorous constraints on the solutions. Alternatively, complete sets of complete 3D exact solutions may be obtained by group techniques alone. For simplicity in this abstract, harmonic time dependence is assumed, leading, e.g., to the simultaneous equations  $\nabla \times [\epsilon^{-1} \nabla \times (\mu^{-1} \mathbf{B})] = \omega^2 \mathbf{B}$ ,  $\nabla \cdot \mathbf{B} = 0$  where  $\epsilon$  and  $\mu$  are complex dyadic functions of position. These are eigenvalue equations of the form  $Tf = \lambda f$ . If an operator  $O_R$  commutes with all the  $T$ 's ( $O_R T = T O_R$ ), then  $O_R f$  is also a solution for the same  $\lambda$ . (Note that  $\nabla \times$ ,  $\nabla \cdot$ , and  $\nabla$  commute with a translation, rotation, or reflection.) If the  $O_R$ 's form a group and the  $T$ 's are linear, a complete set of exact solutions may be chosen such that each solution belongs to a row of an irreducible representation (has a prescribed symmetry, say even or odd). With continuous groups, complete sets of complete solutions may be obtained by these techniques alone, giving rise to the familiar plane, cylindrical, and spherical wave solutions for free space, modes for rectangular and circular guide, and modes for rectangular, cylindrical, and spher-

ical davities including the definitions of the functions involved. The theory provides the modal orthogonality and provides rigorous constraints upon the effects of perturbations, thus increasing the efficiency of ordinary perturbation techniques. These symmetry techniques also yield modal addition theorem, i.e., transformation of the modes under coordinate transformations, leading to efficient data processing for near field scanning with probe correction. Application of non-unitary representations for lossy media and modification for non-linear equations is mentioned. The method does not inquire whether the eigenvalue equation is a differential, integral, integro-differential, variational, or matrix equation or inquire about the T's other than their linearity and a group of  $O_R$ 's which commute with the T's. To a large degree, the technique is independent of whether the solution is a scalar, vector, pseudovector, or spinor field. Hence it integrates wide areas of mathematics and permits one to draw from solutions from diverse physical problems, mathematical formulations, and coordinate systems.

1-8 ON THE FORWARD-SCATTERING APPROXIMATION TO THE ONE-DIMENSIONAL WAVE EQUATION FOR RANDOM MEDIA:

W. Wasylkiwskyj, Institute for Defense Analyses,  
Arlington, Virginia

In the study of electromagnetic wave propagation in random media a variety of approximating assumptions are employed with what appear to be only qualitative justifications. In this paper these approximating techniques are examined in the context of the one-dimensional wave equation, yielding quantitative results that are difficult to obtain in the more realistic but much more complex three-dimensional case. Particular attention is devoted to the so-called forward-scattering assumption. Its validity is shown to be critically dependent on the certain properties of the correlation function of the refractive index fluctuations. It is shown that several commonly employed correlation functions are in fact incompatible with the forward-scattering hypothesis. In particular, this is true of the Diract delta correlation function employed in conjunction with the parabolic wave equation for forward-scattering media.

URSI Session VI-1

1-9 WAVE PROPAGATION IN A RANDOM MEDIUM WITH INHOMOGENEOUS BACKGROUND: R. Woo and F.C. Yang, Jet Propulsion Laboratory, Pasadena, California; and A. Ishimaru, University of Washington, Seattle, Washington

The radio occultation experiment, using the radio link between the earth and spacecraft passing behind planets, has proven to be an important method for remote sensing turbulence in planetary atmospheres. In previous work the atmosphere was assumed to be a medium whose refractive index consisted of small random fluctuations superimposed on a homogeneous background. In reality, however, the background refractive index increases rapidly with depth especially in the case of planets with dense atmospheres, e.g., Venus and Jupiter. In this paper we examine the effects of the inhomogeneous background on the turbulence-induced fluctuations of the radio occultation signal. We assume that the inhomogeneous background refractive index is spherically symmetric and decreases monotonically with altitude. Using Rytov's method along with geometrical optics we derive the integral solutions for the variance and frequency spectrum of the log-amplitude fluctuations. In the case of Mariner 5 the occultation was a central one so that the transverse velocity of the line-of-sight path was in the radial direction. For this special case we find that the effect of the inhomogeneous background is to reduce the variance and narrow the frequency spectrum. Comparison with the Mariner 5 S-band data shows good agreement with the theoretical results.

## ANTENNAS

### URSI COMMISSION VI

Monday, October 20 0900

URSI Session VI-2, Radio Building 1107

Chairman: R.C. Hansen, R.C. Hansen, Inc.

2-1 DIELECTRIC RING LOADED DUAL-MODE CONICAL HORMS:  
M. S. Narasimhan, Department of Electrical Engineering, Indian Institute of Technology, Madras, India

Generation of the  $TE_{11}$  and  $TM_{11}$  modes by a conical dielectric ring of finite length inserted in a uniform conical horn has been studied analytically and experimentally. To start with an accurate analysis of spherical hybrid modes in a conical horn loaded uniformly with a loss-free conical dielectric ring has been carried out employing spherical wave functions and the eigen values of the spherical hybrid modes propagated within the dielectric and axial regions of the horn have been estimated. Accurate estimate of the eigenvalues associated with the spherical hybrid modes have been subsequently used to derive an expression for the mode conversion coefficient for a conical horn of arbitrary flare angle with a conical dielectric ring of finite length inserted in it. (The mode conversion coefficient (MCC) being defined as the ratio of the amplitude of the  $TM_{11}$  to  $TE_{11}$  mode, when the  $HE_{11}$  mode is decoupled into two discrete modes in the unloaded portion of the horn located away from the apex.) An accurate estimate of the MCC in terms of the horn-flare-angle, relative permittivity, and thickness of the dielectric wedge enables one to design a dual-mode conical horn exhibiting rotationally symmetric radiation patterns with suppressed side lobe levels. The MCC calculated through the analysis presented gives excellent agreement with experimental results obtained at X-Band.

2-2 ORTHOGONAL CAVITY-BACKED SLOT ANTENNAS ON A CURVED SURFACE: H. S. Hayre, Electrical Engineering Department, University of Houston, Houston, Texas; and Dean Cubley, SRB Consultants, Inc., Houston, Texas

One of the most significant problems encountered in the design of high performance aircraft is the achievement of adequate antenna pattern coverage due to the dual requirements of high temperature operation and flush mount-

ing. This paper will describe a novel approach in antenna design that has provided an adequate solution for antenna pattern coverage on F102, a high performance aircraft. It was required that near spherical antenna pattern coverage be provided in the frequency range 1650MHz to 1900MHz. The available mounting locations were limited to double curved surfaces of fairly small radii of curvature. The basic antenna element, selected to meet these requirements, was a tee-bar fed cavity-backed slot. In order to achieve broad coverage and circular polarization, two of these slots were orthogonally orientated and interconnected via a specially designed power divider. Due to physical space limitations a resonant dimension design was not possible and, therefore, a high temperature dielectric material was used to load each of the cavities. In the design for these antennas considerable difficulty was encountered due to the effects of the double curvature of the surrounding ground plane. The effects of the different as well as multiple radii of curvature are discussed in relation as to how the optimum design was achieved. Finally, the results of testing of the completed design are found to demonstrate very good performance characteristics as compared to more conventional antennas, while at the same time meeting the stringent environmental and mounting requirements.

2-3 A MOMENT METHOD TECHNIQUE FOR PROBE-FED CAVITY-BACKED SLOT ANTENNAS: Gary A. Thiele and Alan J. Fenn, The Ohio State University Electro-Science Laboratory, Columbus, Ohio

A technique is presented which permits the application of the method of moments to large cavity-backed slot antennas. Of specific interest are slot antennas operating over large bandwidths (e.g., 4:1) so that the aperture distribution cannot be assumed and must be determined according to the type of excitation employed and to a lesser extent by mutual coupling effects.

The technique employed to determine the aperture distribution of a cavity-backed slot involves the application of the electromagnetic form of Babinet's principle. The theory of images is used to remove the walls of the cavity resulting in two infinite arrays of dipoles behind the aperture plane which model the probe in the cavity. These two arrays are then the source of the incident field in calculating the generalized voltage matrix (V). The summation of the fields from the two arrays at the aperture is transformed to a rapidly converging series

by the application of Poisson's Sum Formula. The electric field distribution, or equivalently the magnetic surface current density, is expanded in a piecewise sinusoidal basis and the reaction integral equation is used to compute the elements of the generalized impedance matrix (Z). Solution of the matrix equation  $[Z](K)=(V)$  for the unknown magnetic currents (K) gives the electric field aperture distribution(s). Results will be shown for cavity-backed slots over a 4:1 frequency range that compare well with experimental data.

2-4 ANALYSIS OF A SLOT-MONPOLE ARRAY: A. B. Papierz, S. M. Sanzgiri, and Sharad R. Laxpati, Department of Information Engineering, University of Illinois at Chicago Circle, Chicago, Illinois

This work describes some analytical and numerical results for an excited slot in a ground plane with two parasitic monopoles mounted on either side of the slot. The experimental work carried out by Clavin, et al., (IEEE Trans. on Antennas and Propagation, vol. 22, July 1974, pp. 521-6) has demonstrated that such an antenna has identical E- and H-plane patterns, a desirable characteristic for a reflector feed and also for phased array applications. The equalization of the E- and H-plane patterns depends upon the coupling between the slot and the monopoles and their separation from the slot. The analysis carried out here is based on an equivalent three port network for the structure. Assuming sinusoidal electric and magnetic currents on the monopoles and slot respectively, the mutual coupling coefficients are evaluated using the induced e.m.f. method. A parametric study of the coupling between the slot and the monopole will be presented. The numerical results obtained for the radiation patterns are in close agreement with the experimental data. The paper will also present results and concerning the optimization of the slot-monopole geometry for synthesizing identical E- and H-plane patterns.

2-5 MULTIBEAM ANTENNA PATTERN SYNTHESIS THROUGH OPTIMIZATION TECHNIQUES: R. Mittra and L. Wilson Pearson, Department of Electrical Engineering, University of Illinois, Urbana, Illinois

The problem of pattern synthesis for multibeam antennas, particularly aperture antennas, is of current interest in the area of satellite communications. Such pattern synthesis is directed to selective area coverage on the

earth's surface for reasons of electromagnetic compatibility. This presentation reports the results of an investigation of the feasibility of applying optimization techniques to an objective function which is some norm of the error between the actual pattern and the desired pattern. The investigation was carried out in one spatial dimension, but can be directly extended to two-dimensional patterns. All pattern parameters, including aim, were taken as fixed and the amplitude and phase of the individual beams were modeled as perturbed sinc functions. Perturbations account for non-ideal aim, beam-spreading at the extremes of the reflector, and the effect of phase variation over the pattern. An overshoot phenomenon at discontinuities in the ideal pattern similar to the Gibb's phenomenon in a trigonometric Fourier series is observed when the error is measured by a mean squared norm. This phenomenon suggests the desirability of optimization in the minimax sense.

*minmax*

Norms :  $\frac{1}{2a} \int_{-a}^a e^2(u) du$       ]  
 or      ]  
 $\max_u e^2(u)$       ]  
 may eliminate  
 transition region  
 (discont) for start

$$\text{Norms : } \frac{1}{2a} \int_{-a}^a e^2(u) du$$

$$\text{or}$$

$$\max_u e^2(u)$$

2-6

## NEAR-FIELD ANTENNA COUPLING BY THE PLANE WAVE

SPECTRUM METHOD: Alexander C. Brown, Jr.,  
Atlantic Research Corporation, Alexandria, Virginia

The coupling equation (IEEE Trans. AP Mar. 1970) derived by W.K. Kahn and W. Wasylkiwskyj is practical for computing the near-field coupling between two arbitrary antennas. This equation is expressed in terms of the plane wave spectrum (PWS) of each antenna. Formally, integration over all wavenumber space is required. Practically, for all but supergain antennas, integration need be performed only over wavenumbers corresponding to visible space, as the contribution to the coupling due to integrating the PWS's over wavenumbers corresponding to invisible space is negligibly small for distances greater than a few wavelengths. For large antennas and for most near-field distances, integration can be performed over some smaller region in visible wavenumber space, as according to A. Brown, Jr. (URSI, June 1975), near fields are wavenumber bandwidth limited. The PWS coupling method is exact and is much faster than earlier exact coupling expressions based on fields computed directly from aperture fields. The PWS method requires only a double integration, whereas the earlier method requires a quadruple integration. Comparisons to published coupling data are presented.

2-7 THE ON-AXIS FIELD OF CIRCULAR APERTURE ANTENNAS:  
C.J. Chen, The BDM Corporation, Albuquerque, New Mexico

The knowledge of the power density on the axis of a circular aperture is useful in calculating the maximum safe distance from high power transmitters. Several attempts have been made to calculate the on-axis field by numerical integration or by approximate formulae. Here the exact formulae are presented. These formulae provide not only the means for the efficient and accurate computation of the on-axis field, but also the way to synthesize the far field from the on-axis field. The on-axis fields of a circular symmetric aperture antenna are formulated by the plane wave spectrum integration method. The integrations are performed analytically. The aperture distributions under investigation are (1) uniform, (2) parabolically tapered, and (3) higher order tapered. The distributions in case (3) are of the  $n$ th power of parabolically tapered distribution, where  $n = 2, 3, \dots$ . A recursion formula is given to express the on-axis field of the  $n$ th order tapered aperture in terms of that of the  $n-1$ th order tapered aperture. Since it is always possible to approximate any circularly symmetric aperture distribution by an even polynomial, the formulae presented here enable one to express the on-axis field of such aperture antennas analytically.

2-8 MANUAL FREQUENCY AND ANTENNA SELECTION OF HIGH FREQUENCY BROADCAST FACILITIES: George W. Haydon,  
Office of Telecommunications, Institute for Telecommunication Sciences, Boulder, Colorado

Modern high power multi-antenna high frequency broadcast facilities are becoming increasingly numerous. Computer facilities to assist in the frequency scheduling and antenna selection to optimize the operation of these installations are often not readily available. Recent experiences in the development of broadcast schedules and in antenna selection for the Kingdom of Saudi Arabia are described. The assumption is made that propagation via the F-region provides strong high quality signal levels. Frequency selection to optimize radiation at the vertical angle corresponding to F-region modes is the basis of the scheduling process. The adaption of CCIR materials permits graphical representations of optimum transmission time for each band allocated to high frequency broadcasting. This simple approach is discussed as a contrast to the sophisticated computer-based scheduling. The manual

method described differs from previous manual methods in that "Maximum Useful Frequency" (MUF) or "Optimum Traffic Frequency" (FOT) are not directly involved. The emphasis is on distance coverage along selected azimuth radials as a function of vertical radiation angle and operating frequency. Monitor reports attest to the success of the scheduling effort.

2-9 OTHER TRANSFORMS FOR OPTICAL INFORMATION PROCESSING:  
F. Paul Carlson, Department of Electrical Engineering,  
University of Washington, Seattle, Washington

Optical data processing has generally been limited to the use of Fourier transform concepts. This has followed quite naturally from the simple quadratic phase representation of a lens and simple reduction of the general Rayleigh-Sommerfeld integral equation describing the radiation fields to an easily recognizable form. However, if one examines the class of optical data processing models such as correlation, spectral transforms, ambiguity function, adaptive systems, averaging systems, or just convolutional systems, it is seen that the canonical integral equation is a Fredholm type of which the Rayleigh-Sommerfeld integral equation is a general descriptor. In a simple two-aperture radiating system such as one finds in optical processors, the Fourier transform quite naturally arises with the use of a lens or by observing the far field. This, however, should not limit the realization of other transforms of a Fredholm type, such as Abel, Radon, and Hilbert transforms. This is particularly true in cases where measurements are desired of medium temperature, density, and/or stress profiles; or when one wants to study network amplitude and phase relations or the real and imaginary parts of medium dielectric constants. It appears from our preliminary studies that Abel, Radon, and Hilbert optical transformers can be realized with conventional optical devices. Simple realizations will be described along with experiments involving simple test functions.

NOISE AND INTERFERENCE MEASUREMENTS

URSI COMMISSIONS VIII AND I

Monday, October 20 0900

URSI Session VIII-1, UMC Forum Room

Chairman: M.G. Arthur, National Bureau of Standards

1-1 A THEORETICAL AND EXPERIMENTAL INVESTIGATION OF THE NBS TEM CELL FOR USE IN EM EMISSIONS AND SUSCEPTIBILITY STUDIES: John C. Tippet and David C. Chang, Electromagnetics Laboratory, Department of Electrical Engineering, University of Colorado, Boulder, Colorado; and Myron L. Crawford, Electromagnetics Division, National Bureau of Standards, Boulder, Colorado

The capacitance and hence the characteristic impedance of a TEM cell are found analytically using the method of conformal transformation. In addition, approximate formulas are derived which exhibit the dimensions of the TEM cell explicitly, thus facilitating the design of a cell with given characteristic impedance. The electric field distribution of the TEM mode is derived and used to calculate the radiation resistance of both electric and magnetic dipoles located inside the cell. When the equipment-under-test (EUT) can be modeled by elementary dipoles, our analysis therefore allows one to predict the radiation characteristics of the same EUT in other environments by measuring the power radiated in the TEM cell. The characteristics of the TEM cell have been measured and are in close agreement with the theoretical predictions.

1-2 INTERFERENCE MEASUREMENT: Robert J. Matheson, Office of Telecommunications, Institute for Telecommunication Sciences, Boulder, Colorado

Many types of radiated signals may at one time or another be classed as "interference." In this paper, interference is defined as any energy received besides the desired signal. An extremely important part of the interference measurement process is the decision regarding what aspects of the interference should be measured. This point is illustrated with examples of several different techniques used to measure signals and noise of different types by the Radio Spectrum Measurement System (RSMS) van operated by the Office of Telecommunications (OT). The RSMS van contains a computer-controlled receiving system used for a broad range of measurements in support of a number of spectrum management problems.

One powerful measurement technique developed by OT personnel (called MSCAN) is described. MSCAN tunes rapidly across a band measuring which frequencies are in use, using signal processing to ignore interfering signals such as impulsive noise or radars. This technique also effectively increases the receiving system's sensitivity.

Broadband impulsive noise is a well-known type of interference. Since this type of interference is random in nature, the only reasonable measurements are in probabilistic terms. The measurements must be such that they can be used for the solutions of system design and analysis problems. The techniques used for the measurement of this type of interference are specified in detail.

1-3 C.C.I.R. STUDY GROUP 8 OPINION ON MAN-MADE NOISE:  
Neal H. Shepherd, General Electric Co., Lynchburg, Virginia

The C.C.I.R. has invited both the IEC and CISPR to suggest a method of measuring man-made noise that would be suitable for determining the degradation of performance to receivers used in the mobile services. In view of the urgent need expressed by Study Group 8, it seems appropriate that URSI should also be informed on this subject and be given an opportunity to participate. The IEC has prepared recommended methods of measuring the degradation of performance of mobile radio-receiving equipment due to man-made noise. The C.C.I.R. proposes to use the methods of measurement recommended by the IEC when suitable noise data are available to cover the various possible situations. A description of IEC's method of measurement will be given. Typical presentation of results showing application to FM, data, and AM receivers will be given.

1-4 ELECTROMAGNETIC INTERFERENCE MEASUREMENT PROGRAM  
AT THE NATIONAL BUREAU OF STANDARDS: John W. Adams,  
National Bureau of Standards, Electromagnetics  
Division, Boulder, Colorado

The need for better measurement techniques and instrumentation in the EMC field has long been recognized. Better measurements are the key to solving problems. They are also the key to providing an accurate, reliable data base that can be used in design, testing, etc.

There are several measurement areas in which work is under way. First, isotropic, near-field probes are needed to measure the electric and magnetic fields in the near-field regions, closest to sources, where field strengths are highest, and potentially most damaging. Far field data is scanty, and if extrapolated to near field, is dangerously misleading. Second, enclosures such as TEM cells must have expanded application, both for susceptibility measurements and for emission measurements. Third, better ways (e.g., statistical) must be developed to describe measured data. E- and H-fields vary widely with time, frequency, orientation, polarization, and location. Therefore, much care must be exercised in reporting results unambiguously, clearly, and without omitting these key variables. Terms, definitions and units, as well as format, must be carefully considered if results are to be useful rather than confusing. Specific ideas, techniques, and devices will be discussed; whether or not these user needs is a key item for discussion.

## AUDITORY EFFECTS

### URSI COMMISSION I (BIOLOGICAL EFFECTS)

Monday, October 20 0900

URSI Session B-1a, UMC East Ballroom

Organizer: The entire series on biological effects was organized by A.W. Guy, University of Washington

Chairman: A. H. Frey, Random Line Corporation

Bla-1 MICROWAVE HEARING IN MAMMALS AT 3.0 GHz: Charles A. Cain and William J. Rissmann, Department of Electrical Engineering, Bioacoustics Research Laboratory, University of Illinois, Urbana, Illinois

Several investigators have reported auditory evoked responses in mammals irradiated with pulse-modulated microwave energy. In addition, human subjects report hearing a distinct "click" when irradiated with individual pulses. The purpose of this research was to determine microwave "hearing" threshold parameters for different mammalian species irradiated with microwave pulses at 3.0 GHz. Threshold peak power density levels at different pulse widths were determined for the cat, dog, chinchilla, and a number of human subjects. Threshold levels for non-human species were determined by monitoring auditory evoked responses from the inferior colliculus of the brain or with simple scalp electrodes. All implanted electrodes were glass micropipettes filled with physiological saline. All evoked responses were processed by a computer of average transients program. Eight human subjects were given standard audiograms and microwave "hearing" threshold parameters were subsequently determined. For pulse widths less than 20  $\mu$ sec, the threshold energy density per pulse, averaged for all human subjects, was about 11  $\mu$ J/cm<sup>2</sup>. The threshold energy density per pulse, averaged for the smaller animals, was about 9  $\mu$ J/cm<sup>2</sup>. In addition to the above, an experiment involving two cats rigidly connected together at the skull by a lucite rod was conducted. One cat was irradiated with microwave pulses while the other cat, completely shielded from the incident radiation, was monitored for an auditory evoked response. Results of this experiment will be discussed.

Bla-2 A THEORETICAL STUDY OF MICROWAVE-GENERATED AUDITORY PHENOMENA IN MAMMALIAN CRANIAL STRUCTURES: James C. Lin and Chi-Kwan Lam, Department of Electrical Engineering, Wayne State University, Detroit, Michigan

While there is considerable evidence for the human ability to hear pulse-modulated microwave radiation, a number of questions remain regarding the mechanism responsible for this phenomenon. One explanation suggested by several investigators and which seems most likely is that the impinging microwave pulses produce heating as a result of energy absorption. A rapid thermal expansion of the biological material follows. The stress associated with thermal expansion launches an acoustic vibration which is detected by the inner ear. Until now, however, most theoretical investigations have centered on the one-dimensional problem characterized by a semi-infinite layer of tissue material and an exponential absorption profile. This paper presents a theoretical analysis of the stress and displacement generated by impinging microwave pulses in a spherical model of mammalian cranial structure. Assuming homogeneity of the brain matter, the absorbed energy pattern obtained from the electromagnetic wave equation is used as the source function for the equation of heat conduction in the spherical head. This displacement is found by solving the thermoelastic motion equation with stress free boundary conditions. The solution consists of two parts: a steady state term which is directly proportional to the width of the incident pulse and a transient term made up of an infinite sum of oscillating components. Numerical results will be given to indicate the magnitude of the induced stress and displacement as well as the applicability of the theory to the microwave auditory phenomenon.

Bla-3 MICROWAVE-INDUCED AUDITORY RESPONSE--COCHLEAR MICROPHONICS: C. K. Chou and A. W. Guy, Bio-electromagnetics Research Laboratory, Department of Rehabilitation Medicine, University of Washington School of Medicine, Seattle, Washington; and R. Galambos, Neurosciences Department, University of California, San Diego, La Jolla, California

Previous failures to observe microwave evoked cochlear microphonics (CM) in experimental animals exposed to

microwave pulses are probably due to: (1) the frequency of CM is higher than the frequency response of recording equipment; (2) the microwave energy is too low to elicit a detectable CM; and (3) the CM may be buried in a large microwave artifact. With the above problems avoided or minimized, an electrical potential oscillating at 50 kHz has been recorded from the round window of guinea pigs during irradiation with 918 MHz pulsed microwaves. This potential promptly follows the stimulus, outlasts it by about 200  $\mu$ sec, and measures up to 50  $\mu$ V in amplitude. The potential is time-locked to the onset of the microwave pulses. It precedes the auditory nerve response and disappears with death. Its intensity function versus microwave energy absorption density resembles that of the cochlear microphonics versus sound pressure level. It is reasonable to conclude that this potential is a cochlear microphonic response to the microwave pulses. This cochlear microphonic suggests that the microwave auditory effect is accompanied by a mechanical disturbance of the hair cells of the cochlea.

Bla-4      DISCRIMINATIVE CONTROL OF APPETITIVE BEHAVIOR  
BY PULSED MICROWAVE RADIATION IN RATS:  
R. B. Johnson, D. Myers, A. W. Guy and R. H.  
Lovely, Department Rehabilitation & Psychology,  
University of Washington, Seattle, Washington;  
and R. Galambos, Neurosciences Department,  
University of California, San Diego, La Jolla,  
California

Food deprived albino rats were trained in an anechoic chamber to make a nose-poking operant while restrained in a plexiglass rat holder. During daily 1-1/2-hour sessions, individual animals were presented alternating 5-min stimulus-on/stimulus-off periods during which food was made available as reward for responding only during stimulus-on periods. A response consisted of extending the nose forward and upward to break a light-beam photo cell arrangement. The original stimulus was an 7.5 kHz audible click produced by a high frequency tweeter driven by a 1 V, 3  $\mu$ sec duration square-wave pulse at the rate of 10 pps. Within 2 weeks, these animals learned to sufficiently inhibit responding such that 85-90% of a session's total responses were made during the appropriate stimulus-on periods. During one of the stimulus-off periods in which each animal was not responding, it was exposed for 30 sec to pulsed microwave radiation at the same pulse width and rate as the auditory stimulus and at field strength

< 5 mW/cm<sup>2</sup>. These animals showed definite "orienting responses" and began to respond during the presentation. During subsequent sessions in which microwaves, not the audible clicks, were present during the stimulus-on periods, all animals demonstrated a continued ability to respond at the 85-90% level. Although suggestive of an auditory component in the microwave control of this behavior, the demonstrations also indicate that stimulus control of appetitive behavior can indeed be obtained with pulsed microwaves. This is in contrast to reports that such control cannot be obtained with modulated microwave radiation. These findings also stand in contrast to, and suggest other possible interpretations of, recent reports of detection and avoidance of pulsed microwave radiation in rats.

Bla-5 RF SOUND: POSSIBLE MECHANISMS AS DEFINED BY  
RECENT RESEARCH: Edwin S. Eichert and  
Allan H. Frey, Randomline, Inc., Huntingdon  
Valley, Pennsylvania

The human auditory system response to low power density, pulse modulated, electromagnetic energy is one of the most compelling of the so-called "low-level" biological effects of UHF energy. It is the most easily and reliably replicated of the biological effects of low power density illumination; it may provide a new tool to investigate the human auditory system; and an understanding of the rf sound mechanism may provide new insight into the mechanism of the reported nervous system and behavioral effects.

Here we consider, in the light of recently obtained experimental data, mechanisms that have been proposed. In general, we find that previously proposed mechanisms are derived from model studies and are inconsistent with the recently obtained physiological and psychophysical data. We then consider several alternate possibilities that are consistent with the body of experimental data. For each, we discuss site specific physical phenomena which may explain the rf energy-biological tissue interaction, and we suggest experimentation which should provide an understanding of the rf sound mechanism.

MICROWAVE CATARACTOGENESIS  
URSI COMMISSION I (BIOLOGICAL EFFECTS)

Monday, October 20 1045

URSI Session B-1b, UMC East Ballroom

Chairman: S. Rosenthal,

Polytechnic Institute of New York

B1b-1 BIOLOGICAL THERMAL EFFECT OF MICROWAVE RADIATION  
ON HUMAN EYES: Kadry A. Al-Badwaihy and Abu-  
Bakr Youssef, Department of Electrical Engineering,  
Cairo University, Egypt

Thermal effects of microwave radiation are more dangerous on parts of the human body that are poorly cooled by blood and that may suffer malfunction or damage when overheated. The human eye is one of these parts. This paper considers a spherical model for the head irradiated by microwaves. The two eyes properly located in the head are also assumed spherical with the eye lens in its most probable place inside the eye. The electromagnetic transmission problem is first solved to find the fields in the eye and the heat diffusion equation is then solved in spherical coordinates inside the eye. A constant temperature gradient  $G_1$  is assumed on the cornea and the part of sclera exposed to air. Another temperature gradient  $G_2$  is assumed constant on the remaining part of the eye ball. The constant  $G_1$  accounts for cooling by aqueous humour, eye lid tears, and radiation, whereas  $G_2$  accounts for both metabolic heat generation and blood cooling by means of retinal arteries, and retinal, intrascleral, episcleral veins, etc. Body reaction in the form of increased blood circulation in blood capillaries to avoid such forced temperature rise can be accounted for by an increase in  $G_2$ . Temperature profiles are presented for different levels of the incident plane microwave and for varying degrees of body reactions. The capability of blood circulation to protect the eye lens from overheating is critically evaluated because such blood circulation is not close enough to the eye lens. Safe exposure long term microwave leakage levels are also calculated.

**B1b-2 EFFECTS OF 35 AND 107 GHZ CW MICROWAVES ON THE RABBIT EYE:** L. Birenbaum, Polytechnic Institute of New York, Brooklyn, New York; I. T. Kaplan, Zaret Foundation, CUNY, New York, New York; W. Metlay, Hofstra University, Hempstead, New York; S. W. Rosenthal, Polytechnic Institute of New York, Farmingdale, New York; and M. M. Zaret, Zaret Foundation, Scarsdale, New York

The eyes of anesthetized rabbits were irradiated with 35 and 107 GHz CW microwaves using a circular horn applicator. By this means, the nature of the threshold injury following a single exposure was defined, and the corresponding power levels and exposure times observed.

Effect on the corneal stroma, as seen by slit lamp, was found to be a valid indicator of threshold injury. Although 107 GHz power was more effective in producing immediate stromal damage, it was generally gone by the next day. On the other hand, 35 GHz effects were persistent, almost always present the next day, and associated with high levels of epithelial injury.

Our results were obtained using 56 animals at 35 GHz, 46 for the 107 GHz work, and 11 for sham exposures. Fluorescein staining was employed to detect epithelial damage. Power levels were principally 50 mW and below. Exposure times ranged from 15-80 minutes. The degree of stromal injury seen with the slit lamp was found to correlate well with the degree of derangement of the collagen fibers within the corneal layers, as seen with the electron microscope.

Threshold levels of power dissipated in the eye, measured in our closed-waveguide experiment, are used to estimate free-field planewave incidence thresholds for immediate injury following an acute exposure. Thresholds for chronic low level exposure cannot be deduced from our results but require additional work.

**B1b-3 MECHANISM OF MICROWAVE CATARACTOGENESIS IN RABBITS:** P. Kramar, C. Harris, A. W. Guy, and A. Emery, Bioelectromagnetics Research Laboratory, Department Rehabilitation Medicine, University of Washington School of Medicine, Seattle, Washington

Animal experiments using general hypothermia have shown that the production of heat is necessary for microwave

cataract formation following high level irradiation. These studies, however, have not ruled out the possible existence of a specific non-thermal factor at chronic low-level irradiations. Continuous low level irradiation of experimental animals may resolve this controversy, although this may involve several months to years of irradiation. Another method of investigating this problem is to raise the retrolental temperature to a level known to be associated with cataract formation ( $42^{\circ}\text{C}$  or above for at least 30 min) by means other than microwaves. If cataracts develop under conditions, heat itself is responsible for the lens damage. Rabbits were exposed to conditions of general hyperthermia and their retrolental temperatures maintained above  $42^{\circ}\text{C}$  for over 30 min. The animals were allowed to recover and their eyes examined periodically thereafter. To date no detectable lens abnormalities have been found. Differences and similarities between the two methods of elevating the retrolental temperature are presented.

Blb-4 THE EFFECT OF CATARACTOGENIC DOSES OF MICROWAVE RADIATION ON LENTICULAR TRANSPORT: James R. Rabinowitz, New York University Medical Center, Institute of Environmental Medicine, New York, New York

The acute irradiation conditions necessary to cause lenticular opacities in the rabbit have been established by studies in various laboratories. Recent studies have shown microscopic structural changes at power densities too low to cause opacities in the lens for single doses. These changes are probably the result of a series of biochemical processes. The observed effects depend on the specific metabolism and specialized function of lens tissue. The mechanism by which the absorption of microwave energy initiates these processes could serve as a model for the interaction of microwave radiation with other tissues and at other doses where the results are structurally less apparent. Cell membrane function is known to be non-linearly dependent on physical parameters. We have measured the influx of L-ascorbic acid (C-14 labelled) into unirradiated and irradiated (cataractogenic doses) rabbit lenses, removed, and cultured at various times after irradiation and found the rate of influx (1.2  $\mu\text{g}/\text{hr. lens}$ ) to be the same for irradiated and unirradiated pairs. Further, the rate of influx is too slow for transport to be responsible for the early decrease in the lenticular concentration of ascorbic

acid after microwave irradiation. We have also investigated, using similar procedures, the transport of 3-O-methyl D-glucose, a nonmetabolized D-glucose transport analog, and thymidine and find microwave radiation causes changes in the rate of influx. These changes, however, occur a significant time after irradiation. A discussion on the importance of looking at transport during irradiation will follow.

---

MONDAY AFTERNOON, OCT. 20 1330-1700

---

COMBINED SESSION

Monday, October 20 1330

UMC Center Ballroom

Organizer: J.R. Wait,

U.S. Department of Commerce

Chairman: J.M. Richardson, Office of  
Telecommunications

C-1 OPTICAL SCINTILLATIONS AND THEIR UTILITY FOR  
ATMOSPHERIC MEASUREMENTS: Robert S. Lawrence,  
Wave Propagation Laboratory, NOAA Research  
Laboratories, Boulder, Colorado

Refractive-index irregularities in the clear atmosphere, as well as those produced by precipitation, cause scintillations of a light wave. We shall describe how scintillations can be used to measure the refractive-index turbulence, the crosswind at various portions of the optical path, the rainfall rate, and the raindrop-size distribution. As path length increases, the optical phase-front irregularities increase without limit, while the amplitude (or irradiance) scintillations do not. Scintillations saturate and, when they do, their spatial statistics are modified. It is only recently that saturation has been well enough understood to permit quantitative prediction of its effect on optical-scintillation techniques for measuring wind. The corresponding effect on precipitation-caused scintillations is still under investigation.

C-2 A REVIEW OF REFLECTOR ANTENNA DEVELOPMENT: A. W. Love, Space Division, Rockwell International, Downey, California

Reflector antennas have been used since the radio pioneering era of Lodge, Hertz, and Marconi, but it took the exigent demands of radar in World War II to stimulate a real development in the reflector art. Subsequent interest in the science of radio astronomy and the inception of microwave ground communications links were responsible for a burgeoning growth in the field, so that in the 1940s and 1950s the design principles and requirements for prime focus fed systems were well established. Cassegrain, or secondary focus systems, and horn reflectors came into

## COMBINED SESSION

prominence in the early 1960s with the advent of satellite tracking and communications networks. The desire to maximize the gain, or the gain-temperature ratio, then led to development of sophisticated techniques for properly shaping the illumination over the reflector aperture in order to maximize efficiency and minimize spillover. At first the large radio astronomy dishes tended toward use of prime focus hybrid mode feeds, while the satellite tracking and communications networks leaned toward Cassegrain systems utilizing either the shaped sub-reflector technique and/or multimode feed horns. Now, in the 1970s, there is strong interest in large unfurlable space-borne antennas and in developing special techniques for creating shaped beams for maximum efficiency in total earth coverage from a satellite in circular orbit. Not all reflector antennas utilize paraboloidal surfaces. Some recent developments in line source feeds make the spherical reflector attractive for scanning applications and the conical reflector for deployable, space-borne antennas. The large 1000-foot diameter reflector at Arecibo is a well-known example of the former. Some interesting comparisons can be drawn among some of the larger reflector systems that have been built both for radio astronomy and for space communications.

### C-3 REFLECTIONS ON COMMUNICATIONS SATELLITE SYSTEMS: Pier L. Bargellini, COMSAT Laboratories, Clarksburg, Maryland

Active microwave repeaters carried by man-made satellites placed in geosynchronous equatorial orbit have been in existence for about eleven years. During this relatively short period of time, the technological advances in this field have been extraordinary. The use of satellites within a rapidly expanding network of terrestrial terminals has substantially contributed to increase the information capacity, speed, range, coverage, and reliability of electrical communications on a global scale. The two major characteristics of satellite systems are spectrum availability much greater than otherwise previously used or presently offered by competitive technologies (e.g., cables), and topological flexibility deriving from the multiple access which is an exclusive connotation of this form of communications. Following a review of the progress achieved until now, various foreseeable future technological developments will be discussed. These will satisfy the continued growth of the global systems carrying the two most frequently encountered forms of

## COMBINED SESSION

traffic, i.e., long distance telephone and television. They will also make it possible to offer new services effectively and economically. The growing importance of communications satellites for domestic and regional communications will be illustrated, as well as their role in forthcoming (maritime) or planned (aeronautical) applications.

**C-4 RETROSPECT AND PROSPECT: WILL THE NEXT 50 YEARS OF IONOSPHERIC SOUNDING BE AS FASCINATING AS THE LAST?: O. G. Villard, Jr., Stanford Research Institute, Menlo Park, California**

To some it may seem like only yesterday, but five decades have elapsed since Breit and Tuve made Kennelly and Heaviside's postulated overhead "layer" palpable by means of short radio-wave impulses. This work gave great impetus to a branch of physics which has pleasantly exercised generations of graduate students (and their professors) ever since. Unexpectedly, both the findings and technology thus spawned can be said to have led to practical applications far removed from the original field. In a light-hearted and bi-centennial mood, this paper calls these developments to mind and boldly attempts to extrapolate them into the future.

**C-5 PROSPECTS IN INTEGRATED OPTICS: J. H. Harris, National Science Foundation, Washington, D.C. (On leave from the University of Washington)**

Optical systems promise to provide an important cornerstone for the society of the future, principally through their role in communications, but also in other device applications. Realization of this promise requires the kind of physical control of optical waves that is presently available with lower frequency electromagnetic waves. Integrated optics offers the most apparent method for exercising this control. Within this broadly defined field lie many research opportunities that will lead to materials systems and waveguide designs that can provide efficient manipulation of optical signals. Problems associated with waveguide design are, of course, dependent on developments in materials and fabrication techniques which, in turn, are guided in part by progress in design. In this paper we will review aspects of some of the present and likely future waveguide design problems. These include the coupling problem for waveguide-to-fiber, inter-waveguide,

COMBINED SESSION

and laser-to-fiber coupling, laser cavity design, wave-guide branching techniques, and active component design.

C-6 A ROSE BY ANOTHER NAME IS A CABBAGE:  
Don R. Justesen, U.S.V.A. Hospital, Kansas City,  
Missouri

There are schizophrenia symptoms in the body scientific with respect to the attitudes of scientists, the media, and the public health practitioners toward the hazards of microwave radiation. It would appear that exposure of human beings to fields of high density is common, therapeutic, and viewed with sanguinity by professionals in some sectors, while in other sectors the suspicion that even weak fields are present raises the pejorative finger of anguish and alarm. The nominal, scientific, geopolitical, and parochial bases for this remarkable difference will be summarized as will the author's prognosis for future applications of microwave energy in medicine.

REMARKS ON THE REORGANIZATION OF URSI:  
F. S. Johnson, Chairman, USNC/URSI

---

TUESDAY MORNING, OCT. 21 0830-1200

---

SUB-SURFACE PROPAGATION AND COMMUNICATIONS

URSI COMMISSION II

Tuesday, October 21 0830

URSI Session II-2, UMC 159

Chairman: David Martin,

National Coal Board, United Kingdom

2-1 BASIC CONCEPTS AND LIMITATIONS OF LEAKY FEEDER SYSTEMS IN MINE COMMUNICATIONS:

J. R. Wait, U.S. Department of Commerce,  
Boulder, Colorado

In cooperation with the Pittsburgh Mine Safety and Research Center, we have undertaken to analyze various systems for point-to-point communication in coal mine environments. Of particular interest are coaxial structures that will support guided waves that "leak" energy to the immediate neighborhood of the cable. If such systems are to be properly employed in U.S. coal mines, it is essential that we understand the nature of the factors limiting their performance. For example, the close proximity of tunnel walls may rule out the use of the monofilar mode yet permit the exploitation of the bifilar mode. An attempt is made in this paper to identify the relative importance of the many design parameters that enter into the theoretical formulation of leaky feeder systems for intended use in mine environments. At the same time, for the benefit of our Office of Telecommunications, we call attention to the potential merit of these limited access systems to highway and railway communication and to many possibilities for short paths in urban surroundings.

2-2 EM FIELDS OF A COAXIAL CABLE WITH AN INTERRUPTED SHIELD LOCATED IN A CIRCULAR TUNNEL:

D. A. Hill, OT/ITS, U.S. Department of Commerce, Boulder, Colorado

One general method of long-distance communications in mine tunnels utilizes a leaky feeder cable which supports a mode of low attenuation and also provides continuous access to the signal. The specific type of leaky feeder which is considered here is a coaxial

cable with a series of circumferential gaps in the shield. An integral equation for the electric field in a single gap is derived for an arbitrary cable location in a circular tunnel with imperfectly conducting walls. The integral equation is solved by a quasi-static method, and the resultant solution for the electric field in the gap is used to calculate various quantities of interest. Of particular importance is the coupling efficiency between the TEM mode in the cable and the dominant (monofilar) mode in the tunnel. Numerical results are presented for various frequencies and for various separation distances between the cable and the tunnel wall.

2-3 CALCULATED CHANNEL CHARACTERISTICS OF A BRAIDED COAXIAL CABLE IN A MINE TUNNEL: S. F. Mahmoud, Electrical Engineering Department, Cairo University, Giza, Egypt; and J. R. Wait, Cooperative Institute for Research in Environmental Sciences, University of Colorado, Boulder, Colorado

The braided coaxial cable is studied as a communication scheme in a mine tunnel. A simplified rectangular waveguide model is adopted for the tunnel and the shield of the cable is assumed to behave as a single inductive transfer impedance. Specific results on the attenuation of the monofilar and bifilar (or coaxial) modes of propagation, taking into account the possible existence of a thin lossy film on the cable, are presented. In order to estimate the maximum possible range of communication, we consider the coupling factors of these modes to transmitting and receiving dipoles inside the tunnel and present results on these factors for various cable parameters and over a wide range of frequencies.

2-4 THEORY OF THE PROPAGATION OF LOW AND MEDIUM FREQUENCY RADIO WAVES IN A COAL SEAM: Alfred G. Emslie and Robert L. Lagace, Arthur D. Little, Inc., Cambridge, Massachusetts

A theoretical model has been developed to explain the unexpectedly long communication ranges and marked polarization effects measured by the Collins Radio Group in a coal mine at low and medium frequencies. The model is based on a cylindrical TEM mode of propagation in a low-conductivity horizontal coal seam embedded in high-conductivity rock, with E vertical and H horizontal. For small loop antennas this mode is most efficiently

launched and received when the planes of the loops are oriented so they lie in a common vertical plane, which agrees with the optimum orientation found experimentally. The best overall fit to the experimental attenuation data for this case, over the frequency range 57.5 to 920 kHz, is found for coal and rock conductivities of  $1.4 \times 10^{-4}$  Mho/m and 1.0 Mho/m, respectively, for an assumed coal dielectric constant of 7. These conductivity values are reasonable for the soft bituminous coal and the layers of shale found in the mine. A better fit to the data at the lower frequencies would be obtained if, in the model, the high-conductivity rock extended only a short distance above and below the coal seam instead of to infinity. If the coal conductivity is changed from  $1.4 \times 10^{-4}$  Mho/m to the higher value of  $1.0 \times 10^{-2}$  Mho/m expected in some mines, the attenuation is markedly increased.

## 2-5 THE SUBMARINE-TOWED ELF LOOP ANTENNA:

Michael Burrows, Lincoln Laboratory, M.I.T.,  
Lexington, Massachusetts

The noise generated by a submarine towed ELF loop antenna is more severe and more complicated than that generated by the electrode pair antenna. However, both antenna types must be used in combination if reception is to be maintained over all submarine headings. The talk summarizes the results of several years of work aimed at elucidating the noise mechanisms of the towed loop antenna and developing a less noisy antenna design. The results have been (i) the creation of quantitative mathematical models of the noise sources, including two distinct types of vibration induced noise, and the subsequent identification of a number of noise suppression techniques ("On the Design of a Towed ELF H-Field Antenna,"); (ii) obtaining a gratifyingly low noise, in agreement with the theoretical predictions, when an antenna incorporating these techniques was tested at sea ("The Lincoln Submarine Towed ELF Loop Antenna,"); and (iii) the construction of various laboratory test facilities, the most notable being an antenna towing simulator in the form of a shielded water-flow tunnel ("Performance of the ELF Antenna Water Flow Tunnel,"). The design feature of particular significance for reducing the noise turns out to be the shape of the antenna's sensitivity profile, i.e., the distribution of signal sensitivity along the antenna length.

2-6 BOREHOLE MEASUREMENTS OF CONDUCTIVITY AND  
DIELECTRIC CONSTANT IN THE 300 kHz: R. N. Grubb,  
P. L. Orswell, and J. H. Taylor, National Oceanic  
and Atmospheric Administration, Environmental  
Research Laboratories, Space Environment Laboratory,  
Boulder, Colorado

Two borehole instrumentation systems for the measurement of complex propagation constant in the frequency range 300 kHz and 30 MHz are described. The first system measures the ratio of the signals coupled to two identical receivers in separate boreholes at different ranges from an isolated transmitter in a third borehole. The second system operates in a single borehole by measuring the mutual impedance between two magnetic dipoles aligned parallel to the borehole. This system has an automatic digital data acquisition system based on a programmable calculator which reduces the data to conductivity and dielectric constant versus frequency. Examples of data measured by the systems in actual boreholes will be presented.

RADIO OCEANOGRAPHY SEASAT "A"

URSI COMMISSION II

Tuesday, October 21 0830

URSI Session II-3, UMC Forum Room

Organizer and Chairman: C.T. Swift,  
NASA Langley Research Center

3-1 SEASAT "A": A USER ORIENTED SYSTEMS DESIGN:  
Samuel W. McCandless

The SEASAT program is a space-based operational oceanographic measurement system, which will be capable of providing continuous, all-weather, worldwide, timely data on global ocean dynamics and other physical properties of practical importance to wide community of governmental and private sector users. Program objectives include the demonstration of a capability to measure global ocean dynamics and physical characteristics to include the directional wind field, wave spectra, and temperature of the sea surface and to measure sea surface roughness topography and geoidal height. All of these measurements will be accomplished with an accuracy and coverage not possible using other methods. In addition, SEASAT-A will demonstrate features of a prototype operational ocean dynamics monitoring system, and will demonstrate and define the economic and social benefits to be added by such a monitoring system to user organization products and services.

SEASAT-A is an outgrowth of a diversity of scientific and technology work conducted by NASA, the Department of Defense, the Department of Commerce, and several other institutions in both the measurement of the required physical quantities and the implementation of the appropriate sensors on spacecraft and on the ground.

The SEASAT-A project is described in terms of the definition of sensors employed to make the required ocean physics and dynamics measurements, the design requirements of the satellite system, and the end-to-end data system conceived to return the data from the sensors to the SEASAT-A user community. The demonstration role of SEASAT-A, its goals, and objectives are reflected in the mission requirements, the satellite design performance capabilities, and the ground system required to run the mission and supply the data in the correct form.

3-2 SEASAT-A USER AND INTERAGENCY COORDINATION: John R. Apel, National Oceanic and Atmospheric Administration, Miami, Florida

The measurements of geophysical quantities to be made by the SEASAT-A instrument complement have largely been established by potential users of the data. At the inception of the program, NASA solicited opinion from members of the governmental oceanographic community in terms of both measurement requirements and methods of implementing them. At a later date, an informal users' working group was established to provide continuing guidance and, as necessary, support to the program. This group has since been chartered as a formal subcommittee of the NASA Applications Advisory Committee. Funding for pre- and post-launch participation by users in the SEASAT-A program has been planned by NOAA, Navy, and NSF, with coordinated announcements of opportunity to be issued as a means of enlarging the community of investigators; the disciplines involved are not only oceanography but meteorology, climatology, glaciology, and geodesy.

3-3 SEASAT-A SPACECRAFT AND MISSION DESIGN:  
James A. Dunne, Jet Propulsion Laboratory,  
Pasadena, California

The SEASAT-A spacecraft will be designed, built, and tested by a spacecraft system contractor under the direction of the Jet Propulsion Laboratory. Microwave sensors will be provided by the Langley Research Center (wind field scatterometer), the Wallops Flight Center/ Applied Physics Laboratory, the Johns Hopkins University (altimeter), the Jet Propulsion Laboratory (synthetic aperture radar and scanning multichannel microwave radiometer), and the Goddard Space Flight Center (visual and infrared radiometer). The spacecraft will be launched into a non sun-synchronous, high inclination orbit during calendar 1978. Principal mission design emphasis is on close coordination of spacecraft data collection activities with on-going major oceanographic programs including NOAA Project Stormfury and the First Global GARP Experiment. Primary flight objectives will be the validation of the performance of the microwave sensors in terms of geophysical parameters and the demonstration of certain critical characteristics of an eventual operational oceanographic satellite system. It is presently anticipated that the latter objective will be achieved by close coordination with user agency activities including principally DOD's Fleet Numerical

Weather Central in Monterey, California, and NOAA's National Environmental Satellite Service, National Weather Service, and Environmental Data Service.

3-4 A DESCRIPTION OF THE SEASAT-A RADAR ALTIMETER:  
W. F. Townsend, NASA Wallops Flight Center,  
Wallops Island, Virginia

A radar altimeter having an altitude resolution of 10 cm RMS or less over a range of significant wave heights of 1 to 20 meters is slated to fly onboard the SEASAT-A spacecraft in 1978. The technical approach employed in the design of this system is described in detail. Particular attention is given to implementation of full deramp STRETCH to avoid high speed video processing, generation of a 360 MHz bandwidth linear FM pulse to effectively provide a 3 nsec pulse width, and utilization of an adaptive range tracker to improve range resolution and provide real time estimations of significant wave height. Performance expectations for the resulting system are also discussed.

3-5 AN OPERATIONAL SATELLITE SCATTEROMETER FOR WIND VECTOR MEASUREMENTS OVER THE OCEAN: W.L. Grantham, E.M. Bracalente, W.L. Jones, J.H. Schrader, and L.C. Schroeder, Langley Research Center, Hampton, Virginia; and J.L. Mitchell, LTV, Hampton, Virginia

This paper describes performance requirements and design characteristics of a microwave scatterometer wind sensor for measuring surface winds over the oceans on a global basis. A brief review of microwave scatterometer aircraft and satellite measurements on the ocean is included, showing the sensitivity of this instrument as a remote wind sensor. This wind sensor will be used on the SEASAT-A satellite along with several other remote sensors: a radar altimeter, an imaging radar, and an optical radiometer. Together, this complement of instruments will provide the SEASAT-A user community with scientific and operational type data in the areas of oceanography, meteorology, and geodesy.

The scatterometer specifications are developed from user requirements of wind vector measurement range and accuracy, swath width, resolution cell size, and measurement grid spacing. The manner of transforming wind speed accuracy into instrument accuracy requirements is described in detail. Since the scatterometer is sensitive to both

wind direction and wind speed, special techniques are developed to determine both parameters.

From several options available, the fan beam scatterometer design has been chosen by the SEASAT-A study teams as the one most suitable when considering attitude control, spacecraft interface problems, and performance characteristics. An analysis is performed for a baseline scatterometer design. The analysis includes derivation of the instrument design and its performance capabilities for meeting the SEASAT-A user requirements. Various modes of operation are discussed which will allow the resolution of questions concerning the effects of sea state on the scatterometer wind sensing ability and to verify design boundaries of the instrument.

**3-6 SEASAT-A SYNTHETIC APERTURE RADAR EQUIPMENT:**

W. E. Brown, Jr., Jet Propulsion Laboratory,  
California Institute of Technology, Pasadena,  
California

Currently in the planning and early stages of development is a synthetic aperture radar experiment for the proposed SEASAT-A spacecraft. The purpose of the experiment is to determine the feasibility of monitoring the ocean surface patterns and Arctic ice behavior from an orbiting spacecraft. The experiment presently consists of an L-band radar with solid state transmitter (peak power 800 to 1500 watts), an antenna 10 to 14 meters long by 2 meters wide, a downlink for real time transmission of data, ground data storage, an optical correlator, and preliminary plans to convert the imagery to directional wave spectra, observe currents, and internal wave effects. The resolution is expected to be about 25 by 25 meters and the swath width goal is 100 km or 16 to 24 degrees off-nadir. The nominal parameters of the spacecraft orbit are attitude 800 km, inclination 108 degrees, eccentricity 0.003, and velocity 7450 meters/second.

**3-7 THE SCANNING MULTICHANNEL MICROWAVE RADIOMETER:**

F. T. Barath, California Institute of Technology,  
Jet Propulsion Laboratory, Pasadena, California;  
and P. Gloersen, Goddard Space Flight Center,  
Greenbelt, Maryland

The Scanning Multichannel Microwave Radiometer (SMMR) is being developed for inclusion in both the Nimbus G. and SEASAT-A Spacecraft payloads. The instrument measures microwave radiation in two orthogonal linear polariza-

tions at the wavelengths of 4.5 cm (6.60 GHz), 2.8 cm (10.69 GHz), 1.7 cm (18.00 GHz), 1.4 cm (21.00 GHz), and 8 mm (37.00 GHz). The instrument antenna performs a conical scan at an angle of 42 degrees with respect to the local vertical yielding an incidence angle of 50 degrees on the earth. The scan extent is  $\pm$  25 degrees with respect to the spacecraft orbit plane thus covering a swath width of approximately 650 km. The resolution on the ground, determined by the 80 cm projected antenna aperture and the orbit, ranges from 14 x 22 km to 80 x 122 km and the sensitivity is expected to range from 0.6 to 1.7 K per resolution cell, depending on the wavelength. For SEASAT, the output data will be principally used for all-weather sea surface temperature, surface wind, and atmospheric water content determination; the latter information will also be used to correct the results of the altimeter and scatterometer instruments.

3-8 SEASAT AIRCRAFT TEST PROGRAM: Thomas W. Thompson,  
Jet Propulsion Laboratory, Pasadena, California

The NASA SEASAT Program (Earth and Ocean Dynamics Program, Office of Applications) is planning an aircraft test program to support the satellite SEASAT-A which is scheduled for launch in 1978. This aircraft test program will continue NASA's participation in oceanographic research programs building upon past work such as the joint NASA-NOAA aircraft and SKYLAB observations of hurricane Ava, participation in JONSWAP-II with the NASA Wallop's C-54, participation in GATE with the NASA Ames CV-990, and joint NASA-NOAA observations of fetch limited wave build up in NOAA's Winter-Storm Program, in 1975. For the next four years, there will be more aircraft flights of radar altimeters, radar scatterometers, imaging radars, visible and infrared scanners, and microwave radiometers emphasizing measurement of significant wave height, surface wind speed and direction, wave spectra, sea ice coverage, and sea-surface temperature. Participation in ongoing oceanographic programs is an important part of this aircraft test program. Potential users of SEASAT-A satellite data will have data which will be useful for their own programs. Two or three aircraft expeditions of one month duration or longer will be run every year until SEASAT-A's launch in 1978. Then in 1978 and 1979, a fulltime aircraft program will provide surface truth during mission operations. Participation in

URSI Session II-3

these aircraft tests will be welcomed. Open planning sessions for these aircraft tests will be held in conjunction with the SEASAT Science Steering Group, which meets regularly to advise NASA on the SEASAT experiments and application.

## IONOSPHERIC RADIO SCINTILLATIONS - II

### URSI COMMISSION III

Tuesday, October 21 0830

URSI Session III-2, UMC 157

Chairman: W. F. Utzaut, OT/ITS

2-1 THE SEASONAL PATTERN OF HIGH LATITUDE F-LAYER IRREGULARITIES: Jules Aarons and Gerald S. Hawkins, AFCLR, Hanscom AFB, Massachusetts, and Eileen Martin, Emmanuel College, Boston, Massachusetts

Amplitude fluctuations of VHF signals from geostationary satellites give a measure of the extent and occurrence of F-region irregularities. Fluctuations in the ATS-3 136 MHz signal from 1968 to 1974 were converted to scintillation index (SI) for three stations at sub-ionospheric path intersection invariant latitudes of  $63^{\circ}$ ,  $60^{\circ}$ , and  $53^{\circ}$ . Seasonal contour plots of SI were prepared on a UT-monthly grid for conditions of low and high geomagnetic activity ( $K_p = 0-3$  and  $K_p = 4-9$ ). At the latitude of  $63^{\circ}$  diurnal values increase about 20 units in SI from low to high  $K_p$ . There is a pronounced annual variation with a maximum in April-June; time of maximum for  $K_p = 0-3$  is  $\sim 2$  hours before magnetic midnight. At  $60^{\circ}$  the higher latitude diurnal pattern is repeated for low  $K_p$  with a post midnight maximum and an increase of 20 SI units for high  $K_p$ . At the lowest latitude ( $53^{\circ}$ ), the irregularities in the mean are confined to the hours of darkness; the maximum is from 1-3 hours after midnight. Minimum activity occurs between May-August. For the two higher latitudes the winter data shows only a weak diurnal pattern for  $K_p = 0-3$ . At all latitudes there is a pronounced delay in the onset of irregularities at sunset at the winter solstice. The implication of these results is discussed with reference to the solar terrestrial magnetospheric interaction.

2-2 IONOSPHERIC SCINTILLATIONS AT SHF: Luke K. McSherry, Headquarters, USASATCOM Agency, Fort Monmouth, New Jersey

Ionospheric scintillations refer to amplitude and phase variations of high frequency radio signals transmitted through the ionosphere from outside the earth. Two common signal sources are cosmic noise from outer-space on which scintillations operate and radio signals from

2-6 A FADE-RESISTANT MODEM FOR USE IN A UHF SATELLITE COMMUNICATIONS LINK DISTURBED BY IONOSPHERIC SCINTILLATION FADING: James J. Foshee, Electronic Communications, Inc., A Subsidiary of the NCR Corporation, Dayton, Ohio

Fading due to ionospheric scintillation can seriously effect the reliability of a UHF satellite communications system operating with mobile terminals such as aircraft. Due to the structure of this type of fading and the normal operating margin of the airborne mobile terminal the traditional techniques of improving link performance such as the various types of diversity normally fail to provide any substantial improvement in link reliability. This paper contains a description of a scheme which could be used to improve the reliability in such a communications system. The tradeoffs involved in implementing such a scheme are also discussed. This scheme would not rely on a continuously reliable received signal but would utilize error-correction codes with interleaving. The interleaving would tend to spread the "burst" errors so that the power of the decoder could be used to correct the errors. The scheme would utilize a modulation technique which is comparatively efficient and has essentially no acquisition time. Since a perfect bit-timing is critical to system performance, a technique for extracting a perfect bit-timing from the decision-element in the demodulator is discussed. This scheme is presently being implemented into a unit called the Fade-Resistant Modem and an engineering model should be ready by late 1975 or early 1976.

PLASMA INSTABILITIES IN THE MAGNETOSPHERE - I

URSI COMMISSION IV

Tuesday, October 21 0830

URSI Session IV-2, UMC 158

Chairman: E.G. Fontheim, University of Michigan

2-1 REPORT ON PLASMA INSTABILITIES AT GRENOBLE MEETING:  
E.G. Fontheim, University of Michigan, Ann Arbor,  
Michigan

2-2 SOME EFFECTS OF MAGNETOSPHERIC WAVE PARTICLE  
INTERACTIONS: D. J. Williams, Space Environment  
Laboratory, NOAA, ERL, Boulder, Colorado

Using observations from the Explorer 45 satellite, we will present observations and results pertaining to wave particle interactions occurring in the magnetospheric hot plasma. These and similar results are not only valuable in their own right, but can be used in possible direct tests of theories and hypotheses concerned with the behavior of other remote naturally occurring plasmas such as the solar corona, planetary magnetospheres and ionospheres, pulsars, and the interstellar and intergalactic media. We shall begin with a discussion of protons during geomagnetic storms and briefly present considerations of energy densities, hot-cold plasma interactions, stable and turbulent regions, and SAR ARC generation. If time permits, we will present the behavior of the energetic electron population during quiet and storm times, along with a discussion of the mechanisms responsible for the quiet time and post ejection recovery behavior.

2-3 OBSERVATIONS OF RING CURRENT PROTONS AND THEIR IM-  
PLICATIONS CONCERNING WAVE-PARTICLE INTERACTIONS:  
L. R. Lyons, Space Environment Laboratory, NOAA,  
ERL, Boulder, Colorado

Explorer 45 observations of trapped protons obtained near the geomagnetic equator within  $5.24 R_E$  are used to investigate storm-associated loss processes for ring current protons. Using simultaneous proton and magnetic field observations, it is found that large flux decreases during a storm at energies  $\geq 200$  keV result simply from adiabatic deceleration in response to the stormtime magnetic field decrease. It does not appear necessary to include wave particle interactions in order to explain the apparent loss of these protons. Observations of pitch angle dis-

tributions as a function of particle energy and radial distance during a storm recovery phase show detailed structure which strongly suggests that pitch angle diffusion in the plasmapause region is dominated by resonant interactions with ion-cyclotron waves. Calculations of ion-cyclotron wave growth rates, using the measured proton energy spectra and pitch angle distributions, indicate that ion-cyclotron waves can be significantly amplified by ring current protons in the plasmapause region. However, the effects of wave growth occurring off the equator must be considered to explain the observed time evolution of the proton distributions.

2-4 PLASMA INSTABILITIES OBSERVED IN A LABORATORY  
SIMULATION OF ELECTRON BEAMS IN THE MAGNETOSPHERE:  
H. Leinbach, Space Environment Laboratory, NOAA,  
Boulder, Colorado

Electric field emissions at frequencies of  $(n + \frac{1}{2}) f_{ce}$  have been generated in a large-scale electron beam experiment in NASA's giant vacuum facility in Sandusky, Ohio. These emissions arise when a field-aligned, contra-streaming beam configuration exists, the primary beam consisting of monoenergetic electrons (50 eV to 5 keV), the other beam of lower energy, backscattered secondary electrons. It is suggested that this same mechanism could also be a source of  $3/2 f_{ce}$  emissions at auroral latitudes. There, the field-aligned precipitation which sometimes occurs may interact with the atmospherically backscattered electrons, which are collimated into a beam by the diverging magnetic field. In the absence of the beam-beam instability, weak oscillations at the plasma frequency were observed in the laboratory. In this case, no significant modification of the primary beam velocity distribution occurred and the beam configuration over a distance (20m) corresponding to 1 to 2 gyro-periods is adequately described by single particle motion in the ambient magnetic field.

2-5 HYDROMAGNETIC INSTABILITIES AND EXCITATION OF  
KINETIC ALFVEN WAVES: Akira Hasegawa, Bell  
Laboratories, Murray Hill, New Jersey

Most of the hydromagnetic wave instabilities associated with the coordinate space non-equilibrium excite hydromagnetic surface waves. It can generally be shown that this surface wave dissipates its energy by the linear mode conversion to the kinetic Alfvén wave

(Alfven wave with finite Larmor radius and electron inertia correction) which propagates across the magnetic field. This previously unknown process should present various interesting linear and nonlinear effects in the magnetosphere, which will be discussed in the talk.

2-6 RECENT RESULTS FROM THE WAVE-INJECTION EXPERIMENT AT SIPLE STATION, ANTARCTICA: R. A. Helliwell and J. P. Katsufakis, Radioscience Laboratory, Stanford University, Stanford, California

Recent wave injection experiments using the Siple Station VLF transmitter have produced the following new results:

- (1) Temporal growth (up to 30 db) of a freshly injected pulse is reduced by the presence of an echo of a preceding pulse. A suggested explanation is that the echo broadens the spectrum of the total input wave thereby reducing the efficiency of phase bunching.
- (2) Natural magnetospheric noise is sometimes suppressed by amplified Siple signals. Reductions of the noise by as much as 6 db are observed in a band 50-200 Hz wide situated just below the transmitter frequency. This surprising effect is not understood, but might be caused by a reduction in electron flux that in turn resulted from pitch angle scattering by the Siple signal and its associated emissions.
- (3) Wave growth and triggering are independent of  $df/dt$  for  $|df/dt| < 2$  kHz/s, giving support to a recently proposed feedback model of narrowband wave generation.
- (4) Simultaneous injection of several spectral components (generated by FSK modulation of the carrier) shows that each grows independently of the other when they are spaced more than 30 Hz apart. This result also supports the model.

2-7 NONLINEAR WHISTLER PROPAGATION EXPERIMENTS: R. W. Fredricks and R. L. Stenzel, TRW Systems Group Research Staff, Redondo Beach, California

Recent laboratory experiments have been performed in the TRW Large Magnetized Plasma Source (LAMPS) in which electric dipole and magnetic loop antennas have produced righthand polarized (whistler) mode waves of both small and large amplitude. The LAMPS device is many whistler wavelengths in dimension, thus

wall effects are negligible. It has been found that both electric dipoles and magnetic loops when driven above a critical power level will produce self-ducted r.h. waves confined within an approximately cylindrical flux tube of radial dimension comparable to the parallel whistler wavelength  $\lambda_{||}$ . This effect is density-dependent, occurring more easily as  $\omega_p/\omega_c$  becomes large compared to unity, and for wave frequencies in the range  $0.16 < \omega/\omega_c < 1$ . Resonance cone structures are found at low densities, i.e.,  $\omega_p/\omega_c \lesssim 5-10$ , but these tend to disappear as  $\omega_p/\omega_c > 10$ . The nonlinear plasma effects causing self-ducting of large amplitude waves in the narrow beams observed are not yet understood, but some evidence for self-focusing and phase-bunching of electrons exists in the experimental data. Possible applications to the ionosphere and magnetosphere will be discussed.

2-8 DISTRIBUTION OF ELF CHORUS WITH LOCAL TIME, LATITUDE, AND MAGNETIC ACTIVITY: B. T. Tsurutani, E. J. Smith, and J. D. Mannan, Jet Propulsion Laboratory, Pasadena, California

A systematic statistical study of outer zone ELF chorus ( $f < 10^3$  Hz) has been undertaken using search coil magnetometer data from the entire first year of OGO-5. Positive identification of chorus was assured using real-time spectrum analysis of the signals thereby preventing potential contamination by plasmaspheric hiss or exohiss. The properties of the chorus such as peak power, frequency at the peak, bandwidth, and resultant wave amplitude were determined. This information was merged with geomagnetic indices such as  $K_p$  and  $AE$  onto a single magnetic tape containing OGO-5 trajectory parameters and a multi-parameter analysis was carried out. The peaks in the amplitude, power spectral density, and rate-of-occurrence of chorus were located in two distinct regions: a postmidnight region at 00-02h local time (L.T.) and a more intense region at 06-10 L.T. The latter is characterized by an abrupt onset at dawn. Signal intensity and occurrence rates decrease between 1000h and 1600h L.T. after which little or no chorus is detected. In the midnight to dawn sector, chorus occurs primarily within  $15^\circ$  of the magnetic equator, presumably due to local generation by the cyclotron loss cone instability. From dawn to 16h L.T., chorus occurrence is again found near the equator and is also commonly observed in a second region at high latitude. Although this high altitude region

may extend into the ionosphere, this cannot be determined due to the limitations of the satellite orbit. Principle axis analyses determining wave propagation properties near the magnetic equator and at high latitudes have been carried out. These results give additional information about the source and propagation of these high latitude emissions.

2-9 POLARIZATION AND DIRECTION OF PROPAGATION OF PLASMASPERIC HISS: E. J. Smith and B. T. Tsurutani, Jet Propulsion Laboratory, Pasadena, California; and R. M. Thorne, University of California, Los Angeles, California

Plasmaspheric Hiss is a naturally-occurring Extremely-Low-Frequency ( $f < 10^3$ Hz) emission which is essentially restricted to the plasmasphere. At high altitudes, hiss is observed at essentially all local times and latitudes. At low altitudes, however, hiss is principally a dayside phenomenon restricted to local times between 06 and 18h. Hiss is apparently generated by a cyclotron resonance with trapped electrons having energies of ~ 30 kev. It appears to be the dominant loss mechanism limiting the flux of trapped electrons in this energy range in that portion of the outer zone within the plasmasphere. Hiss can propagate into the inner radiation zone where it can resonate with relativistic electrons causing their precipitation. A complete survey of plasmaspheric hiss has been carried out at both high and low altitudes using the OGO-5 and OGO-6 search coil magnetometer data. Triaxial analog waveforms with frequency components up to  $10^3$ Hz are available from both missions. Waveforms obtained throughout the plasmasphere have been digitized and subjected to a variance analysis to determine the direction of the wave normals. The sense of polarization, ellipticity, and direction-of-propagation of the hiss relative to the ambient magnetic field at various locations will be reported.

MILLIMETER WAVELENGTH TECHNIQUES

URSI COMMISSION V

Tuesday, October 21 0830

URSI Session V-2, UMC 156

Chairman: M. Gordon, NRAO

2-1 CONSIDERATIONS FOR A MILLIMETER-WAVE SITE:

M. A. Gordon, B. E. Turner, and C.M. Wade,  
NRAO, Green Bank, West Virginia

The choice of a suitable site for a millimeter-wave telescope depends primarily on the specific objectives of the observatory. We discuss several locations in terms of water vapor, latitude, and access, with special consideration for the needs of NRAO's proposed 25m telescope.

2-2 THE HAT CREEK MILLIMETER WAVE INTERFEROMETER:

J. Dreher, R. Forster, W. Hoffman, D.D. Thornton,  
M.C.H. Wright, and W.J. Welch, Radio Astronomy  
Laboratory, University of California, Berkeley,  
California

An interferometer which can operate in the wavelength range 1-15 mm has begun operation at the Hat Creek Observatory. The instrument consists of two 20-foot antennas which can be located at various stations along a T-shaped track. Mapping resolution at 1 mm is better than 1 arc second. One antenna has been used at 2.6 mm and 1.3 mm. Synthesis observations are currently in progress at 13 mm both for line and continuum.

2-3 MILLIMETER-WAVELENGTH PERFORMANCE AND PROPOSED IMPROVEMENTS AT HAYSTACK OBSERVATORY: M. L. Meeks,  
NEROC Haystack Observatory, Westford, Massachusetts

The present performance of the Haystack antenna, a 36.6-meter paraboloidal reflector enclosed in a radome, has been measured at a frequency of 43 GHz by observing bright sources of SiO emission and continuum emission from Venus. We have mapped the antenna pattern and measured the aperture efficiency at various elevation angles and with various temperature gradients over the reflector surface and backup structure. We find that thermal conditions can be improved by blowing outside air into the radome cavity and by circulating the air inside the radome. The excellent structural stability of the Haystack antenna and its performance at 7-mm wavelength justify improvement in the system to permit regular operation at least as high

as 50 GHz and to improve appreciably the performance on that side of the oxygen-absorption complex. We have proposed a program that includes (1) replacement of the upper 3/5 of the radome membrane panels with material having lower reflectivity and loss at millimeter wavelengths, (2) improvement in the adjustment of the gravitational compensation system of the dish, (3) modification to reduce surface distortions due to changes in the thermal environment, and (4) a refined survey and resetting of the existing reflector surface.

2-4 THE NRAO 25-METER TELESCOPE FOR MILLIMETER WAVELENGTHS: B. E. Turner, National Radio Astronomy Observatory, Green Bank, West Virginia

The NRAO is designing a new telescope 25 meters in diameter that will have a surface accuracy of  $\leq 0.075$  mm rms. Thus it will work well to about 1 mm wavelength. The design is based upon the concept of homology, i.e., the surface is designed to distort under gravity so as always to approximate closely a paraboloid of revolution. The focal length is a function of elevation angle. The telescope parameters were guided by present scientific needs, by the relationship between achievable diameter and surface accuracy for homology designs, and by the transmission properties of the earth's atmosphere for mm wavelengths. The instrument is alt-az, wheel-and-track mounted. The main back-up structure, which rests on the elevation bearings, is homologous in design. It defines 60 basic homologous points. Upon these points rest intermediate or panel structures, themselves homologous, and upon which are fastened the surface plates. The 528 plates will consist of machined aluminum surfaces supported by rib structures. The pointing and surface accuracy are limited by wind and by temperature gradients. To achieve a pointing accuracy of 1.2 arc sec and a surface accuracy of  $\leq 0.075$  mm (as required at 1 mm wavelength) requires a wind speed  $\leq 10$  mph and a temperature gradient  $\leq 1.5^{\circ}\text{F}$  over the telescope structure. Thus the instrument will be housed in a spaceframe or astrodome. Some possible designs of these structures will be described.

2-5 HIGH-PRECISION MILLIMETER-WAVE ANTENNA: Robert B. Leighton, California Institute of Technology, Pasadena, California

A ten-meter diameter millimeter-wave dish of unusually high surface precision is described. Design features: Eighty-four hexagonal aluminum honeycomb panels are mounted

on a steel support structure, a tubular framework having a high degree of redundancy based on a lattice of equilateral triangles in plan view. Tubing gauges are chosen to optimize stiffness for given total weight. All members are fabricated to precise computer calculated lengths and are assembled using round pins in reamed holes permitting partial disassembly and reassembly with negligible dimensional change. The panels are supported at the triangle vertices by thin laterally flexible steel struts which also serve as differential adjustment screws. The upper honeycomb surface is open-celled (no skin) and is machined using a radially movable template-guided high-speed cutter, and slow rotation of the dish. During assembly and machining the dish is supported on a large air bearing. The reflecting skin is sheet aluminum vacuum-deformed and cemented to the finished honeycomb surface. A prototype unit having a surface rms of 60  $\mu$ m has been completed, and fabrication of an improved unit is underway. Factors which limit the surface precision and design changes which are expected to yield a several-fold improvement are discussed.

2-6 PERFORMANCE OF THE JPL MILLIMETER-WAVELENGTH  
INTERFEROMETER: M. Janssen and E. T. Olsen, Jet  
Propulsion Laboratory, California Institute of  
Technology, Pasadena, California

The interferometer at the Jet Propulsion Laboratory's Table Mountain Observatory consists of a 5.5-meter and a 3-meter antenna on an east-west baseline of 60 meters and operates at a fixed frequency of 36 GHz ( $\lambda$ 8.3mm). Subsequent to the first observations made in May 1974, the interferometer has undergone a period of testing, equipment modification, and calibration. This work is now completed, and our initial design goals have been met. Making use of data from observations now in progress we can demonstrate the sensitivity, gain stability, and phase stability of the interferometer. For example, we have observed terrestrial atmospheric effects as excess phase noise among one-minute integrations taken on a bright point source. This atmospherically-induced phase noise is highly variable, often less than  $5^\circ$  but exceeding  $50^\circ$  at times. Nevertheless, in May of this year we were able to detect radio emission from the rings of Saturn, separate from the emission from Saturn's disk itself. Projects currently in progress include measurement of the limb darkening of Venus and Jupiter at  $\lambda$ 8mm.

2-7 AN ACCURATE ANTENNA GAIN CALIBRATION METHOD:

B. L. Ulich, National Radio Astronomy Observatory,  
Tucson, Arizona

A method is presented for measuring the axial power gain of a microwave antenna. It is particularly applicable to horns with gains in the range 20-50 dB, and an absolute uncertainty (100) of less than 0.1 dB is achievable in most cases. The method is an extension of the "artificial Moon" calibration technique developed in Russia. An absorbing screen with a circular aperture is placed in the far field of the test antenna. The diameter of the aperture is chosen to subtend a smaller angle than the main lobe of the radiation pattern of the test horn. Then two sheets of microwave absorber (one at ambient temperature and the other cooled to the boiling point of liquid nitrogen) are alternately placed behind the aperture in the screen. Next the same two sheets are alternately placed directly in the aperture of the test horn. The antenna temperature differences are measured with a sensitive superheterodyne radiometer and compared. Since the solid angle of the aperture in the far field is known, from the ratio of the antenna temperature deflections one can calculate the e-equivalent solid angle of the antenna and thus its peak axial directivity. Corrections must be applied for near field effects, diffraction at the screen aperture, partial resolution of the aperture by the main lobe, and ohmic losses in the test antenna. A comparison of black disk measurements using a large conical horn at 86 GHz with theoretical calculations confirms the accuracy of this gain calibration technique.

2-8 A CRYOGENICALLY COOLED PARAMP RADIOMETER FOR MILLIMETER WAVES: J. Edrich, Denver Research Institute, University of Denver, Denver, Colorado

Early work on cryogenically cooled varactors led to the first 20°K-cooled parametric amplifier for millimeter waves. At 46 GHz a double sideband noise temperature of less than 60°K and a single-tuned bandwidth of 1000 MHz for a gain of 16 db were achieved. Two free-running klystrons were used as pump and local oscillators for this laboratory model. In order to obtain a field-operational system for the NRAO 36 ft. telescope a synchronously pumped parametric receiver was developed which can simultaneously measure two linear or circular polarizations and requires only one single klystron. This simplification also facilitates the phase locking of the local oscillator for spectral line observations. The system employs the first

cooled mm wave circulators with less than 0.4 db loss and more than 3 GHz bandwidth. Novel cooled doublers for 94 GHz with special input and output filtering are used which exhibit an efficiency of more than 30%. The restriction to a single drive source which is feeding two balanced mixers and two doublers caused a pump power shortage. Therefore the varactors of the paramps could not be fully pumped which resulted in a deterioration of their bandwidth and noise. Despite these compromises the system achieves a rf bandwidth of 300 MHz and a minimum double sideband noise temperature of 105°K at 47.2 GHz. These results and our work on other mm wave paramps indicate that it is possible to obtain rf bandwidths of 1.5 GHz and double sideband noise temperatures of 120°K up to at least 90 GHz.

2-9 SCHOTTKY-DIODE MIXERS FOR MILLIMETER-WAVE  
RADIO ASTRONOMY RECEIVERS: A. R. Kerr,  
Goddard Institute for Space Studies, New York,  
New York

Current room temperature and cryogenic Schottky-diode mixers will be discussed. The factors affecting the performance of a mixer receiver will be examined, including the conversion loss and the anomalous noise observed in many mixers. A comparison will be made between existing receivers and the best possible receivers using Schottky-diode mixers, showing that a factor of two improvement in noise temperature may still be achievable in both the cryogenic and room-temperature cases. Particular attention will be given to the design of the mixer mount and to anomalous mixer noise.

2-10 SUPER-SCHOTTKY MIXER PERFORMANCE: R. J. Pedersen,  
F. L. Vernon, Jr., M. McColl, M. F. Millea,  
M. F. Bottjer, and A. H. Silver, The Aerospace  
Corporation, Los Angeles, California

The super-Schottky barrier diode, a superconducting-semiconductor tunneling junction, is characterized by a highly nonlinear I-V characteristic at temperatures below the superconducting transition temperature and has been shown to be an extremely sensitive direct detector at microwave frequencies. We report the fabrication and performance of super-Schottky mixers at X-band and discuss the near term potential for extending these results to millimeter wavelengths. The diodes are fabricated from Pb on p-GaAs and

operated at 1 Kelvin in 90  $\Omega$  ridge waveguide. In contrast to conventional Schottky diodes at low temperatures, the noise temperature of the diode is of the order of its thermodynamic temperature. The predicted performance is 7.5 dB conversion loss and 2 Kelvin diode noise temperature. Using an optimized local oscillator power of - 41 dBm diode conversion loss and noise temperature were measured to be approximately 10 dB and 2 - 8 Kelvin, respectively. Measurements were performed with a 300 - 400 MHz i.f. radiometer and an X-band reflectometer. Several novel modifications of standard measurement techniques will be described which are dictated by the low temperature environment and low noise of the diodes. Improvement of the mixer performance and extension to higher frequencies will require modifications of the diode material and diode configuration. Two approaches presently being followed to accomplish the desired results will be discussed.

2-11 A QUASI-OPTICAL LOCAL OSCILLATOR INJECTION SYSTEM: J. J. Gustincic, Consulting Engineer, Los Angeles, California

This paper describes a quasi-optical technique for local oscillator injection into single ended mixers at millimeters and submillimeter frequencies. The technique utilizes a novel polarization twisting signal channels. Low signal channel loss is obtained simultaneously with high local oscillator injection efficiency to make the method extremely attractive for low noise radiometric applications at 100 Ghz and above. The quasi-optical configuration eliminates the loss and fabrication problems associated with waveguide circuitry at the shorter wavelengths. A quasi-optical radiometer front end which was constructed to make use of the injection scheme is described. The system was designed to combine the functions of antenna, local oscillator injection, and phase lock detection without the use of waveguide circuitry for a 115 Ghz airborne radiometer which will be used by The Jet Propulsion Laboratory for the measurement of mesospheric carbon monoxide. The measured electrical characteristics of the system are presented and discussed. Other possible quasi-optical configurations are suggested and their relative advantages considered.

$$F = \begin{bmatrix} f_1 & f_2 \\ f_3 & f_4 \end{bmatrix} = \begin{bmatrix} A + B & A z_1 + B z_2 \\ C + D & C z_1^2 + D z_2^2 \end{bmatrix} \quad F^T F = \begin{bmatrix} A^2 & A z_1^2 + B z_2^2 \\ A z_1^2 + B z_2^2 & C^2 + D z_2^2 \end{bmatrix} \quad F^T F A = F^T B$$

## NUMERICAL TECHNIQUES

### URSI COMMISSION VI

Tuesday, October 21 0830

URSI Session VI-3, Radio Building 1107

Chairman: E.K. Miller, Lawrence Livermore

Radiation Laboratory

B = Predicted  
 $n+1 \rightarrow M_0$   
 $(= ?)$

3-1 COMPUTATIONAL DIFFICULTIES IN THE EXTRACTION OF POLES FROM TRANSIENT DATA: H.G. Hudson, F.J. Deadrick, A.J. Poggio, and E.K. Miller, Lawrence Livermore Laboratory, Livermore, California

Several researchers have reported upon techniques based on Prony's method for extracting the complex natural frequencies from transient data. The efforts have dealt mainly with illustrating the feasibility of the process under ideal signal conditions. It is now necessary to investigate the constraints which must be imposed on the data and the effects of degraded input signal quality on the computed natural frequencies. The length of the transient response data record is an important parameter in the pole extraction scheme. It is shown that the required record length (in time) is defined by the minimum time window during which one can observe the effect of the complete transit over the body of contra-directed waves excited at the target extremities. For a straight wire of length L this is shown to vary between  $\frac{2L}{c}$  and  $\frac{4L}{c}$

with a dependence upon the incidence angle and the scattering angle. For other targets, the minimum window length is shown to be bounded through a relationship involving the minimum enclosing sphere. The effects of noise on the quality of the computed poles is being investigated. It is observed that the computed natural frequencies can be severely modified by noise and that filtering of the input data may not improve the accuracy of the computation. Simple cases are used to illustrate these phenomena and methods for correcting the deficiencies are suggested.

3-2 TECHNIQUES FOR THE EXTENSION AND GENERALIZATION OF PRONY'S METHOD: M. L. VanBlaricum and R. Mittra, Department of Electrical Engineering, University of Illinois, Urbana, Illinois

In the past year several workers have demonstrated the usefulness of Prony's algorithm for the direct extraction

of the poles and residues of a system from its transient response. However, to-date application of this technique has been limited to systems containing only simple poles. It has also been hampered by the fact that it is necessary to know the number of poles which are contained in the transient data before Prony's algorithm can be applied. In this paper we will show that Prony's method can be adapted for extraction and identification of multiple poles without a prior knowledge of their presence in the data. We will also present two schemes for systematically determining the number of poles contained in the transient response. This is important since, in Prony's method if one asks for more poles than are effectively contained in the data, the algorithm generates a number of extraneous poles in addition to ones that compare to the true poles. The presence of the extraneous poles causes the residues of the true poles to be inaccurate and results in unnecessary computation time. Similarly, if one underestimates the number of poles, then many of the returned poles may substantially deviate from the true poles. This paper shows that both of these improvements can be achieved with only a straightforward modification of the conventional Prony's algorithm and illustrates the procedure with numerical examples.

3-3 TRANSIENT CHARACTERIZATION OF ARBITRARILY ORIENTED TWO STRAIGHT WIRES AND COUPLING TRANSITION TO ISOLATED CASE: K.R. Umashankar, Department of Electrical Engineering, University of Mississippi, University, Mississippi

The recent transient scattering characterization of thin straight wire in free space and thin straight wire placed above and parallel to perfect conducting ground plane (case of two-body problem) demonstrated successfully the applicability of the singularity expansion method to obtain responses both in the time and frequency domains with ease. The natural resonant frequencies obtained for the wire above ground plane are quite complex in nature as compared to those of the isolated wire in free space. By formulating a general solution procedure to handle two (or more, either joined or not) straight wires with arbitrary orientation and coupling, an attempt has been made to explain the transition from the two-body problem to single body (under uncoupled situation). The pole trajectories of the first and secondary layers are traced as a function of the coupling angle to explain self and mutual resonances. Also considered are the coupling coefficients, responses in the frequency, and time domains for general orientation.

3-4 TRANSIENT EXCITATION OF ANTENNAS WITH GENERAL NON-LINEAR LOADS: NUMERICAL AND EXPERIMENTAL RESULTS: Frederick M. Tesche, Science Applications, Inc.; Tom K. Liu, Dikewood Corporation; and Fred J. Deadrick, Lawrence Livermore Laboratory, Livermore, California

The analysis of an antenna having a non-linear resistive load by using either the measured or calculated frequency domain response of the unloaded antenna has been previously discussed. In this paper, the method of analysis is extended to consider non-linear reactive elements as well. As an example, we consider the case of a diode connected to a linear dipole antenna. The voltage across the diode is a solution to the equation

$$\left( C(v) + v(t) \frac{dC(v)}{dv} \right) \frac{d v(t)}{dt} + C(v) v(t) = i_{sc}(t) - \int_{-\infty}^t y_{in}(t-\tau) v(\tau) d\tau$$

where the diode is assumed to be modeled by a parallel combination of a non-linear conductance  $G(v)$  and the non-linear capacitance  $C(v)$ . This equation is solved, not by the usual iterative process, but by a time stepping procedure.

Experimental data, measured on the transient range at the Lawrence Livermore Laboratory, has been obtained for a 60 cm monopole over a ground plane with a IN-4148 high speed silicon switching diode as a load. The experimental results compare very well with those predicted by the calculations and will be presented in this paper. In addition, calculated results for other types of non-linear loads will be illustrated.

3-5 NUMERICAL SOLUTION OF SPACE-TIME INTEGRAL EQUATION FOR SCATTERING BY OPEN THIN SURFACES:  
C.L. Bennett and R. Hieronymus, Sperry Research Center, Sudbury, Massachusetts

Over the past several years a new technique has been developed for computing the surface currents (and resulting scattered field) on open thin surfaces which are illuminated by an arbitrarily shaped time-domain waveform. This approach consists of first obtaining a space-time integrodifferential equation for the surface currents by

applying the E-field boundary conditions on the surface. This equation is then reduced to a recurrence relation that can be solved by simply marching on in time, thus eliminating the need for the matrix inversion that is required in the analogous frequency domain solution. The numerical implementation also makes use of the manner in which currents are known to vary in the vicinity of an edge. This presentation discusses the numerical detail of this solution technique. Numerical results which are in good agreement with measurements will be presented and discussed for a number of open thin surface shapes.

3-6 TIME DOMAIN SOLUTION OF SCATTERING BY THE TARGETS WITH NEUMANN OR DIRICHLET BOUNDARY CONDITIONS:  
R.M. Hieronymus and C.L. Bennett, Sperry Research Center, Sudbury, Massachusetts

The problem of scattering by a target with either a Neumann or a Dirichlet boundary condition is considered by the use of direct time domain techniques. In the two-dimensional electromagnetic problem, these boundary conditions correspond to either the TE polarization or the TM polarization. In the acoustic problem, they correspond to either a hard or a soft target, respectively. A space-time integral equation is derived for each of these cases and then solved numerically on a digital computer by marching on in time. A second kind equation results for the Neumann boundary condition whose numerical solution yields stable results which are in good agreement with those obtained for the sphere using classical frequency domain and Fourier transform techniques. For the Dirichlet boundary condition, however, either a first or second kind integral equation results.

Straightforward numerical solutions of either of these produce unstable results. A filtering technique is proposed and demonstrated which obviates this difficulty and produces results which are in good agreement with those obtained by classical techniques for the case of a sphere. Results are also obtained and described for a number of other simple geometric shapes for both boundary conditions.

3-7 USE OF A HYBRID EXPANSION IN MOMENT METHOD TO INCORPORATE EDGE CONDITIONS: D.F. Hanson and Paul E. Mayes, Electrical Engineering Department, University of Illinois, Urbana, Illinois

When electromagnetic waves are scattered from conducting

objects with sharp edges, the induced currents may vary quite rapidly near the edges. For such cases, the numerical solution of the integral equation by the method of moments may be expedited by choosing a different expansion function to represent the unknown current in the vicinity of the edge. An appropriate choice should satisfy the edge condition. In this paper a hybrid expansion is compared with a pulse-everywhere expansion in a numerical solution of the classical half-plane problem with plane wave incidence. In solving for  $(I_E - I_{PO})$ , the E-polarization (E vector parallel to the edge) current minus the so-called physical optics current, a hybrid basis function set is used with a  $z^{-\frac{1}{2}}$  expansion function in a half-width segment at the edge and with 199 full-width pulse expansion functions away from the edge. Point matching is used starting at the edge. Matrix elements are evaluated using methods which are demonstrated to yield excellent (at least 10 decimal place) accuracy. An efficient computer routine is obtained by utilizing the almost-Toeplitz nature of the final matrix. The result for the E-polarization current is found to be accurate to less than 1% when compared with the known analytic solution. Near the edge the hybrid expansion is clearly superior to the pulse-everywhere expansion. The solution for the E-polarization current is used to find the H-polarization current by a method described previously by Mayes. The result for  $(I_H - I_{PO})$ , the H-polarization current minus the physical optics current, is shown to be accurate to less than 6% when the pulse-everywhere expansion is used for  $(I_E - I_{PO})$  and to less than 1% when the hybrid expansion is used.

### 3-8 NEW APPROACH TO THE NUMERICAL SOLUTION OF ELECTRIC FIELD INTEGRAL EQUATIONS FOR PLANAR SURFACES:

D.R. Wilton and C.M. Butler, University of Mississippi, Univversity, Mississippi

The electric field formulation for scattering by planar surfaces typically results in integro-differential equations for the induced currents. Numerical difficulties often arise from the derivatives appearing in these equations. These difficulties are generally handled by choosing smooth basis functions to represent the current or using a Galerkin procedure to average the granular fields produced by subdomain basis functions. Both procedures are, however, relatively complicated. A simpler procedure, which has been extensively used for wire structures, makes use of piecewise sinusoidal basis functions as testing functions. In addition to reducing the numeri-

cal difficulties it also has the following properties: (1) the procedure involves only the evaluation of vector potential quantities which always have an integrable kernel, (2) the solution is identical to that obtained from a Hallén-like equation with point-matching and therefore has the approximately basis-independent convergence feature of Hallén's equation, and (3) includes the sinusoidal reaction matching procedure of Richmond as a special case. Because of the latter two properties, the technique can be viewed as extending the well-known high convergence rate of Richmond's method to a wider class of basis functions. The method, originally developed for wire structures, has been extended to planar surfaces with the aid of a useful identity involving the free-space Green's function.

## 3-9 EXTRACTING SINGULARITIES IN EM SCATTERING PROBLEMS:

William A. Davis, Department of Electrical Engineering, Air Force Institute of Technology, Wright-Patterson AFB, Ohio

The separation of the kernels of integral equations into singular and residual parts, which may be integrated by analytical and numerical methods respectively, has become accepted procedure in numerical techniques for electromagnetics. In the past, surfaces have been treated as locally planar while the kernel for wire problems has been expanded to obtain elliptic integrals, which have logarithmic singularities obtained after further expansion. The technique presented is to add and subtract the term giving rise to singularity divided by the Jacobian transforming the given surface to a planar surface. Thus one can obtain a closed form expression for the singularity of the wire problem or the integral of the surface singularity in addition to a bounded residue which may be treated numerically.

## 3-10 USER-ORIENTED GTD COMPUTER PROGRAM FOR CONVEX CYLINDERS WITH ARBITRARY CROSS SECTION:

Nan N. Wang and Jack H. Richmond, The Ohio State University ElectroScience Laboratory, Columbus, Ohio

A user-oriented computer program has been developed for high frequency radiation and scattering from infinitely-long perfectly-conducting convex cylinders. The analysis is based on the self-consistent geometrical theory of diffraction (GTD). The cylinder is modeled as a N-sided polygon. Two cylindrical waves with

unknown amplitudes are assumed to travel in opposite directions on each face of the polygon. The boundary conditions for the corners are applied to set up a matrix equation for  $2N$  unknowns (the amplitudes associated with the traveling cylindrical waves).

Crout's method is used to solve the matrix equation. Once the amplitudes for the traveling waves are determined, the radiation or scattering field is readily obtained via the usual GTD techniques.

Numerical results are presented for radiation and scattering from triangular, rectangular, semi-circular, and circular cylinders. The results show excellent agreement with measurements, moment, and eigenfunction solutions.

INTEGRATED AND FIBER OPTICS - I

URSI COMMISSION VI

Tuesday, October 21 0830

URSI Session VI-4, Radio Building Auditorium

Co-Organizer: R.L. Gallawa, OT/ITS

Co-Organizer and Chairman: C. Yeh, University  
of California

4-1 TRANSMISSION OF INFORMATION VIA OPTICAL FIBER:

James E. Goell, ITT Electro-Optical Products Division, Roanoke, Virginia

Optical fiber communication has advanced rapidly since the prediction of practicality by Dr. C. Kao of ITT-STL in 1964. Fiber with attenuation of 2 dB/km have been drawn. Compact multifiber cables with tensile strength of 500 lbs. and attenuation of 8 dB/km have been produced, and long-lived operation of GaAs lasers and LEDs suitable for use with fibers has been demonstrated. Initially, advantages such as freedom from interference make the use of optical fiber transmission attractive in special systems. Later, optical fibers will be used in conventional point-to-point links. Advantages offered will include reduced cost and increased repeater spacings which, in some cases, will eliminate field repeaters. Optical fibers are also attractive for use in data busses because of their small size and wide bandwidth. Ultimately, the use of fibers will greatly reduce intermachine wiring and permit increased interconnection flexibility. Because of their small size, optical fibers can be incorporated in mechanical and electrical load carrying cables. Thus, once fiber strength problems are solved, they will be used in applications such as TV inspection of undersea drilling operations. Integrated optical circuits will expand the usefulness of fiber optics for communication by increasing the bandwidth of point-to-point systems and allowing efficient multiplexing for data busses. This paper will describe the present state of fiber optic technology and explore advances needed for applications such as those described above.

4-2 SOME DESIGN CONSIDERATIONS FOR OPTICAL WAVE-GUIDE DIGITAL COMMUNICATION SYSTEMS:

R.L. Gallawa, U.S. Department of Commerce,  
Office of Telecommunication, Institute for Telecommunications Science, Boulder, Colorado

Optical fiber transmission systems are receiving consid-

erable attention from theorists and materials specialists and it now appears that their use is almost a certainty. Economic considerations and source longevity remain problems, but much of the operational analysis has been done. In this presentation we will review the options available to the communicator and discuss how those options impact on the selection of components. Discussion will include how the cost of a system may change with changes in component selection. Some economic prognosis will be given to show how the selection of repeater spacing and pulse rate can be changed to improve the normalized system cost.

4-3 BEAMS AND MODES IN OPTICAL FIBERS: L.B. Felsen  
and S.Y. Shin, Polytechnic Institute of New York,  
Farmingdale, New York

Depending on the application and on the operating parameter regime, the fields in a multimode optical fiber excited at one end by a focused Gaussian beam may be conveniently expressed as a guided mode representation or by tracking the multiply-reflected beam. In the former case, the incident field at the entrance plane is conventionally expanded in terms of the guided modes, which then propagate along the fiber. In the latter case, the field is confined initially to the geometric-optical ray path traced out by the beam axis, but successive reflections at the fiber wall lead to beam divergence which eventually prevents the multiply-reflected beams from being individually resolved. As long as the beam remains well collimated, direct tracking is preferable, but converting to guided modes becomes appropriate after the resolution deteriorates. This presentation explores both mechanisms of propagation and the relation between them. The analysis is performed by a new method, the complex-source-point technique, which converts incident spherical wave solutions into Gaussian beam solutions. Thus the point-source-excited field in an optical fiber, either in its guided mode form or in its paraxial ray-optical representation, is basic to our considerations. The beam-to-mode excitation mechanism is quantitatively interpreted in ray-optical terms, as is the periodic focusing and defocusing of the multiply-reflected beam. Special features of the propagation process, especially the role and character of the beam shift on the curved fiber wall, are emphasized.

4-4 THE ANNULAR-TYPE OPTICAL FIBER WAVEGUIDES:  
Tsuneo Nakahara, Masao Hoshikawa, and  
Shuzo Suzuki, Sumitomo Electric Ind., Ltd.,  
Yokohama, Japan

This paper describes single mode and multimode annular-type optical fibers proposed by the authors.

#### Single mode annular-type fibers

One type is a fiber in which the transverse cross-sectional refractive index distribution has an annular ring having the higher refractive index than that of the rest of the part. When the annular ring is very thin or the index difference is very small, this fiber conveys only the fundamental mode, the  $HE_{11}$  mode.

Another possibility is to consider a quasi-single mode transmission of the  $TE_{01}$  mode, where the lower order mode (the  $HE_{11}$  mode) is continuously filtered out by inserting a very fine lossy rod at the center axis.

#### Multimode annular-type fibers

When the annular ring is thick or the index difference is large, this fiber conveys multimode. Both step and gradient index profile can be considered. Theoretical analysis will be given to obtain very small modal dispersion.

#### Experiments and Conclusions

The annular-type high silica fibers were trially manufactured. The attenuation constants of 2~5 dB/km and the smaller modal dispersions were observed.

The advantages of the annular-type fibers are: Relatively easy splicing, smaller dispersion, and easy fabrication.

4-5 CHARACTERISTICS OF PLASTIC CLADDED SILICA FIBER CABLE: C. Kao, G. Bickel, and J.C. Smith, ITT Electro-Optical Products Division, Roanoke, Virginia

Fluoropolymer cladded pure silica fibers are low cost fibers with sufficiently good transmission characteristics (<40 dB/km) for many transmission applications. This paper reports on the loss and dispersion characteristics

of a number of such fibers and discusses the problems in cabling such fibers. The structure is shown to have mode conversion but with high differential modal loss resulting in low dispersion. If, however, the coupling between modes is increased by the presence of microbends, the differential loss causes the total fiber loss to increase rapidly. Theoretical predictions are verified by experimental results.

4-6 PULSE RESPONSE OF A SELF-FOCUSING OPTICAL FIBER TO A RECTANGULAR INPUT PULSE: S. Nemoto and G.L. Yip, Department of Electrical Engineering, McGill University, Montreal, Quebec, Canada

Using analytical expressions for the impulse response of a self-focusing fiber, the pulse response to a rectangular input pulse is calculated. The refractive index profile of the fiber is described by the second- and the fourth-order terms of the radial distance. Assuming that all the excited modes in the fiber carry an equal amount of power, two cases are considered where [1] all the possible propagating modes and [2] only the modes with no azimuthal variations are excited. It is shown that a rectangular input pulse is strongly deformed by mode dispersion in both cases, and that the shape of the output pulse is affected not only by the duration of the input pulse but also by the fourth-order coefficient  $\rho$  of the index profile. In case [1], the duration of the output pulse can be reduced up to 50.4% by increasing  $\rho$  from 1 to  $8/3$  ( $\rho = 1$  corresponds to a parabolic profile and the index profile with  $\rho = 8/3$  gives no dispersion for case [2]). The pulse shape in case [2] is sharper than that in case [1], but the pulse durations in both cases are almost the same as long as  $0 < \rho < 1$ .

4-7 MEASURED DISPERSION IN LONG MULTI-MODE FIBER WAVEGUIDES WITH AND WITHOUT JOINTS: C.K. Kao, G. Bickel, and M. Maklad, ITT Electro-Optical Products Division, Roanoke, Virginia

Dispersion in multimode fibers arises from the intrinsic group velocity characteristics of each propagating mode, the material dispersion, and the differences in modal velocities. Pulse broadening due to these fundamental mechanisms may be modified in practical waveguides by mode-coupling and mode-filtering due to bending, stress, and structural imperfections of the fiber. The initial pulse broadening in a fiber is expected to be linear with length and of magnitude determined by the effective

numerical aperture of the injected pulse. As propagation continues through longer fiber lengths, the mode-coupling and mode-filtering mechanisms modify the initial pulse spreading. Experimental results on three fibers ranging in length from 2 to 4 kilometers indicates sublinear and sub-root-length dependence in fibers with significant mode-filtering (i.e., high differential mode losses). The effects of splices having losses between 0.5 and 1.0 dB on pulse spreading is shown to be negligible in the case studied.

4-8 NONLINEARITY REDUCTION OF LED AND ILD FOR FIBER-OPTIC COMMUNICATION: J.J. Pan and M.P. Arnold, Harris Corporation, Electronic Systems Division, Melbourne, Florida

Linearity of an optical source is of extreme importance in multichannel communications systems. This paper presents an effective and inexpensive "anti-series" push-pull technique to reduce light emitting diode (LED) or injection laser diode (ILD) nonlinearity for fiber-optic communications. A compensation diode of opposite polarity is inserted in RF series with the optical source diode. The direct currents through the diodes are in parallel and are independent adjustables. The Volterra series is utilized as an analytic tool to evaluate LED and ILD nonlinear frequency-dependent characteristics. The intermodulation and harmonics are expressed as a Volterra series in terms of the diode current. The push-pull configuration and balanced scheme can reduce light fluctuations and noises. Two-tone tests have been conducted using two types of compensation diodes under various bias conditions. The second- and third-order intermodulation products (IMP's) were improved more than 25 dB, thus obtaining IMP's of 60 dB below the carriers.

4-9 RECEIVER DESIGN FOR LONG DISTANCE COMMUNICATION: Irvin B. Slayton, Jr., Harris Corporation/Electronic Systems Division, Melbourne, Florida

Optical receiver performance can have a significant influence on the ability to achieve practical long distance optical fiber communications without the aid of repeaters. Poor receiver performance can easily mean the difference between a small semiconductor optical source and an expensive bulky high powered laser source requiring hundreds of watts of input power with critical optics for input coupling. Using a 10-megabit 4-kilometer data link as a case study for discussion, the procedures and general

considerations for maximizing receiver performance are examined. Included are considerations for avalanche photodetector selection, transimpedance preamplifier design, and optimum avalanche gain determination to minimize the amount of received optical power required to achieve a pre-specified bit error rate (BER). Also included are computations of the error performance for received optical power values below minimum and an analysis of system performance using two practical suboptimum threshold detection schemes.

4-10 A UNIDIRECTIONAL OPTICAL COMMUNICATIONS SYSTEM FOR BASEBAND VIDEO AND AUDIO SIGNALS: M.D. Redman and G.L. Yip, Department of Electrical Engineering, McGill University, Montreal, Quebec, Canada

A complete optical communications system developed at McGill University for demonstration and educational purposes is described with special emphasis on the hardware and design consideration involved with its implementation. The basic system is an analog communication link designed for the simultaneous one way communication of a single baseband video signal from a TV camera and a single audio channel using an AM carrier at 6.3 MHz, modulated by a signal from a standard magnetic microphone. The amplitude modulated optical carrier is generated with a narrow beam infrared LED and in an attempt to achieve some system flexibility for demonstration purposes, two potentiometers on the chassis of the transmitter terminal electronics offer independent control of the D.C. and A.C. levels of the LED intensity. This optical output is then launched into 100 meters of a single strand self-focusing optical fiber, and the problems involved with the launching into such a medium will be discussed. A Silicon Avalanche Photodiode is employed at the receiving end for the low noise optical detection. The complete terminal electronics and design considerations involved with the low noise detection and signal demodulation will be presented. Finally, the overall test performance in a general laboratory environment will be discussed.

NOISE AND INTERFERENCE MODELS AND  
RADIO SYSTEM PLANNING  
URSI COMMISSIONS VIII AND VI  
Tuesday, October 21 0830  
URSI Session VIII-2, Radio Building 1103  
Chairman: E.A. Wolff,  
NASA Goddard Space Flight Center

2-1 DEVELOPMENT OF HIGH FREQUENCY BROADCAST SCHEDULES  
IN AN INTERFERENCE ENVIRONMENT: George W. Haydon,  
Office of Telecommunications, Institute for Tele-  
communication Sciences, Boulder, Colorado

The likelihood of interference between high frequency broadcast transmitters is rapidly increasing due to increased numbers and powers of these facilities. Methods of predicting the expected performance of high frequency broadcast facilities in the presence of the unintended radiation environment, i.e., atmospheric, man-made, and cosmic noise have been extended to include intended radiations from other broadcast facilities. These methods based upon an estimation of the interference environment resulting from skywave propagation include the likelihood of an interference path and the expected magnitude of the interference signal. The statistical description of the interference environment is combined with a statistical description of the desired signal to obtain an estimate of the likelihood of satisfactory broadcast operation in the presence of the interference. A quantitative measure of the compatibility between broadcast operations is introduced and illustrative computer determination of these measures are shown. The computer determination involves (1) an estimate of the likelihood of both the desired and undesired propagation paths and (2) an estimate of the distribution of the signal magnitudes over these paths when the paths exist. The likelihood that the desired propagation path will provide an adequate signal to noise ratio in the absence of interference is compared to the likelihood that the desired propagation path will provide an adequate signal to interference ratio in the presence of a potentially interfering transmitter. The percentage change in these likelihoods is introduced as a quantitative measure of the compatibility between the high power skywave broadcast operations being considered.

2-2 TRANSFER OF INFORMATION TO CO-LOCATED RECEIVERS IN INTERFERENCE LIMITED CONDITIONS: Douglass D. Crombie, U.S. Department of Commerce, Office of Telecommunications, Institute for Telecommunication Sciences, Boulder, Colorado

Much effective work has been done on the impact of "noise" on transfer of information by radio links. As a result, some very effective techniques for combatting noise have been developed and applied. However, because of spectrum congestion, for instance, in radio frequency bands used by the microwave common carriers, noise may no longer be a significant limitation. Instead, co-channel interference from similar signals will become dominant, particularly in cities where numerous microwave circuits originate or terminate, as the pressure to share the available radio channels increases.

In this paper the total capacity of many microwave links sharing a common channel, using the same modulation parameters, and converging to a point at which all the receivers are located is examined. In this situation interference to each receiver from angularly adjacent transmitters constitutes the major limitation to total communication capacity, assuming high signal to noise ratios for the individual links. Maximization of the total capacity requires a study of the tradeoffs between capacity per link and the number of links terminating at the receiver location. Factors considered include angular spacing of the links, antenna beam width and side-lobe level, bandwidth expansion, and required output signal to interference ratios. The relative capacity for frequency division multiplexed voice signals, using single sideband amplitude modulation or frequency modulation with various modulation indices, are compared. The results confirm that the use of bandwidth expansion ratios greater than unity is beneficial when attempting to maximize the total amount of information transmitted per unit bandwidth in spectrum sharing situations.

2-3 STATISTICAL FREQUENCY-DISTANCE CURVES:  
R. D. Jennings, L. E. Vogler, and  
J. J. Stephenson, OT/ITS, Boulder, Colorado

Requirements for better tools with which to perform evaluations of electromagnetic compatibility (EMC) between systems which transmit and receive radio signals have stimulated the development of a computer-based model for producing statistical frequency-

distance curves. The statistical frequency-distance curves provide an estimate of the distance separation that is required between an interfering transmitter and a victim receiver as a function of the frequency offset between them. The curves are parametric in the probability, or percent of time, that interference power will not exceed a specified interference criterion. Statistical variations in antenna power gains and propagation loss are used to compute probabilities of interference. Continuing development of the model will allow statistical variations in systems parameters and operational factors also to influence the computed probabilities of interference. Methods used to combine the statistical expressions in producing the statistical frequency-distance curves as well as the concept and utility of statistical frequency-distance curves will be discussed.

2-4 THE EFFECT OF DISTANCE IN ALLEVIATING DEGRADATION TO BASE STATION RECEPTION: Jules Deitz,  
Federal Communications Commission, Washington, D.C.

Last year a progress report was given on the degradation of base station reception due to automotive ignition systems and multipath propagation. The project is now completed and a written report is available. A brief summary will be presented. The summary will include new information on the effect of distance in alleviating degradation from automotive vehicles to base station reception. Distances out to 1300 feet were examined for frequencies 37.5, 87, 154, 450, and 950 MHz. The effect of "super-noisy" vehicles will be included.

2-5 STATISTICAL-PHYSICAL MODELS OF MAN-MADE AND NATURAL ELECTROMAGNETIC INTERFERENCE ENVIRONMENTS: David Middleton, Office of Telecommunications, Institute for Telecommunication Sciences, Boulder, Colorado

Analytical first-order probability densities and distributions, as observed at the output of the initial (linear) stages of typical narrow-band receivers (of bandwidth  $\Delta f_{ARI}$ ), are obtained for the three basic classes of electromagnetic interference. These are, respectively: (i) Class A noise, characterized by input bandwidths  $\Delta f_N$  less than  $\Delta f_{ARI}$ ; (ii) Class B interference, where  $\Delta f_N$  is larger than  $\Delta f_{ARI}$ ; and (iii) Class C noise, which is a linear combination of

Class A and B components. These models combine statistical and physical structures, with the basic statistics poissonian. The emitted waveforms obey appropriate propagation laws and explicitly include the effects of source and receiver beam patterns, relative Doppler, source distributions in space, and other geometrical factors. The results are expectedly highly nongaussian, but are analytically tractable and canonical. Excellent agreement with experiment is found for both Class A and B noise. These quantitative models are needed for: (1) assessment of EM environments, (2) evaluation of receiver performance and optimum receiver design, and (3) determination of system performance in these environments.

2-6 OPTIMUM RECEPTION IN IMPULSIVE INTERFERENCE:

A. D. Spaulding, U.S. Department of Commerce,  
OT/ITS, Boulder, Colorado

The statistical-physical model of impulsive interference recently developed by D. Middleton is applied to a class of optimum signal detection problems. In a previous paper, optimum detection algorithms were developed for coherent detection in narrowband impulsive interference and performance compared to that of the current suboptimum receivers. In this paper, locally optimum Bayes detection (LOBD) receivers are developed for incoherent reception and the performance of these detectors given. Performance comparisons are given between suboptimum and optimum coherent receivers and the incoherent optimum receivers. Various forms of fading signals are considered. The case in which phase estimation (partially coherent) is used is also covered.

2-7 PERFORMANCE OF DIGITAL SYSTEMS IN NOISE AND

INTERFERENCE: John R. Juroshek, Office of  
Telecommunications, Institute for Telecommunication  
Sciences, Boulder, Colorado

This paper presents an approximate method for determining the performance of digital systems in Gaussian noise and cochannel interference. The method uses an approximation based on the geometrical characterization of signals to obtain the performance of a variety of digital modulation techniques as a function of signal-to-noise ratio and signal-to-interference ratio. Performance estimates are presented for coherent phase shift keying (CPSK), noncoherent frequency shift keying

URSI Session VIII-2

(NCFSK), differentially coherent phase shift keying (DPSK) and multi-amplitude-phase keying (M-APK) systems. Curves are presented that show excellent agreement between the approximate method and other theoretical predictions even at bit error rates of  $10^{-9}$ .

THERAPEUTIC APPLICATIONS

URSI COMMISSION I (BIOLOGICAL EFFECTS)

Tuesday, October 21 0830

URSI Session B-2a, UMC West Ballroom

Chairman: J.F. Lehmann, University of Washington

**B2a-1 STEADY STATE TEMPERATURE PROFILES IN MICROWAVE**

**DIATHERMY:** Kadry A. Al-Badwaihy and  
Abu-Bakr A. Youssef, Department of Electrical  
Engineering, Cairo University, Egypt

Body reaction and heat transfer are important factors in predicting steady state temperature profiles in microwave diathermy and hence in determining safe doses of microwaves. This paper shows how to include such effects, which were considered only qualitatively in the past, both in the formulation and numerical solution.

Microwave irradiation of stratified three skin, fat, and muscle layers is first considered. Steady state temperature profiles are calculated by solving the heat diffusion equation and the electromagnetic transmission equation. The metabolic heat generation and blood cooling effects are included in the analysis. Body reaction in the form of increased blood circulation as a result of local microwave heating is then considered for different levels of body reaction. The steady state heat diffusion equation becomes nonlinear when body reaction is taken into consideration. The more interesting geometry of a cylindrical layer of skin enclosing fat and muscle in suitable models is then considered.

Temperature profiles are again presented for these models and for different frequencies, exposure levels, skin and fat thicknesses, blood circulation rates, and levels of body reactions. Results should serve as a more accurate guide for suitable exposures for such treatments. The proposed schemes of body reactions and their influence on the biological effects of microwave radiation are shown to be quite important in determining safe levels of long term microwave leakage hazards.

**B2a-2 PHYSIOLOGIC DESIGN CRITERIA FOR THERAPEUTIC  
APPLICATORS OPERATING AT 915 MHz:**

J. F. Lehmann, Department of Rehabilitation  
Medicine, A. W. Guy, Bioelectromagnetics  
Research Laboratory, Department of Rehabilitation  
Medicine, and J. B. Stonebridge, Department of  
Rehabilitation Medicine, University of Washington,  
Seattle, Washington

Based on the fact that the absorption of microwaves is considerably higher for musculature than for other tissues, microwaves have been considered as the therapeutic agent of choice to selectively heat muscle. While lower frequencies are more desirable because they avoid the reflection at the subcutaneous fat and muscle interface, 915 MHz is the lowest microwave frequency available for therapeutic purposes. The major therapeutic goal when using microwaves is to elevate the temperature throughout the musculature to a therapeutic level. It is also desirable that the temperature be evenly elevated throughout the field of application. Particular designs are compared first as to their heating pattern in a phantom model consisting of subcutaneous fat and musculature. Secondly, temperature distributions produced in human volunteers are obtained. From these temperature distributions, an attempt is made to assess the absorbed power and to determine the cooling rate due to changes in blood flow in various tissues. The results show that 40 watts applied by means of a surface-cooled rectangular aperture can provide an incident power density of up to  $550 \text{ mW/cm}^2$  with a peak absorbed power density of approximately  $120 \text{ W/kg}$  in the musculature. Stray leakage radiation is limited to  $5 \text{ mW/cm}^2$  or less, two inches from the applicator. At these levels a flow cooling rate of up to  $180 \text{ W/kg}$  can be stimulated in the musculature.

B2a-3 MAPPING OF FREE SPACE AND SCATTERED FIELDS IN MICROWAVE DIATHERMY: G. Kantor, H. Bassen, and M. Swicord, Division of Electronic Products, Bureau of Radiological Health, Food and Drug Administration, Rockville, Maryland

Near-field measurements of external electric fields around microwave diathermy applicators (2450 MHz) in free space and in conjunction with planar and limb phantoms were made with a miniature isotropic probe developed by the Bureau of Radiological Health. Spatial variations of the field components were mapped in the vicinity of applicators presently in clinical use. The probe consisting of three orthogonal -2.5 mm long dipoles, has the high spatial resolution necessary for near-field measurements close to applicator apertures. A fiber optically-linked telemeter eliminated metallic cables from the vicinity of the probe and applicator, thus minimizing perturbation of the field and RF interference in the readout electronics. Three-dimensional graphs

presenting the magnitude of each field component as a function of position in a transverse plane were obtained with a digital mini-computer. Corresponding isopower density ( $|E|^2$ ) contours also were plotted. Electric field strength ratios of the longitudinal and transverse components were obtained to evaluate the radiation patterns of spaced applicators in terms of resulting heating patterns.

B2a-4 SHORTWAVE DIATHERMY APPLICATORS: A. W. Guy,  
J. A. McDougall, and M. D. Webb, Bioelectromagnetics Research Laboratory, Department of Rehabilitation Medicine, University of Washington School of Medicine, Seattle, Washington

Guy, et al., (Proc. IEEE, Jan. 1974) have discussed theoretical and experimental evaluations of shortwave diathermy applicators. Using an extension of a new technique for bisecting phantom models (Guy, et al., Proc. Microwave Power Symp., 1975), several shortwave diathermy applicators were evaluated thermographically with phantom materials. It was found that the "induction" type applicator described in Guy, et al., (Proc. IEEE, Jan. 1974) produced a toroidal absorption pattern in the muscle phantom material as predicted. It produced more power absorption in the muscle phantom (255 W/kg) than in the fat phantom (184 W/kg) for  $H = 682$  A/m. Two other "induction" type shortwave applicators of a different coil geometry, wire size, and spacing, including one with an electrostatic shield, were tested. These latter applicators also produced toroidal type heating patterns in the muscle phantom but of different radii dependent on coil size. The heating pattern of the latter two applicators was concentrated more in the fat phantom layer and did not penetrate into the muscle phantom very deeply. The unshielded applicator produced 540 W/kg in the muscle phantom and 304 W/kg in the fat phantom for  $H = 238$  A/m. The shielded applicator produced 138 W/kg in the muscle phantom and 61 W/kg in the fat phantom for  $H = 308$  A/m. The tests indicate the applicability of "induction" type diathermy applicators is strongly dependent on coil geometry and spacing.

B2a-5 MICROWAVE-INDUCED HYPERTERMIA AND RADIATION SENSITIVITY OF MOUSE INTESTINE: Gregory A. Gordon, Gordon Livingston, and Lyle A. Dethlefsen, Departments of Radiology and Bioengineering, University of Utah, Salt Lake City, Utah

Recent data shows that heat alone in both in vitro and in vivo settings selectively kills cancer cells and that heat plus radiation have a synergistic interaction. Normal tissue tolerance has been studied using only hot-water immersion of mouse skin. We are studying the C3H mouse intestine to define normal tissue response more adequately. Quantitation of mucosal response is done by microscopic crypt-cell survival method of Withers. Microwaves are generated by a 2450 Megahertz Microwave Magnetron and delivered through a wave guide which is collimated to encompass the upper abdomen. The mid-upper abdomen temperature of the mouse is monitored continuously with a liquid crystal thermometer inserted into the rectum up to the epigastrium. At a fixed power, microwaves are pulsed until the region of interest has attained the desired temperature (43 and 45°C) which is then sustained for varying periods of time. Immediately post-heating, 1000 rads of whole body radiation are administered and at 3-1/2 days post-treatment, the intestine is removed with histopathological sections prepared and the regenerative crypts counted. With heat alone (45°C for 15 min.), preliminary data suggests survival is reduced to less than 45% (12 to 28 animals). Similar low survival (4/13) is seen with 45° for 2 to 4 min. Crypt-cell survival is strikingly reduced with combination heat and radiation (45° for 2 min.) Presuming the systemic rise in temperature related to vascular heating caused the high mortality, the above technique was altered to improve survival. The subcutaneous temperature was monitored when cool air was blown on a wet mouse and this caused the subcutaneous temperature to remain at or less than normal with no change in mortality. To avoid the vascular organs of the liver, lung, and heart, the distal colon was heated and again there was poor survival (4/28 - 45° for 3 minutes). Heating of externalized bowel resulted in the same low survival. We will pursue these techniques to develop complete radiation dose-response curves and evaluate implanted tumor response.

B2a-6 BIOLOGIC EFFECTS OF PULSED HIGH FREQUENCY ELECTROMAGNETIC RADIATION: B. West and W. Regelson,  
M.C.V./V.C.U., Richmond, Virginia

A pulsed electromagnetic non-ionizing radiation source utilizing a carrier frequency of 27.12 megahertz delivered at one of six pre-selected pulsed frequencies was seen to significantly alter survival time and size of implanted B-16 melanoma and Lewis lung tumors in syngeneic mice.

The highest pulsation rate (600 pulses/sec) had a pulse length of 65 microseconds delivery 975 watts peak power at an average 38 watts. Mice irradiated for 20 mins daily for three days prior to tumor exposure showed an enhancement of tumor growth and a decrease in life span. Post-operated models irradiated at 400 pulses/sec showed increased life span. Effects against the P388 and L1210 ascites leukemia have been equivocal. Biological activity including overall body weight change and speed of drug metabolism were shown to differentiate from controls. Decreases in sleeping time of mice injected with sodium pentobarbital immediately before whole-body high frequency exposure was associated with an increase in liver cytosol protein implying the P450 drug hydrolase system may be stimulated. Significant inhibition of weight gain and differential development patterns in maturing male mice have been noted to occur after 30 min daily exposure for 14 days at the highest pulse frequency. Female mice show a differnt weight inhibitory pattern initiated during the 14-day radiation schedule. Adult weight levels for both controls and treated are similar indicating a temporary effect in developmental gain equalized at approximately two to four weeks. These effects appear to be independent of overall effects on body temperature, and are not associated with any gross alterations in organ to body weight ratios.

DIAGNOSTIC APPLICATIONS  
URSI COMMISSION I (BIOLOGICAL EFFECTS)  
Tuesday, October 21 1100  
URSI Session B-2b, UMC West Ballroom  
Chairman: C.C. Johnson, University of Utah

B2b-1 MICROWAVE RADIATION AS A DIAGNOSTIC TOOL:  
P. C. Pedersen, C. C. Johnson, C. H. Durney,  
and D. G. Bragg, University of Utah, Salt Lake  
City, Utah

A new technique is being developed in which microwave radiation is used for diagnosis and patient monitoring. The technique has special applicability for lung diseases such as pulmonary edema and emphysema, where significant changes in the electromagnetic characteristics of the lung tissue are produced. The microwave technique is non-invasive, is sensitive to the fluid content in the tissue, can be localized, and gives negligible exposure hazards compared with even the most conservative safety standards. It has potential for overcoming some of the inadequacies of the currently available methods. The system consists of a network analyzer coupled to a dual directional coupler, a UHF generator, and an applicator which functions as a receiving/transmitting antenna. With the applicator placed on the chest, a selected part of the lung compartment is irradiated with low intensity microwave energy (in the order of  $1\mu\text{W}/\text{cm}^2$  between 500 and 1000 MHz). Using the incident microwave signal as a reference, the complex reflection coefficient is determined. It has been shown both theoretically and experimentally that phase and amplitude are correlated with the lung respiration inflation/deflation as well as with the ratio (lung tissue + fluid)/(total lung volume) which is changed by lung diseases such as pulmonary edema and emphysema. The theoretical results were based on a model of plane homogeneous tissue layers. The initial experimental results were obtained from a series of measurements of phase and amplitude variation with respiration. Applicator position sensitivity and spirometry correlations were studied. Later experimental results were derived from dog experiments, where pulmonary edema was produced artificially by intravenous infusion of Dextran 40, and where significant amplitude changes following the

development of edema. To investigate in a controlled fashion the factors which affect phase and amplitude, a simulator was built in which respiration as well as lung diseases can be simulated, and where the effect of lung volume, lung shape, fluid content in the lung, lung position relative to the applicator, frequency response, etc., could be studied.

**B2b-2 REMOTE MEASUREMENT OF RESPIRATION IN INFANT PRIMATES USING AN X-BAND DOPPLER RADAR:** F.A. Spelman, C.W. Kindt, D.M. Bowden, G.P. Sackett, and J.E. Spillane, Regional Primate Research Center at the University of Washington, Seattle, Washington; and D.A. Blattman, RACON, Inc., Seattle, Washington

A system has been developed to measure respiration and motor activity of caged infant pigtail macaques (Macaca nemestrina). The 450 gm infants are housed singly in a wooden enclosure (76 x 76 x 61 cm) which is open at the top and illuminated with 10.5 GHz CW electromagnetic energy that is generated by an Impatt diode at the apex of a horn antenna (Gain = 18 db). The maximum power density 9.1 cm above the floor of the enclosure is  $3.7 \mu\text{w}/\text{cm}^2$ . In order to get sufficient return signals for processing, the monkey wears a chest band of soft metallic interwoven cloth (Aris Glove Division of Consolidated Food Corporation, New York). The cloth does not restrict movement, allowing the animal to move freely within the enclosure. The return signal is received by a microwave diode mounted at the apex of a horn antenna (Gain = 18 db), mixed with energy leaked from the transmitting horn, and amplified by an IF amplifier with a maximum gain of 86 db and a frequency response flat within 3 db from 0.11 to 1.1 Hz. The system is being used to assess normal respiratory patterns in sleeping infant monkeys and to monitor for respiratory arrest in premature and high risk infants.

**B2b-3 ANTENNA DESIGN FOR A PASSIVE TEMPERATURE MONITORING AND IDENTIFICATION SYSTEM FOR LIVESTOCK:** J. A. Landt, University of California, Los Alamos Scientific Laboratory, Los Alamos, New Mexico

The need for identification of individual livestock animals and determination of their body temperature has resulted in development of an rf telemetry system employing a passive transponder. The transponder is implanted under the skin of the animal, is interrogated remotely, and is powered solely by rf energy

incident upon the transponder antenna. This paper summarizes developmental work on transponder antenna design to overcome the high attenuation suffered through skin and muscle tissue and the large reflection incurred at the air-skin interface. The antenna design involved a combination of numerical calculations using existing computer codes and experimental validation. This approach indicates that engineering approximations can be made in order to model the real antenna configuration in view of computer code limitations, and yet retain both quantitative as well as qualitative information on the antenna performance in the real environment. The major constraints of transponder size and transponder power requirements have been met with several antenna designs while maintaining at least a safety factor of five over the health safety guidelines of  $10 \text{ mW/cm}^2$ . It is planned to field test this system in a farm environment during the Fall of 1975.

FIELD SURVEY INSTRUMENTS  
URSI COMMISSION I (BIOLOGICAL EFFECTS)

Tuesday, October 21 0830

URSI Session B-3, UMC East Ballroom

Chairman: R. Bowman,  
National Bureau of Standards

**B3-1 E- AND H-FIELD INSTRUMENTATION AND CALIBRATION  
BELOW 500 MHz:** Paul S. Ruggera, Division of  
Electronic Products, Bureau of Radiological  
Health, FDA, Rockville, Maryland

Under P.L. 90-602, The Radiation Control for Health and Safety Act of 1968, the Bureau of Radiological Health is charged with the responsibility to determine levels of radiation emitted from electronic products. During the past two years, the Bureau has been developing capability to generate and measure electromagnetic fields from 0.1 Hz to 500 MHz. Many of the current available electronic products which operate below 500 MHz and emit potentially hazardous radiation have never been accurately measured. The reason for this is that detection equipment has been primarily designed for far field use. In most applications involving electronic products such as diathermy machines, dielectric heaters, induction heaters, anti-theft systems, etc., the exposure to personnel is actually near field in nature. This adds the constraint that both the electric and the magnetic field must be measured for a true assessment of the possible biological consequences of exposure. This paper will discuss commercially available instrumentation and the evaluation procedures utilized by the Bureau. Two three-axis orthogonal magnetic field measuring instruments, one developed under contract and one developed in the Bureau's laboratories for measurement of magnetic fields, will be presented. The operating characteristics of a special three-axis orthogonal version of a commercially available portable electric field meter will also be discussed. The cross polarization reactivity of the orthogonal instruments appears to be greater than 25 dB. The field strength covered will be equivalent to  $10 \text{ mW/cm}^2$  free space power density.

B3-2 MAGNETIC FIELD STANDARD AT FREQUENCIES ABOVE 30 MHz: Hubert Trzaska, Technical University of Wroclaw, Wroclaw, Poland

Up to this time magnetic field standards at frequencies above about 50 MHz have not been built. The interest in the wide frequency range measurements of the magnetic field in the near field, also at frequencies above 30 MHz, as well as suggestions on high biological activity of magnetic field have made it necessary to construct magnetic field probes for near field measurements. The first step here was the necessity to construct equipment for investigations parameters of these probes, i.e., standard magnetic field.

In the work are presented magnetic field standards based upon both the standard field method and the standard antenna method designed for frequency range up to 200 MHz and field intensities up to 100 mA/m. Some factors limiting accuracy of the standards, specific for higher frequencies, e.g., non-uniform current distribution, shape of the antenna being standarized, sensitivity of the standard receiving antenna to the electric field, and others are discussed.

On the basis of the presented accuracy limitations and the literature of the problem the inaccuracy of the built magnetic field standard was calculated as  $\pm 4\%$  in the frequency range up to 100 MHz and  $\pm 5\%$  at frequencies up to 200 MHz.

The standard magnetic field generated with the use of standard field method has been measured at the field level 50 mA/m with the standard receiving antenna method. The result of this comparision shows that the intensities of both standards agree with each other with accuracy better than  $\pm 2.5\%$ . Recent and further works will be done to obtain wider frequency range, higher intensities, and better accuracy of the magnetic field standard.

B3-3 A LOW FREQUENCY H-FIELD RADIATION MONITOR:  
Edward Aslan, Narda Microwave, Plainview, New York

An H-field radiation monitor is described which has a 1 db bandwidth from 10 MHz to 200 MHz. It functions beyond 300 MHz with some additional degradation in sensitivity. The probes response is isotopic and independent

of polarization. Its equivalent plane wave power density range extends dynamically from 20 mW/cm<sup>2</sup> to 20 mW/cm<sup>2</sup>, and with an alternate probe, from 100 mW/cm<sup>2</sup> to 100 mW/cm<sup>2</sup>. The probe consists of three mutually perpendicular coils. Each coil, having a diameter of 9 cm and consisting of two turns. The natural resonance of each turn is well above the frequency range of interest and each coil is resonated slightly below the frequency range of interest with a small lumped capacitance. The coils are each terminated in a thin film thermocouple element having a resistance between thirty and fifty ohms. Very high resistance monolithic leads connect the outputs of the elements to a well shielded preamp. Connections are then made to the metering instrument. The RF induced currents dissipate power and heat the resistive thermocouple hot junctions thereby providing a d.c. output voltage proportional to the square of the RF induced current. The probe makes use of two innovations of an NBS probe design of Ron Bowman, a high resistance film to provide a shield of static changes, and a preamp in the handle which eliminates cable modulation from degrading the performance.

B3-4 COMPLETE MEASUREMENT OF HAZARDOUS ELECTROMAGNETIC FIELDS WITH ELECTRO OPTICAL CRYSTALS: H. Basson and R. Peterson, Bureau of Radiological Health, Food and Drug Administration, U.S. Public Health Service, Rockville, Maryland

An electric field probe capable of wideband measurements of the amplitude and phase of RF electric fields has been developed using an electrically short dipole antenna (30 cm in length) with a small optical crystal at the antenna feed point. No electrical cables or components are in the presence of the detection system. A laser is used to interrogate the crystal, hence minimal perturbation of the field occurs. Standard optical detectors with bandwidths exceeding 100 MHz are used to remotely convert the modulation of the laser beam (polarization rotation) to a linearly proportional electrical replica of the field under study. In the feasibility system, a 1 mm x 1 mm x 20 mm Lithium Niobate crystal was used to provide detection of a 10 Volt/meter electric field whose frequency was swept from 10 to 30 MHz. A signal to noise ratio of 10 dB was observed with a spectrum analyzer having 3 kHz IF bandwidth. Fields over 200 V/m were observed with all harmonics generated by the crystal being more than 20 dB below the fundamental. Excellent linearity is exhibited over a 35 dB range.

B3-5 MEASUREMENT OF ELECTRIC AND MAGNETIC FIELD STRENGTHS FROM INDUSTRIAL RF POWER SOURCES: David L. Conover, Wordie H. Parr, Edwin L. Sensintaffar, and William E. Murray, Jr., NIOSH, DLCD, PAB, Cincinnati, Ohio

This paper describes the performance characteristics of radiofrequency (RF) electric and magnetic field strength meters and the results of surveys performed with these meters. The electric and magnetic field strength meters were constructed and calibrated for use within close proximity (fractions of a wavelength) to RF power sources. The NBS EDM-2 electric field strength meter was developed for the frequency range of 10 to 500 MHz and the NBS magnetic field strength meter was designed to be used from 10 to 40 MHz. The field strength meters were made for NIOSH to assist in the determination of the total occupational exposure from industrial RF power sources. Survey results include measurements of electric and magnetic field strengths generated by various types of industrial RF power sources operable from 13 to 40 MHz. The electric and magnetic field strength measurements were made in locations occupied by the operators of RF industrial power sources. Preliminary survey results indicated that more than half of the measured electric and magnetic field strengths exceed the field strength guides specified in the ANSI C95.1-1974 personnel exposure standard for microwave and RF radiation.

B3-6 METHODS AND INSTRUMENTATION FOR THE EVALUATION AND CALIBRATION OF MICROWAVE SURVEY INSTRUMENTS: M. L. Swicord, H. I. Bassen, W. A. Herman, J. E. Duff, and J. R. Bing, Division of Electronic Products, Bureau of Radiological Health, FDA, Rockville, Maryland

In order to assess electromagnetic radiation hazards, facilities for the evaluation and calibration of microwave power density instrumentation have been established. The calibration facility includes an anechoic chamber which has a movable dielectric cart capable of positioning a receiving antenna at any point along the 7-meter longitudinal axis of the chamber to millimeter accuracy. A laser provides a means of aligning transmitting and receiving antennas with the boresight of the chamber. In the calibration

facility, power density calibrations are accurately performed utilizing the three-antenna technique to determine near zone gain of the transmitting antenna. Power equation techniques allow precise measurements of system mismatches. Special NBS calibrated high power meters have been developed with waveguide input ports whose flange sizes are identical to those of the transmitting antennas. Multipath reflections in the chamber are also accounted for. Absolute power density calibration uncertainties (worst case) of less than 0.5 dB at 2450 MHz and 0.8 dB at 915 MHz are achievable in this facility. The instrument evaluation facility includes (1) a microwave absorber-lined temperature chamber, and (2) a separate slot source and probe positioner permanently mounted in an absorber-lined fixture. In these systems, near field instruments can be evaluated for independence of response to amplitude modulation, polarization orientation, battery voltage, and frequency. Other parameters which can be evaluated are r.f.i. phenomena, drift, pattern, and nonlinearity.

B3-7 MUTUAL COUPLING BETWEEN LINEAR ANTENNAS:

M. L. Swicord, Division of Electronic Products, Bureau of Radiological Health, FDA, Rockville, Maryland; and A. Y. Cheung, University of Maryland, Institute for Fluid Dynamics and Applied Mathematics, College Park, Maryland

A method for calculating the mutual impedance between a linear transmitting antenna located symmetrically along the Z axis and a linear receiving antenna of arbitrary location and orientation is described. Two specific cases are treated. The first case is a transmitting slot antenna and short electric dipole receiving antenna. The coupling is determined as a function of receiving antenna size at various distances and locations. This provides a means of establishing minimum design criteria for a nonperturbing near field dipole detector with direct application to the case of using a dipole for measurement of microwave oven leakage. The second case considers orthogonal wire antennas. Coupling between two short electric dipoles which are perpendicular but have displaced centers is investigated as a function of their relative size and location. An application of the latter is the determination of design criteria for small isotropic electric field probes consisting of three orthogonal components.

MEASUREMENT AND TECHNIQUES

URSI COMMISSION I

Tuesday, October 21 1330

URSI Session I-1, Radio Building 1103

Chairman: G. Birnbaum

National Bureau of Standards

1-1 A SHORT HOODED ANTENNA FOR REDUCING RADIATION MEASUREMENT ERRORS IN SHIELDED ENCLOSURES AT FREQUENCIES BELOW 1 GHz: J. A. Woody, R. S. Smith, and J. C. Toler, EMC Group/ Communications Division/EES, Georgia Institute of Technology, Atlanta, Georgia

Current military standards concerned with the measurement of equipment level radiated emission and susceptibility characteristics require that the test area electromagnetic environment be at a specified level below the performance limits. This generally dictates that the measurements be conducted in an anechoic chamber or a shielded enclosure. The cost and size of anechoic chambers often rule them out as viable options, yet above approximately 20 MHz, shielded rooms yield measurement errors so large as to render test data both inaccurate and nonrepeatable. Research investigations have been conducted recently to develop a short hooded antenna for use at frequencies below 1 GHz. The short hood features light weight and small size while reducing measurement errors to acceptable levels. This paper reviews the errors inherent in shielded room measurements and describes the short hooded antenna developed. The theoretical predictions and experimental data for this antenna are compared and performance compromises are described. The performance of the hooded antenna in a typical shielded enclosure is then compared to performance in an anechoic chamber. In conclusion, the use of antennas with shortened hoods is recommended for radiated measurements in future standards concerned with radiated emission and susceptibility tests.

1-2 THE BUCKET TECHNIQUE FOR RADIOMETRIC MEASUREMENT OF ANTENNA AND RADOME LOSS: K. R. Carver, Physical Science Laboratory, New Mexico State University, Las Cruces, New Mexico

Antenna and radome loss measurements for the Multifrequency Microwave Radiometer (MFMR), which operates at 1.4, 18.0, 22.05, and 37.0 GHz, and for the Passive Microwave Imaging System (PMIS), which operates at 10.69 GHz, have recently been made using the large reflecting bucket enclosure on A-Mountain (at 1.48 km above MSL) near New Mexico State University. The bucket serves to block thermal radiation from surrounding terrain, thus allowing the antenna/radome system under test to be isothermally surrounded by the corresponding equivalent sky temperature for each frequency. The sky temperature is calculated using radiosonde profiles as input data and by using a spherically stratified model of clear-sky radiative transfer, so that measurements are made only on clear-sky nights. Such a technique becomes particularly attractive for (1) large airborne or spaceborne radiometric systems where the loss values must be measured with the antenna and radome in situ, and for (2) multifrequency radiometer systems. Nonetheless, there are several questions which arise naturally concerning the systematic and random errors incurred by such a technique such as (1) possible mutual interaction between the antenna and bucket, or (2) the systematic error incurred in calculating the sky temperature, particularly at 22 GHz. This paper will discuss these errors in detail, as well as user criteria for required bounds on the systematic error in the loss measurement, and will demonstrate that the bucket technique can yield highly accurate loss values.

1-3 MEASURED CURRENT DISTRIBUTION ON MODERATELY THIN WIRE SCATTERERS: B. M. Duff and S. Singarayar, University of Mississippi, University, Mississippi

The current distribution on moderately thin scattering structure has been measured as a function of both angular and axial position on the surface. Data is presented for straight wire and V cross structures above an image plane. Electrical radii of  $ka = 0.04$  and less were studied. The observed angular variation of the current density is of the order of 20% in magnitude and 20 degrees in phase. This angular variation in the surface current has previously been recognized in

theoretical studies of cylindrical scatterers. However, most previous measurements on structures as thin as these have assumed rotational symmetry of the current. This rotational independence of the current is a basic assumption of thin wire theories. This assumption is valid for driven antennas even for relatively large radii. For the scattering case, however, the angular variation can be significant and should be considered when comparisons are made with thin wire theory. In addition to the measurements of current distributions, the response of conventional loop probes is examined. It is shown that the errors in measurement of the current can be considerably greater than expected for nonresonant structures.

1-4 MEASURED DISCONTINUITY OF CHARGE AT THE JUNCTION OF UNEQUAL RADII WIRES: B. M. Duff and S. Singarayar, University of Mississippi, University, Mississippi

The discontinuity of the linear density of charge, which occurs at the junction of thin wires of unequal radii, has been measured. This problem was considered in a previous paper by the authors, but the results were somewhat inconclusive. The principal emphasis in the investigation presented here was placed on accurate experimental calibration of the probes used for the charge measurement. The probe calibration was accomplished by making measurements in a coaxial line containing a step change of radius of the inner conductor. A theoretical solution for this coaxial line problem is well established. It is, therefore, possible to utilize the coaxial line measurements to obtain an accurate calibration of the relationship between the probe response and linear density of charge. Charge distribution measurements were then made on stepped-radius monopole antennas. Three different steps ratios were investigated and the change in linear density of charge across the step has been determined.

1-5 INSTANTANEOUS BROAD-BAND POLARIMETER: Harold Shnitkin, Norden Division of United Technologies Corporation, Norwalk, Connecticut

A decade bandwidth antenna and receiver equipment is described which will measure the complete polarization parameters of an incident radio wave of quarter microsecond long duration.

Axial ratio, sense of rotation, and the orientation angle of the major axis of the polarization ellipse are measured and recorded every 200 microseconds. The equipment consists of orthogonal linear, phase coincident, broadband antennas, a pair of microwave mixers, an IF processor, an eight channel receiver, pulse stretchers, digital interface, and magnetic tape recorder.

The principle employed requires the generation of six IF signals from the signals intercepted by the two orthogonal linear antennas, corresponding to these six polarization components: vertical linear, horizontal linear, +45° linear, -45° linear, righthand circular, and lefthand circular. This is achieved by the IF processor. Subsequent video processing yields voltages representing vertical-to-horizontal ratio, +45° to -45° ratio, and lefthand circular-to-righthand circular ratio. These voltages are quantized and tape recorded in real time. When the tape recordings are played back through a digital computer, the data is converted into axial ratio, sense of rotation, and orientation angle of electric field maximum, which are subsequently printed out on a pulse-by-pulse basis together with signal level and time of arrival.

This paper includes derivations and nomographs to explain the measurement principle, equipment description, and measured data analysis.

#### 1-6 SWEEP FREQUENCY SURFACE FIELD MEASUREMENT

FACILITY: Valdis V. Liepa and Fred P. Rhine,  
Radiation Laboratory, Department of Electrical  
and Computer Engineering, The University of  
Michigan, Ann Arbor, Michigan

Although techniques for measuring surface currents and charges have been known for years, most experimental studies have held the frequency constant while the probe or sensor is moved along the surface to obtain the charge or current distribution. With the present interest in EMP, it has become important to devise techniques for obtaining the transient currents and charges excited on metallic surfaces of complex shape. These can be determined from a knowledge of the CW response as a function of frequency, and an experimental facility is described for the sweep-frequency measurement of currents and charges in amplitude and phase. To demonstrate the accuracy achieved, measured data for a metallic sphere illuminated by a plane

electromagnetic wave are compared with the theoretical values. Similar data for metallized and thick wire model aircraft are also presented, and reveal the resonance properties of the objects. In the latter case, the results are compared with computer-generated data.

1-7 THE ACCURACY/PRECISION OF S-193 RADIOMETER/  
SCATTEROMETER USING SKYLAB-ACQUIRED DATA:  
K. Krishen and D. J. Pounds, Lockheed Electronics  
Company, Inc., Aerospace Systems Division,  
Houston, Texas

This paper provides a statistically based estimate of the precision/accuracy with which the S-193 Scatterometer and Radiometer measured the backscattering cross sections and radiometer temperature respectively, of ground sites. Scientific evaluations of S-193 data leading to earth resources applications will be meaningful only when these estimates are available. The estimate of precision/accuracy is based upon a sensor analysis, and comparisons of the actual S193-acquired/ data with values of the backscattering cross sections or brightness temperatures obtained by simulating the target scene and sensor mathematical model. These comparisons and statistical analysis of S-193 data yielded the upper and lower limits of the precision/ accuracy of the scatterometer and radiometer systems. This analysis provided also a verification of the NASA/Johnson Space Center S193 Production Data Processing (PDP) program.

1-8 JOSEPHSON EFFECT MIXERS: P. L. Richards, J. H. Claassen, and Y. Taur, Department of Physics, University of California, Berkeley, California

After a decade of speculation and exploration, Josephson effect receivers for mm and sub-mm waves are entering a phase of detailed engineering development. Experiments at 36 and 140 GHz have shown that the noise and the conversion efficiency of a Josephson effect heterodyne mixer with external local oscillator are in quantitative agreement with theory. The theory predicts that the mixer noise temperature of a receiver made from a single ideal Nb Josephson junction operated at a temperature of 1.5K should be  $T_M \approx 50K$  for  $v \lesssim 0.3$  THz and  $\approx 135v$  ( $v$  in THz) for  $0.3 < v < 1$  THz. If it proves possible to make mixers from series arrays of ideal junctions, then practical problems such as

impedance matching can be eased and the theoretically predicted  $T_M$  can be reduced by a factor  $\approx 2$ . In this case, we expect  $T_M = 68v$  ( $v$  in THz) for  $0.1 < v < 1$  THz. This is very close to the photon fluctuation limit  $T_M = hv/k = 48v$ . The prospects for making the required arrays and the ways in which actual junctions deviate from ideal performance will be discussed.

1-9 PARAMETRIC AMPLIFICATION BY UNBIASED JOSEPHSON JUNCTIONS: R. Y. Chiao, M. J. Feldman, and P. T. Parrish, Physics Department, University of California, Berkeley, California

Broadband tunable low-noise cryogenic amplification has been achieved at X-band Ka-band by a series of unbiased Josephson junctions. At X-band an electronic gain of 12dB, a bandwidth of 1 GHz (FWHM), a tunability over 4GHz, and an amplifier noise temperature of less than 20K were measured. Ka-band preliminary experiments show a net gain of at least 16 dB, a bandwidth greater than 1 GHz (FWHM), and system noise temperature less than 200K. At Ka-band we used a degenerate mixing scheme in which a single oscillator served both as pump and local oscillator for the second stage mixer. We also operated at below the lambda point. Progress toward a 115 GHz amplifier will be reported. Comparison with theory will be made.

1-10 TRANSMISSION LOSS MEASUREMENTS OF A 14 km CIRCULAR WAVEGUIDE: D. T. Young and S. D. Williams, Bell Laboratories, Murray Hill, New Jersey

A 14 km length of 60 mm diameter waveguide has recently been installed and tested by the Bell System. We describe here a sophisticated computer interfaced measurement set which characterizes the  $TE_{01}$  transmission properties of waveguide medium. The set operates from 33 GHz to 117 GHz with frequency increments as small as 50 MHz. The basic measurement scheme is a straight forward measure of a pulsed signal which is first reflected from a fixed reference point and then reflected from the end of the waveguide under test and compared to the reference. The entire frequency band can be measured in approximately 12 hours with an error less than 1%. The set can operate also in a mode such that the signal return from a moving reflector is measured. Signal return loss of 100 dB can be measured.

The waveguide medium consists primarily of dielectric lined waveguide with 9 meter helix mode filters spaced approxi-

mately 800 meters apart. The waveguide is placed along a typical commercial route which includes 11 route bends. The  $TE_{01}^0$  transmission loss is 1 dB per km at 40 GHz, decreasing to slightly less than 0.5 dB per km at 80 GHz and increasing to 0.8 dB per km at 110 GHz.

PLASMA INSTABILITIES IN THE MAGNETOSPHERE - II

URSI COMMISSION IV

Tuesday, October 21 1330

URSI Session IV-3, UMC 158

Chairman: E.J. Smith, Jet Propulsion Laboratory

3-1 STABILIZATION OF WHISTLER MODE BY RELATIVISTIC ELECTRONS WITH LOSS-CONE ANISOTROPY: Michael Schulz and A.L. Vampola, Space Physics Laboratory, The Aerospace Corporation, El Segundo, California

In the nonrelativistic Vlasov theory of plasma cyclotron waves, instability occurs for propagation parallel to  $B_0$  (unperturbed magnetic field) if  $\omega/\Omega < s/(s + 1)$ , where  $\omega/2\pi$  is the wave frequency,  $\Omega/2\pi$  is the gyrofrequency, and  $s$  is the corresponding particle anisotropy. Thus an electron pitch-angle distribution  $f(\alpha) \propto \sin^{2s}\alpha$  produces instability at some frequency in the whistler mode if  $s > 0$ , and (more specifically) at all  $\omega < \Omega/2$  if  $s = 1$ . The purpose of the present work is to investigate relativistic corrections to the theory, using an equilibrium fission spectrum as prototype. For environmental parameters characteristic of the earth's magnetosphere, relativistic effects are found to reduce the (frequency) domain of instability by  $\sim 40\%$  inside the plasmasphere and by  $\sim 80\%$  outside the plasmasphere. The stabilization at  $\omega/\Omega < s/(s + 1)$  is caused mainly by electrons that have gyrofrequencies  $\Omega/2\pi\gamma$  below the wave frequency, where  $\gamma$  is the ratio of relativistic mass to rest mass. Instability thus occurs only for  $\omega/\Omega \ll s/(s + 1)$  when relativistic effects are properly considered.

3-2 OBSERVATIONS OF STORM-TIME MAGNETOHYDRODYNAMIC WAVES AND THEIR RELATIONS TO HIGH- $\beta$  PLASMA INSTABILITIES: L. J. Lanzerotti, Bell Laboratories, Murray Hill, New Jersey

The sources of geomagnetic pulsations (observed as ULF variations in the earth's magnetic field) remain important unsolved problems of magnetospheric physics. A review is given of recent magnetohydrodynamic wave analyses using data obtained from both ground-based and satellite-based instruments. It is shown that during the magnetic storm conditions in the events analyzed, where sufficiently detailed data are available, high  $\beta$  plasma instabilities such as the mirror instability or the compressional drift wave instability, coupling to resonant magnetospheric

field lines, were likely candidates for producing the observed waves.

3-3 STIMULATION OF PC 1 MICROPULSATIONS BY CONTROLLED VLF TRANSMISSIONS: H. C. Koons, The Aerospace Corporation, El Segundo, California

During controlled VLF transmissions from a site near  $L = 4$ , Pc 1 micropulsations which can be associated with the transmission program were observed by a detector at College, Alaska. The micropulsation event onset shortly after the transmitter began sending a simple repetitive pulse program at 6.6 kHz. The program consisted of a 5 sec pulse transmitted every 30 sec. Following the onset of the event a complex sequence of pulsations appeared between 1.0 Hz and 1.33 Hz. During the simple repetitive program which lasted for 10 minutes, the pulsations recurred about every 90 sec. Subsequently the transmitter was operated in a swept frequency mode with a repetition period of 5 sec. At that time the micropulsation structure simplified to two essentially monochromatic wave packets reappearing at 120 sec intervals. The micropulsations onset 15 minutes after satellite 1972-76B, at low altitude in the conjugate region, observed proton fluxes which could be identified on a one-for-one basis with pulses from the transmitter. Calculations with the same plasmaspheric density model used to obtain the time delay between the transmission of a pulse and the detection of the protons at the satellite suggest that the 6.6 kHz whistler-mode wave and a 1 Hz hydromagnetic wave resonate with protons of the same parallel velocity near  $L = 4.0$ . The bounce period of those resonant protons which mirror low on the field line is about 90 sec. The observations suggest that the micropulsations were stimulated by the VLF transmissions with the protons playing a role in the interaction.

3-4 VLF EMISSION DATA: EVIDENCE DEFINING A SINGLE MECHANISM FOR COHERENT CYCLOTRON INSTABILITY IN THE MAGNETOSPHERE: R. A. Helliwell and T. L. Crystal, Radioscience Laboratory, Stanford University, Stanford, California

Recently observed characteristics of triggered emissions provide evidence that there is a single cyclotron resonance mechanism of coherent instability operating in the magnetosphere. The measured bandwidths

of the generated signals are less than the interaction bandwidth. Controlled injection of VLF triggering signals from the Siple transmitter is being used to determine the growth rate and bandwidth of the process. A wave-particle-interaction model is being developed which has already successfully reproduced several important emission characteristics. Recent computer calculations based on this model now allow us to predict minimum equatorial energetic electron fluxes, based on emission amplitude measurements. The model is general enough that it may also be applicable to interactions involving waves in other frequency ranges. For instance ULF emissions (Pc 1) may result from an analogous mechanism.

3-5 CONCERNING THE EFFECT OF ANOMALOUS RESISTANCE  
ON AURORAL ELECTRIC FIELDS AND CURRENTS:

J. A. Fedder, J. H. Orens, and T. P. Coffey,  
Naval Research Laboratory, Plasma Physics  
Division, Washington, D.C.

Using a simple model for the magnetosphere-ionosphere coupling we will demonstrate the effect of anomalous resistance to field-aligned current on auroral electric fields and Birkeland currents. Examples of fields and currents will be shown for different magnitudes of the resistance. These results serve to illustrate the possible importance of anomalous resistance to field-aligned currents in auroral arcs. We also model the effects of the two commonly suggested resistance mechanisms: unstable field-aligned currents and the Papadopoulos Coffey parametric mechanism. Examples will also be shown for cases where the precipitating electron current is resistance free. In all cases the electric field effect is qualitatively similar, whereas the Birkeland current density is quite sensitive to the resistance model. Finally, a model result for a N-S section of the auroral oval will be shown. The model electric field will be compared to satellite data from the same region, and the very complex ionospheric and field-aligned current patterns will be discussed.

3-6 ULF AND ELF STUDIES IN REGIONS OF DETACHED  
PLASMA: M. G. Kivelson, R. E. Holzer,  
S. Kokubun, C. T. Russell, and H. Singer,  
University of California, Los Angeles,  
California; and C. R. Chappell, Marshall Space  
Flight Center, Huntsville, Alabama

Regions of enhanced plasma density in the outer magnetosphere are expected to be regions of enhanced wave-particle interactions. Energetic particles, stable to plasma wave generation outside these regions, can suddenly become unstable upon drifting into them. Chan and Holzer have shown that such tubes of enhanced plasma density are associated with a characteristic ELF spectrum. Detailed studies of OGO-5 particle and field data in a limited sample of such regions show that these ELF emissions occur for broad ducts when the energetic electrons have loss cone or normal pitch angle distributions and their fluxes are above the predicted stably trapped limit. ULF waves in these regions have also been observed. At times it is possible to use the OGO-5 plasma measurements to infer one component of the electric field of these ULF waves. For some Pc 5 events, the waves are also observable in ground-based magnetic records.

3-7 EVIDENCE FOR ONSET OF ELECTRON CYCLOTRON RESONANCE INSIDE THE PLASMASPHERE:  
J. N. Barfield, Space Environment Laboratory,  
NOAA, Boulder, Colorado

The intensity variation of ELF emissions has been studied during isolated substorm activity. Spectrum channel data from the OGO-6 search coil magnetometer has been analyzed to obtain the probability of occurrence as a function of local time during different phases of the substorm. The data is consistent with cyclotron resonant generation by medium energy ( $\approx$  30 KeV) electrons. Near dawn the ELF emission intensifies during the substorm expansive phase when anisotropic fluxes of electrons are expected to be injected into the outer radiation zone. In the afternoon and dusk sectors ELF signals diminish during the period of active substorm disturbance but then intensify during the drift orbits in the presence of strong substorm convection electric fields. Explorer 45 observations confirm the duskside electron flux reductions during substorms and indicate that 30 KeV electrons near  $L = 5$  fall below the Kennel-Petschek stably trapped flux levels coincident with the disappearance of duskside ELF emissions.

3-8 ANAMALOUS TRANSPORT PROCESSES IN THE MAGNETOSPHERE:  
K. Papadopoulos, U.S. Naval Research Laboratory,  
Washington, D.C.

A review of the computation of anomalous transport coefficients such as resistivity, thermal conductivity, diffusion, etc., is presented with emphasis on their role in the magnetosphere. Such anomalous transport is the result of enhanced levels of electrostatic turbulence driven by magnetospheric plasma instabilities. The methods and framework of the computations are presented, followed by a discussion of their applicability to the magnetosphere.

INTERFERENCE TO RADIO ASTRONOMY AND

CCIR RELATED TOPICS

URSI COMMISSIONS V, III, AND VIII

Tuesday, October 21 1330

URSI Session V-3, UMC 156

Chairman: J. Findlay, NRAO

3-1 THE HISTORY OF THE ITU, THE CCIR, AND THE CCITT:  
Ernest K. Smith, Institute for Telecommunication  
Sciences, Office of Telecommunications,  
U.S. Department of Commerce, Boulder, Colorado

The initials "ITU" go back to 1865 making the "ITU" one of the oldest international organizations. However, during the period 1865 to 1932, these initials stood for International Telegraph Union. The Radio Telegraph Union, born in 1903, was merged with the International Telegraph Union in 1932 and the International Telecommunications Union (the present ITU) dates from that time. The International Telegraph Consultative Committee (CCIF) and the International Telephone Consultative Committee (CCIT) were both created at the Administrative conference of the International Telegraph Union in 1925 and continued in the new ITU until 1956 when a consolidation was effected to form the present CCITT (International Consultative Committee for Telephone and Telegraph). The International Radio Consultative Committee (CCIR) was created at the 1927 Washington Conference of the Radio Telegraph Union. It continued into the present ITU but underwent major reorganization in the Stockholm Plenary Assembly of CCIR in 1948 as ordered by the ITU Atlantic City Conference of 1947. The internal structure of CCIR last underwent significant change at the 1970 CCIR Plenary Assembly in New Delhi. The crucial documents of the ITU are the Convention, the Telephone and Telegraph Regulations, and the Radio Regulations. The latter are scheduled for a complete overhaul in 1979.

3-2 CCIR-URSI RELATIONS: WHY, WHEN, WHAT AND  
WHITHER: Ernest K. Smith, Institute for  
Telecommunication Sciences, Office of Tele-  
communications, U.S. Department of Commerce,  
Boulder, Colorado

Past relations between URSI and CCIR (The International Radio Consultative Committee of the International

Telecommunications Union) have had the checkered history that might be expected between an international scientific organization (URSI) and an applications-oriented treaty-related organization (CCIR). These relations seem now to be in an ascending period both in quantity and quality. Following each Plenary Assembly of the CCIR its director forwards the documents which have been referred to URSI in the CCIR Study Group deliberation to the Secretary General of URSI. He in turn delivers them to the appropriate URSI Commission chairman for consideration at the next URSI General Assembly. The URSI responses then go back through this channel and are prepared as documents to the next meeting of the pertinent CCIR Study Groups. This paper traces the areas, extent, and success of past relations and considers the possibilities and needs for improvement in the forthcoming decade.

**3-3 WORLD ADMINISTRATIVE RADIO CONFERENCES OF THE INTERNATIONAL TELECOMMUNICATIONS UNION:** Samuel E. Probst, Office of Telecommunications Policy, Executive Office of the President, Washington, D.C.

World Administrative Radio Conferences are the arenas in which the Radio Regulations of the International Telecommunications Union (ITU) are developed, supplemented, modified, and approved. This paper deals with the procedures by which WARCs are convened and conducted, U.S. positions for presentation at such conferences are developed, and negotiations on such positions are conducted at the conference itself, with particular emphasis on the forthcoming General World Administrative Radio Conference to be held in 1979. The degree of U.S. obligation to abide by the final results of such conferences is also set forth.

**3-4 RADIO ASTRONOMY PROBLEMS AND PRIORITIES IN PREPARATION FOR THE 1979 WORLD CONFERENCE ON RADIO FREQUENCY ALLOCATIONS:** William E. Howard III, National Radio Astronomy Observatory, Green Bank, West Virginia

The U.S. radio astronomy community has prepared a preliminary working paper outlining its views of the current radio frequency allocation situation in radio astronomy in preparation for the next World Administrative Radio Conference to be held by the International Telecommunications Union in 1979. Together with a band-by-band analysis including scientific justifications of the frequencies

now allocated to or used heavily by the Radio Astronomy Service, the U.S. radio astronomers are attempting to put priorities on improving the interference protection in those bands that are most crucial to the research effort projected for the next decade. This working paper, prepared by the Committee on Radio Frequencies (CORF) of the National Academy of Sciences in liaison with the new frequency management office of the National Science Foundation, will help to determine the U.S. position at the 1979 allocations conference. Technical justification of spectrum usage by the radio astronomy service is provided by the C.C.I.R. and U.S. Study Group 2D, composed of CORF subcommittee members, who continually review the documentation. Particularly important is CCIR Report 224 which cites the harmful interference limits above which radio astronomy measurements become untrustworthy. Points to be emphasized in this talk will include current major allocation problems and their possible solutions, the role played by the committee system as it interacts with the national frequency management community, and an assessment of future prospects.

3-5 FREQUENCY MANAGEMENT AT THE NATIONAL SCIENCE FOUNDATION: R. M. Price, National Science Foundation, Washington, D. C.

Many basic research programs require the use of the radio spectrum for communication, telemetry, or remote sensing. Typical programs are wildlife tracking and monitoring, oceanographic studies using automated data buoys, radio and radar astronomy, and studies of the atmosphere or the ionosphere. The National Science Foundation has appointed a Radio Spectrum Manager to provide the U.S. scientific community with advice in the research use of the spectrum and assistance in obtaining frequency support for experiments. This assistance is available to the national centers sponsored by the Foundation as well as to grantees in the broader research community. The Foundation is a member of the Interdepartmental Radio Advisory Committee (IRAC). NSF representatives are participating in the subcommittees engaged in the preparation for the WARC-79. Additionally, the NSF Radio Spectrum Manager maintains liaison with the Committee on Radio Frequencies (CORF) of the National Academies of Science and Engineering and the U.S. National Committee of URSI.

3-6 WORK OF THE CCIR AND THE IUCAF RELATING TO  
INTERFERENCE TO RADIO ASTRONOMY: John P. Hagen,  
Department of Astronomy, The Pennsylvania  
State University, University Park, Pennsylvania

The relationship of the CCIR and the IUCAF to the I.T.U. and the nature of the studies and recommendations of the two groups relating to interference will be discussed. These two technical groups, the CCIR representing administrations and the IUCAF representing the scientific unions, are the means by which scientific and technical information can be introduced into the decision making process of the I.T.U. Both of the groups will need the assistance of URSI in their preparation for the 1979 World Administrative Conference. The nature of the problems before the two groups relating to interference to Radio Astronomy and its relevance to the work of URSI will be emphasized.

3-7 URSI-CCIR COOPERATION: John P. Hagen, The Pennsylvania State University, Department of Astronomy, University Park, Pennsylvania

The CCIR (International Radio Consultation Committee) is an organization which was established to provide technical advice to the ITU (International Telecommunication Union). The National Committees of the CCIR represent administrations and have a membership drawn from the scientific and technical communities of each administration. Many of the members of the CCIR are also active in URSI. The CCIR is organized in eleven study groups each representing a service such as Space Research and Radio Astronomy or a topic of general interest such as Ionospheric Propagation. The work of the CCIR is published in Reports and Recommendations which are reviewed at a Plenary Assembly and then published in a "Green Book" and in that form are available to the ITU and to the scientific community. Advances in radio science and the emergence of new techniques make it necessary to periodically revise the CCIR Reports and when necessary prepare new reports on topics not previously discussed by the CCIR. In keeping with the advances in radio science the CCIR will in the future by relying more and more on URSI for scientific and technical support in its efforts to insure efficient use of the radio spectrum.

URSI Session V-3

3-8 INTERFERENCE IN THE 2690-2700 MHz RADIO ASTRONOMY BAND FROM THE EXPERIMENTAL BROADCASTING SATELLITE  
ATS-6: Frank J. Kerr, University of Maryland, College Park, Maryland; and H. Hvatum, National Radio Astronomy Observatory, Green Bank, West Virginia

The ATS-6 satellite carries a high power television transmitter operating at a frequency close to the 2690-2700 MHz radio astronomy band. Some of the radiation spills into this band. Observations of the satellite have been made, showing an interference level at the edge of the radio astronomy band 13-15 dB above the level stated in CCIR Report 224-2.

3-9 INTERFERENCE IN THE 1660-1670 MHz RADIO ASTRONOMY BAND FROM METEOROLOGICAL SATELLITES SMS-1 AND SMS-2: H. Hvatum, J. L. Dolan, and C. R. Moore, National Radio Astronomy Observatory, Green Bank, West Virginia

The two geostationary meteorological satellites SMS-1 and SMS-2 transmit weather pictures with a 28 megabit per second signal modulating a 1681.6 MHz carrier. The modulation envelope as well as cross-products among various telemetry carriers and the picture carrier spill into the 1660-1670 MHz radio astronomy band. The radiation from the two satellites has been observed with the NRAO 140-foot telescope. In both cases there are portions of the radio astronomy band where the radiation exceeds the level stated in CCIR Report 224-2 by about 4 dB.

INTEGRATED AND FIBER OPTICS - II

URSI COMMISSION VI

Tuesday, October 21 1330

URSI Session VI-5, Radio Building Auditorium

Co-Organizer: R.L. Gallawa, OT/ITS

Co-Organizer and Chairman: D.C. Chang,

University of Colorado

5-1 GUIDED WAVE OPTICAL DEVICES: E. G. Lean, IBM  
Thomas J. Watson Research Center, Yorktown Heights,  
New York

Some guided wave optical devices have proven to be advantageous over their bulk wave counterparts because of the high efficiency in guided wave structures and the possibility of planar fabrication in integrated forms. The recent results in grating-coupled GaAs lasers, thin film acousto-optic and magneto-optic devices, and thin film waveguide structures in our laboratories will be presented. Their limitations and possible applications will be included.

5-2 UTILIZATION OF  $Ga_{1-x}Al_x$  AS LAYERS FOR OPTICAL WAVEGUIDE CIRCUITS: M.K. Barnoski, Hughes Research Laboratory, Malibu, California

Future guided wave optical circuits fabricated in  $(Ga Al)As$  must be compatible with the spectral attenuation characteristics of low loss glass fiber waveguides. Currently, this requires that the source wavelength be either near 1.06  $\mu m$  [ $(Ga In)As$ ] or in the 0.8 to 0.9  $\mu m$  range [ $(Ga Al)As$ ]. Waveguiding has been experimentally observed in graded  $Al$  concentration, single layers of  $Ga_{1-x}Al_x$  As grown on  $Ga As$  substrates, with absorption coefficients of  $\alpha = 0.17 \text{ cm}^{-1}$  at 1.15  $\mu m$  wavelength and  $\alpha = 1.5 \text{ cm}^{-1}$  at 0.93  $\mu m$  wavelength indicates that  $Ga_{1-x}Al_x$  As waveguides can be used as transmission line links between active devices in a guided wave optical circuit using  $(Ga In)As$  sources. The experimental result obtained at 0.93  $\mu m$  wavelength indicates that band edge absorption in  $(Ga Al)As$  may be a problem for operation at wavelengths compatible with  $(Ga Al)As$  sources. These results will be discussed in detail during this talk.

5-3 INFRARED WAVEGUIDE MODULATOR WITH ONE WATT  $TEM_{00}$  TRANSMITTED POWER: P.K. Cheo, D. Fradin, and R. Wagner, United Technologies Research Center, East Hartford, Connecticut

Efficient coupling of up to 1.2 watts of  $\text{CO}_2$  laser light through GaAs thin-slab waveguides has been obtained. These waveguides are being developed as the electrooptic media for modulation of infrared laser light at microwave frequencies. The waveguides, which are approximately  $25\mu$  thick, are chemo-mechanically and ion-beam thinned with one face bonded onto a flat copper baseplate which serves as a supporting substrate as well as the ground plane for a microwave traveling-wave transmission line. The measured total insertion loss for the  $10.6\mu$   $\text{TE}_1$  guided-wave mode is  $3.8 \text{ dB/cm}$  which includes the loss of two couplers ( $\alpha_c = 1.7 \text{ dB}$ ). Input and output couplings are accomplished by means of two Ge prisms. The measured propagation loss  $\alpha_p$  is  $2.1 \text{ dB/cm}$ , which is consistent with the calculated (P.K. Cheo, et al., *Appl. Opt.* 12, 500, 1973) loss value for the  $\text{TE}_1$  mode in a metal-cladded waveguide. Loss mechanisms responsible for propagation and excitation of various guided-wave modes will be discussed. Effects of coupler types, waveguide tolerance, metal cladding and material imperfections on optical transmission, and output beam quality will be detailed.

5-4 A METHOD FOR MEASURING THE REFRACTIVE INDEX PROFILE OF INTEGRATED OPTICAL WAVEGUIDES: T. Itoh,  
Department of Electrical Engineering, University of Illinois, Urbana, Illinois

Non-destructive determination of the refractive index profile of an optical waveguide is an important problem in integrated optical circuits, because the propagation characteristics of the guide are strongly dependent on the profile function. Itoh and Mittra have recently reported a method for this determination based on the holographic technique combined with a parameter optimization technique. In their method, a planar M-layered dielectric waveguide is illuminated from its exterior by a plane wave, and the amplitude and the phase of the specularly reflected wave are recorded holographically as a function of incident angles. The so-called performance index for the optimization algorithm is defined by

$$F = \sum_{i=1}^N |\rho(\theta_i, \epsilon_m, \sigma_m, d_m, m=1,2,\dots,M) - \rho_0(\theta_i)|^2 \quad (1)$$

where  $\rho_0(\theta_i)$  is the measured complex reflection coefficient with the incident angle  $\theta_i$ ,  $i=1,\dots,N$  and  $\rho$  is the computed reflection coefficient for the trial parameters; dielectric constant  $\epsilon_m$ , loss factor  $\sigma_m$ , and thickness  $d_m$  of the  $m$ -th layer. A set of  $\epsilon_m$ ,  $\sigma_m$  and  $d_m$  which gives the minimum value of  $F$  are considered to be the parame-

ters in the actual waveguide. In this paper the procedure is modified so as to simplify the measurements. Since the phase measurement is difficult at optical frequencies, only the amplitude measurements are retained in the new procedure. Hence, instead of the complex reflection coefficients  $\rho$ , only the power reflection coefficients are used in (1). To compensate for the accuracy lost by the abolishment of phase measurements, the results for both E- and H-polarization cases are included. Numerical experiments have been performed, and it is seen that the accuracy in this new procedure is comparable to that of the previous one.

5-5 DIFFUSE BOUNDARY EFFECTS ON LEAKY-WAVE PROPAGATION IN INTEGRATED OPTICAL WAVEGUIDES: K. F. Casey, Department of Electrical Engineering, Kansas State University, Manhattan, Kansas

Propagation of leaky waves in integrated optical waveguides comprising a dielectric layer joined to a substrate by an inhomogeneous transition region is considered. The characteristic equation for the structure is found by expressing the fields in the transition layer in terms of solutions to Hill's equation, and is analyzed for the permittivity configuration which allows only leaky waves to exist on the structure. The propagation and attenuation constants of the leaky modes are determined using a perturbation analysis and it is found that, while the propagation constants are negligibly affected, the attenuation constants are significantly increased by the presence of the transition layer. When the transition region is absent, the TE modes are less strongly attenuated than the TM modes. As the thickness of the region increases, the attenuation constants of the TE leaky modes rapidly increase while those of the TM modes increase more slowly. When the transition region becomes electrically thick, the attenuation constants of the two mode types become identical.

5-6 LEAKY-WAVE COUPLER FOR INTEGRATED OPTICS: C. Yeh, Electrical Sciences and Engineering Department, University of California, Los Angeles, California; and K. F. Casey, Electrical Engineering Department, Kansas State University, Manhattan, Kansas

Optical coupler is an essential component in integrated optics. When two optical dielectric waveguides whose core media have higher dielectric constants than the

surrounding media are placed side by side with each other and separated by a distance,  $d$ , exchange of energy between guided modes along these guides with similar propagation constants occurs. This effect has been used successfully in the design of optical guided-wave couplers. However, in many important physical situations the dielectric constant of the core region is lower than that of the surrounding media. In this case guiding of the optical wave with low-loss (the leaky modes) may still be present if the dimensions of the core are large compared with the wavelength of the guided light. The purpose of this presentation is to consider the problem of mode coupling between two parallel leaky guides. Detailed coupling characteristics of this leaky-wave coupler will be given.

5-7 HIGHER ORDER INTERACTIONS IN PERIODIC MEDIA: FLOQUET AND COUPLED WAVES APPROACH: D. L. Jaggard and C. Elachi, Jet Propulsion Laboratory, California Institute of Technology, Pasadena, California

We consider wave propagation in sinusoidally periodic media near the first and higher order Bragg resonance using the Floquet theory, a truncated Floquet theory, and an expanded coupled waves (ECW) approach. The standard coupled waves approach gives a physical feel for wave propagation in periodic media near the first Bragg resonance but does not account for higher order interactions. The ECW approach remedies this problem and predicts coupling coefficients  $\chi$  which vary as  $\eta^n$  where  $\eta$  is the magnitude of the periodic perturbation and  $n$  is the order of the interaction. It also gives the band gaps shift away from the exact Bragg frequencies. The results for the second and third order interactions using the ECW method agree well with the ones of the other two methods even for  $\eta$  close to 1. We also investigated the case of non-sinusoidally periodic media where competing processes occur at the high order interactions between the different Fourier components. The results of this study are useful in the calculation of the threshold gain in higher order distributed feedback lasers, higher order filtering, and the propagation of pulses in periodic media.

5-8 SCATTERING AT A CURVATURE DISCONTINUITY IN AN OPTICAL WAVEGUIDE: Edward F. Kuester and David C. Chang, Electromagnetics Laboratory, Department of Electrical Engineering, University Colorado, Boulder, Colorado

At present, continuous radiation of a surface wave propagating around a curved section of an open waveguide is a relatively well-understood phenomenon. Less thoroughly investigated, however, has been the radiation which occurs at a discontinuity in curvature, e.g., at a transition between a straight and a curved section of waveguide. Here, this problem is analyzed by replacing the Hankel functions which describe the propagation on the curved section by their (Debye) asymptotic forms, with the result that an approximate or "asymptotic" continuous mode spectrum for the curved guide appears, permitting a strong (although not complete) analogy to be made with a straight waveguide. This approach also allows examination of each curvature discontinuity separately, whereas nearly all previous approaches must analyze two such junctions together and separate the interaction effects. The relative contributions of continuous radiation and curvature discontinuity scattering to the total radiation loss will be evaluated for the case of a simple optical waveguide structure.

5-9 BEND RADIATION FROM SINGLE AND MULTIMODAL FIBERS:  
A.Q. Howard, Jr., U.S. Department of Commerce,  
Office of Telecommunications, Institute for Tele-  
communication Sciences, Boulder, Colorado

Using general expressions for the field components in an optical fiber, a simple but exact expression for the radial wave impedance is obtained. Radiation loss is described simply in terms of this quantity. The unknown in the impedance is the logarithmic derivative of a modified radial wave function. For a bent fiber, this function must be calculated anew. This is done by replacing fiber curvature with a straight fiber in a fictitious medium which is inhomogeneous in the plane of the bend. For a gently curved fiber, the medium is slowly varying and the WKB method is used to approximate the radial dependence. The radiation loss per unit length is calculated by collecting the power flux over a surface concentric to the fiber. This technique allows mode orthogonality to simplify the relevant multimoded case in a perturbation formalism.

SCATTERING - II  
URSI COMMISSION VI

Tuesday, October 21 1330  
URSI Session VI-6, Radio Building 1107  
Chairman: P.L.E. Uslenghi,  
University of Illinois at Chicago Circle

6-1 SCATTERING BY LINEARLY VIBRATING OBJECTS:  
R. E. Kleinman and R. B. Mack, Microwave  
Physics Laboratory, Hanscom AFB, Massachusetts

The scattering problem for a plane wave incident upon a perfectly conducting linearly oscillating object is investigated both theoretically and experimentally. The theoretical analysis, accurate to order  $v/c$  where  $v$  and  $c$  are the velocities of object and light, respectively, shows that the target oscillation changes the scattered far field of a motionless target only in phase. The oscillation is assumed to be periodic which impresses the same period on the modulation of the scattered field. Spectral analysis of the modulation shows that the power distribution varies with the shape of the motion, wavelength of the incident field, and magnitude of the projections of the oscillation in the direction of incidence and receiver. Power spectra have been calculated for square, triangular, and sinusoidal target motion and, in general, the power content in the higher harmonics is found to increase with carrier frequency and magnitude of oscillation. For backscattering from an object moving sinusoidally along the direction of incidence, the power in the first harmonic is shown to exceed that at the carrier frequency when  $d > .23\lambda$  where  $d$  is the magnitude of the oscillation. These calculations are shown to agree with experimental measurements of the phase modulation of the field scattered from a vibrating disk at X-band. Experimental results were obtained with a cw backscatter equipment at 10 GHz that utilized separate tunnel antennas for transmitting and receiving. The receiving section of this equipment was modified to separately display phase modulation and amplitude modulation characteristics of the backscatter signal in both time and frequency as well as characteristics of the overall modulation envelope. Phase modulations introduced by target oscillators as small as  $\pm 0.005''$  were readily detected, as were amplitude modulations of a few per cent.

## 6-2 ON THE FOCUSING EFFECT OF A GAUSSIAN BEAM IN AN INHOMOGENEOUS MEDIUM: S. Kozaki, Faculty of Engineering, Gumma University, Kiryu, Japan

Theoretical investigations on the propagation of an infinite plane wave in an inhomogeneous medium have been published by many writers. However, under practical and experimental conditions, we are always concerned with more or less bounded beams rather than with infinitely extended plane waves.

A study on propagation of the beam in the inhomogeneous medium has not yet been done both theoretically and experimentally. For the purpose of radio and optical propagation, it is useful to study the behavior of a beam in the inhomogeneous medium. A fundamental problem where a Gaussian beam is obliquely incident on the inhomogeneous medium, whose permittivity decreases linearly, is theoretically analyzed. With increasing propagation distance, the amplitude of the beam becomes increasingly stronger and a very narrow beam is also obtained (focusing effect). In order to corroborate the validity of the theory, a model experiment was performed in the millimeter wave region. Thus the predicted strong increase of the field intensity was observed by measuring the beam along the ray path, so that the focusing effect was also experimentally corroborated.

In the analysis the equiphasic front of the incident and reflected beam in the inhomogeneous medium is also found to have the concave and convex surface respectively. Thus the inhomogeneous medium for the beam acts as a concave or convex lens.

## 6-3 ELECTROMAGNETIC PENETRATION THROUGH SMALL APERTURE IN CYLINDRICAL SHIELD STRUCTURE: S. Sandness and C. T. A. Johnk, University of Colorado, Department of Electrical Engineering, Boulder, Colorado

The problem of electromagnetic penetration through a small aperture into a conducting cylindrical structure of finite length was studied theoretically and experimentally. Energy from a plane wave arriving at arbitrary incidence was coupled through the aperture to excite an interior coaxial structure terminated in a diode detector feeding an output indicator. Response measurements on a pattern range yielded reasonable agreement with a solution by Harrison and Taylor, modified to cover arbitrary angles of incidence. Experimental evidence revealed thin-wire

antenna theory inadequate to the cylindrical system of 0.1 wavelength diameter, showing a distinct pattern change with azimuthal orientation. An optic fiber data link provided decoupling of the cylindrical structure from the pattern recorder system to yield reliable patterns.

6-4 ELECTROMAGNETIC PENETRATION THROUGH DIELECTRIC-SHEET-COVERED SLOTTED SCREEN: Chalmers M. Butler and G. Cooke Lewis, Jr., University of Mississippi, University, Mississippi

An approximate theory is developed for analysis of the problem of electromagnetic penetration through covered slots in infinite screens. Both infinite and finite length slots, which are covered with very thin dielectric (lossy) sheets, are considered. Integral equations are formulated and are solved numerically for the transverse electric field in the covered slots. Numerical data are presented for slots of various widths as well as for different characteristics of dielectric sheets.

6-5 SCATTERING BY MULTI-LAYERED LOSSY PERIODIC STRIPS: Leonard L. Tsai and T.K. Wu, University of Mississippi, University, Mississippi; and Joseph T. Mayhan, M.I.T. Laboratories, Lexington, Massachusetts

Scattering by multi-layered sheets consisting of periodic metal strips interlaced with thin lossy dielectric slabs using integral equation techniques. The strips are infinitely long. Broadside incidence by a plane wave TM to the strip edge is assumed. Applications of the method proved useful for phase-delay-type strip artificial dielectrics. By equating the complex transmitted field between the strip medium and an equivalent actual dielectric slab, for increasing slab thicknesses, the index of refraction can be found. Results thus obtained show excellent agreements with those obtained by classical techniques and measurements. By taking into consideration the conductivity of the lossy dielectric slab region, which simulates the support medium for the metal strips, the power losses in artificial dielectric is now also quantitatively predicted. The integral equations are derived by relating the induced currents to the tangential electric field through equivalent "surface" impedance functions. Their solution is obtained using Fourier series expansions over each sheet and periodicity properties. The resulting matrix ele-

ments require no numerical integration nor special functions. Currents induced on the sheets consisting of air metal-strips are also considered in detail. Convergence is quite rapid in that typically 5 to 7 modes prove sufficient for cell widths  $< 0.5\lambda$ . The results for two-layers-very-close-together converge to the one layer result with no numerical instabilities. Representative current variations are also presented for structures possessing up to nine layers.

6-6 SCATTERING OF A PLANE WAVE BY AN INFINITE RECTANGULAR WIRE MESH: D. A. Hill and J. R. Wait, ITS/OT and ERL/NOAA, U. S. Department of Commerce, Boulder, Colorado

A doubly infinite set of linear equations for the currents induced on a pair of planar wire grids has been found applicable for both the unbonded and the bonded mesh. When the two planar arrays are separated by at least a wire diameter (unbonded mesh), the reflection and transmission properties are highly dependent on the azimuthal and elevation incidence angles. When the arrays are coplanar (bonded mesh), the properties are essentially independent of the azimuthal incidence angle. This behavior is in agreement with one set of previously published theoretical and experimental data, but in disagreement with some more recently published theoretical results. A difficulty in the solution of the bonded case is that many terms are required to accurately represent the current and achieve convergence. However, it is found that when convergence is obtained, the expected current and charge conditions at the wire junctions are satisfied. These conditions do not have to be imposed separately.

6-7 SCATTERING FROM LOSSY DIELECTRIC BODIES OF REVOLUTION: Leonard L. Tsai and T.K. Wu, University of Mississippi, University, Mississippi

The scattering properties of lossy dielectric bodies of rotational symmetry are analyzed by the surface integral equation technique. From Maxwell's equations, Green's theorem and boundary conditions two coupled vector integral equations are formulated. The unknown surface currents (both electric and magnetic) are then solved by first Fourier decomposition and then flat pulse expansion with point matching. For a high permittivity sphere the electric currents agree with the perfectly conducting sphere currents calculated by others. Once the surface currents are found, the scattered fields in the far and

near zone may readily be determined as well. Surface currents on homogeneous dielectric cone-sphere body are also obtained to illustrate the arbitrary geometry capabilities of this integral equation technique. Applications of this theory should be of use for improved rain drop models and electromagnetic hazards to biological bodies.

6-8 THEORY AND EXPERIMENT FOR SCATTERING FROM SUBSONIC AIRFOILS: K. M. Mitzner, S. S. Locus, and H. C. Heath, Northrop Corporation, Aircraft Division, Hawthorne, California

A theoretical and experimental study was made of far field backscatter from NACA Series 00 airfoils, which are widely used in helicopter design. The study was made in the frequency range where the leading edge radius is small compared to the wavelength but not so small that the airfoil behaves like a flat strip. Physical Theory of Diffraction (PTD) was used for the theoretical work. For E perpendicular to the airfoil cross section, the scattered field can be represented as the sum of three effects: A physical optics term, a Ufimtsev edge diffraction term for the trailing edge, and a correction term which accounts for the deviation of the surface current near the leading edge from the physical optics value. As the frequency increases, the importance of the correction term decreases. For H perpendicular to the airfoil cross section, there is a fourth significant effect: a wave returned from the leading edge which accounts for the small amount of scattering that is observed when the airfoil is viewed from behind. Creeping of the edge-diffracted wave along the surface is also significant for this polarization and thus the edge diffraction term persists at observation angles where the trailing edge is not geometrically illuminated.

CELLULAR AND MUTAGENETIC EFFECTS  
URSI COMMISSION I (BIOLOGICAL EFFECTS)

Tuesday, October 21 1330  
URSI Session B-4, UMC West Ballroom  
Chairman: D. McRee, National Institute of  
Environmental Health Sciences

B4-1 RESPIRATORY ACTIVITY OF MITOCHONDRIA EXPOSED IN A COAXIAL AIRLINE TO 2000-4000 MHz MICROWAVE RADIATION: J. A. Elder, J. S. Ali, and M. D. Long, Environmental Protection Agency, Experimental Biology Division, Research Triangle Park, North Carolina

A system was developed to continuously circulate mitochondria through a coaxial airline and oxygen electrode cell so that (1) mitochondria were exposed to microwave radiation while biochemically active, i.e., at 30°C and (2) respiration was measured as the mitochondrial suspension flowed from the airline. Rat liver mitochondria were irradiated for approximately 10 minutes at three frequencies (2450, 3000, and 3400 MHz) at a high absorbed dose rate and at a low dose rate to the frequency range of 2000-4000 MHz at sweep times of 0.1 and 30 sec. The volume of the airline was 14.5 ml; the total volume of the system was 22.5 ml. The absorbed dose rate in the sample within the airline was 41 W/kg at higher power. The absorbed dose rate in the sweep experiments varied with frequency from 1.7 to 2.3 W/kg. The temperature of the sample entering and leaving the airline and in the oxygen electrode cell was measured with thermocouples. The rates of respiration, respiratory control ratios, and ADP/Oxygen ratios were determined at 30°C with succinate, pyruvate, and  $\beta$ -hydroxybutyrate as substrates. No difference in respiration and oxidative phosphorylation of control and irradiated mitochondria was observed.

B4-2 THE EFFECT OF MICROWAVES (2450 MHz) ON LYMPHOCYTE BLAST TRANSFORMATION IN VITRO:  
Ralph J. Smialowicz, Experimental Biology Division, Health Effects Research Laboratory, U.S. Environmental Protection Agency, Research Triangle Park, North Carolina

The proliferative capacity of lymphocytes that are responsible for cellular immune responses (T cells) and humoral immune responses (B cells) was examined following exposure *in vitro* to microwave radiation at

2450 MHz. Spleen cells from BALB/c mice were cultured in 35 x 10 mm plastic dishes maintained at 37°C in a temperature controlled exposure chamber during irradiation for 1-4 hours at an absorbed dose rate of approximately 19 W/kg. Following irradiation the temperature of the cultures did not differ appreciably from controls and cell viability was comparable in both cultures. The ability of exposed lymphocytes to undergo blast transformation in response to mitogens that selectively stimulate either T or B cells was followed by incorporation of  $^3\text{H}$ -thymidine into nucleic acid. No consistent difference was found between the blastogenic response of microwave-irradiated and control splenic lymphocytes cultured in the presence of the mitogens phytohemagglutinin, pokeweed mitogen, concanavalin A, or E. coli lipopolysaccharide.

B4-3 MICROWAVE PERTURBATION ON CELLULAR ENZYMATIC REACTIONS: S. T. Hsieh and Y. J. Seto, Tulane University, New Orleans, Louisiana

In a previous study it was shown that an externally imposed time varying electromagnetic field can be used to modify a planar localized enzymatic system isothermally in such a manner that the modification reflects in a modified Michaelis-Menton constant for charges substrate consumption rate. This paper extends the analysis to account for observed microwave-induced cellular growth effect. It is known that the main energy production pathway for a facultative non-photosynthetic micro-organism is respiration, and that the respiratory apparatus is localized at the inner wall of a prokaryotic cell. The respiratory intermediates are derived from glycolysis and exist in ionized states thus are vulnerable to the influence of electromagnetic fields. Theoretically, a three-dimensional spherical cell model for extra and intra-cellular nutrient transports was invoked. Externally applied electromagnetic field interacting with the transport process of charged nutrient substrates were examined using a perturbation approach and Green's function technique. Solutions correct to second order were obtained. Taking into consideration the localization of respiratory enzymatic systems, a microwave-induced rf-diffusion effect on substrates was found to modify the nutrient consumption rate. The modified Michaelis-constant in the Monod growth rate equation

was shown to alter the batch growth pattern at the deceleration phase isothermally. Analytical results were found to have good agreement with the observed changes of growth pattern in E. coli under low intensity microwave perturbation.

B4-4 A SUMMARY OF CELL AND TISSUE LEVEL EVENTS PRODUCED BY RF FIELDS PREDICTED FROM CONSIDERATION OF REGIONAL HYPERTHERMIA: J.W. Frazer, USAF School of Aerospace Medicine, Brooks AFB, Texas

One of the effects of absorption of electromagnetic energy in any object is an increase in collision probability of its constituent molecules, leading to the production of heat in the statistical mechanical sense. Even in relatively homogenous absorbers, the distribution of this heat is not uniform throughout the absorber, but is critically dependent on the size of the absorber relative to wavelength, the field impedance, and the electrical characteristics of the absorber. Prediction of one set of biologic results from exposure to such a field is dependent on knowledge of the regional thermal environment, and also knowledge of the tissue response to such thermal environment. One set of such interdependencies is outlined by Chamness, et al., showing that release of metals from one organ leads to uptake by another. Other sets of events are becoming clearer as a result of studies of the prospective application of hyperthermia to the treatment of cancer. It has been shown that shifting of division cycling in cultured tumor cells occurs, and in tumors in animals exposed to hyperthermia. Similar events have been seen with many types of normal cells extracted from animals exposed to a variety of electromagnetic fields. Another corollary, as yet unexamined in RF fields, is loss of intracellular materials from such cells, already known to occur, for example, in exercise leading to muscle hyperthermia.

B4-5 EFFECTS OF MICROWAVE RADIATION ON MAMMALIAN CELLS IN VITRO: James C. Lin, Department of Electrical Engineering, and Kuo C. Chen, Department of Biology, Wayne State University, Detroit, Michigan

One of the most pressing and fundamental questions concerning the effects of microwaves on biological systems is the nature of the intrinsic effect of non-ionizing radiation. To attack this problem, we have recently developed a bioengineering approach to

differentiate the thermal and non-thermal factors of microwaves acting on mammalian cells in culture. Cells of a Chinese hamster somatic cell line, V79-122D1, derived originally from the lung of a male animal, were synchronized by treating cells with a suitable concentration of hydroxymen in conjunction with the mitotic shake-off technique. The synchronized cell populations were then exposed to 2450 MHz radiation of both low and high intensities in a wave-guide chamber. The biologic effects of microwave radiation on these cells were shown to be a function of incident and absorbed power densities and duration of exposure. The possibility of non-thermal involvement in the radiation effect at cellular level will be discussed. The present experiments could provide a model system for future studies of the molecular mechanisms of microwave-induced biologic effects in living systems.

B4-6 EVALUATION OF DOMINANT LETHAL TEST AND DNA STUDIES IN MEASURING MUTAGENICITY CAUSED BY NON-IONIZING RADIATION: Man M. Varma and Eric A. Trabculay, Jr., Department of Bio-Environmental Engineering and Sciences, Howard University, Washington, D.C.

Fifty-six day old Swiss mice (Charles River Breeding Laboratories, Massachusetts) were exposed to microwave radiation. In total, two dominant lethal tests and three DNA studies were conducted. In the first experiment of the dominant lethal test, the mice were exposed to 1.7 GHz, 50 mW/cm<sup>2</sup> for 30 minutes and in the second experiment, the mice were exposed to 1.7 GHz, 10 mW/cm<sup>2</sup> for 80 minutes. In the first experiment of the DNA studies, the mice were exposed to 1.7 GHz, 50 mW/cm<sup>2</sup> for 30 minutes; in the second, 1.7 GHz, 10 mW/cm<sup>2</sup> for 80 minutes; and in the third, 0.985 GHz, 10 mW/cm<sup>2</sup> for 80 minutes.

In the dominant lethal test, mice exposed to 1.7 GHz, 50 mW/cm<sup>2</sup> showed that mutagenicity was significant at the 99 percent level in the third week and at the 95 percent level in the fourth, fifth, and sixth weeks. The parallel DNA study showed a change in the Tm from 87°C in the control to 85°C in the irradiated group, with subsequent changes in the based composition and asymmetry ratio. In the second dominant lethal test, mutagenicity was significant at the 99 percent level in the fifth week and at the 95 percent level in the first, second, third, and sixth weeks. The parallel DNA study

showed changes in the  $T_m$  ( $86^{\circ}\text{C}$ ), base composition, and asymmetry ratio.

A third DNA study was performed at 0.985 GHz,  $10 \text{ mW/cm}^2$  for 80 minutes and similar changes in the  $T_m$  ( $85.5^{\circ}\text{C}$ ), base composition, and asymmetry were observed. The change in the optical density of the irradiated DNA supports the possibility that irradiation causes strand separation and reflects a decrease in hydrogen bonding. A point mutation would then result if there is imprecise base matching.

**B4-7 MUTAGENICITY INDUCED BY NON-IONIZING RADIATION IN SWISS MALE MICE:** Man M. Varma, Elbert L. Dage, and R. Joshi, Bio-Environmental Engineering and Sciences Research Laboratory, School of Engineering, Howard University, Washington, D.C.

Testes of male mice were irradiated to microwaves at 2.45 GHz in three experiments: (1) at  $100 \text{ mW/cm}^2$ , a single exposure of 10 minutes; (2) at  $50 \text{ mW/cm}^2$ , three exposures of 10 minutes each in one day; and (3) at  $50 \text{ mW/cm}^2$ , four exposures of 10 minutes each during two weeks. Treated males were tested by the dominant lethal assay for mutagenicity by mating them with untreated females for six weeks. Fertility was not impaired following irradiation but mutagenicity induced was significantly higher subsequent to single exposure and multiple exposures during one day. No effects were observed when multiple exposures were extended over a period of two weeks. Suggesting that high-level acute exposures are potentially more hazardous than chronic exposures at lower power densities.

**B4-8 THE EFFECT OF MICROWAVE EXPOSURE ON BACTERIA: MUTATION INDUCTION:** C. F. Blackman, M. C. Surles, and S. G. Benane, Environmental Protection Agency, Experimental Biology Division, Research Triangle Park, North Carolina

The mutagenic potential of continuous wave electromagnetic radiation at 1.70 and 2.45 GHz was examined with a strain of the bacterium, *E. coli*, which can be used to detect both forward and reverse mutations. Log phase cultures of the bacterial strain were placed in 35 mm diameter sterile plastic tissue culture dishes and irradiated for 3 to 4 hours at  $35^{\circ}\text{C}$ . Exposures at 2.45 GHz were conducted at far field power densities of 10 and  $50 \text{ mW/cm}^2$ , which

correspond to absorbed dose rates of 14 and 69 W/kg, respectively. Exposures at 1.70 GHz, at a near field power density of 2.0 SW/cm<sup>2</sup>, were estimated to correspond to an absorbed dose rate of 2.8 W/kg. Sensitivity for mutation induction was optimized by exposing the bacteria during at least one complete DNA replication cycle. Although positive controls using ultra violet light demonstrated the expected exponential survival curve and increase in mutation induction, no mutagenic activity could be demonstrated for either microwave frequency under the conditions employed.

## EXPOSURE SYSTEMS

URSI COMMISSION I (BIOLOGICAL EFFECTS)

Tuesday, October 21 1330

URSI Session B-5, UMC East Ballroom

Chairman: M. Shore,

Bureau of Radiological Health

B5-1 DEPENDENCE OF TOTAL AND DISTRIBUTED ABSORBED MICRO-WAVE ENERGY UPON SIZE, SHAPE, AND ORIENTATION OF RAT PHANTOMS IN WAVEGUIDE: Aurelija Leicher-Preka, Institute Physiological Biochemistry Medical Facility, Sarajevo, Yugoslavia; and Henry S. Ho, Division of Biological Effects, BRH, FDA, DHEW, Rockville, Maryland

Since the size and shape of the rat as well as its position and orientation in the waveguide influence the absorbed dose, possible absorbed dose related effects of microwaves on the central nervous system of rats exposed whole-body in a waveguide should account for these factors. This work investigates the relationship between the total and distributed absorbed energy in rat phantoms and their sizes and orientations in a waveguide exposed to 2450 MHz microwave radiation. Six models of tissue-equivalent materials are used to simulate the sizes and shapes of rats that are 1, 4, 10, 23, 30, and 60 days old. The measurements are made with all models at the center of the waveguide oriented facing (0°) and opposite to (180°) the direction of the incident wave. For the two smaller models, the orientation is also varied step-wise from 0° to 180°. The patterns of absorbed energy in the cross sections of the phantoms are studied using a thermographic camera. The result indicates that changes in size, shape, and orientation of exposed animal models produce changes in total and distributed absorbed energy. Although the total absorbed energy changes only slightly between the 0° and 180° orientation, there exist large differences in the distribution of absorbed energy in the animal phantoms. With the phantom head facing the incident radiation, in most cases, the head area, including the brain, absorbs the most microwave energy. In the opposite orientation, the maximum absorption concentrates on the tail and abdominal regions. It is concluded that in addition to determining the total absorbed energy, the determination of the distribution of absorbed energy in animal bodies can be important in the interpretation of observed biological and psychological effects.

B5-2 CONSIDERATIONS OF CHAMBER DESIGN, ENVIRONMENTAL CONTROL, AND MICROWAVE FIELD INTERACTIONS IN SMALL ANIMAL EXPERIMENTATION: William M. Houk, James D. Grissett, and Andrew Longacre, Jr., Naval Aerospace Medical Research Laboratory, Pensacola, Florida, and University of New Orleans, New Orleans, Louisiana

The criteria for design and performance of a facility utilized for studying microwave biological effects in rats up to 500 gm in size are presented. The results of using a 1.2 x 1.2 x 1.2 m semi-enclosed anechoic exposure chamber including field measurement techniques, material selection, environmental control, and biological experimental design are discussed, with an analysis of the problems encountered in its use. The problems are related to certain biological parameters studied in a finite experiment dealing primarily with environmental control, field measurements, and the use of several subjects in the enclosure simultaneously. Using the same basic design and performance criteria as the first experimental chamber, a second larger and more sophisticated semi-enclosed anechoic chamber, 1.8 x 1.8 x 1.8 m in size was constructed in the microwave facility at the Naval Aerospace Medical Research Laboratory. This chamber addressed environmental control and microwave field parameters from its inception. Absolute requirements were: (1) for a 2450 MHz microwave reference field located in the far field of a 15 dB standard gain horn showing no greater than  $\pm 1.0$  dB variation over a  $100 \text{ cm}^2$  working area; (2) for absolute temperature control of the environment where the experimental animals were located, in a range of 12.5 to  $45^\circ\text{C}$ , and control of  $\pm 0.5^\circ\text{C}$  at the selected control point; and (3) for uniform air flow over the experimental animals with provision for dumping chamber air rather than recirculating it. Using the NBS XD-1 and EMD-1C microwave sensors, details of the field pattern alterations induced by polystyrene foam products used in the construction of animal enclosures will be presented along with a standardized method of measuring exposure levels. Using analogous techniques, field amplitude patterns around single and multiple experimental animals were derived along with energy absorption estimates made from standing wave patterns created by the animals.

B5-3 CHRONIC EXPOSURE OF A RAT POPULATION BY CIRCULARLY POLARIZED GUIDED WAVES: A. W. Guy, C. K. Chou, and R. H. Lovely, Bioelectromagnetics Research Laboratory, Department of Rehabilitation Medicine, University of Washington, School of Medicine, Seattle, Washington

A system has been developed for economically exposing a large portion of rodents on a long-term basis without disturbing their normal laboratory living patterns. The use of separate cells consisting of cylindrical waveguide excited with circularly polarized guided waves provides relatively constant and easily quantifiable coupling of the fields to each animal, regardless of their position, posture, and moving patterns. The VSWR to each cell is sufficiently low that any number of cells can be coupled to a single source through a power splitter without the need for isolation circuitry. Tests made on ellipsoidal phantom models of a 333 gm rat exposed in various possible shapes and positions in a 20 cm diameter exposure chamber operating at 918 MHz indicated that the subjects absorbed approximately one-quarter of the input power to the cell, regardless of position. Based on a net 1 W input (average incident power density of  $3 \text{ mW/cm}^2$ ) the average absorbed power density varied from 0.79 to 0.92 W/kg and the peak absorbed power density varied from 1.06 to 1.42 W/kg in the phantoms. Measurements were made for the total power absorption as a function of time in a 323 gm live rat exposed for many hours in the chamber. With an incident input power of 1 mW to terminal  $R_F$ , the mean absorbed power was 0.43 mW with a standard deviation of  $\pm 0.07 \text{ mW}$ .

B5-4 MICROWAVE IRRADIATION APPARATUS DESIGN AND DOSIMETRY: Henry S. Ho, Mark R. Foster, and Mays L. Swicord, Bureau of Radiological Health, Rockville, Maryland

Microwave biological and psychological effects will not only depend on external exposure conditions (frequency, field strength and distribution), but also on the distribution of absorbed energy in the specimen. This absorbed energy distribution is affected by the geometry and electrical characteristics of the specimen and the exposure conditions. The Bureau of Radiological Health has constructed in its facilities a variety of apparatus which provides means of irradiating cell samples, hamsters, mice, rats, rabbits, and monkeys and to determine the total and distributed absorbed microwave energy in exposed specimens. These devices consist of waveguides, cavity and anechoic

chambers, and dielectric lenses and are adapted to the need of individual experiments. The specimens can be whole- and partial-body irradiated individually or chronically exposed in groups. The source frequencies are 383 MHz, 915 MHz, 2450 MHz, and 10 GHz. The instrumentation for dosimetry includes phantom tissue materials, thermographic cameras, calorimeters, implantable temperature and E-field probes, and wide band dielectrometers. In order to establish meaningful dosimetric relationships between our biological experiments (quantified in absorbed energy) and health protection, we have initiated a study to determine the total and distributed absorbed energy in phantom human bodies for measured exposure fields.

B5-5 ADRENOCORTICAL RESPONSE IN RATS EXPOSED TO  
MICROWAVES: W. Gregory Lotz and Sol M.  
Michaelson, University of Rochester, Rochester,  
New York

Whole-body acute microwave (2450 MHz, CW) exposure of 120 male Long Evans rats (275-350 gms) has been carried out in the far field of a horn antenna. The rats were housed in non-restraining cages during exposure and sacrificed by decapitation immediately after exposure. Plasma collected from individual rats was analyzed for corticosterone to determine the response of the hypothalamic-hypophysial-adrenal (HHA) axis to this microwave exposure. Circulating corticosterone (CC) levels were significantly higher in rats exposed to 50 mW/cm<sup>2</sup> or 60 mW/cm<sup>2</sup> than they were in control rats, but there was no difference between the CC levels of rats exposed to 10 mW/cm<sup>2</sup> or 20 mW/cm<sup>2</sup> and control rats. Rats exposed to 30 mW/cm<sup>2</sup> or 40 mW/cm<sup>2</sup> showed an inconsistent tendency toward higher CC levels after one hour of exposure, the longest exposure used in this study. The data suggest that for 2450 MHz exposures of up to one hour, the rat HHA axis is not stimulated unless incident power densities of 30 mW/cm<sup>2</sup> or greater are used. The adrenocortical response at the higher power densities in these experiments is analogous to the adrenocortical response to other nonspecific stress stimuli, and appears to be a "thermal stress," since those power densities which result in increased CC levels also increase the rectal temperature of the rat by 1 to 3 degrees Centigrade.

B5-6 A UNIQUE ELECTROMAGNETIC ENVIRONMENTAL SIMULATOR:  
E. R. Graf and D. G. Burks, Electrical  
Engineering Department, Auburn University,  
Auburn, Alabama; and F. E. Cole, Ochsner  
Medical Fnd., New Orleans, Louisiana

An unique electromagnetic environmental simulator designed for investigations on the molecular and microorganism level will be discussed. An active zone 1" x 1" x 1" is provided for the exposure of the sample. A capability to simulate lightning at a regulated rate is provided. The earth's magnetic field, both d.c. and low frequency components, can be simulated. Low frequency electric and magnetic fields perpendicular to each other and mutually parallel to the earth are also provided. All electric and magnetic fields are continuously variable with the capability to control their relative phase in 90° steps. The arc is generated by a 75KV potential, other electric and magnetic fields reach values of 40KV/m and 650 gauss respectively. The range of the low frequency components was chosen as 5-15Hz. The glass test chamber is designed for gas circulation as well as for the easy interchange of the primary arcing electrode. All fields can be activated simultaneously or individually with individual control.

B5-7 FIELD MEASUREMENTS FOR A SERIES OF BEHAVIORAL STUDIES: V. R. Reno and J. O. de Lorge,  
Naval Aerospace Medical Research Laboratory,  
Pensacola, Florida

Preparations for a series of behavioral studies with rhesus monkeys included determinations of the microwave environment affecting the animals. These measurements indicated certain characteristics of the field generated by the magnetron source that may be of significance to interpretation of the results of the studies and could also be pertinent to other biological investigations. Some of the magnetrons used to generate microwave fields for biological research were originally intended for industrial heating purposes and the fields produced by these units are not necessarily identical. They have been variously described as CW, quasi-CW, modulated CW, and pulsed at some multiple of the line frequency with little additional information provided concerning

the actual waveform. The results of experiments conducted with generators producing different waveforms may not be directly comparable since differences in the temporal distribution of energy may alter the biological response. Field measurements for the present series of behavioral studies were designed to minimize this potential problem by determination of both the spatial and temporal distribution of energy incident on the animal.

---

TUESDAY AFTERNOON, OCT. 21, 1330-1630

---

RADIO METEOROLOGY--

OBSERVATIONS, MEASUREMENTS, AND THEORY

URSI COMMISSION II

Tuesday, October 21 1330

URSI Session II-4, UMC 159

Chairman: A.W. Straiton, University  
of Texas

4-1 REMOTE SENSING OF DRIZZLE: Juergen H. Richter,  
Naval Electronics Laboratory Center, San Diego,  
California

One kind of marine fog observed during the summer months in the Southern California coastal area is caused by lowering of the base of the stratus clouds while the height of the cloud tops remains unchanged. Drizzle originating in the stratus layer may account for redistribution of moisture into the drier subcloud layer and therefore may be responsible for the lowering of the cloud base. To verify this hypothesis, a remote sensing capability for drizzle at a 10-20 km range upwind is needed. This paper examines the feasibility of such a radar, its optimum design characteristics, and potential problems caused by refractivity fluctuations, ducting, and sea clutter.

4-2 DELAY AND ITS RELATION TO ATTENUATION IN  
RADIOWAVE PROPAGATION THROUGH RAIN: D. V.  
Rogers and R. L. Olsen, Communications Research  
Center, Department of Communications, Ottawa,  
Ontario, Canada

With the advent of digital communications systems in which various signals must be synchronized to within a few nanoseconds, the need has arisen to determine accurate propagation delay statistics. This paper examines the problem of calculating delays in coherent radiowave propagation through rain, and in particular, the problem of relating delay to attenuation. Although delay statistics are difficult to obtain experimentally, the calculation of delay/attenuation ratios provides a means of predicting delay statistics from existing attenuation statistics. It is shown that the delay/attenuation ratio depends only on the logarithmic

slope  $\Lambda$  of an exponential dropsize distribution  $N_o e^{-\Lambda D}$ . This implies that large " $N_o$ -jumps" in rain-drop spectra as reported recently by Waldvogel are unimportant in the ratio of these two dropsize dependent quantities. Numerical results for the frequency range 1 to 1000 GHz, obtained using Mie scattering amplitudes in Twersky's multiple scattering theory of coherent wave propagation, are presented for the Marshall-Palmer and the Laws and Parsons dropsize distributions. These computations indicate possible limitations in the use of phase and group delays to estimate true propagation delays for frequencies above about 10 GHz.

4-3 20 AND 30 GHz RAIN-INDUCED ATTENUATION RATIO VARIATIONS ON SPACE-EARTH LINKS:

Louis J. Ippolito, NASA Goddard Space Flight Center, Greenbelt, Maryland

The ratio of attenuations for two millimeter wavelength transmissions propagating through the same precipitation volume is a useful parameter for the evaluation of space channel characteristics. A knowledge of attenuation ratio characteristics can provide a means for predicting the attenuation at one frequency, given the attenuation at the another. The attenuation ratio is shown to be sensitive to drop size distribution and path length, and parametric attenuation ratio relationships are developed from existing empirical rain models for the earth-space channel. Measurements of 30 GHz to 20 GHz attenuation ratio at two locations using the ATS-6 downlink transmissions are described. The ratio is shown to vary widely with each rain period, and during the period itself. Ratio variations ranged from 1:1 to 4:1, and correlation with ground measured rainfall rate was not always evident. Finally, an improved technique for predicting attenuation ratio variations by employing long term attenuation statistics is developed, where the ratio uncertainty is reduced by a factor of six.

4-4 FM-CW RADAR WITH DOPPLER DATA PROCESSING:

R. G. Strauch, W. C. Campbell, R. B. Chadwick, and K. P. Moran, NOAA/ERL/Wave Propagation Laboratory, Boulder, Colorado

The S-band FM-CW boundary layer radar has been able to detect refractive index fluctuations in the atmosphere with a range resolution of less than 2 m. These

fluctuations are typically observed in thin layers and often show evidence of wave structure. One of the limitations of this radar has been that velocity information has not been obtained. It has been widely believed that it is extremely difficult, if not impossible, to process the FM-CW data to obtain the complete Doppler velocity spectrum for each range resolution element. However, we have been able to implement Doppler data processing on our FM-CW radar with a method that has been developed for over-the-horizon sea state radars. The theory will be presented and the technique used to implement and test it will be described. Examples of Doppler spectra in precipitation and clear air will be shown, and limitations imposed by the stability of the sweep will be discussed. Since both the first and second moments of the velocity spectra can be estimated, the addition of Doppler processing to the boundary layer FM-CW radar opens up a number of new applications for this device. In addition, the sensitivity of the radar may be significantly improved so that atmospheric returns (and their motion) may be measurable even when the layered structures are not observed. Some of these new applications will be discussed.

4-5 DOPPLER SPECTRA, TEMPORAL GROWTH, AND ENERGY TRANSPORT IN SHORT GRAVITY WAVES: W. J. Plant and J. W. Wright, Ocean Sciences Division, U.S. Naval Research Laboratory, Washington, D.C.

Doppler spectra have been measured in a windwave tank as a function of windspeed and fetch at 4.3 GHz and a bistatic configuration in which the Bragg resonant wavelength is 16.5 cm. Both downwind and upwind going waves were observed and the magnitude of the Kelvin-Helmholtz effect and advection by the wind drift deduced from measurements of their phase speed. Observations of higher order Doppler splittings and the transition to two-scale scattering are compared with theory. Spectral energy transport rates are deduced from the windspeed dependence of the first order Bragg peaks and compared with initial temporal growth rates, which were also measured, in order to elucidate the spectral energy balance responsible for short gravity wave equilibrium.

4-6 MUTUAL COHERENCE FUNCTION, COHERENCE BANDWIDTH, AND COHERENCE TIME OF MILLIMETER AND OPTICAL WAVES IN RAIN, FOG, AND TURBULENCE: S-T Hong and Akira Ishimaru, Electrical Engineering Department, University of Washington, Seattle, Washington

Two-frequency mutual coherence function is the correlation of fields at two different frequencies and at different points in time and space, and its correlation characteristics in frequency and time represent coherence bandwidth and coherence time. A parabolic differential equation for the two-frequency mutual coherence function is obtained for discrete scatterers and turbulence and an approximate solution is obtained when the wavelength is small compared with particle sizes and turbulent eddy sizes. Expressions for temporal spectra of fluctuations are also obtained. Coherence bandwidth, coherence time, and spectra are calculated for millimeter and optical waves in rain and turbulence and optical waves in fog. For rain, we used the Marshall-Palmer size distribution and compared with the results obtained by using the median size given by Laws and Parsons. For fog, we used the data calculated by Deirmendjian based on a modified gamma distribution. The results are applicable to both weak and strong fluctuation cases.

4-7 REFRACTIVE INDEX PROFILE UPDATING USING FM-CW RADAR DATA: V. R. Noonkester, K. D. Anderson, and W. F. Moler, Naval Electronics Laboratory Center, San Diego, California

Unmeasured temporal changes in the vertical refractive index structure can produce errors in the prediction of radio fields. In lieu of launching many radiosondes or making frequent in-situ refractometer measurements to determine the temporal changes, a ground-based remote sensor observing features related to the vertical refractive index profile could be used to assess changes in an initial profile. A method has been developed which uses the changes in the height of the marine layer near Southern California, as sensed by an FM-CW radar, and the changes in the surface temperature, dew point, and pressure to update the refractive index profile initially determined from radiosonde data. Assuming horizontal homogeneity, changes in the re-

fractive index profile are assumed to be caused by adiabatic motion resulting from vertical motion proportional to the height changes of the marine layer. The latent heat of condensation and evaporation is accounted for and no liquid is assumed to precipitate. The technique has been applied to a number of data periods for the California inversion conditions for time periods up to 24 hours. The extrapolated profiles of refractive index were usually more representative of the observed profiles at the end of the data period than the initial profile. The extrapolation technique and examples will be presented.

RADAR OCEANOGRAPHY--  
SEA SURFACE WINDS AND OCEAN WAVES  
URSI COMMISSION II  
Tuesday, October 21 1330  
URSI Session II-5, UMC Forum Room  
Chairman: F.T. Ulaby, University of Kansas

5-1 ACTIVE AND PASSIVE MICROWAVE MEASUREMENT OF  
SEA SURFACE WINDS BY SKYLAB S-193 RADSCAT:  
R. K. Moore, J. D. Young, J. P. Claassen, and  
M. Afarani, The University of Kansas Center for  
Research, Inc., Lawrence, Kansas; and  
W. J. Pierson, V. J. Cardone, J. Hayes, W. Spring,  
C. Greenwood, and R. Salfi, The University  
Institute of Oceanography of the City University  
of New York, Bronx, New York

The Skylab S-193 Radscat measured backscatter and emission from sea surface areas where the equivalent 20 meter elevation wind speeds ranged from calm to over 30 meters/sec. Measurements were taken in a tropical hurricane (AVA), in a tropical storm (Christine), and in portions of extratropical cyclones. The Radscat measurements were compared with independent wind estimates (surface truth) to determine the correlation between surface winds and the microwave measurements. Substantial statistical variance in the data was due to errors in the meteorological wind estimates used for surface truth. Regression analysis was used to determine empirically the relation between surface parameters and the microwave measurements, after correction for atmospheric effects. These results indicate that differential scattering coefficients are nearly proportional to wind speed raised to the 1.5 to 2 power for incident angles from 30° to 50°. Horizontally polarized scattering data show slightly more sensitivity to wind speed than vertically polarized data and the sensitivity increases with incident angle. Microwave measurements from space are shown to provide an accurate method of determining sea surface winds even for cloudy conditions. The specification of these winds on a global basis should contribute substantially to improve weather prediction.

5-2 IMPROVED MEASURE OF OCEANIC WIND FIELDS BY OTH RADAR: Joseph W. Maresca, Jr., and James R. Branum, Stanford Research Institute, Menlo Park, California

Remote measurement of the spatial mean ocean wind speeds, ranging from 4 to 21 meters per second, were obtained using Doppler spectra resolved to .08 Hz from high resolution HF sky-wave radar backscatter measurements of the ocean surface. Accuracies of 2 meters per second resulted from the correlation of observed winds over the ocean and the broadening of the Doppler spectra in the vicinity of the higher first order Bragg line. This broadening, for Doppler spectra unperturbed by the ionospheric propagation, is a direct function of the increase in power caused by higher order hydrodynamic and electromagnetic effects in the vicinity of the Bragg line. At this low spectral resolution, the higher order contributions are separate but not uniquely resolvable from the Bragg line power. Thus the region in the vicinity of the Bragg line broadens with increasing wind speed. The accuracy of the wind speed determination was significantly improved by normalizing the broadening measure by the inverse of the square-root of the radio frequency.

5-3 HIGH-RESOLUTION MAPPING OF OCEANIC WIND FIELDS BY OTH RADAR: James R. Barnum, Sidney M. Serebreny, and Joseph W. Maresca, Jr., Stanford Research Institute, Menlo Park, California

The mean surface wind field in the North Pacific Ocean was mapped on 25 and 26 September 1973 over an area of  $3 \times 10^6$  square kilometers by OTH-B HF radar. A spatial resolution of 60 kilometers in range and 15 kilometers in cross range were used at points spaced by 150 kilometers in range and 80 kilometers in cross range. Wind directions were inferred from the upwind/downwind first order Bragg ratio and the measure of the maximum ratio occurring for radial winds at points near each observation. Detailed measurements of the wind speed and direction were estimated in the vicinity of an atmospheric cold front, an extremely difficult measurement to make in the open ocean. The frontal wind velocity measurements defined the location of the atmospheric front on 25 September 1973 more accurately than the NWS Surface Maps. Range resolutions of 3 km are achieved with the WARF radar and will be essential to the analysis of atmospheric fronts and the gradient of the wind stress.

across intense cyclones. The experiment revealed that scan strategy of large areas should be designed to optimize ionospheric conditions at each measurement point, such that clutter spectra with maximum clarity can be assured.

5-4 SHORT PULSE RADAR USED TO MEASURE SWH AND SURFACE WIND SPEED: D. L. Hammond and R. A. Mennella, Naval Research Laboratory, Washington, D.C.; and E. J. Walsh, NASA Wallops Flight Center, Wallops Island, Virginia

An airborne measurement program conducted jointly by NRL and NASA Wallops Flight Center indicates that wind-speed and sea-surface significant wave height (SWH) can be measured quantitatively simply and remotely with a short pulse (2 NS), nadir looking, wide beam antenna ( $60^{\circ}$ ); 3 cm radar. A measurement program was conducted using the NASA Wallops C-54 and the NRL short pulse radar from November, 1974 to April, 1975. The measurements include data taken over a range of SWH of zero to 15 feet and range of wind speeds from five to 25 knots. The slopes of the leading and trailing edges of the averaged power envelope of the averaged received pulse are used to infer surface wind speed and SWH. The interpretation is based on theoretical models of the effects of SWH on the leading edge shape and rms sea-surface slope on the trailing edge shape. The models include radar system parameters of antenna beam width and pulse width. The results of the experiments show good agreement between the expected pulse shape and the measured pulse shape. It seems possible to design a relatively compact airborne radar to indicate an real-time the sea surface SWH and surface wind speed. The concept involves relative power measurements only and does not need a scanning antenna, Doppler filters, or absolute power calibrations.

5-5 A SCATTER THEORY FOR ANISOTROPICALLY ROUGH SEA SURFACE: A. K. Fung and H. L. Chan, The University of Kansas Center for Research, Inc., Lawrence, Kansas

A theory for radar backscatter from an anisotropic sea surface has been developed using a two-scale roughness model which is based solely upon the measured sea surface slope density function reported

by Cox and Munk and the anisotropic sea spectrum reported by Pierson and Stacy modified by Mitsuyasu and Honda. For small angles of incidence (approximately  $0^{\circ}$ - $25^{\circ}$ ), the difference in upwind, downwind, and crosswind observations are found to depend mainly on the skewness of the slope density function of the large scale waves. In particular, the small dip in the upwind-downwind ratio which occurs near the vertical is due to the fact that the most probable slope is a downwind slope. For large angles of incidence (approximately  $30^{\circ}$ - $80^{\circ}$ ) the level and the increase in the upwind-downwind ratio with the incident angle is due to the nonzero mean slope of the large-scale-wave slope density function defined in the plane perpendicular to the look direction. On the other hand, the level of the upwind-crosswind ratio is dominated by the anisotropic characteristics in the sea spectrum for the small scale waves. The interaction between the large and the small scale waves is found to cause the local minimum in the scattering coefficient versus azimuthal angle curve to shift in location. At large incident angles ( $\theta \geq 30^{\circ}$ ) the increase of the backscattering coefficients with the wind is due primarily to the growth of the sea spectrum with increasing wind speed and, to a lesser extent, to the interaction between the two scales of roughness. Comparisons with some data collected by the Naval Research Laboratory, the Skylab program, the National Aeronautics and Space Administration, Langley Research Center, show satisfactory agreements in angular trends and in some cases also in absolute level.

5-6 BISPECTRUM ANALYSIS APPLIED TO HF DOPPLER RADAR SEA-ECHOES: L. S. Fedor, NOAA/ERL/Wave Propagation Laboratory, Boulder, Colorado

The bispectrum of ocean backscattered radio waves is introduced to give a measured parameter directly proportional to the ocean wave height spectrum. Direct measurement of the ocean wave height spectrum is possible via the first order resonant backscatter power spectrum from ocean waves of wavelength equal to half the radio wavelength. However, at the frequencies of operation of the HF skywave radars ( $> 6$  MHz) the ocean wave spectra is nearly always independent of sea state. Efforts to estimate the ocean wave height spectrum from the second order

backscattered power spectrum determine significant wave height and dominant wave period satisfactorily (surface-wave radar measurements). But dominant wave directions are not readily determinable. It will be shown how a bispectrum analysis of HF backscattered radio wave data will give information about dominant wave period and direction, significant wave height, and beam spread of the ocean waves. A discussion using experimental examples will relate to the given theory.

5-7 A BEAM-LIMITED, TARGET-REFERENCED RADAR FOR OCEAN WAVE HEIGHT MEASUREMENT: E. J. Walsh, NASA Wallops Flight Center, Wallops Island, Virginia, and W. G. Anaya, U.S. Army, MERDC, Fort Belvoir, Virginia

The ability to measure the significant wave height (SWH) of ocean waves is being investigated for a beam-limited, target-referenced radar developed by Fairchild Industries, Inc. The radar transmits a wideband linear FM signal at X-band. The return echoes are mixed with the transmit signal and band pass filtered to isolate the range interval of interest. Squaring and low pass filtering eliminates the range information and results in a signal whose bandwidth is directly proportional to the range extent of the sea. Some data taken at 20 m altitude from a tower 25 km off-shore of Norfolk, Virginia, will be presented. Plans for flight testing the system on a Wallops C-54 aircraft to verify predicted accuracy will be described. The main source of error at low values of SWH is uncertainty in antenna pointing. Reasonable requirements on an operational system might be to measure SWH in the 1 to 10 m range to an accuracy of 0.5 m or 20%, whichever is greater. These requirements could be met at an altitude of 10,000 m using an antenna beamwidth of 1.4° whose pointing is maintained to nadir within a 0.5° standard deviation. Examination of DC-10 and DC-8 aircraft data available indicates that their short term pitch and roll stabilities would satisfy the requirement and only the long term variation in mean pitch would need compensation.

5-8 MAXIMUM LIKELIHOOD ESTIMATION OF OCEAN SURFACE PARAMETERS: Richard P. Dooley and Lowell W. Brooks, Technology Service Corporation, Silver Spring, Maryland

This paper describes a Maximum Likelihood Processor, MLP, for aircraft and satellite ocean monitoring radar altimetry. The MLP provides real-time joint Maximum Likelihood (minimum variance) estimates of altitude, ocean wave-height, ocean reflectivity, and antenna pointing error. The required video processing and underlying assumptions are established and used to develop a feedback loop design which readily lends itself to a practical implementation with a small scale digital computer. An approximate closed-form solution for the shape of the altimeter mean power return in terms of the parameters to be estimated is described. Based on this model for mean power return, estimation accuracies are given for all four parameters. Computer simulation examples are presented to demonstrate the acquisition and tracking performance of the MLP design. MLP performance based on real altimetry data (GEOS-C and/or the AAFE Breadboard Altimeter) will also be described if available.

OBSERVATION OF SPATIAL AND TEMPORAL STRUCTURE  
OF THE IONOSPHERE - I  
URSI COMMISSION III

Tuesday, October 21 1330

URSI Session III-3, UMC 157

Chairman: M.G. Morgan, Dartmouth College

3-1 THE INFLUENCE OF SEASON UPON THE POSITIVE PHASE OF IONOSPHERIC STORMS: Michael Mendillo, Astronomy Department, Boston University, Boston, Massachusetts; and John A. Klobuchar, Air Force Cambridge Research Laboratories, Bedford, Massachusetts

The recent completion of the AFCRL Atlas describing the F-region response to 75 geomagnetic storms has made it possible to search for the effects of season upon average storm patterns at a mid-latitude site ( $39^{\circ}\text{N}$ ,  $70^{\circ}\text{W}$ ,  $L = 2.8$ ). A particularly well-documented storm-induced perturbation is the large enhancement in the ionospheric total electron content (TEC) and peak density of the F-region ( $N_{\text{max}}$ ) which often occurs during the late afternoon period following the commencement of a worldwide magnetic storm. Our long-term observations from Sagamore Hill, Massachusetts, show that the TEC "dusk effect" enhancements tend to peak earlier during winter months and later during summer months in comparison to the spring-fall average of 1800 LT. The magnitude of the average pre-sunset increase is noticeably larger during winter and fall than during spring and summer. Such observations support a mechanism which ties vertical drift effects associated with magnetospheric convection to the normal seasonally-dependent changes in the F-region production/loss processes.

3-2 A COMPARISON OF SEVERAL METHODS OF ESTIMATING THE COLUMNAR ELECTRON CONTENT OF THE PLASMA-SPHERE: K. Davies, Space Environment Laboratory, NOAA/ERL, Boulder, Colorado; G. K. Hartmann, Max-Planck Institute for Aeronomy, Lindau/Harz, West Germany; and R. Leitinger, University of Graz, Graz, Austria

The columnar electron contents of the ionosphere and plasmasphere has been measured near Boulder, Colorado using several techniques: (1) the geostationary ATS-6 multifrequency radio beacon at 36,000 km; (2) the

content up to 1400 km using the radio beacons on the Navy Navigation Satellites; and (3) topside (ISIS-1 and -11) and bottomside ionograms. Data taken between August 1974 and November 1974 have been analyzed for those satellite passes sufficiently close in time and space to merit comparison. It is found that the greatest uncertainty in this comparison is that introduced by horizontal gradients so that individual values show rather poor agreement. However, values averaged over a number of passes show reasonable agreement between the various contents.

3-3 PLASMAPHERIC ELECTRON CONTENT DURING THE EQUINOXES: H. Soicher, Communications/Automatic Data Processing Laboratory, U.S. Army Electronics Command, Fort Monmouth, New Jersey

Since the Applied Technology Satellite (ATS-6) was launched into a geostationary orbit at 94°W in late May 1974, measurements of the total electron content (TEC) using the Faraday polarization-rotation ( $N_I$ ) technique and the dispersive-group-delay ( $N_T$ ) technique have been made at Fort Monmouth, New Jersey, (40.18°N; 74.06°W). The difference between the contents obtained by the two techniques yields the integrated total number of electrons above the ionosphere: the plasmaspheric electron content ( $N_p$ ).

Although diurnal, day-to-day, and seasonal variations of  $N_p$  were observed, they were much smaller than corresponding variations of  $N_I$  and  $N_T$ . The ratio of plasmaspheric-to-ionospheric contents ( $N_p/N_I$ ) varied diurnally, seasonally, and from day to day. The diurnal variation exhibited basically a nearly constant night-time behavior (~50%) and a much lower daytime behavior (~10%), with rapid changes after local sunrise and after local sunset.

3-4 MEASUREMENT OF THE COLUMNAR ELECTRON CONTENTS OF THE IONOSPHERE AND PLASMAPHERE: K. Davies, R. B. Fritz, and T. B. Gray, Space Environment Laboratory, NOAA/ERL, Boulder, Colorado

From June 1974 through May 1975 the columnar electron content ( $N_T$ ) and the ionospheric (or Faraday) content ( $N_F$ ) was measured at Boulder using the multifrequency radio beacon on ATS-6. Monthly median hourly data are presented to show the diurnal and seasonal variations of

$N_T$ ,  $N_p$ , the plasmaspheric content above about 2000 km, and the shape factor  $F$ . It is found that  $N_p/N_T$  varies between about 8 percent by day to around 40 percent on winter nights. Ionosonde data from Boulder have been used to determine the slant slab thickness  $\tau_s$  and this together with  $F$  and topside data are used as the basis of modeling studies using an  $H^+$ ,  $O^+$  ionosphere. A technique has been developed for adjusting the parameters of the model to agree with the observations and acceptable profiles are presented.

3-5 SHORT PERIOD FLUCTUATIONS IN TOTAL COLUMNAR ELECTRON CONTENT: K. Davies, Space Environment Laboratory, NOAA/ERL, Boulder, Colorado; G. K. Hartmann, Max-Planck Institute for Aeronomy, Lindau/Harz, West Germany

Observations of carrier phase of radio signals from the ATS-6 beacon have been recorded at Bozeman, Montana, Boulder, Colorado, and Dallas, Texas. These have revealed small (less than 0.1 percent) sinusoidal fluctuations in total columnar electron content ( $N_T$ ). These oscillations have periods in the range from 30 sec to 50 sec and may continue for several hours near noon on magnetically quiet days. They appear to be associated with micropulsations on the ground and at geostationary heights.

3-6 OPTICAL REMOTE SENSING OF IONOSPHERIC STRUCTURE: R. D. Sears and J. E. Evans, Lockheed Palo Alto Research Laboratory, Palo Alto, California

The spatial distribution of ionization in the E- and F-regions can be determined by optical remote sensing techniques under certain conditions. The measured optical signal is the emission generated in the upper atmosphere by airglow processes or by auroral excitation. Unlike HF to UHF propagation measurements, optical systems are not subject to Fresnel zone size limitations to their resolution over the irregularity range of interest, and the scale sizes of irregularities which can be measured is limited only by optical resolution and by atmospheric seeing conditions. To illustrate the application of the optical remote sensing techniques to propagation experiments we present two quantitative examples (1) the large scale changes in the integrated electron content along a satellite-ground path caused by F-region irregularities of the type observed in the intertropical arcs was com-

puted from the F-region airglow emission structure and (2) the spatial wave number spectrum K of medium scale irregularities in the auroral E-region was determined from photometric measurements of auroral structure. The auroral K spectrum is shown to be similar to that measured in situ by satellite borne ion density probes.

3-7 VARIATION IN THE D-REGION DURING A PCA EVENT AND SOME CONSEQUENCES: Irving L. Chidsey and William A. Dean, U.S. Army Ballistic Research Laboratories, Aberdeen Proving Ground, Maryland; and William Swider, U.S. Air Force Cambridge Research Laboratory, L.G. Hanscom Field, Massachusetts

Measurements of integrated absorption and electron content during the 2 November 1969 PCA event indicated a very high variation in the D-region during individual rocket flights. Peak-to-peak variations in the integrated absorption were comparable to the mean values. For example, at 1512 and 1514 local time, 2 November, absorption along the path to rocket B-4 varied  $\pm 6$  dB about a mean of 17 dB at 18 MHz. Variations of this magnitude make the comparison or combination of rocket and satellite data, or even of data from two separate rockets, however close in time and space, an operation fraught with difficulties.

---

WEDNESDAY MORNING, OCT. 22, 0830-1200

---

SATELLITE COMMUNICATIONS

URSI COMMISSION II

Wednesday, October 22 0830

Session II-6, UMC 159

Chairman: C.I. Beard,

Naval Research Laboratory

6-1 SCINTILLATIONS AND RAPID FADING AT 15 GHz BASED ON ATS-5 SATELLITE DATA: C. A. Levis and V. Ungvichian, The Ohio State University Electro-Science Laboratory, Columbus, Ohio; and S. J. Struharik, USN, Nuclear Power School, Vallejo, California

The ATS-5 satellite failed to stabilize, causing the antenna beam to swing across the receiving antenna. While this complicates the analysis of the received signal variations, it is also an advantage because it enables the discrimination of subtle propagation effects from locally generated noise. In the present analysis, pulses corresponding to the passage of the signal beam over the receiver are lined up in time by correlation and averaged to obtain a replica of the signal. Each pulse is then compared to this replica. The rms value of the differences on a pulse-by-pulse basis measures variations on a time scale shorter than approximately 0.1 second; the changes of the pulse average measures variations on a time scale greater than one second. Signal variations on the order of 0.5 dB can be detected in this manner. Preliminary data indicates a correlation of both the rapid and slower variations with overcast and rain.

6-2 MODELING ATMOSPHERIC EFFECTS AT 15 TO 45 GHz FOR EARTH/SPACE TELECOMMUNICATIONS: E. J. Dutton, M. T. Ma, and H. T. Dougherty, Office of Telecommunications, Institute for Telecommunications Sciences, Boulder, Colorado

A simple transmission channel transfer function at SHF/EHF is derived. Included are the effects of gaseous and spherical raindrop attenuation, phase delay caused by the non-dispersive and dispersive (due to the 22.2 GHz water vapor resonance only) clear air refractive index, and phase delay caused by spherical raindrops.

In addition, engineering formulations at 10 to 40 GHz are obtained to assess the impact of non-spherical raindrops in a rainstorm on both enhanced attenuation and cross-polarization discrimination for a system using dual orthogonal linear polarizations, or orthogonal circular polarizations.

Results presented show the predicted signal-to-interference ratio due to cross polarization distortion of dual horizontal (H) and vertical (V) polarizations, and for dual right-hand circular or left-hand circular (C) polarizations by rainfall expected 1 percent and 0.01 percent of the time at Washington, D. C. on a satellite/earth path where the earth station antenna is elevated at an angle,  $\theta_0=15^\circ$  from the horizontal. Another important result shown is the amount of power relative to that expected at some arbitrary frequency and reliability, plotted as a function of frequency  $f$ , and reliability (time availability)  $q$ . It is suggested that whereas optimum frequency location for operation assessed under clear sky conditions ( $q \leq 50\%$ ) would be near 40 GHz, such a "window" appears non-existent for more standard reliability requirements ( $q \geq 90\%$ ).

**6-3 SCINTILLATIONS OBSERVED ON THE ATS-6 20 AND 30 GHz DOWNLINKS: D. B. Hodge and D. M. Theobold, The Ohio State University ElectroScience Laboratory, Columbus, Ohio**

The characteristics of scintillations observed on the ATS-6 20 and 30 GHz downlinks will be presented. These observations include scintillations in the absence of precipitation on paths having elevation angles of about  $40^\circ$ , scintillations in the presence of precipitation on paths having elevation angles of about  $10^\circ$ , and scintillations in the absence of precipitation on paths having elevation angles below  $5^\circ$ . The amplitudes of these observed scintillations ranged from 6dB at the higher elevation angles to values exceeding 25dB at the lower elevation angles. The predominant frequencies of these observed scintillations ranged from 0.1 to 0.3 Hz. Simultaneous 20 and 30 GHz observations were made at both the OSU Fixed and Transportable Ground Terminals. A portion of the higher elevation angle observations were made with a terminal separation of 7 meters; the remainder of the observations were made with a terminal separation of 13.2 kilometers.

6-4 DEPOLARIZATION MEASUREMENTS USING THE CTS SATELLITE: P. H. Wiley, C. W. Bostian, W. L. Stutzman, E. A. Manus, and R. E. Marshall, Virginia Polytechnic Institute and State University, Blacksburg, Virginia

Orthogonal polarization frequency sharing would double the capacity of the spectrum available to future satellite communications systems, but at millimeter wavelengths its practicality may be limited by cross talk resulting from depolarization in precipitation scattering. Depolarization along ground paths is fairly well understood, but only fragmentary data (taken with ATS-6) exist for an earth-satellite path. This paper describes an experiment which will utilize the 11.7 GHz beacon carried by the CTS satellite to make simultaneous measurements of attenuation and depolarization due to precipitation. Monitoring of the signal on a 24-hour basis will also provide statistical data on clear air depolarization and attenuation. Also included in this paper is a discussion of the difficulties involved in the theoretical prediction of these phenomena for a satellite path. Such factors as raindrop size and shape distributions at high altitudes, the presence of ice and water-ice mixtures in the freezing layer, and the relative orientation of the satellite and earth station can all be expected to affect the observed depolarization. A discussion is included of the feasibility of extending the present ground-path depolarization models to the satellite path.

6-5 FADING CHARACTERISTICS OF A COMPLETE SATELLITE LINK IN THE 1 TO 40 GHz FREQUENCY RANGE: Colin C. Bantin, Telesat Canada, Ottawa, Ontario, Canada

This paper considers the cumulative distribution function of fading or degradation in carrier-to-noise ratio over a complete satellite link. Individual contributions to fading are modelled using empirically derived statistical distributions which are functions of the earth station location and pertinent communications system parameters characterizing the earth station. The link model assumes up-link fading, a noise source at the satellite receiver, a non-linear transponder, down-link fading, and a noise source at the earth station receiver. A computer program was written to evaluate and

combine the individual contributions to fading, according to the link model, in a statistically rigorous fashion. This program has proven a very useful tool in designing satellite links between earth station sites with widely varying geographical locations and a variety of communications system configurations.

6-6      RECEIVING TECHNIQUES FOR PROPAGATION MEASUREMENTS  
          USING 19 and 28 GHz BEACONS ON COMSTAR  
          SATELLITES: D. C. Cox and E. E. Muller, Bell  
          Laboratories, Holmdel, New Jersey

Three COMSTAR domestic communication satellites to be supplied by Comsat General Corporation for use by the AT&T Company early in 1976 will each contain continuously operating 19 and 28 GHz beacons designed to facilitate earth-space propagation measurements. These beacons will radiate +21 dBW EIRP over the continental U.S. at each frequency. A summary will be given of the characteristics of the 19 GHz signals switched between two orthogonal linear polarizations at a 1 KHz rate and of the 28 GHz linearly polarized signals containing modulation sidebands ( $\pm 264$  MHz for two satellites and  $\pm 528$  MHz for the third). Since satellite station keeping is approximately  $\pm 0.1^{\circ}$ , fixed pointed (non-tracking) antennas up to about 8 feet in diameter can be used without incurring detrimental signal amplitude variations. The impact of satellite and beacon characteristics on antenna and receiver design for propagation measurements (rain attenuation, depolarization, and useable bandwidth) will be discussed. Simple narrow band (noise bandwidth  $\approx 30$  Hz) receiver techniques for measuring rain attenuation with an accuracy of about 1 dB over at least a 20 dB range, and techniques for more comprehensive propagation measurements will be described. Since the 19 and 28 GHz beacon signals are coherent (3:2 frequency ratio), coherent receiver techniques can be used to extend the attenuation measuring range at 28 GHz.

6-7      THE QUASI-STATIONARY SATELLITE ORBIT:  
          John C. H. Wang, Federal Communications  
          Commission, Washington, D.C.

The capacity of the geostationary satellite orbit for space communication systems using the same frequency

bands is limited. While the 1971 World Administrative Radio Conference for Space Telecommunications (WARC-ST), did provide some relief through additional frequency bands above 10 GHz for fixed satellite use, these frequency bands are somewhat less desirable than the 4 and 6 GHz bands for geostationary satellites. The quasi-stationary satellite orbit is intended to relieve the burden of the geostationary satellite orbit. Three or four satellites equally spaced in this orbit can provide continuous service to two areas, one in the northern and one in the southern hemisphere. The purpose of this paper is to discuss some of its advantages and disadvantages as compared with geostationary satellite orbit. Topics considered include coverage, antenna pointing angles, Doppler shift, hand-over angles, scintillation and other parameters. Results of a sample system having 11 earth stations and a specific orbit with a reference longitude of 75 degrees west and an inclination of 60 degrees are also presented.

6-8 PRESENT STATUS OF BROADCASTING-SATELLITES:

A. Das, Federal Communications Commission,  
Washington, D.C.

A number of tests have been planned and are being implemented regarding broadcasting-satellites. This paper will discuss these tests with particular regard to the frequency bands to be used and the resulting sharing problems. The technology of the television Broadcasting-Satellite Service has been demonstrated since last summer by the experimental transmissions of the Advanced Technology Satellite-6 (ATS-6) in the 2.50 - 2.69 GHz band. These experiments have been conducted at nearly 120 low cost earth stations in the Rocky mountain and Appalachian regions and Alaska in the health, education, and medical fields. In the summer of 1975, further experiments in the Broadcasting-Satellite Service are planned to be conducted in India in the 860 MHz band after repositioning the ATS-6 over that country. Experiments are planned in the North American Continent from the latter part of 1975 in the 11.7 - 12.2 GHz band utilizing the Communications Technology Satellite (CTS) being developed jointly by Canada and the USA. In 1977 the 11.7 - 12.2 GHz band will be utilized for a Broadcasting-Satellite Service in Japan. Germany is also conducting studies to install a Broadcasting-Satellite

Service in the 11.7 - 12.2 GHz band. Russia recently announced a plan of introducing a television Broadcast-Satellite Service in 1976 in the 714 MHz band. Model sharing criteria will be presented for use of 11.7 - 12.2 GHz band by the Fixed-and the Broadcasting-Satellite Services. A figure of merit will be presented to measure the orbit utilization.

6-9 SMALL DIAMETER ANTENNA EARTH STATIONS:

A. Das, Federal Communications Commission,  
Washington, D.C.

Small diameter antenna earth stations have been introduced and are also planned for use in some of the Fixed- and the Broadcasting-Satellite Services. The parameters of some of these stations are discussed. Published work on the convolution method of calculation of the interference has been extended to calculate the interference from a single channel per carrier circuit(s), used by some small earth stations, to an adjacent satellite. Model sharing criteria will be presented for use of the small diameter antenna earth stations. A figure of merit will be discussed for measuring the orbit utilization.

RADIO METEOROLOGY--RADIO PROPAGATION AND WIND  
MEASUREMENTS IN CONVECTIVE STORMS  
URSI COMMISSION II

Wednesday, October 22 0830

URSI Session II-7, UMC Forum Room

Chairman: A.H. LaGrone,  
University of Texas

7-1 ATTENUATION LEVELS OF PROPAGATION THROUGH RAIN  
AT 13 and 18 GHz CORRELATED WITH PREDICTED  
VALUES USING RADAR: Julius Goldhirsh,  
Applied Physics Laboratory, The Johns Hopkins  
University, Laurel, Maryland

During the summer of 1974 and spring of 1975 the attenuation of propagation through rain was obtained at Wallops Island, Virginia, using 13 and 18 GHz transmitters operating in the uplink mode toward the ATS-6 satellite. Simultaneous with these measurements, rain reflectivity levels were made along the earth satellite path using a high resolution ( $0.4^{\circ}$  beamwidth) S-band radar having a scanning antenna. A system of 4 raingauges and 2 disdrometers were also located in the vicinity of the transmitters. The radar and disdrometer data were used in a modeling program to predict attenuation levels which were subsequently compared to the directly measured fades over near simultaneous time intervals. In the modeling program, the radar reflectivity factor,  $Z$  ( $\text{mm}^6/\text{m}^3$ ) was related to the attenuation coefficient,  $k$  ( $\text{dB}/\text{km}$ ), through the empirical equation,  $k = az^b$ , where  $a$  and  $b$  are frequency dependent constants calculated using a given drop size distribution. The total predicted attenuation was obtained by integrating the variable attenuation coefficient along the earth-satellite path. Calculated attenuation levels were obtained for three drop size distributions; namely, those of Joss, et al., for thunderstorm activity, Marshall-Palmer, and the average distribution measured in the vicinity of the transmitter (APL distribution). Preliminary comparisons between predicted and measured attenuation levels (summer of 1974) show rms differences of 1.4 dB, 1.9 dB, and 2.5 dB at 18 GHz corresponding to drop size distributions of APL, Marshall-Palmer, and Joss, et al., respectively. At 13 GHz the respective rms differences were 1.5 dB, 1.8 dB, and 2.1 dB. Although

the preliminary sample sizes were sparse (101 at 18 GHz and 28 at 13 GHz), the relatively close agreement suggests the validity of using radar to model path attenuation and ultimately arrive at attenuation statistics.

7-2 DUAL-DOPPLER RADAR MEASUREMENTS IN A SEVERE CONVECTIVE STORM: Robert A. Kropfli and L. J. Miller, NOAA/ERL/Wave Propagation Laboratory, Boulder, Colorado

The three-dimensional kinematic structure of a northeast Colorado convective storm has been revealed by the dual-Doppler radar system at the Wave Propagation Laboratory of NOAA. Data to be presented were obtained within a storm in its late-mature stage during the National Hail Research Experiment (NHRE). Data acquisition and reduction procedures utilized the COPLAN method in which two X-band Doppler radars are constrained to scan in common planes tilted with respect to the horizon. Features believed to be characteristic of many convective storms have been revealed by the data. These include a backward sloping updraft overriding a precipitation filled downdraft, middle-level intrusion of cold dry air into which the precipitation falls, and a well defined gust front. Quantitative results such as the updraft entrainment rate and the fluxes of mass, water vapor, energy, vorticity, and momentum will also be discussed.

7-3 AIRFLOW AND PRECIPITATION STRUCTURE OF A CONVECTIVE STORM FROM DUAL-DOPPLER RADAR MEASUREMENTS: L. J. Miller, NOAA/ERL/Wave Propagation Laboratory, Boulder, Colorado

The dual-Doppler radar coplane method of scanning and data reduction has been used to determine the internal airflow and radar reflectivity structure of a convective storm. Cumulus convection growing in a moderately sheared wind environment resulted in a nonsteady moderate intensity thunderstorm. Precipitation fallout and downward moving air are found downshear of an updraft inclined in the downshear direction. Rapid storm translation, vertical shear of the ambient wind, and slow subcloud ascent of inflow air act to establish this observed draft configuration. The absence of significant cold air outflow and its attendant gust front at the surface is attributed to (i) appreciable inflow of slow moving air into the downdraft at the middle layers

and (ii) the fact that the potentially coldest air was located too low to contribute significantly to a deep downdraft circulation.

7-4 KINEMATIC MODELS OF A DRY CONVECTIVE BOUNDARY LAYER COMPARED WITH DUAL-DOPPLER RADAR OBSERVATIONS OF WIND FIELDS: Earl E. Gossard and A. Shelby Frisch, NOAA/ERL/Wave Propagation Laboratory, Boulder, Colorado

In this paper we first compare the kinematic structure of the convective boundary layer, observed by a dual-Doppler radar system, with the structure predicted by simple inviscid shear models. Model 1 assumes a linear ambient wind profile from the surface through the boundary layer and a constant wind above. The shear layer is assumed to be statically neutral, but static stability is permitted in the region above the shear. Model 2 has a hyperbolic tangent ambient wind profile, and some degree of static stability is assumed to be present. After considering the inviscid models, we incorporate some of the effects of viscosity into the models in a crude way and compare the results. We conclude that the kinematic structure is relatively independent of the details of the wind and temperature profile, but that viscosity has important effects, especially near the critical level where the disturbance velocity is equal to the wind speed. The patterns predicted by both models agree very well with the dual-Doppler radar observations when viscosity is included in the models.

7-5 REFLECTIVITY PROFILES AND SPATIAL STRUCTURE OF RAIN STORMS FOR VARIOUS GEOGRAPHICAL LOCATIONS DERIVED FROM RADAR OBSERVATIONS: Thomas G. Konrad, Applied Physics Laboratory, The Johns Hopkins University, Laurel, Maryland

Statistical descriptions or models of rain storms are required in the prediction of attenuation and scatter interference between earth-satellite and terrestrial communication links sharing the same frequency. The question, however, is whether a statistical model developed for one geographical location can be applied to any other location or, alternatively, to what extent are the rain cells in one location similar to those at some other geographical location. The fond hope, of course, is that showers and thunderstorms are similar in character wherever they occur. If such is the case the

effect of geographical location is simply in the frequency of occurrence of storms of various types. This paper compares the characteristics of rain storms as determined from radar observations for various locations in this country and abroad. Rain cells are characterized in terms of the frequency distributions of the peak or core reflectivity at various altitudes, profiles of the mean and median core reflectivity, the frequency distribution of cell heights, the distribution of the height of the maximum reflectivity, the ratio of the maximum core reflectivity to the reflectivity at ground level, and the spacing between cells.

7-6 MULTIPLE ALTITUDE THREE-VECTOR WIND MEASUREMENTS  
WITH THE SUNSET VHF METEOROLOGICAL RADAR:  
J. L. Green, T. E. VanZandt, J. Warnock, R. Winkler,  
and W. Clark, NOAA/ERL, Boulder, Colorado

The Aeronomy Laboratory of NOAA is using a large VHF radar to study winds, waves, and turbulence in the troposphere and stratosphere. This facility is located 16 km west of Boulder, Colorado, near the town of Sunset, Colorado. The operating wavelength of this radar is 7.4 m so that the velocities associated with 3.7 m variations of the refractive index of air can be measured. This radar has a typical height resolution as small as 150 m in lower troposphere and 1 km in the upper troposphere and lower stratosphere; its velocity resolution is 0.37 m/sec. Because of its location just east of the continental divide, this radar is useful in the study of vertical and horizontal wind velocities of mountain lee waves. Recently the capability of measuring wind velocities at 16 altitudes simultaneously and in three directions sequentially has been added to this facility. This addition makes possible, for example, the measurement of the east-west, north-south, and vertical components of wind velocity at every 1 km interval between 4 km and 20 km above sea level with a 300 second time resolution. Digital recording equipment has also been installed so that the time variation of wind velocity due to atmospheric waves can be studied.

7-7 MEASUREMENT OF THE MICROSCOPIC PARAMETERS OF  
TURBULENCE WITH THE SUNSET RADAR:  
T. E. VanZandt and J. L. Green, NOAA/ERL,  
Boulder, Colorado

From Sensem radar measurements of the Doppler spectral

width, the vertical shear of the horizontal wind, and the reflectivity, the following quantities can be derived: the energy in turbulence, the energy dissipation rate, the outer and inner scales of the inertial subrange, the eddy diffusivity, and the structure constant of the refractivity. The derived magnitudes are consistent with other observations of these parameters in the winter, mid-latitude tropopause region. For example, in measurements made to date, the energy dissipation rate ranges between 10 and  $1000 \text{ cm}^2/\text{s}$ , the eddy diffusivity ranges between 2 and  $17 \text{ m}^2/\text{s}$ , and the structure constant is about  $20 \times 10^{-16} \text{ m}^{-2/3}$ .

7-8 CONVECTIVE BOUNDARY LAYER OBSERVATIONS OF THREE-DIMENSIONAL WIND FIELDS USING A DUAL-DOPPLER RADAR SYSTEM: A. S. Frisch and R. B. Chadwick, NOAA/ERL/Wave Propagation Laboratory, Boulder, Colorado

Three-dimensional wind fields have been measured in the convective boundary layer using chaff as an air motion tracer. These measurements reveal the structure of convective cells having a horizontal diameter of about 2 km and extending from the ground to over 1 km. The spatial spectra of velocity, calculated by the maximum entropy method, show sharp peaks at 2 and 5 km scales.

OBSERVATION OF SPATIAL AND TEMPORAL STRUCTURE  
OF THE IONOSPHERE - II  
URSI COMMISSION III

Wednesday, October 22 0830

URSI Session III-4, UMC 157

Chairman: J.W. Wright, NOAA

4-1 PRELIMINARY RESULTS FROM A STATISTICAL SURVEY  
OF TRAVELLING IONOSPHERIC DISTURBANCES DEDUCED  
FROM A THREE-STATION IONOSONDE NETWORK IN  
NORTHERN NEW ENGLAND: K. A. Ballard and  
M. G. Morgan, Radiophysics Laboratory,  
Thayer School of Engineering, Dartmouth  
College, Hanover, New Hampshire

A reliable, abbreviated technique has been developed for the statistical investigation of travelling ionospheric disturbances (TID's) deduced from ionograms obtained every two minutes at three stations mutually 150 Km apart in northern New Hampshire and Vermont. Rather than reducing every ionogram to true-height, a task of immense proportion, the virtual height at a single frequency (optimized for the season and time-of-day) was scaled and analyzed for the existence of TID's. The technique incorporates the capability for handling data-blocks containing missing values, for varying the data-window sizes, and for the determination and removal of the diurnal trend. The results obtained with this technique are compared to those from a complete true-height analysis for seven events in 1969. The agreement is excellent although the comparisons of apparent horizontal velocity are imperfect because the true-height of the abbreviated measurement is not known and both techniques reveal that there is a height-dependence of the apparent horizontal velocity. The wavefront vertical tilt angle, which must be combined with the apparent horizontal velocity to obtain the "true" velocity, cannot be obtained from the abbreviated technique. Results from a sample statistical study of seven daytime hours for the full week of January 10-16, 1969, are reviewed. This sample indicates that the TID's move predominantly toward a south or south-easterly direction with apparent horizontal velocities ranging from about 100 to 500 m/sec, and with dominant periods between 50 and 240 minutes. The sample results show an approximately direct dependence of the apparent

horizontal velocity on the dominant period, in substantial agreement with gravity wave theory, whereas an inverse dependence has sometimes been reported by other investigators.

4-2 THE THOUGHTFUL IONOSONDE: K. Bibl and B. W. Reinisch, University of Lowell Research Foundation, Lowell, Massachusetts

Digital data collection has widened the application of ionosondes fundamentally. Simplicity, reliability, and versatility are nonexclusive functions in ditigal designs. An integrated computer--software or hardware programmed either locally or remotely--collects, processes, and compresses data with new simple algorithms. A fast-tuning frequency-switched transceiver provides full frequency selection capability from pulse to pulse. Coherent integration and spectrum analysis produce a powerful tool in spite of limits in sounding energy and time. Thus the three-dimensional structure of the ionosphere can be routinely studied at a single station. All features of the new Digisonde can be fully utilized in a combined acoustic and radio sounding experiment for the investigation of the whole atmosphere.

4-3 TRAVELLING IONOSPHERIC DISTURBANCE (TID) MODELLING FOR HF RADIO SOURCE LOCATION: K. E. Hoover and N. Narayana Rao, Department of Electrical Engineering, University of Illinois, Urbana, Illinois

Early attempts at ionospheric modelling for the purpose of HF radio source location of ionospherically propagated signals involved the plane earth/vertical plane specular ionosphere assumption, and then later the plane earth/tilted plane ionosphere assumption. These static models of the ionosphere were most useful when the signal of interest could be observed over periods of several hours before a "fix" had to be made. This permitted the effects of dynamic ionospheric perturbations to be largely averaged out. Recently more sophisticated dynamic ionospheric models have been proposed to include the effects of TIDs and thus permit more accurate fixing on signals of shorter duration. The first dynamic model employed was that of a moving single-corrugation, specular ionosphere. Direction of arrival (DOA) data collected from a vertical incidence sounder collocated with the direc-

tion finder will be presented that clearly indicate a more general multiple-corrugation ionospheric model to fit with the observed data. Simulated DOA fluctuation data from a multiple-corrugation ionosphere will be shown to fit the observations more closely. Finally, cross-spectra of DOA fluctuations from several pairs of transmitters of known locations will be presented to illustrate a method of determining all parameters of such a multiple-corrugation model, and will also indicate the possible domain of coherence of such a model.

4-4 A COMPARISON OF IONOSPHERIC PARAMETERS AT A CONSTANT GEOMAGNETIC LATITUDE: Jay R. Hill,  
Naval Electronics Laboratory Center, San Diego, California

A comparison is made between vertical incidence sounder measurements at Point Arguello (34.73N, 120.52W) and La Posta (32.68N, 116.43W), California. The two stations are at the same geomagnetic latitude and are separated by 440 km. Values of  $f_0F2$  and  $h'F2$  at the two sites are compared and they indicate a general tilt in the F-layer which affects calculations of oblique HF propagation. Comparison of spread F and sporadic E conditions between the stations and estimates of the size and speed of sporadic E clouds are made.

4-5 VIRTUAL HEIGHTS AND IONOSPHERE MODELS:  
Newbern Smith, National Geophysical and Solar-Terrestrial Data Center, National Oceanic and Atmospheric Administration, Boulder, Colorado

Satisfactory ionosphere models are needed for radio communications use as well as for ionospheric and other geophysical research. These models must be consistent with, and derivable from, the virtual heights obtained by ionosondes. Models thus far proposed usually consist of simple elements such as parabolas, sine or sine-squared functions, and segments that are linear (or constant) with frequency, electron density, and  $\log$ -(frequency), and are usually "no-magnetic-field" models. To use these various elements to generate a virtual height, we have computed the group retardation for each type, using both the "o" and the "x" modes. The results of these calculations and their influence on modeling are presented. Examples are given from

modeling work done at NOAA and elsewhere, and are compared with true height profiles calculated using the NOAA inversion program. It is concluded that: (1) No model derived from an ionogram can be considered satisfactory unless the effects of the earth's magnetic field are included, (2) a most important criterion is that the virtual height generated by a model must reasonably resemble the virtual height profile on the original ionogram, and (3) the validity of oblique propagation calculations using a "no-field" model and equations may possibly be questionable.

4-6 AN IMPROVED ALGORITHM RELATING THE F-LAYER PEAK TO M(3000)F2: Jay R. Hill, Naval Electronics Laboratory Center, San Diego, California

An equation relating the F-layer peak altitude with M(3000)F2 has been developed which is similar to the formula of Bradley and Dudeney (1973). Our equation yields physically realistic results over a wider range of values of X, the ratio of foF2 to foE, than the previous equation which gives non-physical results with X less than 1.7. The cusp structure shown on summer ionograms has necessitated the modeling of the F1 and F2 regions by more realistic layers than those used in previous models.

4-7 A SHORT-TERM foF2 FORECASTING ALGORITHM: Tom Hopper and Jay Hill, Naval Electronics Laboratory Center, San Diego, California

A model is presented for short-term predictions of foF2 values on past observations alone. This model was developed using the three-step Box Jenkins technique of identification, estimation, and diagnostic checks. Optional forecasts with approximate probability limits at any lead time follow at once from the structure of the identified stochastic model. Application of this model to observations of the mid-latitude ionosphere is presented. The results show that the one hour ahead root mean square prediction error for foF2 is .5 MHz.

4-8 GLOBAL IONOSPHERIC MODELS FOR PREDICTING THE PERFORMANCE OF HIGH FREQUENCY COMMUNICATION SYSTEMS: Margo Leftin, Office of Telecommunications, Institute for Telecommunication Sciences, Boulder, Colorado

Basic to predicting the performance of high frequency communication systems is a reliable model of the spatial and temporal variations of the ionosphere. Numerical maps have been developed to represent these variations for the more important ionospheric characteristics. The available ionospheric models and their reliability will be reviewed. A detailed analysis of the accuracy of the predicted median F2 critical frequencies for the current solar cycle will be presented. The application of numerical maps of ionospheric characteristics to predicting an average electron density profile will be discussed.

PRECIPITATION AND PLASMAS

URSI COMMISSION IV

Wednesday, October 22 0830

URSI Session IV-4, UMC 158

Chairman: J.C. Siren,

University of California at San Diego

4-1 PROBING THE MAGNETOSPHERE WITH ULF PRECIPITATION PULSATIONS: R. R. Heacock and R. D. Hunsucker, Geophysical Institute, University of Alaska, Fairbanks, Alaska

Pulsations in the ULF range below 1 Hz, detected simultaneously in the magnetic field, in the riometer recordings, and by the Chatanika radar, furnish several kinds of information about the magnetosphere. Characteristics of electron precipitation pulsations from the plasma sheet and inverted V-regions are studied from ground recordings of Pi pulsations. A few strong Pc 1-2 events are identified in the riometer and magnetometer recordings. On the assumption that the proton cyclotron resonance instability produced the Pc 1-2 events, some features of the trapped energetic proton population and some characteristics of the instability are disclosed. Pi 1 precipitation pulsations may be used to define the location of the plasma sheet in morning hours during substorms.

4-2 A RADAR TECHNIQUE FOR DERIVING THE ENERGY DISTRIBUTION OF INCIDENT AURORAL ELECTRONS: Richard R. Vondrak, Radio Physics Laboratory, Stanford Research Institute, Menlo Park, California

A technique has been developed by which ground-based measurements made by the Chatanika radar can be used to determine the energy distribution of the incident auroral electrons. An altitude profile of electron density is deconvolved into an incident energy spectrum by use of a library of ionization production profiles for monoenergetic electrons. The accuracy of the method has been assessed by application to synthetic ionization profiles produced by known electron energy distributions. Results indicate that the incident energy distribution can be recovered with high precision (deviations typically < 25%) for incident energies between 1 and 20 keV. The technique is generally insensitive to the original pitch-angle

distributions of the incident electrons. The method has been applied to several density profiles obtained at Chatanika during auroral activity and the equivalent of satellite-measured inverted "V" structures have been seen.

4-3 INCOHERENT SCATTER RADAR OBSERVATIONS OF ELECTRIC FIELDS AND CURRENTS ASSOCIATED WITH AURORAL ARCS:  
Odile de la Beaujardiere, Murray J. Baron, and Richard R. Vondrak, Radio Physics Laboratory, Stanford Research Institute, Menlo Park, California

Using the Chatanika incoherent scatter radar, the electric fields and currents associated with auroral arcs have been studied. The radar observations have been correlated with visual arc brightness, position, and motion as determined from both low-light boresite TV camera data and all sky camera data. When the radar is directed parallel to the magnetic field line, the line-of-sight ion velocity is very small in amplitude ( $\leq \pm 20$  m/s) and shows no consistent patterns as arcs drift through the beam. From the ionization profile we determine the energy distribution of the incoming auroral electrons, their mean energy, and the component of Birkeland current carried by the incident auroral electrons. This component of current can be as large as  $20 \mu\text{A}/\text{m}^2$  during intense auroral events. When the radar is directed toward the magnetic west, the northward electric field and the westward currents are simultaneously measured with a time resolution of less than one minute. On several occasions, a decrease in the northward electric field is observed as arcs appear in the beam. This decrease may be interpreted as a southward polarization field of typically 20 to 50 mV/m due to large conductivity gradients.

4-4 RADAR MEASUREMENTS OF THE LATITUDINAL VARIATION OF AURORAL IONIZATION: Richard R. Vondrak and Murray J. Baron, Radio Physics Laboratory, Stanford Research Institute, Menlo Park, California

On March 12, 1975, the Chatanika incoherent scatter radar was operated in an elevation scan mode along the magnetic meridian. Approximately 40 consecutive scans were made with each scan taking about 3 minutes and covering about 150 km in north-south extent. Measurements were made of the auroral E-region electron density with a spatial resolution of about 5-km; line-of-sight ion velocity measure-

ments were also made. During the experiment several visual auroral arcs were present. The data show the latitudinal variation of ionization associated with the arcs. The motion of the auroral forms is determined from comparison of successive scans of the radar. Other quantities derived from the data are the ionospheric conductivity, energy deposited by the primary auroral electrons, and energy distribution of the incident electrons, all as functions of latitude and time.

4-5 REMOTE SENSING OF SOLAR WIND TURBULENCE:

W. M. Cronyn, F. T. Erskine, and S. D. Shawhan,  
Department of Physics and Astronomy, University of  
Iowa, Iowa City, Iowa

The only technique currently available for taking routine global observations of the interplanetary plasma more than a few solar radii from the sun is the monitoring of IPS (interplanetary scintillation) activity of a grid of small angular diameter celestial radio sources. The Cocoa Cross radio telescope, with one of the largest effective collecting areas in the world (18 acres--about twice the maximum effective collecting area of the Arecibo dish), is a facility dedicated primarily to the exploitation of IPS as a means of remotely sensing electron density turbulence in the solar wind. For example, our observations for the period June-December 1974 reveal 11 recurrent solar-magnetic-sector-boundary-associated enhancements in IPS activity. The IPS activity was well correlated with geomagnetic and space craft magnetic field and particle activity. Our observations and those of others indicate that the IPS remote sensing technique shows great promise in two ways: it is a means of (1) studying physical conditions in the solar wind and (2) forecasting geophysical phenomena such as magnetic storms and ionospheric disturbances which are the result of solar plasma ejections impacting the magnetosphere.

4-6 LOCATION AND MAPPING OF TERRESTRIAL KILOMETRIC RADIATION FROM LUNAR ORBIT: M. L. Kaiser,  
J. K. Alexander, R. G. Stone, and J. Fainberg,  
Goddard Space Flight Center, Greenbelt,  
Maryland

The Radio Astronomy-Explorer-2-spacecraft in lunar orbit has viewed hundreds of occultations of the earth's magnetosphere between July 1973 and July 1975. From occultation timings it has been possible to develop two dimensional maps of the apparent source

location of each terrestrial kilometric radiation (TKR) event as a function of frequency. Our initial findings confirm that the TKR is associated with the earth's polar regions. Most events are complex, often suggesting multiple "hot spots" or simultaneous emission from both poles and the magnetotail. The sources generally show a steady outward progression from the earth and an increasing size with increasing wavelength. The large radial distances from the earth of many TKR events is difficult to explain in terms of current theories. We will show a variety of TKR events viewed from a range of perspectives around the earth and discuss the implications of the source locations on emission mechanisms.

GALACTIC AND EXTRAGALACTIC OBSERVATIONS

URSI COMMISSION V

Wednesday, October 22 0830

URSI Session V-4, UMC 156

Chairman: A. Moffet,

California Institute of Technology

4-1 SPECTRAL LINE VLBI OBSERVATIONS OF STELLAR OH MASERS: M.J. Reid and D.O. Muhleman, California Institute of Technology, Pasadena, California; J.M. Moran, Smithsonian Astrophysical Observatory, Cambridge, Massachusetts; and K.J. Johnston and P.R. Schwartz, Naval Research Laboratory, Washington, D.C.

A direct Fourier inversion of VLBI data is reported for observations made on the 1612 MHz maser lines of VY CMa. These observations are part of a VLBI program of inferring source structure from the full complex fringe visibility. The complexity of the spectral maps for VY CMa indicates that there are many widely spaced maser components at the same velocity. Fourier inversion of this VLBI data, even with very limited u-v coverage, has proven to be more efficient and less biased than direct model fitting for the resolution of such source structure. In addition to generating maps for VY CMa, we have attempted to determine apparent sizes and separations of the individual maser components of the 1612, 1665, and 1667 MHz OH emission from many OH/IR (Mira variable) stars. Generally the maser components at all these frequencies appear large ( $\gtrsim 0.25$  arc sec) and complex. An important and unique exception is U Ori whose dramatic flare-up at 1612 MHz was reported in 1974 by Pataki and Kolena (IAU Circular No. 2680). Our observations show that the emission is highly polarized and originates in several compact components ( $\lesssim 0.1'$ ) separated by  $0.15'$ .

4-2 VLBI DETECTION OF THE COMPACT RADIO SOURCE IN THE GALACTIC CENTER: K.Y. Lo, Owens Valley Radio Observatory, California Institute of Technology, Pasadena, California

A compact radio source in the Galactic Center has been detected at 3.7 cm on the Very Long Baseline Interferometer comprising the Goldstone 64-m and the Owens Valley 40-m telescopes. The correlated flux density of the source is  $\sim 0.7$  Jy. The fringe amplitude is constant as

the projected baseline varies from 3.6 to 4.4 times  $10^6\lambda$ . The position of the source is the same as that of the  $<0''.1$  radio source reported by Balick and Brown (1974, Ap. J., 194, 265), and is presumably the same object. The brightness temperature of the source is  $\gtrsim 3 \times 10^7$  K assuming a size  $\lesssim 0''.02$ . This indicates a nonthermal source with a linear size smaller than 200 A.U. or  $10^{-3}$  pc at the Galactic Center. Comparison with previous observations of the Galactic Center suggests that the source is varying with time and therefore likely to have a smaller angular size ( $<0''.02$ ). This has to be verified with further observations. The nature of the radio source will be discussed.

4-3 COMPACT RADIO SOURCES IN THE NUCLEII OF EXTERNAL GALAXIES: Richard T. Schilizzi, California Institute of Technology, Pasadena, California

The nucleii of 39 galaxies associated with large scale radio emission (typically minutes of arc in size) have been searched for compact radio components using VLBI techniques. A single baseline, 240 km in length, between the OVRO 40m and Goldstone 64m telescopes was used for 15 minute observations of the sources. The detection level for compact structure was 60 to 70 mJy. Approximately one third of the galaxies searched have compact components in their nucleii. The implications of this and earlier results will be discussed in the light of models for radio source evolution.

4-4 MODELS OF 3C 84 from VLBI AMPLITUDES: N. W. Brotén; Herzberg Institute of Astrophysics, NRC, Ottawa, Ontario; M. H. Cohen, Owens Valley Radio Observatory, California Institute of Technology, Pasadena, California; and G. H. Purcell, National Radio Astronomy Observatory, Charlottesville, Virginia

3C 84 has been observed at 2.8 cm in two different series of observations involving, in various combinations, ARO, Chilbolton, Bonn, NRAO, Fort Davis, and OVRO. Models based on fringe amplitudes have been constructed independently by three people, using two techniques. The models have a high degree of similarity despite different initial assumptions.

4-5 THE CORRELATION OF X-RAY AND DECAMETRIC EMISSION BY EXTRAGALACTIC SOURCES: W. C. Erickson, T. A. Matthews, and M. R. Viner, Clark Lake Radio Observatory, Astronomy Program, University of Maryland, College Park, Maryland

The Clark Lake catalog of radio sources at 26.3 MHz has been compared with the 3U catalog of X-ray sources. Twenty-one identifications are found. Of these, four are galactic supernova remnants, three are well known strong sources (Per A, Vir A, Cyg A), five are previously suggested identifications (3C66, 3C129-129.1, 3C264, Coma C, 3C 345), and nine are new identifications. Of the new identifications, three are with uncataloged sources that have such steep spectra that they are below the flux limits of the 4C or other higher frequency surveys. Most of the identified extragalactic sources have very steep spectra with spectral indices in the range from -0.9 to -2.5. This strengthens the correlation between X-ray and decametric emission.

4-6 21-CM ZEEMAN EFFECT MEASUREMENTS WITH A TURNSTILE JUNCTION POLARIMETER: T. H. Troland and C. E. Heiles, Department of Astronomy, University of California, Berkeley, California

We have constructed a turnstile junction polarimeter for use at 21-cm on the Hat Creek 26-m telescope. The turnstile is a six-port waveguide junction. Attached to the feed horn of the telescope, it provides opposite senses of circular (or linear) polarization at two of its ports. It is superior to dual-linear polarimeters for Zeeman effect experiments because a hybrid circuit is not needed for circular polarization and because the turnstile cannot introduce assymmetries in the polarized sidelobes of the telescope. The two output ports of the turnstile are alternately connected to a single paramp through a 100Hz ferrite switch, the difference between hydrogen line profiles in opposite senses of circular polarization is obtained with a 100-channel filter bank. We are conducting a long-term program of 21-cm Zeeman effect measurements with this system. The emphasis is upon high-latitude emission features, particularly the prominent filamentary structures at least some of which are aligned with the magnetic field. We report upon the initial results of this program.

4-7 THE STRUCTURE OF HI AS VIEWED IN SMALL VELOCITY RANGES: Carl Heiles, Astronomy Department, University of California, Berkeley, California

"Photographs" of the 21-cm line intensity in the sky, integrated over small ranges in velocity, have been generated from the Berkeley 21-cm line survey for  $|b| > 10^{\circ}$ . The restriction to a small velocity range allows narrow spectral features to be visible which are otherwise rendered indistinguishable when mixed with emission at other velocities. These features are often large and roughly circular in shape. In some cases the diameter of the circle depends on velocity, which suggests that the gas is distributed in an expanding shell. On smaller scales, structures of many shapes are visible.

INVERSE SCATTERING  
URSI COMMISSIONS VI AND I  
Wednesday, October 22                    0830  
URSI Session VI-7, Radio Building Auditorium  
Chairman: H.E. Bussey,  
National Bureau of Standards

7-1 EXACT INVERSE SCATTERING: Norbert N. Bojarski,  
Department of Defense, Moorestown, New Jersey

The exact inverse scattering and radiation problem (the inverse source problem) for the inhomogeneous (time-reduced) Helmholtz wave equation is formulated in terms of the unknown sources in an arbitrary volume and the known scattered or radiated field on the surface bounding this volume as a proper Fredholm integral equation of the first kind. The known surface fields appear in the form of a modified Kirchhoff surface integral. A numerical method of solution of this integral equation is presented, which is applicable to the case of a priori knowledge of finite support of the unknown sources (finite-sized scatterers). This method consists of a generalization of this author's  $k$ -space method, yielding a very efficient deconvolution (finite and discrete) method, using the Fast Fourier Transform algorithm.

Shown are computer-reconstructed source distributions (currents) of a half-wave dipole antenna, a point source, and two synchronous point-sources separated by one-half-wavelength, from computed synthetic far-field scattering data. Super resolution (i.e., resolution beyond the classical Rayleigh diffraction resolution limit) was achieved.

The inverse source problem associated with the time-dependent inhomogeneous wave equation is similarly formulated. The resulting integral equation involves the causal (time-retarded) as well as the inverse-causal or effectal (time-advanced) fields.

The scalar-field inverse source formulations and solutions are generalized to the vector-fields (Maxwell's equations). It is shown that for the inverse scattering case the unknown constitutive equations/boundary conditions (e.g., complex conductivity) are obtainable. The ill-conditioning effects of incomplete aspect angle information are discussed.

## 7-2 PHYSICAL OPTICS FAR FIELD INVERSE SCATTERING IN THE TIME DOMAIN: Norman Bleistein, University of Denver, Denver, Colorado

Recently, N. N. Bojarski has developed a physical optics far field inverse scattering (POFFIS) identity which relates the phase and range normalized scattering cross section to the Fourier transform of the characteristic function of the scattering obstacle. (The characteristic function is equal to unity in the domain occupied by the scatterer and equal to zero elsewhere.) The result is derived for the time reduced field. The analogous result in the time domain is not readily derived from this identity because of the approximations and algebraic manipulations performed in the derivation. By considering the time dependent problem directly, we derive a POFFIS identity for the fields observed in space-time. This result is compared to the time transformed identity and also to ray tracing-time delay methods presently employed to solve inverse problems.

## 7-3 ON SOLUTIONS OF A CLASS OF INVERSE PROBLEMS IN ACOUSTICS AND ELECTROMAGNETICS: Jack K. Cohen, University of Denver, Denver, Colorado

This paper presents certain consequences and extensions of the recent formulation of the inverse source problem which is due to N. Bleistein and N. Bojarski. These authors derived a three-dimensional integral equation for the source function of the scalar wave equation in terms of observed data on a surface which contains the support of the source function. Here we use this integral equation to derive information about the Fourier Transform of the source. Unfortunately, this information is not sufficient to identify the source completely in the general case. However, in some special cases this complete identification can be made. The two most important of these are: (1) The time dependence of the source is known, *a priori*, and is of a certain type; and (2) The far field response to an arbitrary harmonic is prescribed. Both near and far field observation surfaces are considered and the analogous results are obtained for Maxwell's Equations.

## 7-4 NUMERICAL CHECKS ON RECENTLY DEVELOPED REMOTE SENSING IDENTITIES: Robert D. Mager, University of Denver, Denver, Colorado

Recent progress in the field of remote sensing has been

achieved by Bojarski, Bleistein, and other co-workers. The techniques that have been developed lead essentially to a determination of the characteristic function of the scattering obstacle (inverse scattering problem) or to a determination of the source function (inverse source problem). These various approaches will be briefly discussed in terms of the Helmholtz equation, and numerical evidence attesting to the validity and feasability of the techniques will be presented.

7-5 APPROXIMATE SOLUTION OF INVERSE PROBLEMS WITH  
PIECEWISE CONTINUOUS SOLUTIONS: William L. Perry,  
Department of Mathematics, Texas A&M University,  
College Station, Texas

In some inverse problems that arise in detecting information about unknown structures we expect solutions that are piecewise continuous. For example, the problem of determining the size and shape of an orbiting satellite from backscattered far field measurement, or the problem of determining crop populations from infrared radiation data. Moreover, these problems are ill-posed which means among other things that accurate determination of solutions from noisy data is difficult, if not nearly impossible, unless special steps are taken. One class of methods dealing with these difficulties is regularization. In this paper, a regularization scheme is shown for finding approximate solution of inverse problems which (a-priori) possess piecewise continuous solutions. A numerical example is given.

7-6 UTILIZATION OF POLARIZATION-DEPOLARIZATION CHARACTERISTICS IN PROFILE INVERSION OF A PERFECTLY CONDUCTING PROLATE SPHEROID: Sujeeet K. Chaudhuri and Wolfgang M. Boerner, Department of Electrical Engineering, University of Manitoba, Winnipeg, Manitoba, Canada

During the past decade a great deal of interest has been generated in the inverse scattering field, however the demand for new basic model theories is as strong as ever, as these model theories are fundamental to remote sensing problems. The existing techniques, owing to the exhaustive amount of imput information requirements, seem increasingly unfeasible.

The polarization-depolarization characteristics which have had very little importance in the inverse scattering

investigations so far appear to have the potential to add new dimensions to inverse scattering techniques. Thus the purpose of this study is to use polarization-depolarization characteristics of electromagnetic wave scattering as a basic tool in developing improved techniques which can be applied successfully to the recovery of radar targets under various difficult situations.

A new model for the solution of the inverse problem of electromagnetic scattering by smooth, convex shaped, perfectly conducting, 3-dim. scatterers has been developed. Certain geometrical as well as physical optics approximations were used to incorporate the concept of the "Minkowski problem" of differential geometry into the space-time integral solution of electromagnetic scattering. This enables the formal solution for the recovery of the surface profile of the scatterer from the scattered field data. Application of this inverse scattering model to the test case of a perfectly conducting prolate spheroid has been undertaken. Various results, along with errors and limitations, are discussed in this paper.

7-7 APPLICATION OF ALGORITHMS FOR THREE-DIMENSIONAL IMAGE RECONSTRUCTION FROM MULTIPLE TWO-DIMENSIONAL PROJECTIONS TO ELECTROMAGNETIC INVERSE SCATTERING: Yogadhish Das and Wolfgang M. Boerner, Department of Electrical Engineering, University of Manitoba, Winnipeg, Manitoba, Canada

In radar identification of perfectly-conducting convex objects, a need arises to reconstruct a three-dimensional body from a knowledge of its area functions. It is known that this problem can be solved by using the inverse Radon transform. It is shown here that this problem is analogous to the well-known problem of three-dimensional image reconstruction from multiple two-dimensional projections, which occur in such diverse fields as electron microscopy, radio astronomy, tomography, interferometry, geophysical exploration, etc. The data inversion algorithms developed in these various fields have been used to estimate the shapes of radar targets from their area functions, which are obtained from their far field, back-scattered ramp responses using the physical optics approximation. Far field measurements of the back-scattered ramp responses for various directions of incidence or of

some function from which they can be computed are assumed to be available.

7-8 THEORETICAL LIMITATIONS OF COHERENT IMAGING IN THE PRESENCE OF ANGULAR AND APERTURE NOISE:  
Giorgio V. Borgiotti, AFCRL, Hanscom AFB, Massachusetts

An optimal procedure is established for the reconstruction of the angular object distribution in a given field of view (FOV). The procedure is "uniformly" optimal in the sense of minimizing for each direction belonging to the FOV the statistical r.m.s. difference between the object distribution-modeled as an "angular" random process, and its reconstructed image. The observable aperture voltage distribution is due not only to the incident field scattered by the object but also to background angular noise from inside and outside the FOV, and to "measurement noise" generated on the aperture. The reconstruction algorithm consists of summing a truncated series of special functions--prolate spheroidal for the linear case and their generalizations for two-dimensional apertures--weighted by appropriate coefficients. These coefficients depend upon the observed aperture field and upon the relative power densities associated with the object field and the various types of noise. The series is truncated to a number of terms ("degrees of freedom" of the image) determined through an information theoretical method: Each term of the series, suitably ordered, provides an information gain lesser than the preceding one, and the information gain goes rapidly to zero. When this happens the conditional entropy of the term in the series for the image reconstruction is equal to the entropy of the corresponding term in the series representation of the object process, and no advantage is obtained by adding extra terms to the series.

7-9 SOME EFFECTS OF WAVE POLARIZATION, FREQUENCY, AND FOCUSING IN MICROWAVE IMAGING: E. L. Rope, G. Tricoles, and On-Ching Yue, General Dynamics, Electronics Division, San Diego, California

Several experiments have demonstrated the feasibility of imaging concealed weapons with microwaves; however, the experimental conditions have been somewhat limited. This paper describes three experiments that illustrate some effects of wave polarization, frequency, and focusing on the quality of microwave images. In the first

experiment, images of a G-shaped aperture were formed by illuminating the aperture with 35 GHz waves, measuring forward-scattered intensity, forming a hologram, and reconstructing with laser light. Image quality depended on wave polarization direction and the spatial frequency content of the aperture. In the second experiment, a metallic triangle partially obscured an antenna that radiated 15.3 GHz waves. The forward-scattered field was probed and encoded into a detour-phase hologram which was illuminated with laser light. Images of the triangle were formed, and distinct images of the radiating antenna were formed by changing the focus of a lens in the reconstruction setup. In the third experiment, images of metallic cylinders and a more complex composite object were formed by measuring back-scattered fields and computing images with an algorithm that was based on the angular spectrum concept. Images depended on the orientation of the object relative to the plane of wave polarization. The effect of optically opaque dielectric covers on image quality is illustrated.

TOPICS IN COMMUNICATION THEORY  
URSI COMMISSIONS VI AND VIII  
Wednesday, October 22 0830  
URSI Session VI-8, 1107 Radio Building  
Chairman: J.K. Wolf,  
University of Massachusetts

8-1 CAPACITY COST OF PAM-TRANSDUCING NOISY FILTER CHANNELS INTO DISCRETE-TIME MEMORYLESS ONES:  
Robert Price, Sperry Research Center, Sudbury, Massachusetts

Miyakawa and Harashima in 1969 conceived the analog communication, nonlinear equalization technique of generalized transmitter modulo-feedback ("MT") precoding, for eliminating inter-symbol interference (ISI) in Pulse Amplitude Modulation (PAM) systems; digital partial-response methods constitute a special case. For noisy filter channels this operation naturally combines with Forney's whitened-matched-filter reception; when in addition operated at the optimum number of levels, such MT-PAM provides relatively efficient though uncoded digital communications as shown in the author's ICC '72 paper. The present study seeks to determine the capacity reduction incurred in applying the above PAM transduction technique (together with implied error-correction coding of unlimited complexity) to a frequency-attenuating channel perturbed by stationary Gaussian noise. Thereby, a memoryless sample-data channel is created. It is found that the modulation yielding maximum information transfer is discrete-time memoryless and equiprobably occupies an amplitude-level continuum. Using an on-off pulse energy spectrum (that best conserves average transmitter power) and modulating at the optimum pulse rate, the reduced capacity may be found from an entropy table for the Theta function, once the effective energy transfer factor at that rate has been deduced from the attenuation contour of the original channel. Quite generally, the MT-PAM transduction capacity-loss at high channel snr's approaches 1.53 dB in equivalent transmitter power penalty; numerical analysis for an underwater-acoustic-path example exhibits similarly modest loss over the whole snr range. These results argue that in modem design the familiar separation of pulse-by-pulse equalization from error-control coding is not unduly dichotomous, and often may not be seriously suboptimal in combatting ISI (relative to invoking maximum-

likelihood sequence estimation via the Viterbi algorithm).

8-2 ON THE CHARACTERIZATION OF A NEW CLASS OF COMMUNICATIONS CHANNEL: THE RANDOM DELAY CHANNEL:

Mario A. Blanco and F. S. Hill, Jr., Department of Electrical and Computer Engineering, University of Massachusetts, Amherst, Massachusetts

There has been a great deal of interest in the problems of analyzing the effects of random channels on communication reliability over the last several years. Many models have been developed to represent the effects of multipath transmission and scattering on tropospheric and ionospheric channels, underwater sonar channels, and in satellite communication systems. We introduce the pure delay channel, which causes a signal to suffer a time-varying and random delay during transmission. In this manner an impulse input at time  $t$  produces an output impulse at time  $t + \theta(t)$ , where  $\theta(t)$  is in general a random process. The impulse response of such a channel follows from this definition, and we show necessary and sufficient conditions on  $\theta(t)$  to make the channel physically reasonable. An alternative impulse response is determined that guarantees conservation of energy, thus permitting one to isolate effects of propagation loss and signal distortion in an actual transmission situation. This model is generalized to the multipath random delay case, and compared with other models developed over the years. Additional applications in the areas of speaker recognition studies and random path networks are presented. Focusing primarily on the single path delay case, various aspects of the statistical characterization of the output signal are developed. It is shown how all the multidimensional distribution functions of the output signal can be computed in principle if one has complete statistical knowledge of both the process  $\theta(t)$  and input signal. Special emphasis is then given to the mean and autocorrelation functions, and several examples are given. Further, the stationarity of the output signal is analyzed, and necessary conditions on the delay function  $\theta(t)$  and input signal are presented to insure that the output signal is strictly stationary, wide sense stationary, or cyclo-stationary. The problem of minimum mean-squared error (MMSE) estimation of randomly delayed signals in additive noise is considered, and expressions for the optimal linear filter are obtained for stationary and some special cases of nonstationary delay functions  $\theta(t)$  and wide sense stationary input signals. The problem of MSEE estimation of a pulse of known shape with a randomly time-varying delay

and additive noise is also analyzed, and both optimal and suboptimal results are given.

8-3 REFLECTIONS ON CODING AND MODULATION: Julian J. Bussgang, Signatron, Inc., Lexington, Massachusetts

For many years coding and modulation were regarded as two separate disciplines in radio communications art. One of the reasons has been that coding related to the transmission of binary data while modulation dealt primarily with the transmission of analog waveforms. The trend towards digital communications leads us to restudy the problem of digital transmission of analog data. One finds that, for the best system performance, it is necessary to apply an integrated approach utilizing properly both coding and modulation since both represent a waveform transformation. Following this transformation, the new signal occupies more bandwidth than the original signal. One feature of the combined design approach is that one can attain performance close to the theoretical rate distortion in a specified signal-to-noise ratio region.

8-4 CODING FOR MULTI-USER COMMUNICATION CHANNELS: Jack Keil Wolf, Department of Electrical and Computer Engineering, University of Massachusetts, Amherst, Massachusetts

Most of the previous analyses of communication systems has been concerned with the transmission of information from a single source to a single receiver. In many communication networks, the simultaneous transfer of information amongst several users is required. Recent work in information theory has been concerned with calculating the channel capacity (region) for several different channel configurations. Such calculations make use of a random coding argument and do not concern themselves with the performance of specific codes. In this paper the use of deterministic codes for several channel configurations (such as the broadcast channel and the multiple access channel) is investigated.

8-5 MULTIPLE-USER SHANNON THEORY: A.D. Wyner, Bell Laboratories, Murray Hill, New Jersey

In this introductory talk we will discuss several multiple-user communication systems and corresponding Shannon-theoretic results. One such communication system is the "multiple-access" channel in which two or

more separated transmitters seek to communicate with a single receiver via the same channel (as for example in a satellite "up-link"). In this situation the theory yields "tradeoff" curves between achievable transmission rates at the various transmitters.

8-6 CHANNEL MODELING AND SIMULATION FOR EVALUATION OF TRANSIONOSPHERIC COMMUNICATION SYSTEMS: Rodger E. Ziemer, University of Missouri, Rolla, Missouri

In this paper two general communication channel models, which are applicable to transionospheric scintillation channels, are discussed. These are termed the linear time-varying filter and the probabilistic transition-mechanism channel models to the transionospheric scintillation channel are given. Their use for communication system performance evaluation via computer simulation is illustrated by considering typical digital data-transmission systems. In order to do so, phase-quadrature components of the instantaneous channel gain must be synthesized, as only envelope data is available from present channel measurements. A method for simulating these components using the Rino correlated-Gauss-quadrature model is described, and the computer-generated synthetic components are compared with actual data on the basis of amplitude and fade-duration statistics.

8-7 COMMUNICATION POSSIBILITIES FOR CHIRP-PULSE REFLECTION FROM THE IONOSPHERE: Alfonso Malaga and Robert E. McIntosh, University of Massachusetts, Amherst, Massachusetts

The feasibility of using the dispersive property of the ionosphere for the design of intermediate and long range chirp-pulse communication systems is considered in this paper. Transmitted pulses can be synthesized such that the reflecting ionosphere acts as a "matched filter," i.e., the optimum transmitted signal is a translated version of the impulse response of the ionosphere. However, since these signals tend to have complicated envelopes and frequency modulation, we treat the near-optimum case where the transmitted signals have rectangular or Gaussian envelopes and linear frequency modulation. It is found that an appropriate selection of the frequency sweep rate results in high compression (10-20 dB) ratios at the receiver for a wide range of carrier frequencies. Furthermore, an analysis of the pulse compression ratio in the neighborhood of the receiver for these pulses

shows that at certain carrier frequencies the pulse compression is strongly dependent on the receiver location. Finally, the effects of randomness of the ionospheric profiles on the choice of carrier frequency and sweep rate and the resulting compression ratios are discussed.

BEHAVIORAL EFFECTS (LOW LEVEL EXPOSURE)

URSI COMMISSION I (BIOLOGICAL EFFECTS)

Wednesday, October 22 0830

URSI Session B-6a, UMC East Ballroom

Chairman: D. Justesen,

Veterans Administration Hospital,

Kansas City

B6a-1 STUDY OF THE MICROWAVE-INDUCED PERTURBATIONS OF THE BEHAVIOUR BY THE OPEN-FIELD TEST INTO THE WHITE RAT: J. Gillard, B. Servantie, G. Bertharion, A. M. Servantie, J. Obrenovitch, and J. C. Perrin, Ecole d'Application du Service de Santé pour la Marine et Centre d'Etudes et de Recherches Biophysiques Appliquées à la Marine, Hôpital d'Instruction des Armées Sainte-Anne, Toulon Naval, France

We have explored the effect of a microwave field into white rats with the open-field test. The spontaneous behaviour of the animal is studied with four parameters: locomotor activity, exploration activity, vigilance, and emotionality. Rats (106 control and 82 irradiated animals) have been exposed during two weeks to an X-band 9.4 GHz pulse-modulated microwave field with an average power-density of  $0.7 \text{ mW/cm}^2$ . In control animals, locomotor activity, emotivity, and vigilance decrease during the test, when exploratory activity increases. In irradiated animals, exploratory activity increases more slowly, vigilance at first increases then decreases, and locomotor activity is uniform.

B6a-2 "AVOIDANCE" BY RATS OF A 2.88 GHz PULSE MICROWAVE FIELD: E.L. Hunt, Walter Reed Army Institute of Research, Washington, D.C.; N. W. King and R.H. Lovely, University of Washington, Seattle, Washington; and R.D. Phillips, Battelle Pacific Laboratory, Richland, Washington

B6a-3 ALTERATIONS IN THE SLEEP PROCESS OF THE RABBIT AS A FUNCTION OF CHRONIC LOW INTENSITY ELECTROMAGNETIC RADIATION EXPOSURE: R. C. Manthei and Z. R. Glaser, Biomedical Research Laboratory, Naval Surface Weapons Center, Dahlgren, Virginia

Data have shown brain electrical activity associated

with sleep states to be biologically constant for any given species. Further, nonionizing radiation exposure has been shown to alter brain electrical activity. The sleep process is characterized by cyclic fluctuations between alertness (W), slow wave (SW), and paradoxical (REM) stages. Rapid eye movement sleep (REM) is a very active state metabolically and is functionally defined as that period of sleep in which cortical activity paradoxically reveals low voltage, fast activity characteristic of the awake phase, concurrent with rapid eye movement, and atonus of neck muscle. Chronic recordings of electrocorticogram (ECOG), electro-oculogram (EOG), and electromyogram (EMG) were obtained daily from adult male rabbits on a 24-hour basis following daily 2-hour microwave exposure at  $5 \text{ mW/cm}^2$  for sixty days. The surgical implant assembly was designed to allow chronic post-irradiation recording while allowing no metallic elements to be associated with the subjects during microwave exposure. A unique application of logic circuitry allowed the investigator to quantify both the frequency and duration of REM stage episodes. The hypothesis is advanced that prolonged exposure of an organism to microwave radiation will decrease the frequency and duration of REM stage sleep. The sleep process is viewed as a potential index of CNS adaptation to prolonged EMR exposure.

B6a-4 THE EFFECTS OF 1.7 AND 2.45 GHz MICROWAVES ON DRUG-INDUCED SLEEPING TIME IN THE RABBIT: S. F. Cleary, Department of Biophysics, Virginia Commonwealth University, Richmond, Virginia

Exposure of anesthetized rabbits to 1.7 and 2.45 GHz pulsed and CW microwave radiation led to a dose dependent decrease in mean sleeping time. The 2.45 GHz irradiations caused a greater decrease than 1.7 GHz microwaves at all power densities in the range of from  $5$  to  $50 \text{ mW/cm}^2$ . 2.45 GHz exposures produced a 15% decrease at  $5 \text{ mW/cm}^2$ , CW, in contrast to 1.7 GHz radiation which did not significantly reduce sleeping time at this intensity. The effect of the thermal stress on the reduction in sleeping time was investigated by rectal temperature measurements in irradiated, sham-irradiated, and animals exposed to thermal stress by increased environmental temperatures. The effects of pulse modulation and variation in drug dosage were also investigated in an attempt to ascertain the extent to which the sleeping time alterations are dependent upon alteration of body temperature in the rabbit.

B6a-5 MODIFICATION OF INTERNAL DISCRIMINATIVE STIMULUS  
CONTROL OF BEHAVIOR BY LOW LEVELS OF PULSED MICRO-  
WAVE RADIATION: John R. Thomas, Stephen S.  
Yeandle, and Linda S. Burch, Naval Medical Research  
Institute, Bethesda, Maryland

The behavioral effects of pulsed microwave radiation were determined on rats performing on a reinforcement schedule regulated by internal stimulus control. The reinforcement schedule required that at least eight consecutive responses be made on one response lever before a response on a second lever would be reinforced with food. If the animal switched to the second lever before the count of eight, the sequence of eight responses has to be restarted. Baseline performances over a 6-month period indicated the existence of a discrimination of the number of responses counted on the first lever, as switching responses occurred with the largest frequency following eight or more responses. Exposure to a pulsed 2.45-GHz radiation source for 30 minutes with power densities of 5, 10, or 15 mW/cm<sup>2</sup> produced changes in the performance on the fixed consecutive number schedule. All power densities led to increased frequency of premature switching, with the highest power producing the most disruption of the counting discrimination. Premature switching responses due to radiation exposures were associated with pronounced reductions in the percentage of correctly performed response runs that produced reinforcements. Microwave radiation had no effects on overall or running response rates or on response variability. Performance changes were not related to induced hyperthermia.

BEHAVIORAL EFFECTS (HIGH LEVEL EXPOSURE)

URSI COMMISSION I (BIOLOGICAL EFFECTS)

Wednesday, October 22 1040

URSI Session B-6b, UMC East Ballroom

Chairman: E. Hunt,

Walter Reed Army Institute of Research

B6b-1 BEHAVIORAL EFFECTS OF RESONANT ELECTROMAGNETIC POWER ABSORPTION IN RATS: John A. D'Andrea and Om P. Gandhi, Departments of Electrical Engineering and Bioengineering, and Raymond P. Kesner, Department of Psychology, University of Utah, Salt Lake City, Utah

Previous experiments have indicated that RF absorption by an animal in a plane wave field depends strongly on the polarization and frequency of the electromagnetic field (Gandhi, 1974). Two experiments are being performed to determine the effect of RF absorption on the awake active rat. To determine the resonant absorption frequency, fifteen male Long Evans rats, 350-380 grams in body weight, were each habituated for 30 minutes a day for four days to a cylindrical Plexiglass restraining chamber (6.5 x 24 cm). On RF exposure days, each rat was fitted with a liquid crystal fiberoptics temperature probe (3 cm rectally). Each rat was given 10 minutes exposure to RF radiation within a TEM parallel plate waveguide at fifteen frequencies within the 220-500 MHz band. RF absorption at 500 MHz with the length of the rat body parallel to the electric field was three times greater than the average absorption of the other frequencies. RF absorption at 500 MHz in the electric field orientation was fifteen times greater than with the rat body parallel to the direction of propagation. To determine the effect of RF absorption on a well trained behavior, six male Long Evans rats were trained to press a Plexiglass lever for dry food pellets on a variable interval 30-second reinforcement schedule while in the parallel plate waveguide. Preliminary results indicate that resonant (500 MHz) RF exposure in the electric field orientation disrupts lever-pressing behavior sooner than RF exposure at nonresonant frequencies. RF absorption measurements will be extended to 750 MHz.

B6b-2 THE EFFECTS OF MICROWAVE RADIATION ON BEHAVIOR AND TEMPERATURE IN RHESUS MONKEYS:

John O. de Lorge, Naval Aerospace Medical Research Laboratory, Pensacola, Florida

Male rhesus monkeys, trained to respond on a vigilance task, were exposed to vertically polarized 2450 MHz microwaves in an anechoic room. Power densities of 4, 16, 32, 42, 52, and 62 mW/cm<sup>2</sup> (measured at the level of the animal's head) and exposure times of 30, 60, and 120 minutes were used. The transmitter system was a Holaday Magnetron with up to 1500 watts of RF output and, while all levels employed continuous waves, pulsed waves were also used at 4 and 16 mW/cm<sup>2</sup> (PRF = 1 sec, P.D. = 0.1 sec). The vigilance task required the monkey to press a lever to produce one of two different auditory stimuli. A response on the other lever in the presence of the correct stimulus delivered a food pellet. Responses on the other lever during the incorrect stimulus and at other times postponed food delivery. The monkeys performed the task in a styrofoam restraint chair while being irradiated from the front. Body temperature was monitored during exposure at all but the lowest power density. Vigilance performance was not affected until 52 and 62 mW/cm<sup>2</sup> illuminations occurred and even in these instances behavior was only minimally and inconsistently changed. Mild body heating (0.4° C to 1.7° C) was associated with the higher densities (32-62 mW/cm<sup>2</sup>) although body temperature was not related to observed behavioral changes at these same levels.

B6b-3 MICROWAVE AND INFRARED RADIATION EFFECTS ON AN OPERANT RESPONSE IN RHESUS MONKEYS: R.D. McAfee, Medical Research Department, Veterans Administration Hospital, New Orleans, Louisiana (and S. Thomas Elder, R.J. Lipscomb, J.G. May, and M.G. Holland

Four unrestrained rhesus macaques were trained to lever press for a reward which could be obtained if they placed their mouth on an acrylic drinking tube positioned so that drinking from it would place the rhesus' eyes in the center of a 9.3 GHz microwave field. They were irradiated for 15 minutes at power densities ranging from 350 mW·cm<sup>-2</sup> to 450 mW·cm<sup>-2</sup>. Microwave irradiation did not suppress their lever press rate, a finding which suggests that the power density and times used in the experiment were not aversive to the rhesus.

B6b-4 MICROWAVE-INDUCED AVOIDANCE BEHAVIOR IN THE  
MOUSE: John C. Monahan and Henry S. Ho,  
Bureau of Radiological Health, Rockville,  
Maryland

Previous research has established that microwave radiation is capable of effecting behavioral changes in an organism. A report on our waveguide apparatus has shown that the measured percentage of forward power absorbed by a mouse can vary according to the orientation and position of the animal in the waveguide. The purpose of this investigation is to quantify the ability of low level 2450 MHz CW microwave energy to generate avoidance behavior in the male mouse (30-34 gms). Subjects were irradiated in an environmentally controlled waveguide assembly at incident power levels of .84, 1.6, 2.4, 3.2, 4.0, and 4.8 W. At 1.6 W and higher, the percent absorption decreased after the initial five minutes and remained lower for the duration of exposure. Subjects exhibited an average maximum of 57% absorption at .84 W and this decreased with increasing power to an asymptote of approximately 35% at 3.2, 4.0, and 4.8 W. Although no visual observations were possible during irradiation, it is assumed that the subjects are actively decreasing their potential dose of microwave energy by altering both their orientation and their position within the waveguide assembly. This data suggests that the subjects are capable of detecting average dose rates of as little as 28 mW/gm. Furthermore this level of irradiation, while not producing core temperature increases of more than 0.5°C, is aversive and will cause the animal to actively try to avoid the microwave radiation.

B6b-5 PHYSIOLOGICAL AND BEHAVIORAL EFFECTS OF CHRONIC  
LOW LEVEL MICROWAVE RADIATION OF RATS: K. E. Moe,  
R. H. Lovely, and A. W. Guy, Bioelectromagnetics  
Research Laboratory, Department of Rehabilitation  
Medicine and Department of Psychology, University  
of Washington, Seattle, Washington

Eight male rats were irradiated for three months with 918 MHz microwaves pulse-modulated at 11 Hz, for 8 hours/day, and at field strengths of 10 mW/cm<sup>2</sup> or less. Exposure was during the active part of the day-night cycle. The exposure apparatus consisted of a cylindrical wave-

guide capable of delivering circularly polarized guided waves (TE<sub>11</sub>) mode) and a living chamber designed and shown to be compatible with normal laboratory living conditions required by rats. The cylindrical waveguide allowed for easy quantification of the fields for each exposed animal independent of other rodents being simultaneously exposed. Biological and behavioral comparisons between the 8 irradiated and 8 sham-irradiated controls included food and water intake, body weight, blood sugar, metabolic hormones, and behavioral repertoire during the exposure period. These variables were assessed every three weeks, and the effects of chronic irradiation by 918 MHz pulse-modulated microwaves on them will be presented.

ASSESSMENT OF POWER DEPOSITION IN TISSUES BY

MATHEMATICAL AND PHANTOM MODELS

URSI COMMISSION I (BIOLOGICAL EFFECTS)

Wednesday, October 22 0830

URSI Session B-7a, UMC West Ballroom

Chairman: H. Schwann,

University of Pennsylvania

B7a-1 THEORETICAL CALCULATIONS OF POWER ABSORBED BY MONKEY AND HUMAN SPHEROIDAL AND ELLIPSOIDAL PHANTOMS IN AN IRRADIATION CHAMBER: Habib Massoudi, Carl H. Durney, and Curtis C. Johnson, University of Utah, Salt Lake City, Utah, and Stewart Allen, Brooks AFB, Texas

The electromagnetic field perturbation technique which has been used previously to obtain the internal electric field strength, the absorbed power density distribution, and the total absorbed power in tissue prolate spheroids irradiated by planewaves with wavelengths long compared to the spheroid dimensions is applied here to the calculation of the total absorbed power in a near-planewave irradiation chamber for purposes of comparing experimental and theoretical values. The measured values of electric and magnetic field strength in the empty irradiation chamber are used in the calculation of the absorbed power. Since the measured values of  $E$  and  $H$  do not have the plane-wave impedance of  $377 \Omega$ , a theoretical technique has been developed in which the power absorbed in the prolate spheroid phantoms in the presence of two oppositely traveling planewaves is calculated. This method gives the power absorbed in an irradiation field in which the  $E/H$  impedance ratio is not necessarily equal to  $377 \Omega$ . Calculated data for power absorbed by monkey and human phantoms from 10 MHz to 50 MHz are presented and discussed. For the monkey phantoms, data are given for the three principal polarizations: electric, magnetic, and cross, but for the human phantom, data are given only for magnetic and cross polarization because the phantom is too long to allow measurements with electric polarization. Calculations were made for the power absorbed by twenty monkey phantoms because the power absorbed by fewer phantoms is too small to be measured accurately.

B7a-2 MEASUREMENT OF RADIOFREQUENCY POWER ABSORPTION IN MONKEYS, MONKEY PHANTOMS, AND HUMAN PHANTOMS EXPOSED TO 10-50 MHz FIELDS: S. J. Allen, W. D. Hurt, J. H. Krupp, and J. A. Ratliff, USAF School of Aerospace Medicine, Radiobiology Division, Brooks AFB, Texas; C. J. Durney and C. C. Johnson, University of Utah, Salt Lake City, Utah

Realistic EMR hazard assessment requires careful analysis of total power absorbed and distribution in the test specimen. Test methods must consider such factors as size, orientation, complex shape, and complex dielectric properties of the exposed specimen as well as exposure frequency. Previous experiments were conducted using a rectangular human size phantom. These data showed excellent comparison to calculations using a prolate spheroid model. As a follow-on to this experiment, a 70 kg prolate spheroid human phantom and twenty 3.5 kg prolate spheroid monkey phantoms were constructed, filled with a saline solution having a conductivity 0.6 mho per meter, and the power absorption measured using differential power measurement techniques for 10 to 50 MHz exposures. Twenty Rhesus monkeys averaging 3.5 kg were also used to compare power absorption of primates with the equivalent primate phantoms. Monkeys and monkey phantoms were exposed for electric, cross, and magnetic polarization. The human phantom was exposed for cross and magnetic polarization. Experimental techniques will be presented and comparison of experimental and theoretical results will be discussed.

B7a-3 POWER DEPOSITION IN A MULTILAYERED SPHERICAL MODEL OF THE HUMAN HEAD: S. M. Neuder, Division of Electronic Products, Bureau of Radiological Health, FDA, Rockville, Maryland; and D. H. Hill, and R. B. Kellogg, Institute of Fluid Dynamics & Mathematics, University of Maryland, College Park, Maryland

A theoretical investigation has been conducted of the magnitude and spacial variations of power depositions in a multilayered spherical model of the human head exposed to plan wave electromagnetic (microwave) radiation of various frequencies in the ISM band. Numerical and graphical results are presented, locating hot spots within the spherical regions and the fields both within and external to the spheres.

B7a-4 DISTRIBUTION OF ELECTROMAGNETIC ENERGY DEPOSITION IN MODELS OF MAN WITH FREQUENCIES NEAR RESONANCE: Om P. Gandhi, Kazem Sedigh, Gary S. Beck, Departments of Electrical Engineering and Bioengineering, University of Utah, Salt Lake City, Utah; and Edward L. Hunt, Department of Microwave Research, Walter Reed Army Institute of Research, Washington, D.C.

Experimental results are described for whole-body absorption (for orientations  $\vec{E} \parallel \vec{L}$ ,  $\vec{k} \parallel \vec{L}$  and  $\vec{H} \parallel \vec{L}$ ) of a series of saline-filled and biological-phantom figurines of major lengths (L) that varied from 0.4 to 1.5  $\lambda$ . Measurements are also reported of  $\alpha$  parameter values (ratio of mW/gm of absorbed energy to mW/cm<sup>2</sup> of incident field energy) for different regions of the body. The energy distribution is measured for 12.1 and 18.4 cm tall figurines under free space irradiation at both 985 and 2450 MHz using the liquid crystal temperature probe. These results are compared to those obtained in the TEM parallel plate chamber, namely, of whole-body values for the 220-750 MHz frequency range with 12.1 and 18.4 saline-filled figurines and prolate spheroids of  $a/b=6$ . The highest intensity of energy deposition is observed for the neck region of the body in both free space and parallel plate exposure conditions. The  $\alpha$  for the neck region is approximately 30 times that observed for the whole-body average. The  $\alpha$  values for other parts of the body, in descending order of magnitude, are reported for the thighs, shins, chest, pudendal region, and the eye region. For figurines with the feet touching the ground plate of the parallel-plate chamber, maximum energy deposition is observed for the shins, with  $\alpha=12$  at 240 MHz ( $L/\lambda \approx 0.15$ ). A monopole-above-ground chamber is presently under construction to permit assessment of ground effects and measurements of  $\alpha$  values using this chamber will also be presented. The technical support by J. H. Jacobi and P. B. Brown, Department of Microwave Research, WRAIR, is gratefully acknowledged.

B7a-5 MODELS OF BIOLOGIC INTERACTION WITH ELECTROMAGNETIC FIELDS: J. W. Frazer, USAF School of Aerospace Medicine, Brooks AFB, Texas, and J. MacDougal, M. Webb, and A. W. Guy, University of Washington, Department of Rehabilitation Medicine, Seattle, Washington

Guy, et al., have previously reported investigations of the power distribution in man models as a function of

frequency below resonance. It was found that field impedance was a very important factor in the distribution of absorbed power below resonance, with magnetic coupling producing toroidal currents predominating in low impedance fields and electric coupling resulting in peak power deposition wherever current "pinches" occurred in high impedance fields. Allen, et al., have explored the power deposition in prolate ellipsoids in a variety of HF band fields, and found reasonably good agreement between a theoretical prediction of Durney, et al., and power absorption measurements performed in the USAFSAM/NS HF band exposure system. We have found that simple rectal temperature measurements in rats exposed to strong magnetic fields (40 amp meter-1) at 19 mhz in the USAFSAM near-field synthesizer demonstrates a qualitative agreement with theory in that increase in diameter was accompanied by more rapid heating over a narrow range of animal radii. Distribution of absorbed energy was measured in rats sectioned along their long axis at frequencies of 19 mhz and 1600 mhz, and in two specially designed head inactivators at 2450 mhz using electric and magnetic field concepts. In addition, energy distribution in prolate ellipsoids was measured at 19 mhz with a field impedance  $\sim 337$  ohms, in the near field synthesizer with field impedance of  $\sim 100$  ohms and  $\sim 1000$  ohms, as well as at 1600 mhz with field impedances of  $\sim 377$  ohms. It was found that eddy current-induced heating at 19 mhz varied with the aspect to the field, as expected, and that even in a uniform ellipsoid distinctly non-uniform heating patterns were produced in electric and magnetic fields.

DIELECTRIC PROPERTIES OF TISSUES  
URSI COMMISSION I (BIOLOGICAL EFFECTS)

Wednesday, October 22 1048

URSI Session B-7b, UMC West Ballroom

Chairman: H. Schwann,  
University of Pennsylvania

B7b-1 A TWO-IMPEDANCE METHOD FOR WIDE RANGE DIELECTROMTRY: M. Swicord and J. Saffer, Division of Electronic Products, Bureau of Radiological Health, FDA, Rockville, Maryland; A. Cheung, University of Maryland, Institute of Fluid Dynamics & Applied Mathematics, College Park, Maryland

A method is described for measurement of complex dielectric constants which is useful over a frequency range of from 200 MHz to 18 GHz. Two different sample lengths may be required if the entire frequency range is to be covered. Dielectric constant values from 1 to 50 with a loss tangent of as much as 0.5 are measured with an accuracy dependent on the sensitivity of the particular system used. Transmission line theory for lossy dielectrics is employed, but the need to solve transcendental equations has been eliminated. The method is particularly adaptable to use with automated systems but can also be used with slotted lines. A distinct advantage of the method is its independence of measured sample lengths and the easy construction of a sample holder. The method is expanded to include corrections for the sample holder. Comparative data using an automatic network analyzer and a slotted line is presented.

B7b-2 WIDE-BAND CHARACTERIZATION OF DIELECTRIC AND HEAT PROPERTIES OF SIMULATED BIOTISSUES:

Augustine Y. Cheung, David W. Koopman, and Mays L. Swicord, Institute for Fluid Dynamics and Applied Mathematics, University of Maryland, College Park, Maryland

Simulated muscle-phantom suitable for modeling (full size and scaled) biological exposure experiments have been developed for x-band frequencies. These tissues consist of mixtures of saline solution, polyethylene, and Super Stuff and their dielectric properties can be varied over a wide range by simply changing their composition ( $30 \leq \epsilon \leq 45$ ;  $.1 \leq \tan \delta \leq .4$ ). The frequency (1-18 GHz) characteristics and temperature dependence of the dielectric properties of these phantoms were studied using

Time Domain Techniques at various temperatures (25-45°C) and they are found to be governed by a Debye type relaxation process with a temperature sensitive relaxation time  $\tau$  centered at ~ 50 psec. The temperature effect showed up as a one percent change in  $\epsilon$  and three percent change in  $\tan\delta$  per degree centigrade which is also measured over the x-band range by short-circuited waveguide techniques. Specific Heat and Thermal conductivity were also studied. The specific heat, measured by calorimetry, was found to vary from .62 to .88 and the thermal conductivity, measured by a modified Fitch Conductivity Apparatus, was found to be  $\kappa \sim 2-6 \times 10^{-3} [\text{cal/cm} \cdot ^\circ\text{C} \cdot \text{sec}]$ .

B7b-3 THE ATTENUATION FUNCTION FOR BIOLOGICAL FLUIDS AT MILLIMETER AND FAR-INFRARED WAVELENGTHS: K. H. Illinger, Department of Chemistry, Tufts University, Medford, Massachusetts

We present a derivation of the attenuation function,  $\alpha(\omega)$ , for a fluid, exhibiting relaxation and resonance absorption of electromagnetic radiation, via a theoretical model which evades the (physically) incorrect limit for  $\alpha(\omega)$  for a Debye-type relaxation process. The collisional interruption of absorption and emission of electromagnetic radiation by molecular fluids is treated in terms of a formulation describing the efficiency of collisional perturbation as a function of the field frequency,  $\omega$ , and the correlation times characteristic of molecular motion. The attenuation function, and hence the depth of penetration,  $[1/\alpha(\omega)]$ , is computed on the basis of this model for a series of systems of interest. The results of the theory are compared to existing experimental results for liquid  $\text{H}_2\text{O}$ , and typical biological tissue. Consequences of the foregoing considerations for the description of the interaction between biological fluids and electromagnetic radiation at millimeter and far-infrared wavelengths are discussed.

B7b-4 ELECTRIC DIPOLE INTERACTIONS FOR MICROWAVE PULSES AND DAMAGE TO EMBRYOS: S.D. Pyle, C.L. Hu, R. Caldwell, F.S. Barnes, Department of Electrical Engineering, University of Colorado, Boulder, Colorado

The results of some experiments on the application of high power microwave pulses to zebra fish embryos are reported. Microsecond pulses with electric field strengths between 5 and 15 kV/cm at 2.7 GHz have been used to kill fish embryos

in a temperature-controlled environment. Evidence will be presented showing a partial temperature independence for damage and indication that the orientation of asymmetric dielectric bodies may be responsible for death by changes in osmotic pressure. Low frequency data on electrically-induced birefringence changes in blood plasma will also be presented.

RADIO OCEANOGRAPHY--WAVE SPECTRA, SYNTHETIC  
APERTURE RADARS, AND RADIOMETERS

URSI COMMISSION II

Wednesday, October 22 1330

URSI Session III-8, UMC Forum Room

Chairman: D.E. Barrick, NOAA

8-1 DESIGN CONSIDERATIONS FOR A DIRECTIONAL OCEAN  
WAVE SPECTROMETER: L. Brooks, R.P. Dooley, and  
F. Nathanson, Technology Service Corporation  
Silver Spring, Maryland

This paper examines a short pulse wide-band radar technique for measuring ocean wave spectra. A spectral analysis of the amplitude modulation (caused by ocean waves) on the return signal is performed at a given analysis direction. A slow mechanically conical scanned antenna then permits the spectral measurement every  $\Delta\theta^0$  over the full  $360^0$  scan. The required receiver processing and underlying assumptions are established and used to develop design equations for the gravity wave spectrum of the ocean surface. It is shown that the input to the spectrum analyzer consists of two noise processes, one being the desired modulation of  $\sigma^0$  and the other due to the fact that the modulation is riding on a noise process whose mean is  $\sigma^0$ . An approximate expression is developed which gives the probability of detecting the desired modulation on  $\sigma^0$ . This expression provides a useful system design constraint. The limiting design constraint is derived from an expression for the standard deviation of the ocean wavelength measurement. The design equation for measurement accuracy exhibits a saturation effect which occurs when the "signal-to-noise" into the spectrum analyzer,  $(S/N)_{isa}$ , is near unity. Thus a further increase in  $(S/N)_{isa}$  beyond this value provides little improvement in measurement accuracy. However, the  $(S/N)_{isa}$  is found to be a function of modulation index,  $\lambda$ , and the number of resolution cells per ocean wavelength. To achieve unity  $(S/N)_{isa}$  with a 2 dB (peak-to-peak) modulation it is necessary to resolve to the order of a 19th of a (water) wavelength.

8-2 MEASUREMENT OF SEA SURFACE MULTIPATH PHENOMENA  
USING UHF SIGNALS FROM GOES-2: K. R. Carver,  
Physical Science Laboratory, New Mexico State  
University, Las Cruces, New Mexico

This paper describes the results of an extensive sea surface multipath measurement program conducted in June, 1975 at Waihi Beach, New Zealand, where the apparent arrival angle was near  $90^\circ$ . The 468.8 MHz circularly polarized signal from the GOES-2 spacecraft (subsatellite point on equator at  $115^\circ$  W. long.) was recorded on strip-chart at antenna heights from 1 to 9.6 m above sea level, using both linearly and circularly polarized antennas. The resulting height-gain profiles, which agree essentially with recent theoretical predictions, show a well-defined lobing structure with height as well as oscillatory power spectra at fixed heights corresponding closely to visually observed ocean wave spectra. The total atmospheric ray bending was calculated by using measured refractivity profiles from radiosonde taken concurrently with the height-gain measurements. These data confirm the predominance at UHF of the coherent portion of the sea-scattered energy and point to the importance of optimizing mounting heights for Data Collection Platform (DCP) antennas on buoys and ships. The ratio of diffuse to coherent scattered energy is shown to depend strongly on the antenna height as well as sea state and spectra. Thus for a practical buoy/ship DCP communication link an estimate of the fraction of time spent in a null (and the related ability of the link to maintain PSK lock) will depend not only on the Rice distribution but also on swell dynamics and platform stability.

8-3 SHIPBORNE HF SYNTHETIC APERTURE OBSERVATIONS  
OF DIRECTIONAL OCEAN-WAVE SPECTRA: Calvin C.  
Teague, Center for Radar Astronomy, Stanford  
University, Stanford, California

Shipborne synthetic aperture observations of directional ocean-wave spectra were made from the R. V. Thomas Washington during the 1974 NORPAX "Pole" experiment in the North Pacific centered at  $35^\circ$ N,  $155^\circ$ W. The observations were made at 4.80, 6.78, 13.38, and 21.77 MHz with the Stanford portable four-frequency radar, using ground-wave propagation. The transmitting antenna was a set of quarter-wave

vertical wires suspended from the ship's mast, and the receiving antennas were individually-tuned loop and sense antennas adjusted for cardioid operation and mounted near the bow. A large aperture antenna was synthesized by steaming at constant velocity for about 350 m on each of 4 or 6 straight courses, separated by 90° or 60°. This gave a maximum theoretical resolution of better than 10°, although the radar-inferred directional spectra were smoothed to remove noise, resulting in a final resolution of about 30° at the half-power points. Techniques were developed to optimize the antenna directional responses and to identify and reject those data segments which were corrupted by strong interference. Several multi-frequency ocean-wave directional spectra were obtained which showed a broad, flat maximum, typically 120° to 180° wide at the half-power points, centered on the mean wind, with front-to-back ratios of 10 to 15 dB.

8-4      IMAGING AND HEIGHT MEASUREMENT OF OCEAN WAVES  
        USING SYNTHETIC APERTURE IMAGING RADARS: C.  
        Elachi and A. Jain, Jet Propulsion Laboratory,  
        California Institute of Technology, Pasadena,  
        California

Ocean waves and a variety of surface patterns have been observed with synthetic aperture imaging radar. The radar provides high resolution two-dimensional imagery of surface waves; however, it is not well understood yet what the surface parameters are which lead to the modulation of the image brightness with the same spatial periodicity of the existing wave pattern. In this presentation we consider three models which might explain the generation of the radar image: 1) a tilt modulation model where the Bragg backscatter cross section is modulated by the surface average slope, 2) a roughness modulation model where the Bragg backscatter cross section is modulated by the magnitude of the small waves, and 3) an orbital velocity modulation model where the backscattered wave is Doppler modulated by the wave orbital velocity. These three models are analyzed numerically and compared to experimental data taken with the JPL L-band imaging radar. We also present some preliminary results of a "speckle technique" which we used to determine the height of the waves from the radar image. This technique basically evaluates the decorrelation between imagery generated

at neighboring radar frequencies. The technique was tested over three different types of sea: 20 ft. waves off Point Conception, California, 10 ft. waves during a cross-Atlantic flight, and 3 ft. waves off Point Mugu, California. As expected from the theoretical analysis, the higher the waves, the faster the multifrequency images decorrelate.

8-5 SYNTHETIC-APERTURE RADARS: MECHANISMS PRODUCING OCEAN-WAVE IMAGES: Robert H. Stewart, University of California, San Diego, La Jolla, California

An L-band synthetic aperture radar flown by the Jet Propulsion Laboratory has shown clear images of longer hectometer ocean waves. Since the radio waves scatter from short centimeter ocean waves, some modulation of the scattering cross section with phase of the longer waves is necessary to produce images of these much longer waves. There are at least four possible mechanisms involved: 1) tilting of the sea surface by the longer waves, 2) modulation of the shorter wave's amplitude by the spatial velocity field associated with the longer waves, 3) enhanced generation of short waves on the long wave's crest, with dissipation in the trough, and 4) distortion of the SAR Doppler mapping from frequency to image space due to additional Doppler imparted by the long-wave orbital velocity. The first process is expected to produce modulations of the scatter cross section on the order of 10 dB for depression angles around  $20^\circ$  to  $40^\circ$ . The contrast is greatest when the radar looks perpendicular to the wave crests and vanishes when it looks parallel. The second and third processes should produce a weaker image, but one that is independent of the orientation of the long waves. The last process may be important for spaceborne radars, although, surprisingly enough, the effect decreases as wave height increases if wave slope is held constant.

8-6 PHASE AND DOPPLER ERRORS IN A SPACEBORNE SYNTHETIC APERTURE RADAR IMAGING THE OCEAN SURFACE: K. Tomiyasu, General Electric Company, Valley Forge Space Center, Philadelphia, Pennsylvania

A conventional side-looking synthetic aperture radar (SAR) assumes a linearly moving platform, stationary targets, and uniform propagation path. With a

spaceborne SAR imaging the ocean surface, consideration must be given to earth rotation, orbit eccentricity, moving ocean waves, and ionospheric granularities. The first three effects will introduce perturbations to the Doppler frequency shift, and if the data were processed assuming otherwise, the images will be displaced in azimuth position. The fourth effect will introduce phase dispersion and time delay variations, and hence may produce degraded images. Against earth rotation effects two compensation methods are suggested; these are: (a) shift the receiver local oscillator frequency to reposition the zero-Doppler frequency direction to fall within the SAR antenna beamwidth, and (b) rotate the SAR antenna beam in yaw angle (yaw axis along nadir) to reposition the antenna boresight in the direction of zero-Doppler frequency. Satellite altitude variations due to orbit eccentricity can be calculated from ephemeris data quite accurately, and it should be possible in principle to program the receiver local oscillator frequency to negate this effect. A difficulty in this method is that the orbit perigee can migrate thereby making compensation more difficult. The magnitudes of these non-negligible phase and Doppler frequency errors will be discussed in terms of their impact on a hypothetical SAR and the processing of ocean wave images.

8-7 MULTI-FREQUENCY HF RADAR MEASUREMENTS OF THE DIRECTIONAL SEA SPECTRUM FROM .14 TO .5 Hz:  
Dennis B. Trizna, John C. Moore, and Robert W. Bogle, Naval Research Laboratory, Washington, D.C.

Radar data from the San Clemente Island HF Radar facility have been collected in the surface wave mode with  $4^{\circ}$  azimuthal resolution over a range of  $40^{\circ}$  in azimuth, from 2 to 25 MHz. Directional sea spectra have been deduced from these data for a variety of sea and wind conditions, and have been compared with the various models proposed for the directional spreading function.

8-8 EQUATIONS FOR PRECISE CALCULATION OF DIELECTRIC CONSTANT OF SEA WATER AT MICROWAVE FREQUENCIES:  
Lawrence A. Klein and Calvin T. Swift, NASA-Langley Research Center, Hampton, Virginia

Newly developed precision microwave radiometers have

created a need for accurately computing the dielectric constant of sea water as a function of water temperature and salinity. Experimental evidence indicates that the dielectric constant  $\epsilon$  may be expressed by  $\epsilon = \epsilon_{\infty} + (\epsilon_s - \epsilon_{\infty}) / (1 + (i\omega\tau)^{1-\alpha}) - i\sigma/\omega\epsilon_0$ , where  $\epsilon_s$  and  $\epsilon_{\infty}$  are the static and high frequency dielectric constants, respectively;  $\tau$  is the relaxation time;  $\sigma$  is the conductivity;  $\epsilon_0$  is the permittivity of free space;  $\omega$  is the radian frequency; and  $\alpha$  is a parameter that accounts for a distribution of relaxation times. This equation reduces to the Debye equation when  $\alpha=0$ . Until now there have not been sea water data available from which to generate  $\epsilon_s$  or  $\tau$  as functions of temperature and salinity. However, recent measurements by North American Rockwell of the real and imaginary parts of the dielectric constant of sea water at 1.43 GHz now make it possible to obtain an accurate expression for  $\epsilon_s$ . The new solution fits the data to within 0.17% on the average, as compared to 2.3% for the best previously available fit. Similar measurements of dielectric constant at 2.65 GHz show that  $\tau$  for sea water seems to be slightly higher than that given by Stogryn's equation based on NaCl experimental results. The new expressions for  $\epsilon_s$  and  $\tau$  are used to advantage in inverting accurate brightness temperature measurements of the ocean surface to give surface temperature and salinity to within rms accuracies of 0.2°C and 1‰, respectively.

EFFECTS OF NATURAL AND INDUCED IONOSPHERIC DISTURBANCES

URSI COMMISSION III

Wednesday, October 22 1330

URSI Session III-5, UMC 157

Chairman: T.E. VanZandt, NOAA

5-1 A COMPARISON OF RF SCATTERING FROM A HEATED  
IONOSPHERIC VOLUME AND THE RADAR AURORA:  
J. Minkoff, Riverside Research Institute,  
New York, New York

Significant similarities between the RF scattering characteristics of a heated ionospheric volume and natural phenomena such as the radar aurora have been observed. Because such heating experiments offer a means of study of ionospheric processes, from which a greater understanding of natural ionospheric phenomena may be obtained, it is of interest to attempt to make a quantitative comparison of the scattering cross sections. In both cases the scattering takes place from field-aligned irregularities for which the cross section can be formulated as a product of two independent factors. One factor describes the aspect sensitivity of the scattering, which can be characterized by a longitudinal scale size  $L$  such that the width of the scattering lobe is  $\sim \lambda/L$ . Measurement of  $L$ , however, requires much greater spatial-resolution capability on the part of the radar system than has been available in such measurements to date. The other factor,  $b(k) = r_e^2 \langle |\Delta n|^2 \rangle S_T(2k)$  (where  $r_e$  is the classical electron radius,  $\langle |\Delta n|^2 \rangle$  the variance of the fluctuations in the electron density distribution and  $S_T$  the spectrum of the fluctuations normal to the earth's magnetic field,  $\vec{B}$ ), is a measure of the turbulence in the electron density distribution on the scale of half the radar wavelength  $\lambda = 2\pi/k$ . The process of determining  $b(k)$  from radar measurements is discussed. The major difficulty arises from the uncertainty in the aspect sensitivity, the effect of which is analyzed quantitatively. It is shown that, because of the uncertainty in  $L$ , only a lower bound on  $b(k)$  can be established definitively. For both the radar aurora and ionospheric heating experiments this lower bound is calculated to be  $8P_T R^2 / \pi P_R D^3 \Delta$  where  $P_T$  and  $P_R$  are the transmitted and the received power,  $R$  is the range to the scattering center,  $\Delta$  the range resolution cell, and  $D$  is the effective

antennal diameter. Using UHF (398 MHz) radar auroral measurements carried out at Homer, Alaska, in March 1975, during a time of very strong activity, it is found that the lower bound on  $b(k)$  for  $\lambda = 0.74$  m exceeds by  $\sim 21$  dB that produced by ionospheric heating with an incident HF power density of 40  $\mu$ -watts/m. This result is used in an evaluation of an experiment to detect field-aligned plasma-line scattering in the radar aurora, the results of which appear in a companion paper.

5-2 A SEARCH FOR PLASMA-LINE SCATTERING IN THE RADAR AURORA: J. Minkoff and M. Laviola, Riverside Research Institute, New York, New York; and R. Pressnell and R. Tsunoda, Stanford Research Institute, Menlo Park, California

This experiment was motivated by results of VHF/UHF radar observations of a heated ionospheric volume at the White Sands Missile Range (WSMR). Backscatter at WSMR was observed both at the transmitted frequency,  $f$ , (Center Line Scattering [CLS]) and as a pair of sidebands at  $f \pm f_h$  where  $f_h$  is the HF heating frequency (Plasma-Line Scattering [PLS]). Similar observations have been made at the Arecibo Ionospheric Observatory (AO), which have been explained theoretically on the basis of parametric instabilities in which the HF heating field acts as the pump. These theories, however, do not apply to the WSMR results both because of the orthogonal geometry relative to the geomagnetic field,  $\vec{B}$ , and the extremely narrow spectral widths observed. This suggested that PLS might also occur as a consequence of the natural processes giving rise to the radar aurora, without the presence of a background coherent electric field. In this case the precipitating solar particles in transferring energy to the electrons would play the part of the HF heating signal, and the wave motion necessary for the observed frequency offsets could be produced by oscillations at the natural plasma frequency,  $f_p = (ne^2/\pi m)^{1/2}$ , resulting from the perturbations of the ambient electron density distribution. This explanation is consistent with the WSMR results since PLS was always observed at the altitude of maximum heating, where  $f_h$  was equal to the local plasma frequency, and is therefore equivalently described as a pair of sidebands at  $f \pm f_p$ . This NSF-sponsored experiment was carried out between 11-16 March 1975 using the SRI radar at Homer, Alaska. Conceptually, the experiment

consisted of detuning the receiver to  $f \pm f_p$  where  $f_p$  was the local plasma frequency at the desired observation altitude in the auroral volume. No plasma-line scattering was observed at either VHF or UHF (139 and 398 MHz) although UHF RAS signal-to-noise levels as large as 44 dB were observed. In contrast, for the WSMR results the UHF (435 MHz), PLS and CLS levels were nominally equal. This fact, together with the discussion presented in the preceding companion paper, provides strong indication that the mechanism responsible for the WSMR PLS results is not present in the radar aurora; the importance of the coherent HF heating field is also indicated, although existing parametric instability theories do not as yet adequately explain the WSMR results.

5-3 VLF AND LF OBSERVATIONS OF IONOSPHERIC MODIFICATION IN THE D-REGION: B. Wieder and C. J. Chilton, U.S. Department of Commerce, Office of Telecommunications, Institute for Telecommunication Sciences, Boulder, Colorado

Experiments by Jones, et al., (1972) have shown strong changes in the D-region of the ionosphere as a consequence of high radio frequency energy inputs into the ionosphere from a transmitter at Platteville, Colorado (Utlaut, 1970). The experiments involved cross-modulation measurements using WWVI, and WWVB signals from Fort Collins, Colorado, measured at Bennett, Colorado, for the wanted signals, and linearly polarized HF signals from Platteville as the disturbing signals.

These experiments have been extended to measure the frequency and power dependence for both ordinary and extraordinary circularly polarized disturbing signals. Marked increases in cross modulation occur over the linearly polarized cases. For extraordinary polarization and full power from the Platteville transmitter, cross modulation of up to 30% was detected. The effects of extraordinary polarization was much stronger than for ordinary polarization, as expected.

Two solar flares occurred during times when the disturbing transmitter was on for long periods. The percent modulation measured prior to the flares was reduced in both instances by a factor of four at the peak of the flare.

## URSI Session III-5

5-4 EVIDENCE FOR PRECIPITATION OF ENERGETIC PARTICLES BY IONOSPHERIC 'HEATING' TRANSMISSIONS: J. W. Wright, NOAA/ERL, Space Environment Laboratory, Boulder, Colorado

On the infrequent occasions when the Platteville, Colorado, 10 MW transmitter radio frequency matched the F-region peak plasma frequency, intense localized sporadic E-layers occurred at low altitudes (< 95 km). After excluding various alternatives, it is concluded that energetic particle precipitation from the plasma-sphere may occur under these circumstances.

5-5 SIMULTANEOUS OBSERVATIONS OF PRECIPITATING RADIATION BELT PARTICLES AND ANOMALOUSLY LOW ELF SIGNAL STRENGTHS: J. B. Reagan, W. L. Imhof, and E. E. Gaines, Lockheed Palo Alto Research Laboratory, Palo Alto, California; T. R. Larsen, Norwegian Defence Research Establishment, Kjeller, Norway; and P. R. Bannister, Naval Underwater Systems Center, New London, Connecticut

Measurements of ELF signals transmitted from the U.S. Navy Wisconsin Test Facility (WTF) to the Connecticut receiving site have revealed anomalously low horizontal magnetic field strengths on certain nights compared to preceding or following nights. As an example, on 30 October 1972 the nighttime field strength at 75 Hz started out at a level of -147.1 dBAm, increased from 2130-2230 to -145 dBAm and then steadily decreased to a level of ~ -149 dBAm at 0100 on 31 October. The following nighttime field strength remained at this level until about 2200 and then began to increase. During the next night, 1-2 November, the measured field strengths returned to the previous -147.1 dBAm level. During this period particle detectors in the Lockheed payload on the polar-orbiting 1972-076B satellite measured significant fluxes of energetic electrons and protons precipitating into the atmosphere on local nighttime passes across the Wisconsin-Connecticut propagation path. From the measured energy spectra and pitch-angle distributions of the particles, ion-pair production profiles have been calculated. Using previously measured effective electron loss rates, electron density profiles in the D- and E-region resulting from the particle precipitation have been determined. Comparisons of the temporal and altitude variations of the enhanced electron densities with the ELF field strength will be

presented along with a discussion of the cause-and-effect relationship between the precipitation and the low field strength.

5-6 THE PCA POLAR D-REGION: P. E. Argo, Naval Electronics Laboratory Center, San Diego, California

Using a model that relates trans-polar propagating VLF phase advances to the solar proton flux during PCA's, it is shown that the polar cap region affecting VLF propagation during PCA events is significantly larger than the polar cap extent found by Hakura using HF riometer data. An indication that an oval shape exists is, at present, unverifiable. The effective electron loss rates were derived for the polar D-region during PCA events for summer and winter night conditions using the phase advance model. The results show that the summer daytime loss rates are several times higher than the winter daytime rate; the winter nighttime loss rate is ~100 times greater than the winter day.

5-7 SOLAR-FLARE INDUCED IONIZATION ENHANCEMENTS IN THE E AND F REGIONS: R. F. Donnelly, R. B. Fritz, D. N. Anderson, K. Davies, and R. N. Grubb, Space Environment Laboratory, NOAA/ERL, Boulder, Colorado

SITECs (Sudden increases in total electron content,  $N_T$ ) were studied together with SFD observations of the E and F1 region effects of the X-ray and extreme ultraviolet (EUV) bursts of solar flares. X-ray and microwave burst observations were used as inputs to model the impulsive and slow components of the X-ray and EUV flares. The impulsive component of solar flare radiation, which is strong in the 100-911 Å range that is important for producing  $O^+$  (and  $H^+$ ) at high altitudes where electron loss rates are low, is the major source of a SITEC and dominates the rapid rise of  $N_T$  and the large  $dN_T/dt$  values. The slow components of flare radiation are a significant secondary source of SITECs and are particularly important during the peak and decay phase of the event. The time  $t_N$  of the peak of the SITEC ( $\Delta N_{T, \text{max}}$ ) always exceeds the peak time  $t_I$  of the impulsive flare component and varies from one event to another from near  $t_I$  to later than the time  $t_S$  of the peak of the slow flare component according to whether the decay

time of the impulsive emission and the ionospheric electron loss rates are small or large, respectively. The ionospheric electron loss rates are low for the early flares of evolving active regions during quiet ionospheric conditions while the loss rates are high for later SITECs that occur during the ionospheric and magnetic storms produced by earlier flares.

KEEVE M. SIEGEL MEMORIAL SESSION

URSI COMMISSION VI

Wednesday, October 22 1330

URSI Session VI-9, Radio Building Auditorium

Chairman: T.B.A. Senior

University of Michigan

Speakers:

F.S. Johnson, University of Texas, Dallas,  
Texas

S. Silver, University of California, Berkeley,  
California

C.J. Sletten, AFCRL, Bedford, Massachusetts  
R. Timman, Technical University of Delft,  
Delft, Netherlands

N. Marcuvitz, Polytechnic Institute of New  
York, New York, New York

G. Sinclair, Sinclair Radio Laboratories, Ltd.,  
Concord, Ontario, Canada

H. Gomberg, KMS Fusion, Inc., Ann Arbor,  
Michigan

ATMOSPHERIC AND MAN-MADE NOISE

URSI COMMISSION VIII

Wednesday, October 22 1330

URSI Session VIII-3, Radio Building 1107

Chairman: A.D. Spaulding, OT/ITS

3-1 COMMENTS ON URSI OPEN SYMPOSIUM C ON THE TELECOMMUNICATIONS NOISE AND INTERFERENCE ENVIRONMENT, LIMA, PERU, AUGUST 1975: G.H. Hagn, Stanford Research Institute, Menlo Park, California

3-2 SWEEPERS - A SOURCE OF MAN-MADE RADIO NOISE: W.R. Vincent, Develco, Inc.

3-3 GLOBAL MAPPING OF RADIO NOISE AND INTERFERENCE ABOVE THE IONOSPHERE: John R. Herman, Radio Sciences Company, Lowell, Massachusetts; and Robert G. Stone, NASA Goddard Space Flight Center, Greenbelt, Maryland

The HF radio environment above the ionosphere on frequencies greater than foF2 has been surveyed by the Radio Astronomy Explorer 1 (RAE-1) satellite in a circular orbit at altitude 5850 km. The data base is used for global mapping (to + and - 60° latitude) of the composite noise and interference level in local time blocks. On the average, the 6.5 and 9.2 MHz noise on the day side of the earth consists mainly of cosmic noise background. On the night side, however, maps based on 3-month averages at given local times and satellite positions reveal semi-permanent regions of high noise magnitudes. Those over and near continental land masses are attributable to noise and interference from below the ionosphere, while those over subauroral latitudes (~ 60° geographic) may stem from sources in the topside ionosphere. The spatial distributions of the noise contours suggest that the HF radio environment at 6000 km altitude can be predicted reliably only if the source distribution (both natural noise and operating transmitters) and trans-ionospheric propagation conditions can be accurately specified. It is concluded that, on a global basis, the near-space radio environment can be more accurately determined by in situ measurements than by extrapolations from ground-based data.

3-4 ANALYSIS OF THE CRICHLow GRAPHICAL MODEL OF  
ATMOSPHERIC RADIO NOISE AT VERY LOW FREQUENCIES:  
K. E. Wilson, TUSLOG Det 16-2, APO, New York;  
and R. A. Reinman, Wright-Patterson AFB, Ohio

In this paper the model used by Crichtlow and the National Bureau of Standards group for the amplitude-probability distribution for atmospheric radio noise was analysed. This model consists of two straight lines connected by a circular arc in a Rayleigh coordinate system. By using the transformation of coordinates between the Rayleigh coordinate system and the underlying rectangular coordinate system, it was possible to derive analytic formulas for the probability distribution and density function of the amplitude random variable in each of the three regions, the two straight lines and the circular arc. These analytic formulas are parameterized the same way that the NBS group used; the slope  $X$ , and the intercepts  $A$  and  $C$ . The Newton-Raphson convergence method was applied to the analytic formulas for the probability densities, in conjunction with numerical integration using Simpson's rule, to solve for  $X$ ,  $A$ , and  $C$  in terms of the statistical moments represented by the  $V_d$  and  $L_d$  ratios. Using the assumption, employed by the NBS group, that the  $V_d$  and  $L_d$  ratios are linearly related, values of  $X$ ,  $A$ , and  $C$  were determined which produced densities and distributions of the amplitude random variable which were characterized by a specified  $V_d$  ratio within a tolerance of 0.01 db. These refined values were then used to work the coherent Binary and M-ary phase shift keyed communication problem, under the assumption of uniformly distributed phase on the noise. A series of error performance curves were drawn to demonstrate the effect of increasing impulsiveness (increasing  $V_d$  ratio) on the communication system.

3-5 BALL LIGHTNING--AN ELECTROMAGNETIC ORIGIN:  
John B. Smyth, Smyth Research Associates,  
San Diego, California

A positively charged spherical blob has been postulated as the basis for "ball-lightning." Relationships between observables were derived which are in good agreement with many of the characteristics reported at the URSI Boulder Meeting, August 4, 1973. More recently an exact solution of Maxwell's equations which describes lightning adequately for the first

time presented at URSI Boulder Meeting, October 15, 1974, is used to demonstrate how a fundamental process active in charge separation may under extreme conditions produce visible blobs: that is, lightning balls.

3-6 DETERMINATION OF LIGHTNING DISCHARGE CURRENT FROM THE RADIATED ELECTROMAGNETIC FIELD: D. C. Chang, S. W. Maley, and H. Haddad, University of Colorado, Boulder, Colorado

Lightning discharges in the atmosphere can be studied, in part, by measuring the electromagnetic field at various distances from the discharge and then inverting this data to obtain the current in the discharge channel as a function of position and time. In most previous work the ground has been considered perfectly conducting and the ionosphere has been neglected. A study has been conducted to determine the consequence of these simplifications and to determine the magnitude of the errors resulting from the fact that the inversion is carried out using electromagnetic field data at only a limited number of points.

3-7 ANALYSIS OF IONOSPHERICALLY PROPAGATED ATMOSPHERICS RECEIVED WITH A WIDE APERTURE HF ARRAY: Walter B. Zavoli, Stanford Research Institute, Menlo Park, California

A 2.5 km filled high frequency array was used to observe features of remotely propagated atmospherics. In one such experiment this wide aperture HF array, located in California, was steered to receive atmospherics emitted from thunderstorms in New Mexico. ELF atmospherics were simultaneously recorded with equipment operated close to these thunderstorms. Comparison of the line-of-sight ELF records with those obtained via HF skywave reception shows that the structure of ionospherically propagated atmospherics is preserved with sufficient detail to enable the remote identification of various lightning processes such as stepped leaders, and return strokes. Experimental results will be discussed which demonstrate the capability of a wide aperture array to locate desired lightning events accurately in azimuth while rejecting atmospherics from a potentially large number of thunderstorms at other bearings.

CNS EFFECTS - I  
URSI COMMISSION I (BIOLOGICAL EFFECTS)  
Wednesday, October 22 1330  
URSI Session B-8a, UMC East Ballroom  
Chairman: R. Adey, UCLA

B8a-1 ELECTROMAGNETIC RADIATION EFFECTS ON THE BLOOD-BRAIN BARRIER SYSTEM OF RATS: Kenneth J. Oscar, U.S. Army Mobility Equipment R & D Center, Fort Belvoir, Virginia, and American University, Washington, D.C., and T. Daryl Hawkins, Department of Microwave Research, Walter Reed Army Institute of Research, Washington, D.C.

A study was conducted to assess the effect of microwave energy on the blood-brain barrier (BBB) system of rats. A quantitative radioactive isotope method was used in an attempt to verify the increased BBB permeability of rats reported by A. H. Frey, who used a flourescien dye technique. Male, Walter Reed Army Institute of Research, WISTAR derived, 230-270 gram rats were subjected to microwave energy at a frequency of 1.3 GHz. The permeability measurement, after the method of W. H. Oldendorf, uses two radioactive labeled indicators which are injected simultaneously into a common carotid artery of the anesthetized rat. One test substance is labeled with  $^{14}\text{C}$  and the other with tritiated water which is highly diffusible in the brain tissue and provides a standard for comparison. The rats are sacrificed 15 sec after injection and tissue samples from 5 different regions of the brain counted. This quantitative technique measures the uptake of a test molecule into the brain tissue relative to water, which differentiates between a true BBB alteration and vasodilation or stasis. The study used controls (sham-irradiated) and animals exposed to microwaves with various modulation parameters. The study was conducted doubly blind with D-Mannitol as the test substance in most experiments, although substances of other molecular weight were used also. The results, to date, indicate a statistically significant increase in BBB permeability with both pulsed and CW microwave energy at average power levels considerably below  $10 \text{ mW/cm}^2$ . The possible differences between CW and pulsed energy, molecular weight of test molecule, functional dependence of the BBB alteration with microwave parameters, and duration of BBB alteration are discussed.

B8a-2 REDUCTION IN SENSITIVITY TO AUDIOGENIC SEIZURE FOLLOWING A SINGLE, 2450 MHz, CW IRRADIATION OF RATS: T. Daryl Hawkins and Edward L. Hunt, Department of Microwave Research, Walter Reed Army Institute of Research, Washington, D.C.

Wistar rats of both sexes from sound-sensitive breeding lines which have been developed at Walter Reed were assessed for convulsive response to high intensity sound 2 min after the termination of a 30-min period of 2450 MHz, CW irradiation. Subjects were preselected for sensitivity to a random noise signal (105 db, 11-14 KHz, 60 sec) which was presented twice weekly during the growth period of 3-5 weeks of age. Experimentation began at 6 weeks of age. Individual exposures occurred in a plane-wave field with the E-vector parallel to the long axis of the rat. The effects of exposure at 50 mW/cm<sup>2</sup> were evaluated with 12 rats. Seven of the subjects were irradiated initially and 5 were given a sham treatment. A second treatment was given 4 days later with the conditions reversed for each rat. Effects of a 50 mW/cm<sup>2</sup>, 30-min exposure were not significant. Only 2 of the 12 rats failed to respond to the sound challenge following their irradiation. A second study was conducted in a similar manner with 11 new subjects. Exposure for 30 min at 75 mW/cm<sup>2</sup> produced a highly significant reduction in audiogenic response. Nine rats showed no response whatsoever following irradiation. By contrast, these 9 rats did respond following their sham treatment. Recovery of responsiveness within 4 days was indicated in all rats for which the sham treatment had followed the microwave treatment. The present data show that audiogenic convulsive responses can be attenuated by a single, 30-min, CW exposure. Pulsed irradiation and repeated exposures which have been used by previous investigators are apparently not required to produce a decrease of CNS sensitivity as reflected by this measure.

B8a-3 NON-THERMAL EFFECTS OF ELECTROMAGNETIC FIELDS ON THE CENTRAL NERVOUS SYSTEM: H. Kritikos and S. Takashima, Department of Bioengineering, University of Pennsylvania, Philadelphia, Pennsylvania

A series of experiments in the RF (1-30 MHz) and Microwave region (2.45 GHz) have been conducted in vitro to determine whether E.M. fields induce any non-thermal effects on the activities of the central nervous system. In the RF region the giant axon of the *myxicola* worm in constant temperature (6-8°C) saline solution was exposed to current densities of

approximately 100 mA/cm<sup>2</sup> corresponding to heat deposition rate of .6 w/cc. It was found that the triggering threshold level does not change and that there were no detectable effects on the shape of the action potential. RF pulses of approximately .5 ms duration did not trigger the nerve. It was found that triggering was possible only in the low frequency region by .5 ms pulses from DC to 20 KHz. In the microwave region the sciatic nerve of the Rana Pipiens frog while immersed in a constant temperature Ringer solution was exposed to power densities of .5 w/cc. It was found that no effects were induced in the triggering threshold level, pulse shape and that it was not possible to trigger the nerve with microwave pulses. Higher exposure rates (1.5 w/cc) associated with temperature rise up to 39° did, however, damage the nerve. In both cases it was observed that electrode pick-up induces artifacts and may present a potential electromagnetic hazard.

B8a-4 LIGHT AND ELECTRON MICROSCOPIC INVESTIGATION OF BRAINS EXPOSED TO NON-IONIZING RADIATION:

Earnest Albert, Department of Anatomy, The George Washington University Medical Center, Washington, D.C.

Chinese hamsters were exposed to power densities of 10, 25, and 50 mW/cm<sup>2</sup> at 1700 and 2450 MHz frequencies for 30 minutes to 10 weeks. The brains were serially sectioned for light microscopy but only selected areas were examined for electron microscopy. The light microscopic examinations were conducted on paraffin and frozen sections that were stained with Nauta, cresyl violet, thionine and hematoxylin and eosin. Neuronal histopathology was observed in most of the irradiated animals in the hypothalamus and subthalamus; whereas cerebral and cerebellar cortices, pons, medulla, and spinal cord appeared normal. The affected neurons exhibited swelling, vacuolation, and chromatolysis. The blood vessels appeared normal. There was no suggestion of edema, hemorrhage, or congestion. The details of the experimental procedures and significance of the results will be discussed at the presentation.

CNS EFFECTS - II

URSI COMMISSION I (BIOLOGICAL EFFECTS)

Wednesday, October 22 1524

URSI Session B-8b, UMC East Ballroom

Chairman: S. Cleary,

Virginia Commonwealth University

B8b-1 MICROWAVE-INDUCED SHIFTS OF GONADOTROPIC ACTIVITY  
IN ANTERIOR PITUITARY GLAND OF RATS: H. Mikołajczyk,  
Institute of Occupational Medicine, Łódź, Poland

Quantitative changes of gonadotropic activity in pulsed pituitary glands of rats exposed to microwave radiation have been previously demonstrated in this laboratory. This summary presents the results of reinvestigated hormone activities in individual pituitaries of control and of irradiated rats. Twelve 35-day-old male rats (I) were exposed 6 hours daily for 6 days weekly for 6 weeks to microwaves (2860 - 2880 Mc, c.w., 10 mW/cm<sup>2</sup>). Each day the animals were caged randomly in a perforated polyvinyl box spaced for pairs of animals and the box was placed in unechoic chamber before horn antenna in far field. The incident power density was verified with calorimetric and power meter methods. At the same time twelve control rats (II) manipulated and caged in comparable manner were placed in separate unechoic chamber without radiation source. Microwave-irradiated and control rats were killed on the next day (8:00 - 10:00 a.m.) after last exposure and separated anterior pituitaries were stored for 48 hours in cold acetone. The saline extracts of individual pituitary homogenates were tested separately according to schedule: extract of single pituitary tested in single immature hypophysectomized rat. Thus six pituitaries of each group of animals (I and II) were tested for FSH (ovaries augmentation) and for GH (tibia enlargement) and the other six pituitaries were tested for LH (prostata augmentation). NIH-FSH-S7, NIH-LH-S15, and NIH-GH-S were used as standards. The following quantities of hormones have been found in  $\mu\text{g}/\text{pituitary}$  ( $\bar{X} \pm \text{S.D.} \pm \text{S.E.}$ ): (I) in irradiated rats - FSH:  $655 \pm 123 \pm 50$ ; LH:  $302 \pm 81 \pm 33$ ; GH:  $140 \pm 37 \pm 11$ ; (II) in control rats - FSH:  $635 \pm 84 \pm 33$ ; LH:  $197 \pm 34 \pm 14$ ; GH:  $134 \pm 41 \pm 13$ . The amount of LH was significantly higher (at  $p < 0.05$ ) in pituitary gland of irradiated than of control rats. The results of this investigation support the earlier suggestion about the possible shifts of gonadotropic activities in pituitary gland of rats exposed to microwave radiation.

B8b-2 THE EFFECT OF 1.6 GHz CW FIELDS ON TRACE METAL CONTENT OF SPECIFIC REGIONS OF RAT BRAIN:

F. Chamness, H. Scholes, S. Sexauer, and  
J. W. Frazer, USAF School of Aerospace  
Medicine, Brooks AFB, Texas

Studies of neurochemical changes in brain areas (Merritt, et al.) and trace metal content of brain areas (Stavinoha, et al.) had shown that fields of sufficient magnitude could produce alterations in trace metal content, which are regionally quite specific when animals were exposed to HF band fields. MacDougal, et al., have shown that the energy distribution in rats at 1.6 GHz possessed considerable asymmetry, but with fairly large amplitude power deposition in the floor of the brain. Utilizing the same exposure technique, rats were exposed to 80 mW/cm<sup>-2</sup> plane wave fields at 1.6 GHz in the USAFSAM anechoic chamber. Fields were determined with the NBS EDM-1B probe. Companion studies were made on the brains of animals exposed to an environment of 80°C in a warm air oven for an equivalent period of time. Brain areas analyzed included cortex, corpus striatum, hippocampus, hypothalamus, midbrain, cerebellum, and medulla with a modified dissection scheme for rats used by Glowinski and Iversen. Metals analyzed were Na, K, Ca, Mg, Fe, Cu, and Zn, all by atomic absorption. Major differences from controls were found in the magnesium content of the hypothalamus in both hyperthermal and RF exposed rats. Interpreting the iron changes as due primarily to alterations in blood distribution, it appears that intracerebral circulatory changes were produced by hyperthermal environments which were not produced by RF exposure. Decreases in zinc content were found previously in liver and increases in the zinc content in brain cortex of animals exposed to HF band radiation. The present results are quite similar to the latter findings and show that some cerebral effects are produced indirectly as a result of primary effects on other organs.

B8b-3 INTERACTION OF MODULATED ELECTROMAGNETIC FIELDS WITH NERVOUS STRUCTURES: Chuan-Lin Wu and James C. Lin, Department of Electrical Engineering, Wayne State University, Detroit, Michigan

Low level electromagnetic fields amplitude modulated at brain wave frequencies have been shown to influence the conditioned and spontaneous electroencephalographic patterns in cats and to increase the calcium efflux from isolated brains of neonatal chicks. One hypothesis offered was that the electric fields induced in the brain were modifying the membrane characteristics of neurons either by triggering configurational changes on the surface macromolecules or by inducing small displacements of the surface-bound cations. This paper examines the theoretical considerations for the induced fields immediately surrounding the central neurons. By using a "greater membrane model" as a basis, the possibility is discussed of the interaction of impinging low level electromagnetic fields with the central nervous system. A comparison between the effects of amplitude modulated and continuous wave radiations will also be presented.

B8b-4 THE EFFECT OF 1.6 GHZ RADIATION ON NEURO-TRANSMITTERS IN DISCRETE AREAS OF THE RAT BRAIN: James H. Merritt, Richard Hartzell, and James H. Frazer, Radiobiology Division, USAF School of Aerospace Medicine, Brooks AFB, Texas

A considerable body of literature has evolved implicating radiofrequency radiation in effects on the central nervous system. The tissue of the CNS responds to changes in temperature so that changes in neurotransmitter content are expected if synthetic and degradative pathways have different temperature coefficients. We have exposed rats to 1.6 GHz radiation at a measured power density of  $80 \text{ mW/cm}^2$  for 10 min, and have determined power distribution thermographically. Rectal temperature rise was  $4^\circ\text{C}$ . Serotonin and its metabolite 5-hydroxyindole acetic acid, dopamine and its metabolite homovanillic acid, and norepinephrine were measured in seven discrete brain areas; namely hypothalamus, corpus striatum, midbrain, hippocampus, cerebellum, medulla-pons, and cortex. Parallel hyperthermal and normothermal controls were also examined. The hyperthermal controls were maintained in a  $75^\circ\text{C}$  environment for 10 min which resulted in a rectal temperature rise of  $4^\circ\text{C}$ . A significant decrease in hypothalamic norepinephrine content was noted in the irradiated and

hyperthermal groups compared to the normothermal controls. The hippocampal content of serotonin was decreased in the irradiated but not the hyperthermal animals. Conversely, cerebellar and cortical serotonin concentrations were decreased in the hyperthermal but not the irradiated rats. The dopamine content of the corpus striatum was significantly lower in the irradiated group but not in the hyperthermal animals. The decrease in hypothalamic norepinephrine agrees well with other data suggesting that this neurotransmitter subserves a neuronal system to lower body temperature. The other changes noted above in this study fit well with thermographic imagery of rats exposed to 1.6 GHz radiation. The data reported here appear to indicate that the effects seen on the neurotransmitters are a result of RF radiation induced hyperthermia and not a direct effect on innervated tissue.

ASSESSMENT OF POWER DEPOSITION IN TISSUES

BY NUMERICAL METHODS

URSI COMMISSION I (BIOLOGICAL EFFECTS)

Wednesday, October 22 1330

URSI Session B-9a, UMC West Ballroom

Chairman: A.W. Guy,

University of Washington

B9a-1 NUMERICAL STUDY OF ELECTROMAGNETIC POWER  
DEPOSITION IN BIOLOGICAL TISSUE BODIES:  
P. W. Barber, Department of Bioengineering,  
University of Utah, Salt Lake City, Utah

The interaction of electromagnetic (EM) waves with the biological system of man is a problem which is currently receiving considerable attention from the medical and scientific communities. An important area of interest involves a determination of the power absorption characteristics of man as a function of the polarization, orientation, and frequency of the incident EM wave. The Extended Boundary Condition Method (EBCM) has been applied to the problem of obtaining quantitative power absorption information for a homogeneous prolate spheroid model of man. Preliminary work, which has previously been reported, has shown that this technique can readily be applied to power deposition calculations for man at relatively low frequencies. The EBCM and the long wavelength analysis method give exactly the same results at 10 MHz. More recent work has been concerned with making calculations at higher frequencies to determine the frequencies of maximum absorption, i.e., the resonant frequencies of man. Extension of the numerical work to bodies which are electrically larger has required the consideration of some interesting numerical problems. The calculation requires the solution of a rather unusual set of simultaneous equations. Although the matrix involved is not ill-conditioned, the wide variation in the amplitude of the elements can result in appreciable error in the solution due to the finite precision arithmetic of the computer. This behavior, which is a consequence of the large dielectric constant of the muscle tissue used in the model, appears to limit the application of the EBCM to frequencies below 100 MHz. This, however, does permit a determination of the first resonance. The numerical results give the average power absorption and peak power absorption for man as a function of frequency, polarization, and orientation through the first resonance.

B9a-2 FINITE ELEMENT-VARIATIONAL CALCULUS APPROACH TO THE DETERMINATION OF ELECTROMAGNETIC FIELDS IN IRREGULAR GEOMETRY: S. M. Neuder, Division of Electronic Products, Bureau of Radiological Health, FDA, Rockville, Maryland; and P. H. E. Meijer, Catholic University of America, Washington, D.C.

The problem of determining the fields and power deposition within dielectric bodies exposed to external electromagnetic radiation has been solved exactly only for a limited number of geometrically-idealized cases. This paper describes a theoretical formulation based on the finite element method and the variational calculus for the approximate calculation of internal fields in lossy dielectric media of asymmetric or irregular geometry. One application of this technique is that of determining dosimetric distributions in biological systems exposed to microwave radiation.

B9a-3 HIGH VOLTAGE ELECTRIC FIELD COUPLING TO HUMANS USING MOMENT METHOD TECHNIQUES: R.J. Spiegel, IIT Research Institute, Washington, D.C.

With the advent of EHV transmission lines and the almost certain possibility of UHV lines, it becomes increasingly important to be able to accurately describe the transmission line electromagnetic field interaction with life forms. This paper develops a numerical method for predicting current and normal electric field distributions induced on humans situated in the near vicinity of the lines. The technique is based on the method of moments in which the human body is modeled as a collection of straight cylindrical sections. Various scenarios are considered, e.g., a well insulated person standing on the ground beneath the transmission line, an individual in good contact with the earth, or a lineman working in very close proximity to an energized conductor. The position of the arms is varied; for example, arms extended or down at the side. The question of biological hazards from exposure to fields of these systems is also considered.

B9a-4 ELECTROMAGNETIC POWER ABSORPTION IN LOSSY WIRE MODEL OF MAN: K.R. Umashankar and C.M. Butler, Department of Electrical Engineering, University of Mississippi, University, Mississippi

An initial attempt is made to "model a man" by the junctions of six straight lossy circular cylinder sections to represent various structural parts of the human body. In the presence of electromagnetic plane wave incident, this model is theoretically investigated and a computer program developed to calculate currents induced in the various portions of the lossy model for both vertical and horizontal polarizations of the incident field. Peak-induced currents are observed at the arm junction and the growing near resonance situation. For the various frequencies the electromagnetic power absorbed is considered.

B9a-5 NUMERICAL SIMULATION OF THE EFFECTS OF NON-IONIZING MICROWAVE RADIATION UPON THE HUMAN BODY:

A. F. Emery, Department of Mechanical Engineering,  
A. W. Guy, Bioelectromagnetics Research Laboratory,  
Department of Rehabilitation Medicine,  
K. K. Kraning, Department of Dermatology, and  
R. Short, Department of Mechanical Engineering,  
University of Washington, Seattle, Washington

The human body was modelled by a finite difference numerical procedure to compute the thermal response of a man subjected to microwave irradiation of the entire body and the head only. Transient head and body temperatures and sweating rates were computed to determine the maximum levels of irradiation permissible for long time and short time exposures. Since the thermal response is strongly affected by the local sweat rate, four different models were used in which the hypothalamus, average skin and local skin temperatures, and the time rate of change of these temperatures were the controlling parameters. The best of these different models, as judged by comparison of the results with measured data, was then used in the microwave simulations.

POLARIZATION EFFECTS  
URSI COMMISSION I (BIOLOGICAL EFFECTS)

Wednesday, October 22 1600  
URSI Session B-9b, UMC West Ballroom  
Chairman: A.W. Guy,  
University of Washington

B9b-1 COLONIC TEMPERATURE CHANGES DURING MICROWAVE EXPOSURE: Sandra H. Githens, T. Daryl Hawkins, and John Schrot, Department of Microwave Research, Walter Reed Army Institute of Research, Washington, D.C.

Colonic temperature increases during microwave, plane-wave exposures were found to be dependent on microwave frequency, E-field orientation, and the type of animal subject, revealing strong parallels to previously obtained lethality data. Each of the experimental subjects was anesthetized and exposed once to a  $100 \text{ mW/cm}^2$  signal for exactly 4 min. Colonic temperature changes of exposed subjects were determined from pre-exposure and post-exposure temperature measurements and were compared to those of comparable sham-irradiated subjects. Exposures during which the E-vector was parallel to the long axis of the subject consistently resulted in higher temperatures than did exposures with a vertical E-vector. For each type of animal differential frequency effects were most pronounced during exposures with a parallel E-vector. Mice (25-30 g) showed larger temperature increases at 1700 and 2450 MHz than at 710 MHz. Small rats (100-125 g) and large rats (380-420 g) exhibited highest temperatures at 710 MHz. Comparing the temperature changes across the groups of subjects of different size, an interaction of frequency and size was indicated. At 1700 and 2450 MHz, a general inverse relation between temperature increase and body size was evident. At 710 MHz, the rank ordering was reversed, indicating a direct relation between temperature increase and the body size of the respective subjects. These colonic temperature changes are suggestive of differential absorption which is complexly determined by frequency, E-field orientation, and the dimensions of the experimental subject.

B9b-2 MICROWAVE FREQUENCY AND E-FIELD ORIENTATION INTERACT WITH ANIMAL SIZE: John Schrot and T. Daryl Hawkins, Department of Microwave Research, Walter Reed Army Institute of Research, Washington, D.C.

The interaction between microwave frequency, E-field orientation, and animal size was investigated using elapsed time to tonic-clonic convulsion as the dependent variable. The frequencies employed were: 710, 985, 1700, 2450, and 3000 MHz. The subjects were exposed in two E-field orientations at each frequency; namely, E parallel and E vertical to the long axis of the animal's body. At each frequency-orientation combination, groups of 11 mice (25-35g), small rats (100-125g), and large rats (380-420g) were exposed. Individual exposures took place in an anechoic chamber (16' X 16' X 32'), with the animal restrained in a plexiglas enclosure. All exposures were performed with a 150 mW/cm<sup>2</sup> CW signal. The results clearly demonstrate that the frequency, orientation, and body size variables contribute significantly in determining elapsed time to convulsion. The horizontally aligned E-field produced consistently faster times to convulsion across animal size and frequency. In general, increasing animal size produced greater vulnerability (shorter convulsion times) with lower frequencies. For example, mice were most vulnerable in the 1700-2450 MHz range, small rats at 985 MHz, while large rats convulsed most quickly at 710 MHz. The frequency-vulnerability relationships were most clearly demonstrated with the E-field polarized horizontally. These data indicate the importance of considering frequency, orientation, and subject size when evaluating vulnerability to microwave exposure.

INSTRUMENTATION AND TECHNIQUES

URSI COMMISSION V

Wednesday, October 22 1330

URSI Session V-5, UMC 156

Chairman: J. Welch,

University of California

5-1 APERTURE SYNTHESIS WITH A LINE ANTENNA:

R. A. Perley and W. C. Erickson, Astronomy  
Program, University of Maryland, College Park,  
Maryland

We describe a method in which we use the E-W arm of the Clark Lake "TPT" as an aperture synthesis instrument. Because of the unique phasing capabilities of the array, we can steer the N-S fan beam formed by the E-W arm to any desired position. Starting at hour angle -6 hr., and running for 12 hr., we then obtain a series of strip scans of the region in the sky of interest. Because the source rotates with respect to the beam, each strip scan contains new information on the source structure. By properly superimposing these strip scans in a computer, the source brightness distribution, convolved with an effective beam, is recovered. Computer software programs then perform a limited deconvolution of this map so that a total intensity map can be obtained. We have utilized this technique to synthesize maps of 15 Abell clusters of galaxies at two frequencies, 38 MHz, and 26.3 MHz, in an attempt to detect low frequency radio emission.

5-2 EXPERIENCE WITH DUAL-HYBRID-MODE FEEDS:

Alan T. Moffet, Owens Valley Radio Observatory,  
California Institute of Technology, Pasadena,  
California

Two dual-hybrid-mode feeds have been constructed following the designs of Minnett and Thomas of C.S.I.R.O., Australia. These are for use at the prime focus of a parabolic antenna with  $f/D = 0.4$  and at wavelengths of 2.8 and 13.1 cm. Efficiencies, bandwidth, and other details of operating experience with these feeds will be discussed.

5-3 OPTICAL PROCESSING FOR RADIO ASTRONOMY:  
M. C. H. Wright, Radio Astronomy Laboratory,  
University of California, Berkeley, California

Two optical information processors are described which could have advantageous application in radio astronomy data reduction. The first device is an acousto-optical spectrometer providing up to 1000 channels in a 100 MHz bandwidth. The spectrometer uses the Bragg interaction between a coherent light beam and a travelling acoustic wave generated from the radio signal. The bandwidth and resolution is appropriate for 7 mm wave spectroscopy at a cost far lower than traditional spectrometers. The second processor described is a convenient way to optically process the complex two-dimensional Fourier transform required in aperture synthesis. Examples are given of its use in optical post-processing and display of multichannel aperture synthesis maps.

5-4 MICROWAVE MEASUREMENT OF MESOSPHERIC CARBON MONOXIDE: J. W. Waters, Jet Propulsion Laboratory, Pasadena, California; and W. J. Wilson and F. I. Shimabukuro, The Aerospace Corporation, El Segundo, California

The  $J=0 \rightarrow 1$  rotational carbon monoxide transition at 115,271.2 MHz has been measured in the solar absorption spectrum. The measured absorption line is due to carbon monoxide in the earth's upper atmosphere which is produced by photodissociation of carbon dioxide. The strength and shape of the observed line have provided the first measurements of carbon monoxide at altitudes above 50 km in the terrestrial atmosphere. The measurements also have significant implication on vertical transport in the upper mesosphere and lower thermosphere.

5-5 AN AUTOMATIC TELESCOPE WITH REMOTE CONTROL:  
J. C. Webber, K. S. Yang, and G. W. Swenson, Jr.,  
University of Illinois, Urbana, Illinois

The 120-foot radio telescope of the Vermilion River Observatory has been completely automated. A dedicated minicomputer controls telescope positioning and data acquisition, operating unattended according to a pre-determined observing list. Remote system access is provided via telephone line and modem, permitting direct

observing or program change from any remote location. Effective utilization of telescope time for the repetitive measurements necessary for variable source monitoring has been achieved. The implication of this success is that remote control and synchronization of large or widely-spaced telescope arrays is feasible at low cost.

---

THURSDAY MORNING, OCT. 23, 0830-1200

---

WORKSHOP ON NEW NEEDS FOR TELECOMMUNICATION

MEASUREMENTS

URSI COMMISSION I

Thursday, October 23 0830

URSI Session I-2, UMC 159

Chairman: Robert C. Powell,

Telecommunications Analysis Division, OT

The following subject areas will be covered:  
energy, data communications, local distribution, susceptibility, and new technology.

ATMOSPHERIC EFFECTS

URSI COMMISSION II

Thursday, October 23, 0830

URSI Session II-9, UMC Forum Room

Chairman: C.M. Crain, RAND Corporation

9-1 SIMULTANEOUS REMOTE SOUNDING OF ATMOSPHERIC WINDS AND STRUCTURE: D. R. Jensen and V. R. Noonkester, Naval Electronics Laboratory Center, San Diego, California

An acoustic bistatic wind sensor system capable of measuring the vertical wind profile has been operated simultaneously with a monostatic acoustic sounder and an FM-CW radar. These simultaneous observations show the nature and characteristics of low level wind systems associated with atmospheric structures in the marine layer such as multiple layers, wave motions, and turbulence. The bistatic acoustic sounder system used for the real-time readout of the vertical wind profiles will be discussed. Examples of simultaneous observations of wind profiles and associated atmospheric structures will be presented.

9-2 EFFECTS OF PHASE-FRONT DISTRIBUTIONS AND SHIELDING ON ACOUSTIC ANTENNA PATTERNS USING A TAPERED CYLINDRICAL STRUCTURE AS A MODEL: S. A. Adekola and Dean T. Davis, The Ohio State University, Columbus, Ohio

This paper presents the formulation of a more general nearfield and farfield integral equation of a three-dimensional cylindrical model of a shielded aperture antenna for acoustic echo-sounding, employing the free-space Green's function and the Kirchhoff-Fresnel Diffraction formula. The formulation starts with the reduced time-independent wave equation and the free-space Green's function is applied in the Kirchhoff-Fresnel diffraction physical optics formula resulting in the pressure field formulation of an acoustic wave. The redrafted, largely self-explanatory relative gain patterns, are reported for typical wavelengths. From the 70 dB sidelobe reduction obtained in the 20° region between 70° and 90° (where 90° corresponds to ground level), 40 dB is achieved through shielding and 30 dB through a proper choice of phase coefficient  $\beta$ , with only a corresponding 2° beamwidth increase of the mainlobe. The 90° sidelobe level reduction obtained by shielding ranges from 5 dB at  $H$  equals 1 ft. to

39 dB and 40 dB at H equals 12 ft. and 13 ft. respectively. Phase distribution effects and causes of pattern distortions are considered. The results are in excellent agreement with available experimental data reported in the literature and also supplied through private communication with other investigators. The linear and cubic phase distributions distort the antenna beams by nullifying the major-lobes creating conical beam patterns. Quadratic phase distributions smooth the nulls and raise the sidelobes. Periodic phase-front distributions produce a loss in gain. The contour plots, shown for typical angles and scale factors, give the three-dimensional visualization of the acoustic antenna patterns.

9-3 VARIABILITY OF ATMOSPHERIC OXYGEN SPECTRA  
BETWEEN 40 AND 140 GHz: Hans J. Liebe and  
Jerry Hopponen, Office of Telecommunications,  
Institute for Telecommunication Sciences,  
Boulder, Colorado

The variability of  $O_2$  spectra with frequency, pressure, and temperature was studied under conditions occurring in the atmosphere. Accurate line parameters, determined from controlled laboratory experiments, are used in analyses of attenuation and dispersion rates and their sensitivities to small temperature and pressure changes. Results are presented covering conditions encountered over the first ten kilometers of altitude (200-300°K, 190-760 torr). They are based on Rosenkranz's band shape theory that takes into account line inferences caused by pressure-broadening. The discussion centers on the usefulness of such information when treating problems of bandwidth limitations impaired by turbulent air and remote sensing atmospheric state.

9-4 MEASUREMENT OF DIRECTIONAL SURFACE WAVE SPECTRA  
USING A TWO-FREQUENCY CORRELATION TECHNIQUE:  
D. L. Schuler and B. J. Zimmerman, Naval  
Research Laboratory, Washington, D. C.

Recent experimental studies (Plant, W. J., "Studies of Backscattered Sea Return with a Dual Frequency X-band Radar," USNC-URSI Digest 1975 Symposium, Urbana-Champaign, Illinois) of the backscattered return from two-scale wave systems have demonstrated the feasibility of measuring long gravity wave spectra

with a compact two-frequency CW X-band radar interferometer. Gravity waves, through tilting and bunching of local capillary waves, create a propagating spacial modulation pattern which can be observed, under certain conditions, as a high correlation between the returns at the two closely-spaced transmitted frequencies. These conditions are that (1) the Bragg resonance condition be satisfied for the difference frequency and (2) the modulation is sufficiently well developed so that the effect is greater than the background Doppler spectra. The correlation is detected as a Doppler-shifted line in the spectrum of the product of the returns at the two frequencies. Improvements in the original radar's antenna configuration and method of signal processing have been effected in an effort whose aim is the production of directional surface wave spectra in a much shorter length of time than was previously possible. The advantages of making rapid directional spectra are that (1) the spectra will be derived from wave statistics which represent a nearly stationary temporal process and (2) the method then may be used as the eventual basis for a practical survey instrument mounted in an aircraft or satellite. Results with the radar operating in a swept frequency mode with real-time signal digitalization and recording indicate that a single directional spectra (10 complete spectra spaced over a  $120^{\circ}$  sector) can be obtained in 8 minutes with a spectral resolution of .02 Hz. Performing sufficient averaging (5 independent spectra) to reduce fluctuations increases the processing time to 40 minutes. Preliminary results of spectra will be presented and compared to wave staff data and to directional spectra obtained from photographs. A pulsed two-frequency L-band radar system (under construction) which will perform the necessary spectral averaging on a pulse by pulse basis will also be described.

9-5 RADIOMETRIC DETECTION OF ATMOSPHERIC WAVE ACTIVITY:  
C. I. Beard, L. U. Martin, Naval Research Laboratory,  
Washington, D.C.; Douglas R. Jensen, V. Ray  
Noonkester, Juergen H. Richter, Naval Electronics  
Laboratory Center, San Diego, California

Microwave (22 GHz) radiometers have detected atmospheric internal wave activity and localized it in altitude. Varying the intersection height of a narrow ( $3^{\circ}$ ) beam with that of a wide ( $22^{\circ}$ ) vertically pointing beam al-

lowed localization of the source height. An objective of the experiment was to determine what information, complementary to other remote sensors, microwave radiometers could furnish. The ground-based radiometers were located at NELC, San Diego, in a joint experiment in which NELC provided "atmospheric truth" with the FM-CW radar for comparison with the radiometer data. The acoustic sounder, lidar, radiosondes, and other meteorological data completed the remaining "atmospheric truth." First results show both correspondences and differences between the microwave radiometers and FM-CW radar. Quiet periods and gravity-wave trains extending to an hour in length show correspondence between sensors. These results and differences between sensors will be presented and discussed.

**9-6 A PROTOTYPE TWO-CHANNEL MICROWAVE RADIOMETER:**

T. R. Larson, Mark H. Alspaugh, Ball Brothers Research Corporation, Boulder, Colorado

A two-channel microwave radiometer operating at 21.5 GHz and 37.0 GHz has been developed as a prototype for the front end of a satellite radiometer. Proper choice of components allows operation in either a Dickie or a whole-power mode. System performance in either mode is measured using a twenty-channel on-line computer data acquisition system. Real system performance will be compared with predicted. The results of extensive tests to measure gain variations as a function of component physical temperature and supply voltage will be summarized. The feasibility of operating a whole-power microwave radiometer on a satellite will be discussed.

**9-7 DEDUCING REFRACTIVE TURBULENCE PROFILES FROM STELLAR SCINTILLATION MEASUREMENTS:** G. R. Ochs, Ting-i Wang, R. S. Lawrence, and S. F. Clifford, National Oceanic and Atmospheric Administration, Environmental Research Laboratories, Boulder, Colorado

We observe stellar scintillation, caused by atmospheric turbulence, with a set of spatial filters on the ground. By linearly combining the signals, observed at different spatial wavelengths, with appropriate weights, we synthesize a path-weighting function centered at a specific height. The location and height-resolution can be controlled by changing the coefficients and spatial wavelengths of the linear combination.

Experimental data have been taken with a fourteen inch telescope. It turns out that the atmosphere can be divided into four independent layers with reasonable accuracy. The results agree roughly with the  $C_n^2$  profiles measured previously using aircraft-mounted or balloon-borne in situ sensors.

THEORETICAL DEVELOPMENT OF ELECTROMAGNETIC PROBLEMS

URSI COMMISSION II

Thursday, October 23 0830

URSI Session II-10, UMC 158

Chairman: W.S. Ament,

Naval Research Laboratory

10-1 TRANSIENT ELECTROMAGNETIC RESPONSE FROM  
NONUNIFORM LAYERED MODELS OF THE EARTH'S CRUST:  
E. Bahar and M. Fitzwater, Electrical Engineering  
Department, University of Nebraska, Lincoln,  
Nebraska

The transient electromagnetic response from various nonuniform layered models of the earth's crust is determined for Loran C pulse excitations. A full wave solution for the steady state electromagnetic fields is the basis for these investigations. The solutions are shown to satisfy the reciprocity relationships in electromagnetic theory. The complete expansion of the electromagnetic field consists of the radiation term (continuous spectrum of vertically polarized waves) and the surface waves (discrete set of vertically polarized guided waves of the structures).

The principal motivations for this work are: (i) to determine the distortions a radio wave pulse undergoes when it is scattered by a nonuniform stratified model of the earth's crust and (ii) to determine whether it is possible to extract from these electromagnetic signatures information regarding the electrical and geometrical characteristics of the earth's crust. Thus the distortions of the envelope of the plane wave and surface wave response are examined for various values of the overburden complex permittivity and for different gradients in the overburden depth. Special attention is also given to the effects of the nonuniform overburden parameters upon the time of arrival of the response. These investigations are relevant to problems of navigation (by determining Loran-Ground effects) and to problems of geophysical prospecting.

10-2 DYNAMIC RADAR SCATTERING FROM AN ENSEMBLE OF  
DISCS: Thomas M. Smith, M.I.T. Lincoln Labora-  
tory, Lexington, Massachusetts

The dynamic radar cross section (RCS) for an ensemble of

circular discs is analyzed as a function of wavelength (frequency), polarization and disc size. Separate analytical expressions characterize the RCS of the disc in the Rayleigh and optics regions. Two different probability distributions are assumed to describe aspect angle positions: one distribution is uniform over a solid angle, the other is pseudo stable about the trajectory velocity vector of the ensemble. Joint distributions,  $p(\text{RCS}, \text{area})$ , dependent on disc RCS and area, and normalized to a square wavelength, are developed for both right and left circular polarizations. Marginal RCS distributions,  $p(\text{RCS})$ , are determined from  $p(\text{RCS}, \text{area})$  and assumed marginal area distributions,  $p(\text{area})$ . The  $p(\text{RCS})$  curves are converted to cumulative RCS distributions which are used to develop frequency scaling relationships for the ensemble of discs. Being able to frequency scale dynamic radar data can save the time and expense required to remeasure targets or environments whose characteristics are already known at another frequency. Results from this study are applied to fragmentation clutter problems which occur when plate like structures break up while re-entering the earth's atmosphere. Ensembles of discs are used to model the extended clutter environment produced by a complex of plate fragments with arbitrary sizes and shapes. This model indicates that an ensemble of discs frequency scales such that the RCS is proportional to wavelength.

## 10-3 CALCULATIONS FOR TROPOSPHERIC DUCTING ENVIRONMENTS:

R. A. Pappert, Naval Electronics Laboratory  
Center, San Diego, California

Full wave (Airy function) solutions for waveguide modes associated with trilinear refractivity layering will be presented. The ducting environments considered include both ground-based and elevated ducts and the method of solution allows for the inclusion of whispering gallery type modes. Comparisons between height gain and range measurements and the numerical modelling results will be presented for frequencies ranging between about 65 and 3000 MHz. Although in most instances approximate agreement between measurements and calculations is found, some disparities suggest extraneous mechanisms such as mode conversions due to turbulence.

10-4 WAVELENGTH DEPENDENCE IN RADIO-WAVE SCATTERING  
AND SPECULAR POINT THEORY: G. Leonard Tyler,  
Stanford University, Stanford, California

Radio-wave scattering from natural surfaces contains a strong near-forward, quasi-specular component that at fixed wavelengths is apparently consistent with specular-point theory. Some surfaces exhibit a marked wavelength dependence in this scattering that contradicts the usual assumptions underlying the specular-point models. Wavelength dependence can be introduced into quasi-specular scattering by a physical approximation that modifies the effective scattering surface with changes in wavelength. Gaussian curvature is taken as the controlling parameter. Wavelength dependence of the scattering, as expressed in terms of the mean-square tilt of the filtered surface, depends on an integral of the two-dimensional surface power spectral density. A uniform low-pass filter model of the scattering process yields explicit solutions for mean-square tilt versus wavelength. Interpretation of experimental results from planetary surfaces indicates that the asymptotic height-squared spectral densities fall at least as fast as an inverse third-power law of spatial frequency. Wavelength independent surfaces fall at least as fast as an inverse fifth-power law.

10-5 PROPAGATION IN A STRATIFIED ATMOSPHERE:

George Hufford, OT/ITS, United States  
Department of Commerce, Boulder, Colorado

Another method for computing fields in stratified media is presented. This one uses ray tracings and derives an integral which can be evaluated numerically. Results, surprisingly, show that microwave fields within a radio hole exhibit considerable variability. This apparent fading arises from a diffraction fringe system. One conjectures that its appearance in nature is not uncommon, and that this may very well be an important mechanism for the fading that is observed on microwave and millimeter wave links.

10-6 PROBABILITY DISTRIBUTION OF IRRADIANCE

FLUCTUATION OF BEAM WAVES IN A WEAKLY TURBULENT ATMOSPHERE: Y. Furuhama, National Oceanic and Atmospheric Administration, Environmental Research Laboratories, Boulder, Colorado

The integral expression for the Nth-order moment of irradiance fluctuations of a finite beam wave traversing a weakly turbulent atmosphere is derived

by the parabolic-equation method. The expression for the Nth-order moment, evaluated within the framework of the first-order perturbation theory, is the same form as the Nth-order moment of the log-normal distribution. This fact shows a necessary condition for the log-normality of the irradiance fluctuation of the beam wave, although the log-normal distribution is not uniquely determined by the method of series expansion of the moments. This result is valid at all distances from the axis of the beam and the distribution function depends upon that distance. For the plane-wave limit, the value of the variance coincides with the results of the usual first-order perturbation theory, and log-normality also holds.

10-7 SCINTILLATIONS DUE TO AN EXTENDED SOURCE IN EXTENDED STRONG TURBULENCE: V. H. Rumsey,  
University of California, San Diego, La Jolla,  
California

The effect of the angular width of an incoherent source on the spectrum of intensity fluctuations due to strong turbulence extended over the path of propagation is expressed in closed form. It is more complicated than the Cohen-Salpeter formula for a concentrated layer of turbulence. However, the scintillation index  $m$  for an isotropic turbulence spectrum  $\phi_n$  is simple. For example, when the turbulence is uniform over path length  $z$ ,  $\phi_n(q) \sim q^{-\alpha}$ ,  $2 < \alpha < 4$ , and the source has a Gaussian brightness distribution of angular width  $\theta_0$ ,

$$m^2 = 1 - \sqrt{\pi} \times \epsilon^x^2 [1 - \text{erf}(x)]$$

$$\text{where } x = \frac{3U\theta_0}{2\pi} \sqrt{\frac{z}{\lambda}}, \alpha = 3,$$

and  $U \gg 1$  is the intensity randomization (the Born approximation for  $m^2$  due to an incident plane wave). Thus for  $z \approx 10^{10}\lambda$ ,  $\theta_0 \approx 10^{-8}$  rad  $\approx 2 \times 10^{-3}$  arcsec,  $m^2$  remains at unity for  $4 < U < 1000$  and then decreases sharply for  $U > 2000$ . As in the case of a concentrated layer, the exponent  $\alpha$  in  $\phi_n$  is directly found from the variation of  $m$  with strength of turbulence.

10-8 INCOHERENT BACKSCATTER FROM ROUGH SURFACES-  
THE TWO-SCALE MODEL RE-EXAMINED: J. Carl Leader,  
McDonnell Douglas Research Laboratories,  
McDonnell Douglas Corporation, St. Louis,  
Missouri

A mathematical description of surface roughness as a superposition of two independent random height distributions of different scales provides an excellent model of many rough surfaces of interest. If initially-coherent radiation is scattered by such a surface, the small-scale roughness can diffract the radiation while the large-scale undulations determine the angular distribution and superposition of the diffracted energy. A recent derivation of the mutual coherence function caused by the interaction of spatially separate, rough-surface elements showed that this contribution could be identified as the coherent component. The cross section contribution resulting from the integrated intensity of the radiation scattered by the small-scale roughness is identified as the incoherent contribution. This paper reports new calculations of the incoherent cross section contribution using a physical optics model for the small-scale scattering process. The tilt angle of the local surface normal, with respect to the incident polarization vector, is considered, resulting in a first-order depolarized component of the backscatter cross section. Cross section angular distributions are calculated using numerical integration techniques and are compared with results of a double, stationary-phase integration for various values of the surface roughness parameters. The stationary phase calculations show that the stationary phase angle increases with increasing backscatter angle resulting in a reduced effective incident angle which is commensurate with the physical optics assumption. The calculated cross section distributions are shown to correspond to measured scattering data.

FEASIBILITY OF SCATTER RADARS ON THE SPACE SHUTTLE - I

URSI COMMISSIONS IV AND III

Thursday, October 23 0830

URSI Session IV-5, UMC 157

Chairman: M.J. Baron,

Stanford Research Institute

- 5-1 SPACE SHUTTLE CAPABILITIES: C.R. Chapell, Marshall Space Flight Center, Huntsville, Alabama
- 5-2 AMPS MISSION PROGRESS: ATMOSPHERIC AND MAGNETO-SPHERIC PLASMAS IN SPACE: F. Crawford, Stanford University, Stanford, California
- 5-3 INCOHERENT SCATTER RADAR - I: Pierre Bauer, NASA Goddard Space Flight Center, Greenbelt, Maryland (representing CNET, France)
- 5-4 INCOHERENT SCATTER RADAR - II: Pierre Bauer, NASA Goddard Space Flight Center, Greenbelt, Maryland (representing CNET, France)
- 5-5 INCOHERENT SCATTER RADAR - III: M.J. Baron, Stanford Research Institute, Menlo Park, California
- 5-6 INCOHERENT SCATTER RADAR - IV: M.J. Baron, Stanford Research Institute, Menlo Park, California
- 5-7 TECHNIQUE OF COMPUTER SIMULATION OF SHUTTLE BACKSCATTER RADAR SIGNALS: F. S. Mozer, University of California, Berkeley, California
- 5-8 TEST RESULTS OF SIMULATION OF SHUTTLE BACKSCATTER RADAR SIGNALS: F.S. Mozer, University of California, Berkeley, California

5-9 BISTATIC INCOHERENT SCATTER RADAR EXPERIMENTS INVOLVING THE SPACE SHUTTLE: Jan C. Siren, Department of Applied Physics and Information Science, University of California, San Diego, La Jolla, California

Incoherent scatter radar transmitters are too massive for flight aboard the space shuttle. Receivers, however, are relatively light and a combined orbiting package comprising a receiver, high-gain deployable antenna, timing, and data reduction equipment may be feasible for ionospheric studies. The orbiter would receive the scattered VHF waves transmitted by incoherent scatter radars at fixed sites. Because the orbiter would be in the vicinity of high-latitude radars only four times per day, and in the vicinity of near-equatorial radars only twice per day, the receiver must be sufficiently flexible to tune to the various transmitters' operating frequencies. Similarly, the timing equipment must have sufficient capability to synchronize the receiver to the various radars' pulse transmissions. Synchronization of the fixed radars' pulses to Universal Time (which has not been generally implemented at this date) as well as that of the orbiter's, would be necessary. Vector ion velocities within the scattering volume defined by the intersection of the two beams, would be measurable. World-wide patterns of ionospheric convection and densities, could be discerned from the near-simultaneous measurements made at widely scattered points. Establishment of a southern hemisphere incoherent scatter radar is recommended.

SOLAR AND PLANETARY OBSERVATIONS - I

URSI COMMISSION V

Thursday, October 23 0830

URSI Session V-6, UMC 156

Chairman: T. Clark, NASA Goddard SFC

6-1 OUT-OF-ECLIPTIC TRAJECTORIES OF LOW FREQUENCY TYPE III BURSTS: H. Alvarez, F. T. Haddock, and W. H. Potter, University of Michigan, Ann Arbor, Michigan; J. Fainberg, R. J. Fitzenreiter, and R. R. Weber, Goddard Space Flight Center, Greenbelt, Maryland

Spin modulated radio astronomy data of traveling type III solar radio bursts at low frequencies have been used to determine the path of energetic exciter electrons through the interplanetary medium between the Sun and 1 AU. Since the electrons follow interplanetary magnetic field, this technique has yielded the first radio visualization of the spiral structure of the magnetic field projected in the ecliptic (Science, 178, 743, 1972). By utilizing simultaneous measurements from 2 spinning spacecraft, RAE-2 (GSFC experiment, spin axis in ecliptic) and IMP-6 (University of Michigan experiment, spin axis perpendicular to ecliptic) it is possible to determine the out-of-the-ecliptic trajectory of measured type III bursts. Several type III bursts occurring on June 22, 1973, have been analyzed. A striking feature of these bursts is that the path of radio emission close to the Sun moves out northward of the ecliptic but at progressively longer distances it shifts southward. The trajectory crosses the ecliptic at about 0.5 AU. At 67 kHz the observed direction of arrival of the type II radiation is over 50 degrees south. Considerable structure of the interplanetary magnetic field in 3 dimensions is indicated. Several models of the radio trajectory inferred from this data will be presented.

6-2 LF OCCULTATION OBSERVATIONS FROM LUNAR ORBIT:  
R. R. Weber, J. Fainberg, and R. G. Stone,  
Goddard Space Flight Center, Greenbelt, Maryland

In the frequency range of 25-83 kHz the RAE-2 lunar orbiter often measures sporadic 20-30 dB noise enhancements. Lunar occultations indicate at least two source directions: the sun and the earth. In the case of solar occultations the average apparent source direction is a few degrees west of the sun, suggesting

that the high noise levels observed are of local origin and associated with the solar wind. Correlations between the low frequency noise levels and interplanetary plasma parameters will be discussed. A smaller number of occultations of the earth are observed in the data. These occultations appear over a much wider angular range and are of magnetospheric origin.

6-3 INTERPLANETARY SCINTILLATION OBSERVATIONS  
WITH THE 34.3 MHz COCOA CROSS, MAY-DECEMBER 1974:  
A COMPARISON WITH SPACECRAFT OBSERVATIONS OF  
THE SOLAR WIND: F. T. Erskine, W. M. Cronyn,  
and S. D. Shawhan, University of Iowa, Iowa City,  
Iowa

Interplanetary scintillation (IPS) observations have been carried out with the 34.3 MHz Cocoa Cross array during the second half of 1974 in order to locate and map both corotating and transient features in the solar wind. Scintillation index and square root second moment of the intensity spectrum have been measured for a group of over 60 scintillating radio sources having ecliptic latitudes between  $-30^{\circ}$  and  $+74^{\circ}$ . Comparisons are made between IPS activity on individual sources and many-source averaged IPS properties for sources at high latitudes, and sources east or west of the sun. In addition, comparisons are made between IPS data and spacecraft measurements of solar wind particle density, velocity, and interplanetary magnetic field near 1 A.U., as well as with ground based geomagnetic data.

6-4 SIMULTANEOUS MEASUREMENTS OF RADIO BURST INTENSITY  
AND FAST ELECTRON FLUX AT 1 AU: R. J. Fitzenreiter  
and L. G. Evans, Goddard Space Flight Center, Green-  
belt, Maryland; and R. P. Lin, University of Calif-  
fornia, Berkeley, California

Direct observations in the near-earth interplanetary medium have shown that electrons of energy  $\sim$ 10-100 keV are the excitors of solar type III radio bursts at 1 A.U. (Lin, et al., *Astrophys. Lett.* 14, 191, 1973). Space experiments which measure plasma parameters, particle fluxes, and radio waves provide a particularly suitable opportunity to test quantitative theories of the radio burst phenomenon. We compare simultaneous IMP-6 measurements of the intensities of the radio emission (Goddard Space Flight Center experiment) and the flux of fast electrons (University of California experiment). We find that there

are two regimes in the generation of type III radiation: one where the radio intensity is linearly proportional to the electron flux, and a second regime, which occurs above a threshold electron flux, where the radio emission is proportional to the electron flux to the ~2.5 power. These two regimes of radio emission are interpreted as a distinct change in the emission mechanism of type III bursts, i.e., that there is a transition from one mode of burst generation to another more efficient mode when the electron flux reaches a critical value.

6-5    IMPLICATIONS OF PIONEER-11 MAGNETIC FIELD MODELS FOR JUPITER'S DECAMETRIC RADIO EMISSION: R.A. Smith, J.K. Alexander, M.L. Kaiser, Goddard Space Flight Center, Greenbelt, Maryland

Models of Jupiter's magnetic field derived from measurements with the Pioneer-11 flux gate and helium vapor magnetometers have been analyzed with a view towards understanding the origin of the decameter-wave radio emission (DAM) from the planet. In particular, we have calculated the geometry and electron gyrofrequency predicted for both the North and South feet of the Io-threaded flux tube at several altitudes as a function of sub-Io longitude for the multipole field models of Acuna and Ness (1975) and Smith, et al. (1975). The Smith, et al., model predicts a maximum surface gyro-frequency equal to the observed high frequency limit of the DAM; the Acuna and Ness model predicts distortion of the field that would result in all the classical "sources" being located in the same vicinity of the Northern auroral zone; and both models tend to favor a mechanism involving transverse propagation from a source in the Northern hemisphere. Although a detailed understanding of the DAM cannot be derived from either model, our calculations indicate that the beaming pattern of the emission may be determined by reflection from the ionosphere rather than by inherent beaming from the source region.

6-6    RESULTS OF LONG-TERM SYNOPTIC MONITORING OF JUPITER'S DECAMETRIC RADIATION: J. K. Alexander and M. L. Kaiser, Goddard Space Flight Center, Greenbelt, Maryland

The GSFC Jupiter Monitor Network has provided synoptic observations of Jupiter's emission at 16.7 and 22.2 MHz for the past 9-1/2 years, and this report presents the results of analysis of the large homogeneous set of measurements for the apparitions of 1966-1974. We present

an update of the radio rotation period determination of Kaiser and Alexander (Astrophys. Lett. 12, 215, 1975) which includes provision for beaming effects due to variations in  $D_E$  (the Jovocentric declination of Earth). Some estimates of the magnitudes of possible long-term variations in rotation period are also discussed. The data clearly show the Io-independent emission features associated with the System III central meridian longitudes of all three major Io-related source regions as recently reported by other workers. In addition there is some evidence for heretofore unrecognized Io-related emission features which are apparently independent of central meridian longitude. We suggest the possibility of three kinds of emission: namely, (1) Io-stimulated, sharply beamed emission; (2) Io-independent, sharply beamed emission; and (3) Io-stimulated, broadly beamed emission.

SUB-SURFACE PROBING  
URSI COMMISSIONS VI AND I  
Thursday, October 23 0830  
URSI Session VI-10, Radio Building 1107  
Chairman: L. Peters, Jr.,  
The Ohio State University

10-1 ELECTROMAGNETIC SCATTERING BY A THREE-DIMENSIONAL INHOMOGENEITY IN A DISSIPATIVE HALF-SPACE FOR HORIZONTAL ELECTRIC DIPOLE EXCITATION:  
M. Cauterman, P. Degauque, B. Demoulin, and R. Gabillard, Lille University, Electronics Department, Villeneuve d'Ascq, France;  
F. Berthelot, Institut Francais du Petrole, Rueil, France

Some geophysical prospection techniques use the measurement in a borehole of the vertical electric field radiated by an electric horizontal dipole situated on the ground surface. The field amplitude may be used to determine the geometry of subsurface inhomogeneity. In order to improve the geophysical method, we develop a theoretical solution for the electromagnetic response of a three-dimensional inhomogeneity in a conductive half-space excited by a horizontal antenna. We assume that the emitting frequency is sufficiently low in order to use the quasi-static approximation. The solution is obtained in the form of an integral equations system which is reduced to a matrix equation and solved numerically. The cartesian components of the electromagnetic field in the inhomogeneity are determined. Therefore, the vertical electric field in the earth is calculated by integrating the half-space Green's functions over the scattering currents. We apply this theory in the case of a thin horizontal and resistive inhomogeneity. The numerical results are compared with those obtained with scale model experiments.

10-2 NUMERICAL STUDY OF THE EFFECT OF TWO-DIMENSIONAL CONDUCTORS ON THE SURFACE FIELDS OF A BURIED VERTICAL MAGNETIC DIPOLE: Charles H. Stoyer and James R. Wait, Cooperative Institute for Research in Environmental Sciences, University of Colorado, Boulder, Colorado

Using a finite-difference method, the errors resulting from a laterally inhomogeneous overburden in source location of a buried magnetic dipole are determined.

Several idealized two-dimensional models are adopted. Particular attention is paid to longitudinal conductors that will channel the currents induced by the primary magnetic dipole source. In order to provide insight, we present equi-value contours of various field quantities observed on the surface. Of particular interest are the derived ellipticities of the magnetic field vectors in both the horizontal and the vertical plane. It is shown that the source location error, when using the tilt angle of the vertical polarization ellipse, is relatively small. Finally, some suggestions are made on field procedures to determine the conductivity structure of the overburden in order to predict the location error in a given case.

#### 10-3 MICROWAVE REMOTE SENSING OF BOUNDED RANDOM MEDIA:

L. Tsang and J.A. Kong, Department of Electrical Engineering and Computer Science, and Research Laboratory of Electronics, Massachusetts Institute of Technology, Cambridge, Massachusetts

In passive remote sensing of the earth with microwaves, the brightness temperature reading of a radiometer depends on its angle of observation and on the microwave emissive properties of the observed area. Using the model of a half-space random medium with a laminar structure and nonuniform temperature profile, we solve for the brightness temperatures with a radiative transfer approach. For constant absorption and scattering coefficients, the brightness temperature is determined by a simple closed form formula. Physical interpretations and numerical results are illustrated and compared with previous theories and experimental data. In places such as ice or snow covered land or water, the half-space model fails to apply. A straight forward solution of the radiative transfer equations, which only accounts for incoherent effects, for a two-layer random medium found unsatisfactory in interpretation of experimental data which demonstrate high degree of coherent effects. We resort to the Dyson equation and the Bethe-Salpeter equation and derive a set of "modified" radiative transfer (MRT) equations that incorporate coherents. The temperature is assumed to be a constant. The nonlinear approximation, instead of the more popular bilocal approximation, is applied to the Dyson equation in deriving the MRT equations. Under this approximation the principle of conservation of energy is shown to be preserved. The MRT equations are then solved and compared with solutions obtained from the Born approximation within their common

domains of validity. The results are in simple closed form and apply to both active and passive remote sensing.

10-4 MICROWAVE REFLECTION FROM A UNIFORM COAL SEAM WITH A NON-UNIFORM SLATE BACKING: D. C. Chang, E. C. Read, and J. R. Wait, Cooperative Institute for Research in Environmental Sciences, University of Colorado, Boulder, Colorado

There is a current need to determine the roof thickness of coal-mine tunnels in a continuous fashion. It has been proposed by J. W. Adams and D. Ellerbruch of NBS to utilize interference phenomena when the roof is illuminated by a swept-frequency microwave beam. In order to understand non-uniformities in the roof structure, we in CIRES have undertaken to examine several relevant analytical models. Here we discuss a model that consists essentially of a uniform slab of coal that is backed by a relatively highly conducting slate region that can be characterized by a locally defined surface impedance. The latter is taken to have a laterally periodic variation in its properties, but this is not an essential restriction. For an obliquely incident plane wave, we have calculated the actual surface impedance and wave tilts as seen at the coal-air interface. These results are then compared with the corresponding calculations where we assume that the structure is uniformly stratified in a local sense. This quantitative comparison is important in order to have confidence in simpler and more convenient layered media formulations that form the basis of previously developed inversion schemes. Other kinds of errors in such schemes result when the layer interfaces are non-planar; we shall discuss these briefly and mention the work in CIRES of J. Lytle and W. J. Hughes who implemented some analytical studies in this regard as part of our cooperative program with the Pittsburgh Mining & Safety Research Center of the U.S. Bureau of Mines.

10-5 DISCRIMINATION OF RADAR TARGETS IN THE PRESENCE OF NOISE: C. W. Chuang, and D. L. Moffatt, The Ohio State University ElectroScience Laboratory, Department of Electrical Engineering, Columbus, Ohio

The capability of discriminating radar targets is degraded in the presence of noise. This paper investigates the noise effect on the predictor-correlator processing applied to noise-corrupted ramp response waveforms of radar targets which can be synthesized with 10 discrete spectral scatter-

ing data. The end results of the predictor-correlator processing are curves of unity minus the normalized squared error between a measured ramp waveform and a calculated (using the dominant natural resonance of the target being sought in a difference equation) ramp waveform as a function of the sampling interval along the waveform. It is shown that in the presence of noise the discrimination capability using the predictor-correlator processing is degraded by a factor of  $(1-N/S)$  where  $N/S$  is the total noise-to-signal power ratio of the ramp response waveform.

#### 10-6 CHARACTERIZATION OF SUBSURFACE TARGETS:

D. L. Moffatt and C. W. Chuang, ElectroScience Laboratory, The Ohio State University, Columbus, Ohio

Electromagnetic pulse soundings of subsurface structures yield amplitude vs. time records of the reflected signal. The response from a given geological or man-made anomaly is visually evident over isolated portions of the sounding record. In this paper, a characterization of these isolated responses via application of Prony's method is suggested. Prony's method is simply an algorithm for fitting a finite exponential sum to a known function. When applied to transient response waveforms from free space radar targets, the resulting complex decay factors can be associated with the size, shape, and composition of the radar target. In the case of subsurface targets, the interpretation of the decay factors is much more difficult since they represent some complex combination of the antenna, the medium, and the target. Only in rare instances can the antenna and medium effects be removed. Nevertheless, the decay factors (and residues) are characteristic of the waveform and therefore at least partially characteristic of the subsurface target. This type of essentially automatic classification of pulse soundings appears somewhat simpler than laborious comparisons of time and frequency (FFT) records in an attempt to identify similar characteristics for a given target. The method is illustrated using pulse soundings of various dielectric and metallic pipe in a soil medium. Examples where the decay factors can be associated directly with a dimension of the target are given. Other cases where the decay factors are entirely fictitious, in terms of the targets' physical properties, are also shown.

## 10-7 GEOPHYSICAL SUBSURFACE PROBING WITH THE ELECTROMAGNETIC INTERFERENCE FRINGES (EIF) METHOD:

J.A. Kong, W.C. Chan, and L. Tsang, Department of Electrical Engineering and Computer Science, and Research Laboratory of Electronics, Massachusetts Institute of Technology, Cambridge, Massachusetts

The electromagnetic interference fringes (EIF) method was first used in 1955 by ElSaid to probe the underground water in Egyptian deserts. The interference patterns of the field components can either be measured as a function of frequency or as a function of distance. The distance EIF method has been studied extensively. The mathematical approaches used in evaluating the interference patterns involve (1) the saddle point method, (2) the residue series method, and (3) the fast Fourier transform method. In this report we extend the similar approaches to study the use of vertical and horizontal magnetic dipoles in the EIF method. The results are compared with those for the horizontal electric dipole. In particular we find from the radiation pattern plots that the horizontal magnetic dipole (HMD) may be more effective in subsurface probing than the horizontal electric dipole (HED). In the endfire direction, the angle of maximum power coupling for the HMD occurs at  $\sin^{-1}(2/(n^2+1))^{1/2}$  while for the HED it occurs at  $\sin^{-1}((n^2+1)/2n)^{1/2}$ . In the broadside direction, the angle of maximum power coupling for both dipoles occurs at the critical angle. However, for the HMD, the power is more concentrated in the critical angle direction which results in a sharper peak in the interference pattern.

## 10-8 SUBSURFACE RADAR SOUNDING EXPERIMENTS IN ARCHAEOLOGY: Roger S. Vickers and Lambert T. Dolphin, Radio Physics Laboratory, Stanford Research Institute, Menlo Park, California

A family of very short pulse radars operating between 10 and 250 MHz has been developed by SRI for subsurface remote sensing in archaeology, mining, and geophysics. Three different archaeological experiments using the equipment are described to illustrate the potentials and limitations of subsurface radar techniques. These include sounding experiments at the pyramids of Giza searching for hidden chambers, a radar survey at Chaco

Canyon, New Mexico, where numerous walls, kivas, and other Indian pieces lie buried in dry alluvium, and a search for buried Bristlecone pine stumps in alluvial fans of California's White Mountains.

ARRAYS

URSI COMMISSION VI

Thursday, October 23 0830

URSI Session VI-11, Radio Building Auditorium

Chairman: A.A. Ksieinski,

The Ohio State University

11-1 ADAPTIVE ARRAY PROCESSING FOR HF SKYWAVE BACK-SCATTER RADARS: T.W. Washburn and L. E. Sweeney, Jr., Stanford Research Institute, Menlo Park, California

Adaptive beamforming techniques have been applied to an HF skywave backscatter radar. This radar utilizes a repetitive sweep-frequency CW signal format to produce range-Doppler maps and also employs a 2.5 km linear receiving array for 1/2 deg azimuthal resolution. Signals from eight subarrays of the receiving antenna were processed with coherent receivers whose audio voltage outputs were digitized for minicomputer beamforming processing prior to range-Doppler analysis. In one experiment the radar was pointed at a repeater located at a range of 1300 km, while a controlled interfering transmitter was operated at the same range but about 1½ deg away in radar azimuth. Comparisons are given between interference rejection capabilities of a conventionally formed beam (with a modified Dolph taper) and an adaptively formed beam. Algorithms for both recursive time-domain adaptation and covariance-matrix-inversion adaptation were implemented. The characteristics of HF backscatter signals when processed via these beamforming techniques are described and compared.

11-2 ADAPTIVE MULTIPLE-BEAM RECEIVING ARRAY:  
R. E. Langseth and Y. S. Yeh, Bell Telephone Laboratories, Holmdel, New Jersey

A self-cophasing adaptive array which is capable of simultaneously receiving PSK modulated cochannel signals from different arriving angles is described. Instead of using pilots, the desired cophasing information is derived by processing the modulated carriers. This simplifies the transmitting formats and also provides better cophasing performance since the full signal power is used to derive the phase information. The system requires that the carrier frequencies be separated by a small fraction of their modulation bandwidth. The output signal from the array combiner is fed back to each individual

array element and mixed with the input signal. The upper sideband product then contains broadband PSK cross products and several carrier terms. Each carrier term is separated in frequency but contains exact phase information for the cophasing of that array element. A narrow band filter can then be used to pick out one particular carrier and the array will be cophased to receive one of the many cochannel modulations. An experimental 4-element array has been tested.

11-3 VALLEY FORGE RESEARCH CENTER ADAPTIVE ARRAY:

Earl N. Powers and Bernard D. Steinberg, Valley  
Forge Research Center, Moore School of Electrical  
Engineering, University of Pennsylvania,  
Philadelphia, Pennsylvania

Valley Forge Research Center has a continuing research program in the area of large thin random conformal arrays. Such systems can yield high resolution, narrow beamwidth antenna patterns without the necessity of the very expensive, mechanically and electrically well defined structures implied by classical array theory. During the last year Valley Forge Research Center has applied this theory to the implementation of an experimental bistatic radar system. This system operates at L-band and employs a thin random array consisting of 16 receiving elements spread over a region about 100 wavelengths in length. This array has a main lobe beamwidth of 10 milliradians. The array beam can be scanned over the target region. The array elements are self-standing units which detect and measure the phase of the target wavefront and return this measurement to a central processor. The central processor is a real time, special purpose digital system which manipulates the outputs of the array modules to compute the beam pattern and to generate the appropriate phase correction to scan the beam. The target is illuminated by a separate transmitter located several hundred feet from the receiving array. This paper will describe the system structure and its performance in terms of beamforming and scanning.

11-4 A BROADBAND ANTENNA ARRAY FOR SEA SCATTER

MEASUREMENTS: M. T. Ma and L. H. Tveten,  
Institute for Telecommunication Sciences,  
Office of Telecommunications, U.S. Department  
of Commerce, Boulder, Colorado

A nonuniformly spaced array of twenty-five side-terminated vertical half rhombics is synthesized for

the entire high frequency band. The array is to be used for both transmitting and receiving, as a skywave Doppler radar for sea scatter measurements. The array has the capability for providing a maximum transmitting-receiving product gain in the order of 60 dB at low take-off angles, a product azimuth pattern with a nominal beamwidth of  $2^{\circ}$ , a  $40^{\circ}$  sectoral coverage, a final product sidelobe level of -38 dB, and a grating-lobe level of -30 dB.

11-5 A COMPARISON OF GAIN-PHASE AND SINGLE CHANNEL RECEIVER PROCESSING IN AN ADAPTIVE HF ARRAY:

Lloyd J. Griffiths, Department of Electrical Engineering, University of Colorado, Boulder, Colorado

Data for this study were obtained using the Wide Aperture HF Radio Research Facility which is located in the central valley of California and is operated by Stanford Research Institute. This facility is operated as a one-hop over-the-horizon radar system and utilizes transmitter and receiver arrays which are separated by about 100 km. Signal transmissions consisted of a linear, sawtooth CW waveform. Received signals were recorded on 8 adjacent subarrays which spanned a total aperture of 2.56 km. Each subarray was composed of 32 linearly spaced monopoles with an interelement spacing of 10 meters. The 8 subarray outputs were deramped using a common local oscillator, converted to baseband and simultaneously digitized for purposes of off-line processing. The receiver bandwidths and digitizing rate were 960 Hz and 1921 Hz, respectively. Previously reported results using this system have demonstrated that simple adaptive beamforming methods can be used to combine the subarray outputs such that significant improvements in output signal-to-noise ratio may be obtained. The purpose of the present study was to compare performance of this adaptive processor with that achieved when in phase and quadrature receivers were employed at each subarray output prior to adaptive combining. Quadrature signals were synthesized using a 32-point non-recursive digital filter and a sampling rate equivalent to one-half of the original rate. Comparative examples are presented demonstrating the performance of the two processors using identical data sets recorded during periods of high HF interference levels. It is concluded that single channel adaptive processing offers significant advantages in this application.

## 11-6 COMPARATIVE STUDY OF OPTIMIZATION METHODS FOR YAGI ANTENNA ARRAYS: E.K. Yung and D. Kajfez, University of Mississippi, University, Mississippi

Three optimization methods, namely, the Rosenbrock method, the Fletcher and Reeves method, and the Davidon method via Fletcher and Powell (abbrev. DFP), were compared for their efficiencies to optimize the directivity of a six-element Yagi-Uda antenna array by varying the element lengths. The efficiency of the particular optimization method was measured by the total number of function evaluations required to optimize the antenna within the prescribed accuracy. It was found that when the number of optimization variables was fewer than five, the DFP method was the best among the three methods studied. However, the Rosenbrock method was more suitable for an optimization problem with a relatively large number of independent variables, or when the starting point of the search was badly chosen such that it was far away from any local minimum. The DFP method was used to optimize the directivity of the antenna by adjusting the element spacings. It was found that further improvement was possible as compared with the optimized results already published. Also included were two attempts to reduce the sidelobe level. The first example was to optimize the root-mean-square sidelobe level by the DFP method. After optimization, the average sidelobe level was reduced from 16.16 db to 22.87 db, with slight sacrifice (.7 db) in directivity. The second trial was to minimize the largest sidelobe by the so-called minimax formulation. In this case, the Rosenbrock method was used as the DFP method was not applicable, since the objective function had discontinuous first derivatives. The optimized radiation pattern exhibited equal-rippled sidelobes as expected, and the largest sidelobe was -25.2 db below the main lobe.

## 11-7 DIGITAL PROCESSING FOR ENHANCEMENT OF RESOLUTION AND SIDE-LOBE RATIO IN IMAGING RADARS: Lewis R. Wilson, Hampton Technical Center, LTV Aerospace Corporation, Hampton, Virginia

A Quadratic Convex Programming Method is described for the design of linear digital filters (tapped delay lines) which operate simultaneously on the quadrature components of the If data of an Imaging Radar prior to envelope detection. The optimization criteria are: (1) the max-

imum side lobe is minimized and/or (2) the width of the central peak is decreased by a prescribed amount while the side-lobe ratio is simultaneously maximized.

It is shown that the price paid for these improvements is (1) a loss in (S/N) out as compared to the conventional Matched Filter Receiver and (2) an increased sensitivity to phase errors due to spurious motions of the target or receiver. Moreover, the analytical problem becomes increasingly difficult as greater improvements are sought. Specifically, greater improvements require longer filters (more delay line taps), giving rise, in the numerical solution procedure, to matrices which are increasingly large in dimension and increasingly ill-conditioned.

11-8 ELEMENT PATTERN BOUNDS IN UNIFORM PHASED ARRAYS:

W. Wasylkiwskyj, Institute for Defense Analyses,  
Arlington, Virginia; and W. K. Kahn, The George  
Washington University, Washington, D.C.

This paper delineates limits within which the radiation pattern of a single excited element in an infinite regular array of terminated elements may be modified through a uniform feed or matching network. In the absence of grating lobes the pattern is limited by the universal  $\cos \theta$  bound. When the array spacing admits grating lobes, it will be shown that this bound is effectively reduced by a factor dependent on the radiating elements employed in the array. The factor may be computed from any element pattern, e.g., from the pattern of a single excited element in the open-circuited array environment. These results lead to a classification of the conditions resulting in "blindness" of an array. Certain instances of "blindness" are necessary in that they cannot in principle be removed by an adjustment of the feed network, while others can, in principle, be tuned out. Detailed analysis of an array of slots covered by a dielectric slab is presented as an illustration of the general theory.

11-9 CORRELATION MATRIX METHOD FOR THE ANALYSIS

OF FINITE PHASED ARRAYS: A. I. Zaghloul and  
R. H. MacPhie, Department of Electrical  
Engineering, University of Waterloo, Waterloo,  
Ontario, Canada

A novel and simple method is introduced to analyze finite phased array antennas, and is based on

calculating the cross-correlation integration between the elements' electric fields. This takes care of both the mutual coupling effects and the edge effects. The correlation integrals lead to the mutual powers between the elements and thus to the total power contributed by every element. Applying the principle of conservation of power, we calculate the elements' admittances and reflection coefficients. The latter are employed to determine the electric fields across the element apertures which were used for the correlation integrals in the first place. This closed loop procedure produces a set of linear equations with the element reflection coefficients as their variables. The equations are solved by simply inverting the matrix that results from the correlation integrals; this is called the correlation matrix. The elements of the correlation matrix are scan-independent integrals multiplied by relative phasing factors, thus very convenient for fast calculations. The method is applied to arrays of narrow slots to show the behavior of the elements' reflection coefficients with the scanning direction. The relative amplitudes and phases of the electric fields across the different slots are then calculated in a simple and exact form. The method can be extended to arrays of wide slots with a consequent complication in the formulation.

11-10 ANALYTICAL AND NUMERICAL STUDY OF A LENS ARRAY SYSTEM FOR LIMITED SCAN: Giorgio V. Borgiotti, AFCRL, Hanscom AFB, Massachusetts

It has been shown recently that the dimensionality or the "number of degrees of freedom" of a beam scanning in a limited sector is given by the product of aperture in wavelengths by scan sector (measured on "sin $\theta$ " space). In this paper a design method and numerical simulation results are presented for an antenna system for limited two dimensional scan. The system uses a number of phase shifters equal to the theoretical number  $N$  of degrees of freedom, and features independent controls of sum and difference beam shapes. The radiating aperture consists of a "boot lace" lens, with a linear outer and circular inner profile. This lens geometry plays a basic role in the good scan and wide band performances of the system. An array, whose size is determined by the scan requirement and lens focal length, is located on the focal plane and is focused on the inner lens profile. The array is fed by a Butler matrix having  $N$  input ports.  $N$  variable

phase shifters are inserted between the input ports of the Butler matrix and a beam forming network, having two separate inputs for independent control of sum and difference patterns.

EFFECT OF ELF FIELDS ON BIOLOGICAL SYSTEMS - I

URSI COMMISSION I (BIOLOGICAL EFFECTS)

Thursday, October 23 0830

URSI Session B-10a, UMC East Ballroom

Chairman: R. Philips,

Battelle Northwest

B10a-1 EFFECTS OF WEAK LOW FREQUENCY ELECTRIC FIELDS ON CALCIUM EFFLUX FROM ISOLATED CHICK AND CAT BRAIN:  
S. M. Bawin and W. R. Adey, Departments of Anatomy and Physiology and Brain Research Institute, University of California, Los Angeles, California

Freshly isolated chick cerebral hemispheres were equilibrated with a calcium Ringer's solution containing  $^{45}\text{Ca}^{2+}$  for 30 minutes. Washed tissue portions were then exposed to sinusoidal electric fields at either 1, 6, 16, or 32 Hz, with electric gradients of 5, 10, or 56 V/M in air for each frequency for 20 minutes.  $^{45}\text{Ca}^{2+}$  efflux was then measured in 0.2 ml of supernatant and compared with efflux from unexposed control samples. All tissues were maintained at 36°C and checked for specific activity after the experiments. A frequency sensitive "tuning curve" showed sharply reduced efflux of 15 to 20 per cent at 6 Hz ( $p<0.05$ ) and 16 Hz ( $p<0.01$ ) for 10 V/M fields. Similar but slightly smaller reductions ( $p<0.05$ ) occurred at 56 V/M. Threshold was around 10 V/M, but non-significant trends occurred at 5 V/M. Cat visual, auditory, suprasylvian, and sensorymotor cortex tested at 1, 6, 16, 32, or 75 Hz, 56 V/M showed significantly decreased effluxes at 6 Hz ( $p<0.05$ ) and 16 Hz ( $p<0.01$ ), but with non-significant trends at all other frequencies tested. At 10 V/M, non-significant decreases occurred at 6 and 16 Hz. Oscillating ELF fields at 6 to 30 Hz thus reduce Ca efflux, whereas, weak VHF fields amplitude modulated at the same frequencies increase efflux (Bawin, Kaczmarek, and Adey, 1975). A model for both effects based on cooperative interactions of Ca with fixed charges on stranded biopolymers is proposed.

B10a-2 LONG-TERM EFFECTS OF WEAK 45-75 Hz ELECTROMAGNETIC FIELDS ON THE SLIME MOLD, PHYSARUM POLYCEPHALUM:  
B. Greenebaum, E. M. Goodman, and M. T. Marron, Division of Science, University of Wisconsin-Parkside, Kenosha, Wisconsin

Cultures of the slime mold, Physarum polycephalum, have been continuously exposed to weak (2.0 G, 0.7 V/m) 75,

60, and 45 Hz electric and magnetic fields, applied simultaneously to simulate electromagnetic radiation. As a result of exposure to this radiation, nuclear division (mitosis) is slowed. The onset of the effect appears to be frequency dependent; the time for two cell cycles (normally 14-16 hr) is increased by 1-2 hr after 90-120 d of exposure at 75 Hz and after shorter exposure times at 60 and 45 Hz. If cultures showing the delay are removed from the fields, the mitotic delay slowly diminishes, becoming indistinguishable from the control after about 30 days. Other effects induced by exposure to electromagnetic fields include a slowing of reversible protoplasmic streaming and a depression in the rate of respiration ( $O_2$  uptake/mg protein/min). Exposure does not affect the ability to complete either the sexual or asexual life cycles. Experiments seeking thresholds have found no significant mitotic delay in cultures exposed to 0.4 G, 0.15 V/m 75 Hz fields. Experiments are in progress to determine whether these effects are due to electric, magnetic, or a combination of fields.

B10a-3 EFFECTS OF THE FIELD FREE SPACE ON THE CIRCADIAN ACTIVITY RHYTHM OF THE HOUSE SPARROW, PASSER DOMESTICUS, AND OF THE SONG SPARROW, MELOSPIZA MELODIA: Virginia Bliss and Frank Heppner,  
Department of Zoology, University of Rhode Island,  
Kingston, Rhode Island

Experiments were performed to test the hypothesis that changes in the earth's electromagnetic field can act as a Zeitgeber for birds that normally demonstrate pronounced circadian rhythms. Two identical Helmholtz coils were constructed. Each coil contained eight nonmagnetic cages arranged symmetrically within the computed field-free space. The birds' activity was monitored with an event recorder. The experiment was conducted in a soundproof room at a constant temperature. Oscillations in background noise from the power supply and recording apparatus were masked by a white noise generator. Eight birds (one bird/cage) were placed in each coil. Each group consisted of four House Sparrows and four Song Sparrows. All birds were entrained to an LD 9:15 cycle. The experimental group was placed on an electromagnetic field 9:15 cycle (9 hours field-free space: 15 hours earth's electromagnetic field) that coincided with the LD cycle. All birds were maintained at the LD 9:15 cycle. After several weeks, all birds were placed in constant darkness. The electromagnetic field 9:15 cycle was maintained for the experimental group, and all activity was tested for periodicity.

B10a-4 EFFECTS OF 45 HERTZ ELECTRIC FIELD EXPOSURE  
ON RATS: N. S. Mathewson, G. M. Oosta,  
S. A. Oliva, and A. P. Blasco, Armed Forces  
Radiobiology Research Institute, Defense Nuclear  
Agency, Bethesda, Maryland

This is an investigation to determine if vertical sinusoidal electric field exposure at 45 Hz can affect the adolescent rat. Exposures were conducted in six identical chambers which are horizontal air gap parallel plate capacitors. Each chamber can have its applied electric field individually varied, and contains 16 uniformly illuminated cages. The cages are designed to house one animal, to allow the food and water consumption to be measured and to produce a minimum perturbation of the applied field. Electric and magnetic field map data indicate that 45- and 75-Hz magnetic field levels were less than 2 mG and electric field variations within the cage areas are typically  $\pm 5\%$ . Exposures at electric field strengths from 2 to 100 V/m were performed for 28 days. Animal growth during the exposure period was estimated by monitoring the body weights of all animals. Gross metabolism was estimated by monitoring the food and water consumption on a per animal and per gram of body weight basis. At the termination of the 28-day exposure period animals were sacrificed and the following analyses performed. A complete blood count was obtained on each animal. The serum protein and lipid fractions of each animal were monitored by performing selected serum biochemical assays. A necropsy was performed on selected animals of control and irradiated groups. An analysis of data from 18 groups of 16 animals each at five electric field strengths is in progress. Preliminary indications from this analysis suggest that 45-Hz vertical electric field exposure does not significantly affect rats.

B10a-5 EXPOSURE OF DOMESTIC FOWL TO ELF ELECTRIC AND MAGNETIC FIELDS: W.K. Durfee and P.R. Plante, Department of Animal Science, and P. Martin, S. Muthukrishnan, and C. Polk, Department of Electrical Engineering, University of Rhode Island, Kingston, Rhode Island

The domestic fowl (Gallus domesticus) was used in two series of experiments designed to evaluate the influence of continuous wave, extremely low frequency (ELF) magnetic and electric fields upon: (1) growth, develop-

ment, and hatchability of the chick embryo; (2) early post-natal growth and development of the chick; and (3) growth of the sexually immature bird. Special equipment was constructed to provide uniform ELF fields at identical frequencies and amplitudes for continuous exposure of embryos and chicks throughout the preincubation holding, incubation, and hatching periods and through the first four weeks of brooding. Continuous (non-modulated) magnetic fields at frequencies of 45, 60, and 75 hertz, and electric fields at 60 and 75 hertz were used. The magnetic fields were maintained at 1, 5, 8, or 30 gauss and the electric fields were maintained at 1, 10, or 3600 volts per meter. These ELF fields had no significant or consistent effects on: (1) hatchability of fertile eggs; (2) embryonic survival during the most critical stages of development; (3) early post-embryonic growth (to four weeks of age); and (4) learning and memory consolidation in the neo-nate chick. Growth and development to ten weeks of age was not affected by earlier (four-week) exposure. A 60 hertz, 5 gauss magnetic field had no effect on metabolic activity of chick embryos as determined by embryo growth rate and  $\text{CO}_2$  production. Similar experiments using modulated fields are currently in progress.

EFFECT OF ELF FIELDS ON BIOLOGICAL SYSTEMS - II

URSI COMMISSION I (BIOLOGICAL EFFECTS)

Thursday, October 23 1024

URSI Session, B-10b, UMC East Ballroom

Chairman: L. Birenbaum,

Polytechnic Institute of New York

B10b-1 EFFECTS OF WEAK ELF ELECTRIC FIELDS ON SCHEDULE-CONTROLLED BEHAVIOR OF MONKEYS: Rochelle G.

Medici, Brain Research Institute, University of California, Los Angeles, California

Behavior of monkeys in weak, low frequency fields has been extensively evaluated in a recently completed three-year study. Schedule-controlled behavior of the kind used to assay low doses of drugs was shown to be sensitive to weak electric fields in an earlier study (1970). In the present series of experiments, frequencies from 7 to 75 Hz at voltages from 1 to 100 V/m were randomly presented in three different experiments to performing macaques (both implanted with EEG electrodes and unimplanted). Significantly shorter interresponse time and reduced variability of responding were observed for a specific frequency (7 Hz) at 10 V/m. At higher voltages the effect occurred at other frequencies as well, and the magnitude of the change was markedly increased.

B10b-2 EFFECT OF AC ELECTRIC FIELD APPLICATION UPON

HUMAN VISUAL THRESHOLD: S. Sugiyama and K. Mizuno, Kwansei Gakuin University, Nishinomiya, Hyogo, Japan

Contrary to the fact that the DC E.F., having either minus or plus polarity, affect the human visual threshold in such a way that the CFF is elevated or depressed according to the polarity, the AC E.F. whose frequency is 60 Hz did not change CFF level and the 20 Hz AC E.F. whose frequency is lower than the CFF level depresses successive CFF. In Sugiyama's book (1970), he suspected that the 60 Hz AC E.F. application to a human subject whose visual threshold is depressed by other reasons neutralizes his functional level. This means that there seems to be a threshold of human visual functioning to accept the outer energy of the AC E.F. whose frequency is different. It was again suspected that the AC E.F., whose frequency is below a certain level of threshold depresses the photic CFF, while above the threshold there is no facilitatory or inhibitory

effects, but, such higher frequency E.F. neutralizes the excessive functional state due to other reasons such as visual fatigue. In this experiment a 90 Hz AC E.F. was applied at the same time when CFF was depressed by application of low frequency photic stimulus in order to depress the functional state. The result was compared with the depression state made by application of low frequency photic stimulus. The result shows that depressed functional state could be normalized to some extent by application of 90 Hz AC E.F.

B10b-3 IMPACT OF EXTREMELY LOW FREQUENCY ELECTROMAGNETIC FIELDS ON ANIMALS IN NATURE: Bernard Greenberg, Professor of Biological Sciences, University of Illinois at Chicago Circle, Chicago, Illinois

A study is reported of long-term biological impact of extremely low frequency low intensity antenna radiations and electromagnetic fields at the Navy's project Sanguine Wisconsin Test Facility. Population cycles and densities, predator-prey proportions, oxygen consumption, and respiratory quotient of various test and control animal populations living in nature have been monitored for up to 6 years. The animals belong to 4 phyla and include soil arthropods (mites and springtails), 2 species of earthworms, a slug, the woodlouse, and the redbacked salamander. They are all sedentary and some produce large populations and several generations a year, giving reasonable assurance that adequate size populations are continuously exposed over many generations. A marginal difference ( $0.05 > p > 0.025$ ) in  $O_2$  consumption of woodlice was noted in 1972 but not in subsequent years, and a like difference in redworm was noted in 1974 but not previously. Otherwise there were no significant differences in  $O_2$  consumption and RQ between test and control animals measured in summer or fall for 3 years. Between-year and within-year population analyses of mites and springtails living in various habitats and soils under the antenna and in control plots do not reveal any significant alterations attributable to the operation of the Sanguine antenna. In addition, we have no evidence from observations of the animals in nature and microscopically of any differences in gross behavior, habitat selection, or external features and pigmentation.

B10b-4 PHYSIOLOGICAL BASIS OF HUMAN ELECTRIC SHOCK

THRESHOLD: William P. Moran, University of Tulsa,  
Department of Physics, Tulsa, Oklahoma

Quantitative analysis of threshold responses of humans to electric shock as a function of frequency and waveform using passive cable membrane models based on physiological data shows: (1) there are stimulus-independent frequency-independent (d.c. to 100 kHz) thresholds for detection and let-go, (2) the Falk-Fatt impedance measurements on animal muscle can be fitted by the same model, (3) the model shows that Falk and Fatt incorrectly model the seat of the electrical excitation, (4) the model identifies a cable parameter responsible for variations of the threshold over population as a resistive impedance outside the membrane, (5) the in vivo response of muscle may be related to the thresholds of the Hodgkin-Huxley theory for multiple action potentials. Deviations of the constant parameter sub-threshold cable model from the data are similar to those observed by Schwartz and by Falk and Fatt. Mechanisms of rectification, distributed time constants, and negative differential conductivity will be considered in characterizing the deviations. Applications in transmission line hazard assessment and other safety problems will be covered. Suggestions for new in vitro measurements will be given.

MEASUREMENT OF POWER DEPOSITION IN  
BIOLOGICAL TISSUES

URSI COMMISSION I (BIOLOGICAL EFFECTS)

Thursday, October 23 0830

URSI Session B-11, UMC West Ballroom

Chairman: T. Rozzell, Office of  
Naval Research

B11-1 USE OF DIELECTRIC MICROPROBES FOR ELECTROMAGNETIC  
FIELDS MEASUREMENT: A. Deficis, Microwave Department,  
O.N.E.R.A.-C.E.R.T., Toulouse Cedex, France

Since 1971, our research department has been studying dielectric probes for measuring the penetration of electromagnetic waves in not-clearly defined media. These probes call for the following technology: dielectric light conductors; a dielectric thermo-sensitive system; an electromagnetic waves absorbing coating. These devices allow measurement of power density of irradiated waves in ambient media, nearby dioptres, or even near metallic conductor areas. The techniques we are proposing permitted us to reach some quite interesting characteristics which justify their use in many fields such as: fundamental research for the study of microwave penetration in phantoms or real media; medical research for the control and dosimetry of radar radiations; industry for the study and optimisation of irradiators and microwave ovens. The probes, we realized, operate in the ambient temperatures (10 to 40°C) range and their sensitivity depends on the temperature range width of the liquid crystals used. The transducer response speed depends on its mass, i.e., on its thermal inertia. Measurement of the field must be obtained before any thermal exchanges are established with the outside medium. A previous calibration must, however, be made at each frequency. Therefore, we can say that there is a maximal sensitivity of 0.5 mW/cm<sup>2</sup> with a 10 mS response time. The transducers dimensions are small: their diameters are <500 $\mu$  (not sheathed) and <2 mm (P.T.F.E. sheathed). These characteristics are given only as guidance, but we are ourselves improving our techniques. As a consequence of the above, these probes can be used in very many fields.

B11-2 PERFORMANCE OF THE LCOF PROBE IN CALORIMETRIC AND  
TISSUE TEMPERATURE MONITORING APPLICATIONS: G.K.  
Livingston, C.C. Johnson, and C.H. Durney, University  
of Utah, Salt Lake City, Utah; and T.C. Roz-  
zell, Office of Naval Research, Arlington, Virginia

Since heat has been shown to exert an inhibitory effect on malignant tumors, hyperthermia is receiving intensive study at many biomedical research centers. Accurate determination of tissue temperature is of paramount importance in studies of this type. Where microwaves are employed to produce heat, conventional thermometric methods are unsuited because of perturbations induced by metallic components of the sensor. The metal-free design of the liquid crystal optical fiber (LCOF) temperature probe obviates this difficulty. The electronic, fiberoptic, and liquid crystal systems and their integration into a thermal-sensing device have been described elsewhere. This paper presents reflectance vs. time data obtained during a series of calorimetric and hyperthermic experiments which provides a critical evaluation of LCOF probe performance parameters such as stability, accuracy, and longevity. Experimental results have consistently shown that reflectance for the body temperature probe (32-45°C) does not remain constant over the course of one day's experiments, but drifts gradually downward, perhaps an inherent problem associated with liquid crystal fatigue. If the shift in the probe's response is monitored by periodic calibration, the accuracy can be held to 0.1°C and often less. Otherwise, the drift problem would result in errors of up to 0.25°C when only one calibration is performed per day. The drift problem is less serious in lower temperature probes. Probes of 8-10 months age are still functional and providing reliable data.

B11-3 A BIREFRINGENT CRYSTAL OPTICAL THERMOMETER FOR  
MEASUREMENTS OF ELECTROMAGNETICALLY-INDUCED HEAT-  
ING: T. C. Cetas, Division of Electronic Products,  
Bureau of Radiological Health, FDA, Rockville,  
Maryland

A thermometer has been developed which uses the optical activity of a Y-cut single crystal of  $\text{LiTaO}_3$  as the temperature-sensitive element. Polarized light propagates through the crystal in two modes, the ordinary ray and the extraordinary ray, which have indices of refraction  $n^o$  and  $n^e$ . At room temperature,  $n \approx 2.2$ ,  $B \equiv n^e - n^o = 0.004$ , and  $dB/dT = 4.4 \times 10^{-5}/^\circ\text{C}$ . The intensity of light passed through a sandwich of properly aligned

sheet polarizer, crystal, and analyzer is a function of B and hence also is temperature dependent. A thermometer probe was constructed by bonding this sandwich to a bundle of optical fibers (along with a dielectric mirror so that the sensor would be at the probe tip). Half of the fibers conduct light from a light emitting diode (LED) to the sensor tip while the other half conduct light from the sensor to a photodiode detector. The prototype uses a crystal 0.1 mm thick. A temperature range of 30°C with an 0.1°C resolution is attained. Slow drifts equivalent to 0.5°C/16 hr (i.e., 1%/16 hr in output signal) resulted for various prototypes and have been associated with photodiode and LED drifting. A model now under construction uses an optical switch to permit periodic referencing of the photodiode to the LED output. Hence component drifts will be eliminated from the calibration. Tests of the probe in air and in phantom materials while being irradiated by microwave fields of up to 1000 mW/cm<sup>2</sup> showed no direct probe heating.

B11-4 OPTICAL ETALON TEMPERATURE SENSOR FOR MICROWAVE  
TISSUE HEATING APPLICATIONS: D. A. Christensen,  
Departments of Electrical Engineering and Bio-  
engineering, University of Utah, Salt Lake City,  
Utah

For monitoring tissue temperature changes in the presence of microwave fields in bioeffects, thawing, and hyperthermia applications, we have developed a non-metallic measurement system which uses a small optical etalon as the temperature sensor connected to the display module by an optical path. This avoids the metallic connectors and associated field perturbations normally encountered with thermistor-type systems. When the temperature of the etalon (a small optical flat coated on opposite sides to form a cavity) varies, linear thermal expansion and changes in the index of refraction will cause a shift in the resonant wavelengths, thereby shifting the wavelength positions of nulls in reflectivity from the etalon. One method for tracking the amount of wavelength shift, and thus the temperature change, utilizes an external voltage-tunable Fabry-Perot interferometer whose transmitted wavelengths are locked to the etalon's reflectivity nulls by a synchronous detection technique. Theory predicts, and experiments have verified, that the d.c. tuning voltage to the interferometer is linearly proportional to the temperature variation of the sensor. We have experimen-

tally tested two etalon types with this system. The first etalon, fabricated from 0.145 mm thick crown glass, was tested from 22°C to 70°C over its extrapolated temperature range of 154°C, while the second sample, made from 3.2 mm thick fused silica, gave a range of 11.1°C. Temperature resolution was better than 0.5°C and 0.05°C, respectively, over these temperature ranges.

#### B11-5 A TEMPERATURE PROBE FOR RF HEATED MATERIAL:

R. R. Bowman, National Bureau of Standards,  
Boulder, Colorado

Measuring temperature of radio frequency (RF) heated material would be easy except that conventional thermocouples and thermistors use leads that grossly distort the internal field and also produce heat directly due to the induced currents. An effective solution to this problem is to use leads made with materials that have low conductivities. The probe described below uses leads made from carbon-loaded PTFE that has a conductivity of only 4 S/m. When small cross section leads of this material are encased within insulators to make a temperature probe, the heat produced by the probe can be less than that produced by an equal volume of material with a conductivity of 0.5 S/m (muscle tissue has a conductivity of about 1 to 2 S/m). The probe described here uses a thermistor for a temperature sensor. To minimize the errors that could result from the large and unstable lead resistances, a high-resistance thermistor is connected to two pairs of the high-resistance leads to permit a "four terminal" measurement. Several models of this type of probe are under development. For EM bioeffects research a probe has been developed with a one millimeter O.D. plastic tube, a "flake" thermistor, and plastic high-resistance leads with about 160kΩ/cm lineal resistance. Using a current injection of about 0.3 μA, the d.c. heating in the thermistor is less than 0.1 μW and the heating along the leads is less than 0.05 μW/cm. The 90% response time of the probe is about one-half second. The direct heating of the thermistor by the RF induced currents in the high-resistance leads is less than 0.01°C for a heating rate of 1°C/minute in the surrounding material. The sensitivity (0.01°C) and stability are much better than existing probes, and the relative cost should be low. Thermographic tests of the probe

in simulated tissue models will be presented to demonstrate that the probe causes only small field perturbations.

**B11-6 QUANTIFICATION AND MEASUREMENT OF INDUCED FIELDS INSIDE FINITE BIOLOGICAL BODIES:**

K. M. Chen, B. S. Guru, and D. P. Nyquist,  
Department of Electrical Engineering and Systems  
Science, Michigan State University, East Lansing,  
Michigan

When a finite biological body with heterogeneous electrical properties and an irregular geometry is exposed to an incident EM field, the induced internal EM field can be very much complicated. A tensor integral equation method is used to quantify the internal electric field induced by an incident EM field in various finite biological bodies. Numerical results on the internal electric field will be interpreted. Experimental method to measure the induced internal electric field will be described. The major difficulty in the probing of the internal field in a finite conducting body is the calibration of an implantable probe. The probe (dipole or loop type) response is proportional to the strength of electric or magnetic field at the probe location, but is also influenced by the medium parameters at the location and the geometry of the body. The later dependence arises because the internal impedance of a probe and the probe driving voltage are strongly dependent on the heterogeneity of the medium and the relative location of the probe in the body. Thus, a position dependent calibration factor for a probe is needed before one can deduce the induced internal field from the measured probe response. Experimental results on the dependence of the probe impedance upon the probe location in a volume of salt-water and the induced field distribution in the volume excited by an incident EM field will be presented.

**B11-7 EXPERIMENTAL CALIBRATION OF A MINIATURE ELECTRIC FIELD PROBE WITHIN MUSCULAR TISSUES:**

A. Y. Cheung, M. L. Swicord, and H. I. Bassen,  
University of Maryland, Institute for Fluid  
Dynamics and Applied Mathematics, College Park,  
Maryland; and Division of Electronic Products,  
Bureau of Radiological Health, FDA, Rockville,  
Maryland

A miniature ( $\ell \sim 2.5$  mm) isotropic electric field probe consisting of three non-interacting components has been successfully calibrated for near field measurements in free space. Analysis employing the transmission line theory of a buried insulated antenna was performed. For the 1 to 12 GHz frequency range for this particular probe's dimensions and geometry, the impedance modification due to probe-medium interaction is frequency dependent but is insensitive to changes in dielectric parameters of the tissue over a wide range. The coupling modification is less than an order of magnitude except when the probe is placed close to an interface (muscle-bone, muscle-fat, etc.). The above theory suggests that for deep implantation measurement, there is no ambiguity caused by changes in  $\epsilon$  and  $\tan\delta$  due to temperature rise within the sample. The probe can be used for implantation measurement from 1 to 12 GHz without design modification. The probe was experimentally calibrated inside large slabs of simulated muscle tissue with assorted dielectric properties ( $35 \leq \epsilon \leq 45$  and  $.1 \leq \tan\delta \leq .4$ ) situated in a known "plane wave" field generated within an anechoic chamber.

---

THURSDAY AFTERNOON, OCT. 23, 1330-1700

---

EM PROBING AND SUB-SURFACE PROPAGATION

URSI COMMISSION II

Thursday, October 23 1330

URSI Session II-11, UMC 159

Chairman: D.A. Hill, OT/ITS

11-1 EFFECTIVE WAVE TILT AND SURFACE IMPEDANCE OVER A LATERALLY INHOMOGENEOUS TWO LAYER EARTH: W. J. Hughes and J. R. Wait, Cooperative Institute for Research in Environmental Sciences, University of Colorado, Boulder, Colorado

Using a perturbation method, we consider the effect of a simple two-dimensional model on the electromagnetic fields at the surface of the Earth for a postulated down coming plane wave. We examine the calculated change in the surface impedance and wave tilt due to lateral inhomogeneities. It is found that the magnetic wave tilt ( $H_z/H_x$ ) is most seriously affected by such anomalies. This may have important consequences on electromagnetic probing of non-uniform portions of the earth's crust.

11-2 THEORY RELATING TO REMOTE ELECTROMAGNETIC PROBING OF A NONUNIFORM COAL SEAM: R. Jeffrey Lytle, CIRES, University of Colorado, Boulder, Colorado

The effect of lateral inhomogeneities on electromagnetic remote probing of layered structures is considered. The excitation is taken to be a plane wave incident at angle  $\theta_0$ . We determine the variation of the fields ( $E_y$ ,  $H_x$ , and  $H_z$ ), the surface admittance  $Y_s$ , and the wave tilt  $W$  with angle of incidence  $\theta_0$ , with distance from the air-coal interface, with electrical contrast, and with the layer profile (e.g., sinusoidal, step, and slant profiles). Both low frequency and high frequency cases are illustrated and compared with corresponding results with no lateral inhomogeneities. We find that the surface admittance and the fields  $E_y$  and  $H_x$  are "good" indicators of the local structure, whereas the field  $H_z$  and the wave tilt are not. However, the wave tilt is a good indication of subsurface anomalies. As the observation point is moved away from the air-coal interface, the

"information content" regarding the lateral inhomogeneities rapidly decreases. Thus measurements performed on the surface or measurements dependent upon the fields at the surface, e.g., reflection coefficients, are more sensitive to lateral inhomogeneities than measurements performed away from the surface.

11-3 IN SITU HIGH FREQUENCY DETERMINATION OF THE ELECTRICAL PROPERTIES OF ROCK: R. Jeffrey Lytle, Lawrence Livermore Laboratory, Livermore, California

Experiments were conducted to determine the in situ relative dielectric constant  $\epsilon_r$  and conductivity  $\sigma$  of hard rock with respect to propagation of high-frequency radio waves. The experiments were performed in Yosemite National Park and in the Brooks Range in northern Alaska. The experiments at Yosemite involved propagation through more than 1,000 feet of granite. The Alaskan experiments involved propagation through more than 550 feet of limestone in a permafrost state. The experiments involved the use of pulse, continuous wave, and swept frequency measurements of time of arrival, signal amplitude, phase shift, and polarization to discern the relative influence of the dominant propagation paths. The experimental data was reduced to models of varying complexity including a single homogeneous layer, and up to fourteen individually homogeneous layers. The effect of seasonal variations (for Yosemite) and temperature (for Alaska) is evident in the data. For this high frequency sampling of large volumes of rock, relative dielectric constants of 5-15 and conductivities of  $2 \times 10^{-4}$  and  $2 \times 10^{-3}$  S/m were obtained.

11-4 A REMOTE PROBING METHOD FOR DETERMINING THE THICKNESSES AND CONSTITUTIVE PROPERTIES OF PLANAR LAYERED MEDIA: R. Jeffrey Lytle, CIRES, University of Colorado, Boulder, Colorado

A technique is given for determining the thicknesses and the electrical constitutive parameters of a planar layered medium such as a coal seam in a mine environment. Time-domain experimental data are analyzed with Prony's method to determine the natural frequencies of the layered medium. Explicit relations are given (for dielectric layers) for

determining the thicknesses and dielectric constants from the experimentally determined natural frequency results. Explicit expressions are also given (for conductive layers) for calculating the electrical thickness from natural frequency results. These natural frequency results are useful when using either a pulse excitation or a swept frequency excitation. Extensions of the technique to a non-planar medium and practical implications of the method are discussed. The basic concept is also applicable in acoustical probing.

**11-5 ELECTRICAL CONDUCTIVITY STRUCTURE OF THE INTERIOR FOR A NON-SPHERICAL EARTH-MODEL:**

Janardan G. Negi, Instituto de Geociências e Instituto de Física, Federal University of Bahia, Federacão, Salvador, Bahia, Brazil and U. Raval, National Geophysical Research Institute, Hyderabad, India

Spherical-earth models have dominated the global solutions of the electromagnetic induction in the earth's interior. The relaxation of the classical geometrical condition even by small magnitudes has considerable influence in determining the electrical parameters of interior. Powerful perturbation theory is applied on well-known spherical solutions to quantitatively demonstrate the influence of deformation of spherical models.

**11-6 A TRANSIENT UNDERGROUND RADAR FOR BURIED PIPE**  
**LOCATION: Jonathan D. Young, ElectroScience**  
**Laboratory, Columbus, Ohio**

The problem of locating pipes, conduits, and drain tiles is common to municipalities, utilities, and contractors. This paper describes the development of a new device for sensing both metallic and non-metallic pipes called a transient underground radar. The three fundamental parts in a transient underground radar are a transient generator, an antenna, and a time-domain receiver-processor. The mode of operation resembles a time-domain reflectometer, except that radiated electromagnetic fields are used rather than the confined fields of a circuit. The transient generator produces a periodic ramp or step, which is radiated downward by the antenna probe. When the downward-propagating energy impinges on any region

of constitutive parameter change an echo is produced. Thus a plastic pipe ( $\epsilon$  change), a non-ferrous metal pipe ( $\sigma$  change), and a ferrous metal pipe ( $\sigma$  and  $\mu$  change) will all produce an echo. Furthermore, free-space studies have shown that the transient return of such scattering is unique with respect to object size and shape as well as material composition. Several features of the prototype implementation of this system concept are to be described. In particular, the basic antenna and processor properties to achieve adequate target illumination and good clutter discrimination are discussed. Finally, some preliminary results of field tests will be presented.

11-7 PULSE PROPAGATION BETWEEN TWO LINEAR ANTENNAS  
IN A HOMOGENEOUS ISOTROPIC LOSSY MEDIA:  
Geoffrey A. Burrell and Leon Peters, Jr.,  
ElectroScience Laboratory, Columbus, Ohio

The operation of subterranean radar systems is strongly dependent upon the characteristics of the medium and the antenna. Normally the antenna would be mounted on a ground-air interface. Determining the range of such a subterranean radar involves computing the return pulse transmission loss for a given depth for finite length antennas on the interface. The presence of the interface involves the Sommerfeld integral and would lead to excessive integration time. We have computed the transmission loss for pulse propagation between two linear finite length antennas in an infinite ground medium using the Method of Moments and the Fast Fourier Transform algorithm. The computations have been done for a wide range of pulse widths, antenna lengths, and ground parameters. The effect of the ground-air interface is then approximated by simple reflection theory. The results are summarized in a set of design curves. Physical explanations are given for the various characteristics of these design curves. The transmission loss for pulse propagation presented in the design curves is a pertinent design parameter because the frequency response of the radar is almost constant up to a certain cutoff frequency (the Low Frequency Window). Hence the design curves are good for any signal which is approximately band-limited within the Low Frequency Window. Insulated, partly insulated, and non-insulated elements have been considered.

11-8 IMPULSE RADAR SOUNDING IN PERMAFROST: A. P. Annan  
and J. L. Davis, Geological Survey of Canada,  
Ottawa, Ontario, Canada

A VHF impulse radar system operating on the ground is a viable technique for mapping the near surface geological structure and electrical properties of permafrost. A fixed antenna configuration transported over the surface yields a reconnaissance map of two-way travel times for subsurface reflectors. Wide angle reflection and refraction (WARR) sounding determines propagation velocity versus depth when performed in layered areas. To obtain a WARR sounding, one measures travel time versus antenna separation. These techniques were field tested in the Tuktoyoktuk region of the Mackenzie River delta N.W.T. Data recording was on a graphic display for initial field analysis and on analog magnetic tape for subsequent processing. Reconnaissance surveying has mapped structural features at various depths between 3 and 30 m. The electrical loss of the soils at a site limits the penetration depth. Clays and silts attenuate the radar signal more than sands and gravels. WARR soundings have determined dielectric constant versus depth in layered areas. Digital processing has permitted better interpretation and identification of features not easily visible in the graphically recorded data.

11-9 PERFORMANCE OF DIGITAL FILTERS FOR NOISY  
GEOPHYSICAL INDUCTION SIGNATURES: E. A. Quincy  
and H. C. Wu, Department of Electrical Engineering  
and Department of Geology, University of  
Wyoming, Laramie, Wyoming

The average probability-of-error for matched digital filters used to classify noisy electromagnetic induction signatures is derived and evaluated as a function of signal-to-noise ratio. Known induction responses from two geophysical models are considered. They are the conducting half-space and the horizontal thin sheet. The received data consists of one or the other model response plus additive independent Gaussian random noise. Each model response is assumed to have equally-likely occurrence. The minimum probability-of-error receiver for classifying these noisy responses is comprised of parallel digital filters with one matched to each model response. Then the outputs are summed and compared to the optimum threshold in order to decide

which model response is present. The digital filters are matched to the model responses in the frequency domain since the available model data is given in that domain. Many induction systems operate at a single frequency or at two frequencies while some systems use wideband techniques. Consequently, performance is evaluated for these three cases showing the effect of using more frequency measurements on probability of error. The analytic performance is compared to empirical performance obtained by Monte Carlo simulation of the receiver. Performance for these highly correlated models is also compared to the case of uncorrelated models.

11-10 PREDICTING THE ELECTROMAGNETIC PROPERTIES OF SOILS IN REMOTE AREAS BY THE STUDY OF THEIR CLIMATOLOGICAL AND GEOLOGICAL ENVIRONMENTS:

Louis Mittelman, Jr., and Robert A. Falls, CM/CI Department, USAMERDC, Fort Belvoir, Virginia

Over the years, there has been an increasing need by Government agencies and industry to determine the electromagnetic properties of soil textural types (sand, sandy loam, silt, silty loam, or clay) under various climatic conditions. One objective of this research would be the ability to recommend the most suitable electromagnetic underground radar for a particular climate and region. This paper intends to show that the collection of climatological data and soil textural information would help in the prediction, within reasonable limits, of the electromagnetic properties of soils on a continental or world scale. Accurate data on attenuation and permittivity for major soil textural types has been obtained under laboratory conditions. Attenuation and permittivity of soils are primarily a function of temperature, moisture, and density. The potential for forecasting the electromagnetic "climate" within the near surface of a geographical region at VHF/UHF frequencies has been demonstrated at a few locations, and its practical application depends in part on the availability and resolution of climatic and soil textural data.

REMOTE SENSING

URSI COMMISSION II

Thursday, October 23 1330

URSI Session II-12, UMC Forum Room

Chairman: E. Gossard, NOAA

12-1 PROGRESS AND PROBLEMS IN REMOTE SENSING OF ATMOSPHERIC PARTICULATES BY LIDAR: V. E. Derr, G. T. McNice, R. E. Cupp, and N. L. Abshire, National Oceanic and Atmospheric Administration, Environmental Research Laboratories, Wave Propagation Laboratory, Boulder, Colorado

Hydrometeors and lithometeors of the earth's atmosphere have important effects on radiation balance and climate. The measurement of particulate characteristics by remote sensing is a formidable problem, but is necessary to avoid expensive and unrepresentative in-situ measurement. Progress has been made in partially identifying and measuring the concentration of lithometeors by the use of multiwavelength, polarization sensitive lidar, with the aid of minimal in situ calibration. Thus lidar may be used to determine the concentration of lithometeors and their motion through diffusion and advection. Hydrometeors in clouds may be analyzed for relative ice and water concentration when multiple scatter is small. The theory will be examined and experimental results obtained with a multiwavelength polarized lidar beam will be presented. The talk will conclude with a discussion of outstanding problems.

12-2 THE POTENTIAL OF PROBING POLLUTION-PRONE PLACES BY FM-CW RADAR: R. B. Chadwick and K. P. Moran, NOAA/ERL/Wave Propagation Laboratory, Boulder, Colorado

During the winter of 1975, an FM-CW radar was operated in an upland valley in the mountains west of Denver. A variety of other sensors participated in the experiment and several joint observations of atmospheric phenomena were recorded. In addition, it was found that the FM-CW radar was a very reliable predictor of when the effluent from a small kiln would pose a pollution hazard in the valley. Results of the experiment will be discussed and implications for oil-shale development pointed out.

12-3 DIELECTRIC PROPERTIES OF SOILS AT X- AND L-BAND FREQUENCIES: J. W. Rouse, Jr., R. W. Newton, and W. R. McClellan, Texas A & M University, College Station, Texas

The remote measurement of soil moisture content with active and/or passive microwave sensors is dependent upon the complex permittivity of soils at various moisture levels. An examination of these behavior characteristics was made using a waveguide method at 3.0 cm and 21.4 cm wavelengths. Measurements of the complex permittivity of clay, clay loam, sandy clay loam, and sand were obtained for moisture levels from dry to saturated. The L-band results show a pronounced transition region in the real permittivity data as the water accumulation increases from a state of absorbed water (tightly bound water layer surrounding soil particles) to a state of relatively free water (solvate and pore water). The position of the transition region is heavily influenced by the percent clay in the soil. Dielectric measurements for moisture levels below the transition region are virtually independent of soil type. The results obtained are compared with earlier measurements and with theory.

12-4 MEASUREMENT OF DIURNAL VARIATIONS OF VEGETATION SCATTERING COEFFICIENT: Fawwaz T. Ulaby and Percy P. Batlivala, The University of Kansas Center for Research, Inc., Remote Sensing Laboratory, Lawrence, Kansas

Although diurnal variations of the scattering characteristics of plants in the optical part of the spectrum have been extensively reported in the literature, prior to the measurements presented herein, no such note had been reported at microwave frequencies. Measurements of the backscattering coefficient of densely planted fields of sorghum were conducted using a radar spectrometer mounted atop a 20 meter truck-mounted boom. Data were acquired at 8 frequencies between 2 and 8 GHz, 2 polarizations (HH and VV), and 6 incidence angles ( $0^{\circ}$  to  $50^{\circ}$  in  $10^{\circ}$  steps) at several times during the 24-hour diurnal cycle. The results indicate that off-nadir, the scattering coefficient of all fields exhibited a diurnal pattern having a peak close to dawn and a minimum around 6 p.m., and that the magnitude of this variation is most pronounced at the lowest frequency in the 2-8 GHz band with HH polarization. As an example, at a  $30^{\circ}$

angle of incidence the difference between dawn and 6 p.m. is 5.5 dB at 2.75 GHz, decreasing to less than 0.5 dB at 7.25 GHz.

12-5 COMPARISON OF SKYLAB ACTIVE AND PASSIVE  
MICROWAVE MEASUREMENTS WITH SIMPLE  
THEORETICAL MODELS: Arun Sobti, R. K. Moore,  
and F. T. Ulaby, The University of Kansas,  
Remote Sensing Laboratory, Lawrence, Kansas

The 13.9 GHz Skylab radiometer-scatterometer measured the response of ocean and land surfaces at thousands of points on the earth. These measurements at angles near vertical have been used in the geometric optics, and the exponential correlation function physical optics, models for scattering, and the plane surface model for emission, to show the type of surface parameters indicated by the models. The geometrical optics model was used to calculate the measured mean slope and dielectric constants based on returns from forest, from farmland, and from sandhills; and the computations were repeated using a version of the exponential-correlation coefficient physical optics model used by radar astronomers. Similar computations were made for the ocean and for an ensemble of all data from North America. Mean slopes between  $3.9^{\circ}$  and  $5.6^{\circ}$  were indicated for the different terrains, with rather good correspondence between results obtained using the two models. Voltage reflection coefficients ranged from 0.144 (exponential, forest) to 0.53 (ocean, both models). The low value obtained for the ocean may be in part due to saturation of the instrument on the very strong returns from vertical incidence. Oceanic brightness temperatures were compared with the theory for emission from a smooth surface with various assumptions about the sea physical temperature. The shape of the angular response is in accord with theory, but the responses are biased higher than theory predicts. This can be explained by elevation of the measured temperatures by presence of intervening clouds whose characteristics cannot be known because of lack of information.

12-6 CORRELATIONS BETWEEN MICROWAVE SCATTERING AND EMISSION FROM LAND AND SEA AT 13.9 GHz FOR VARIOUS INCIDENCE ANGLES AND POLARIZATIONS:  
Arun Sobti and Richard K. Moore, The University of Kansas, Remote Sensing Laboratory, Lawrence, Kansas

The Skylab 13.9 GHz scatterometer-radiometer was operated over a wide variety of ocean and land areas. The correlation between returns to the scatterometer at various angles and polarizations, to the radiometer at various angles and polarizations, and between radiometer and scatterometer, was obtained from the consolidated land and ocean data sets. Over the ocean a strong correlation was obtained between polarizations at all angles of incidence, except vertical where pointing errors can make a big difference. Strong correlation exists between like-polarized responses over the ocean at incidence angle between  $30^{\circ}$  and  $50^{\circ}$ , but the correlation between cross-polarized responses at these angles is weaker. The scattering return at  $15^{\circ}$  is poorly correlated with that at any other angle, with a correlation of only 0.55 even with  $30^{\circ}$ . The cross-polarized response is, however, well correlated with like-polarized response at the same angle. Over the land the correlation between responses at different angles is weaker, and a negative correlation that is significant exists between  $44^{\circ}$  and  $17^{\circ}$  responses for vertical polarization scattering. Possible consequences of these correlations are discussed for various types of application.

12-7 THE SCANNING MULTICHANNEL MICROWAVE RADIOMETER:  
F.T. Barath, California Institute of Technology,  
Jet Propulsion Laboratory, Pasadena, California

12-8 THE BACKSCATTER SPECTRUM SIGNATURE OF PERIODIC WATER WAVES OBSERVED FROM NADIR:  
David E. Weissman, Department of Engineering and Computer Sciences, Hofstra University, Hempstead, New York

The spectrum of the backscattered signal received by a nadir-aligned stationary CW microwave radar that illuminates several wind driven water waves at any instant shows discrete spectral enhancements and depressions caused by the periodic variation of the reflectivity of the surface. The water waves travel perpendicular to

the beam axis of a simple narrow beamwidth horn. Observation of the spectrum of the synchronously detected signal indicate that separated scattering areas such as wave crests and troughs which maintain some coherence during their translation across the illuminated area cause this continuous spectrum to have peaks and valleys. These can be directly related to their differences in range and relative time delays along the water wave trajectory. A single isolated moving scatterer imposes a linearly varying Doppler frequency modulation on the returning signal and is characterized by a smooth monotonic spectrum. However, the presence of two or more scatterers within the beam produce identical but delayed signals whose instantaneous frequencies are displaced and they combine at the receiver to yield a resultant signal whose fluctuating amplitude displays beats due to these frequency differentials. Measurements of the spectrum displaying this effect, obtained with a laboratory X-band radar and wind wave tank, will be presented and a theoretical interpretation will be discussed.

ELF - HF PROPAGATION

URSI COMMISSION III

Thursday, October 23 1330

URSI Session III-6, UMC 158

Chairman: D.D. Crombie, OT/ITS

6-1 THE SCREENING OF MICROPULSATION SIGNALS (1-100 mHz) BY THE ATMOSPHERE AND IONOSPHERE: W. J. Hughes, CIRES, University of Colorado/NOAA, Boulder, Colorado; and D. J. Southwood, Department of Physics, Imperial College, London, England

A study is made of the screening effect of the atmosphere and ionosphere which lets only part of a micropulsation signal (1-100 mHz) reach the ground. Using four ionospheric models, we find that the previously predicted ionospheric rotation occurs under all conditions, but that at night the ionosphere reflects much less of the incident energy, that is, it becomes a much better energy sink. We also find that the ionosphere-atmosphere system strongly attenuates signals with large cross-field wave numbers ( $k > 1/50 \text{ km}^{-1}$ ). This results in only the gross structure of magnetospheric wave fields being observed on the ground. This may explain some of the discrepancies between model calculations and observational results. It also means that we will not be able to determine the scale size of a magnetospheric resonance from earth-based observations if the scale size is much less than about 100 km at ground level.

6-2 ANALYSIS OF SPE-PRODUCED PROPAGATION DISTURBANCES:  
B. Gambill, Jr., J. D. Illgen, and R. R. Rutherford, General Electric - TEMPO, Santa Barbara, California

This paper describes the effects of a SPE (Solar Proton Event) on several VLF and LF propagation paths in terms of signal amplitude and phase. Theoretical values are compared with the observed VLF and LF values using VLF and LF propagation prediction techniques. VLF analyses include both WKB approximations (slow variation in the direction of propagation and a crude approximation of magnetic field effects) and solutions which consider magnetic field effects and mode conversion when WKB does not apply. The LF analysis included

a ray theory approximation. Electron and ion density models used in the analysis are briefly described. The VLF data was complicated by path geometry, day/night terminator relationships, and low earth conductivity (Greenland). Because of the complexities, the data provides a stressing test on VLF models. Satellite measurements are briefly illustrated to substantiate the observed effects.

6-3 NIGHTTIME PROPAGATION ANOMALIES OBSERVED AT TWO VERY LOW FREQUENCIES: F. K. Steele and A. H. Diede, U.S. Department of Commerce, Office of Telecommunications, Institute for Telecommunication Sciences, Boulder, Colorado

Recent nighttime phase and amplitude anomalies have been observed on the 10.2 and 13.6 kHz signals from Trinidad, West Indies, as received at Boulder, Colorado. The anomalies, in some cases, are comparable in size to the normal diurnal variations on these signals and occur predominantly at 13.6 kHz. These observations, when taken with independent confirming observations, suggest a localized ionospheric anomaly that may be significant to radio navigation.

6-4 RADIATION FIELDS ON THE EARTH'S SURFACE DUE TO LINE SOURCES IN THE IONOSPHERE: T. M. Chu, F. Einaudi, and J. R. Wait, CIRE, University of Colorado, Boulder, Colorado

The radiation fields of specified sources in the ionosphere are formulated. A stratified planar model is adopted for the ionosphere. An equivalent scattering matrix of an anisotropic inhomogeneous region is derived for a plane wave with an arbitrary incident angle. The plane wave spectrum representation is obtained for the primary waves in the source slab and for the fields on the earth's surface with the aid of appropriate scattering matrices. Finally, the wave fields are found by evaluating the plane wave representations. Extensive numerical results are presented. The frequency range is from 75 Hz to 10 kHz. The effects of dip angle and height of the source on the amplitude of the field are investigated. The six Cartesian field components on the earth's surface are calculated for the range from the point just below the source to ten megameters for both east-to-west and west-to-east propagation. The accuracy

of final results due to using slabs of finite thickness and a finite number of plane waves are demonstrated. Wave impedances, phase velocities, and attenuation rates are derived from the results and compared with some analytic and experimental data.

6-5 COMPARISON OF THE RATES OF CHANGE OF PHASE-PATH AND GROUP-PATH DUE TO THE MOTION OF THE OBSERVER:  
S. Silven, GTE Sylvania Incorporated, Mountain View, California

If an observer of an electromagnetic field is in motion with respect to the source of the field, he measures a frequency which differs from the source frequency. The difference is the Doppler frequency, which thereby provides a measure of a component of his velocity. This component, known as the "Doppler velocity," is equal to the rate at which the observer crosses the surfaces of constant phase-path from the source. If the medium of propagation is dispersive, this is not identical to the rate at which the observer crosses the surfaces of constant group-path. A derivation is presented of the relationship of the Doppler velocity to the time rate of change of group-path. In the geometrical-optics approximation the difference is shown to depend on orientation of the velocity vector with respect to the wave-fronts and on the dispersive effect of the medium. Based on the derived relationship, a method for possible determination of velocity components both normal and tangential to the ray path is suggested. Application is made to the case in which the observer is moving horizontally near the earth's surface, in which the propagation medium includes the ionosphere.

6-6 MEASUREMENT OF MULTIPATH PROPAGATION DELAY TIMES:  
R. L. Johnson, Southwest Research Institute,  
San Antonio, Texas

An algorithm has been developed to measure intermode propagation delay times in a multicomponent wave field. The technique exploits the effects of wave interference in somewhat the same manner as was done by Appleton and Barnett in their experiments of 1925 demonstrating the existence of downward reflections from ionospheric layers. The measurement is independent of the source modulation, and hence does not require the use of a coherent transmitter. Multiple delay time measurements can be made simultaneously since the

algorithm is not inherently constrained to two propagation modes. A mathematical model is presented which characterizes the signals received at two spatially separated antennas. The complex degree of coherence function is then computed which, in turn, provides a measurement of the intermode delay times. Results of computer simulations are given which demonstrate performance of the algorithm under two and three mode conditions. Finally, results are presented from experiments over the Ava, New York to San Antonio, Texas HF propagation path during which delay times were measured between one hop and two hop skywaves.

6-7 HORIZONTALLY POLARIZED WAVES IN IONIZED MEDIA WITH VARYING ELECTRON DENSITY AND COLLISION FREQUENCY--ENERGY CONSERVATION AND RECIPROCITY RELATIONSHIPS: E. Bahar and B. S. Agrawal, Electrical Engineering Department, The University of Nebraska, Lincoln, Nebraska

Considerable effort has been made to derive full wave solutions for the electromagnetic fields in horizontally stratified media in terms of mathematical functions tabulated in Handbooks. While they do not provide solutions to the general problem in which the complex permittivity of the media is assumed to vary arbitrarily, they provide an important basis for the analysis of electromagnetic waves in inhomogeneous media. Thus using the Green's function technique, for instance, the solutions are formulated in terms of integral equations involving comparison functions that are chosen from the list of permittivity profiles for which closed form analytical solutions are known.

The method employed in this paper to compute horizontally polarized electromagnetic fields in an ionized media with varying electron density and collision frequency profiles is based on the conversion of Maxwell's equations into a set of loosely coupled first order differential equations for the wave amplitudes. Special attention is given to permittivity profiles with critical coupling regions where the familiar WKB approach fails.

The reflection and transmission coefficients and the characteristic surface impedance for a horizontally stratified layer of finite thickness is computed as a function of the transverse wave number and excitations of both propagating and evanescent waves are considered.

The reciprocity and realizability relationships are formulated and the numerical results are in agreement up to at least four significant figures. The computed values for the reflection and transmission coefficients and the characteristic surface impedance are also shown to be in good agreement with those derived from closed form analytical solutions for special permittivity profiles.

6-8 A COMPARATIVE STUDY OF MEDIUM-FREQUENCY  
SKYWAVE FIELD STRENGTH PREDICTION METHODS:  
John C. H. Wang, Federal Communications  
Commission, Washington, D.C.

Recently CCIR stressed the needs for continued study on nighttime medium-frequency propagation curves and formulas for worldwide applications. Several prediction methods such as the FCC method, European Broadcasting Union method, and the new USSR method have been documented by CCIR. FCC has taken extensive field strength measurements in 26 propagation paths. Altogether 261 path-years of data covering a full sunspot cycle were released in 1971. Recently FCC engineers have applied different CCIR prediction methods to these propagation paths. This paper presents the results of these calculations. Calculated and measured field strengths will be compared and analyzed. Possible refinements of existing methods for U.S. application will be discussed.

FEASIBILITY OF SCATTER RADARS ON THE SPACE SHUTTLE - II

URSI COMMISSIONS IV AND III

Thursday, October 23 1330

URSI Session IV-6, UMC 157

Chairman: F.S. Mozer,

University of California

6-1 MAPPING AURORAL ELECTRIC FIELDS FROM THE SPACE SHUTTLE WITH HF RADAR: F. W. Perkins, Princeton University, Princeton, New Jersey and G. D. Thome, Raytheon Company, Sudbury, Massachusetts

In this paper we suggest an experiment in which a coherent HF radar on board the Space Shuttle is used both for mapping the auroral field and for studying the spectrum of the "turbulent" field-aligned density striations found in the auroral ionosphere. These density irregularities present large scattering cross sections to HF radars when viewed normal to the earth's magnetic field. At F-region altitudes we expect these irregularities to move with the local  $E \times B$  velocity and therefore we expect that the Doppler shift of the HF returns from a scattering volume at this altitude will be a measure of the local electric field. The geometry of the situation is such that ground based radars can look normal to the earth's field over only a very limited portion of the auroral F-region. By putting the radar in space the geometrical constraints are greatly reduced and as the spacecraft moves it should be possible to produce for each orbit a "snapshot" of the electric field distribution over much of the polar F-region. In contrast to conventional topside sounders, an HF radar for auroral mapping must be coherent and must be able to resolve returns in angle of arrival. Power requirements are higher and frequency flexibility, though desirable, is not essential. A representative monostatic radar on board the Space Shuttle would operate at 30 MHz, would have a two-dimensional phased array antenna 100 meters on a side, and would require a kilowatt of average power. Alternately, a bistatic configuration could be used in which the transmitter and a small non-directive antenna would be on board the Space Shuttle and the phased array receiving antenna would be on the ground. This would eliminate the need for a large antenna in space, but would complicate the operation and analysis of the experiment.

## URSI Session IV-6

6-2 COMPUTER SIMULATION OF THE IONOSPHERIC EXPERIMENT OF THE APOLLO-SOYUZ TEST PROJECT (ASTP): Mario D. Grossi and Ray H. Gay, Smithsonian Astrophysical Observatory, Cambridge, Massachusetts

A computer simulation has been performed of the ionospheric experiment of the Apollo-Soyuz Test Project (ASTP). ASTP is the first example of USA/USSR cooperation in space and is scheduled for Summer, 1975. The experiment consists in performing dual-frequency Doppler measurements (at 162 and 324 MHz) between the Apollo Command Service Module (CSM) and the ASTP Docking Module (DM), both orbiting at 221 Km height and at a relative distance of 300 Km. A network of ground stations will also operate and will collect differential and rotating Doppler data in DM-to-ground radio paths. The computer simulation has shown that, with the Doppler measurement resolution of approximately 3 millihertz provided by the instrumentation (in 10 seconds integration time), ionospheric-induced Doppler Shifts will be measurable accurately at all times, with some rare exceptions occurring when the radio path crosses regions of minimum ionospheric density. The computer simulation has evaluated the ability of the experiment of measuring changes of columnar electron content between CSM and DM (from which horizontal gradients of electron density at 221 Km height can be obtained) and of measuring variations in DM-to-ground columnar content (from which an averaged columnar content and the electron density at the DM can be deduced under some simplifying assumptions). The simulation has confirmed the expectation that simultaneous measurements of horizontal gradients and space-to-ground columnar content substantially increase the accuracy of data inversion.

6-3 THE INVERSION OF DIFFERENTIAL AND ROTATING DOPPLER DATA COLLECTED BY THE IONOSPHERIC EXPERIMENT OF THE APOLLO-SOYUZ TEST PROJECT (ASTP): Ray H. Gay and Mario D. Grossi, Smithsonian Astrophysical Observatory, Cambridge, Massachusetts

The preparation of the analytical approach and of the related software to be used in the inversion of the differential and rotating Doppler data that the ionospheric experiment of the Apollo-Soyuz Test Project

(ASTP) will collect has been recently completed. These data will be collected in space-to-space paths (between the ASTP Docking Module and the Apollo Command Service Module that will orbit both at a height of 221 Km, at a relative distance of 300 Km) and in space-to-ground paths (between the Docking Module and ground). The Doppler links will operate at 162 and 324 MHz and will have an accuracy better than 3 millihertz over 10 seconds integration time. The ASTP Mission is scheduled for Summer, 1975. While waiting for the actual experiment data, the inversion approach has been tested with the "dummy" data obtained with a computer simulation. We found that a measurement accuracy of 1 to 10% in the value of the horizontal electron density gradient at 221 Km altitude can be achieved, in space-to-space paths. For space-to-ground paths near the orbital plane, we have identified and compensated for, possible effects of the horizontal gradients on the received differential Doppler shifts. In the two cases that we have considered, it was possible to reduce the gradient-associated errors in the inversion that leads to the columnar electron content by approximately one-half. Accuracies of 5 to 10% in columnar electron content are achievable with this gradient-compensation technique.

6-4 THE APPLICATION OF GROUND-BASED DIGITAL IONOSONDE CONCEPTS TO EXPERIMENTS ABOARD THE SPACE SHUTTLE: J. W. Wright and R. N. Grubb, NOAA/ERL, Space Environment Laboratory, Boulder, Colorado

The design concepts for a modern research ionosonde involve programmable (minicomputer) control over all aspects of user interaction, system function and monitoring, scheduling, data acquisition, data processing, display and retention. From an RF transmission standpoint, these system concepts include active pulse and CW capabilities throughout the 0.1-30 MHz range at substantial radiated power levels. They include a wide variety of signal reception and processing capabilities for echo recognition and parameter digitization (in active sounding modes) and for passive observations of natural and externally generated signals. High time, frequency, and parameter resolution is maintained throughout. We believe that these concepts correspond almost identically to those desirable within the shuttle for a general-purpose HF ionospheric and plasma research facility.

This paper describes our ground-based hardware prototypes in further detail and illustrates some relevant software in action.

6-5 TRANSMITTER POWER REQUIREMENTS FOR SPACE SHUTTLE SCATTER RADAR EXPERIMENTS: Kenneth J. Harker, Institute for Plasma Research, Stanford University, Stanford, California

A study has been made of the transmitter power requirements for scatter radars on the Space Shuttle for three different types of experiments: (1) measurement of the ionic component of the incoherent scatter spectrum; (2) measurement of the plasma line enhanced by natural processes such as energetic photoelectrons; and (3) measurement of the spectrum of the plasma line artificially enhanced by ionospheric modification with high-power HF radio waves. Our study consisted of calculating the power required for the radar transmitter to produce a backscattered signal equal to the system noise level for a sequence of ranges between 1 and 200 km. In the case of the modification experiment, calculations were also made of the HF transmitter power required to produce a power flux at the reflection point equal to twice that required for exciting the parametric decay instabilities. Results of these calculations and conclusions regarding the feasibility of the experiments will be presented.

SOLAR AND PLANETARY OBSERVATIONS - II

URSI COMMISSION V

Thursday, October 23 1330

URSI Session V-7, UMC 156

Chairman: J. Broderick,

VPI and SU

7-1 ELIMINATION OF MULTIPATH EFFECTS DURING PLANETARY OCCULTATIONS: Thomas A. Croft, Stanford University, Stanford, California

During a planetary radio occultation, a spacecraft may encounter one or more regions of multipath propagation. The associated receivers make use of phase-lock techniques which discriminate against the weaker modes; either the strongest mode controls the receiver or else the mode mixture leads to a result which is useless for occultation study. For downlink signals, (i.e., from the spacecraft to earth) this problem has been overcome through wide-band predetection recording followed by elaborate variable-band Fourier analysis in digital computers. This has permitted the tracking of multiple-frequency loci as evidenced by multi-peaked spectra. So far no investigator has succeeded in extracting amplitude measurements from a multipath occultation of sufficient quality to permit derivation of planetary parameters. No method for extraction of either frequency or amplitude has heretofore been found for uplink multipath. Here it is shown that a dispersive delay can be applied to the signal-plus-noise before detection or other processing, with the result that multipath is eliminated. This benefit is based upon the geometric observation that only one propagation mode exists for any one height of ray asymptote; the added dispersion has the effect of changing the time axis into an asymptote-height axis. Since the dispersive delay is added before any signal processing or detection, this approach may permit phase-lock receivers to track all the strong and weak signals. This removes the main barrier which has prevented the complete reception of multipath occultations by phase-lock receivers, with the result that spacecraft may be able to perform this task. Such an added capability would make uplink occultations practical, and it would also make outer planet relay radio links better able to serve the needs of occultation science.

7-2 LOW FREQUENCY RADIO EMISSION FROM THE OUTER  
PLANETS: Larry W. Brown, Goddard Space Flight  
Center, Greenbelt, Maryland

Low frequency radio emission from Jupiter, Saturn, and possibly Uranus have been observed by the IMP-6 space-craft. These emissions were identified through a direction-finding analysis of the phase of the observed modulated signal detected from the spinning dipole antenna. The data covered a period of 500 days from April 1971 to October 1972. Over 300 Jovian events were observed at 25 frequencies between 425 and 9900 kHz. The spectrum shows a primary flux peak at 8 MHz and a secondary peak at 1 MHz. Correlation with System III longitude shows a similarity between frequencies near the primary peak and the lowest frequencies of earth-based observations. Near the secondary peak other sources play a larger role. Correlations with satellites Io and Europa appear weak. The first Saturn bursts were similarly identified at 15 frequencies between 375 and 2200 kHz. About 24 Saturnian events were observed with a peak flux near 1 MHz. The RAE-2 spacecraft in lunar orbit has confirmed this observation through the detection of bursts using occultations of Saturn by the Moon. The IMP-6 data has been analyzed for possible emission from Uranus. The angular separation of Uranus and the Earth is small, but 4-7 possible Uranus events have been observed at times of greatest apparent separation. These are unique in spectral behavior, peaking at 475 kHz and observable only at 4 frequencies between 375 and 600 kHz.

7-3 PRELIMINARY RESULTS FROM ARECIBO RADAR  
OBSERVATIONS OF CANDIDATE VIKING C-SITE  
LANDING AREAS ON MARS: R. A. Simpson and  
G. L. Tyler, Center for Radar Astronomy,  
Stanford, California; D. B. Campbell, Arecibo  
Observatory, Arecibo, Puerto Rico;  
G. H. Pettengill, Department of Earth and  
Planetary Sciences, MIT, Cambridge, Massachusetts

Preliminary results from Mars observations taken with the new S-Band system at Arecibo will be presented. These were obtained during August-September 1975 and cover latitudes of 0-12°S. Areas proposed as Viking lander C-Sites will be emphasized. The 1975 S-Band data will be compared with those obtained during the last opposition at Haystack (3.8 cm), Goldstone (12.5 cm; vid Downs, et al., Icarus, in press), and

Arecibo (70 cm) observatories. Analysis in 1973 showed: (1) Mars surface is very heterogeneous, (2) radar scattering is essentially independent of wavelength, (3) radar behavior is only poorly correlated with photography, (4) rms surface slopes range from  $0.5^{\circ}$  to  $3^{\circ}$ , and (5) dielectric constant varies from 1.7 to 3.5.

7-4 MARTIAN TOPOGRAPHY DETERMINED BY RADAR DURING THE 1971 AND 1973 OPPOSITIONS: P. E. Reichley and G. S. Downs, Jet Propulsion Laboratory, California Institute of Technology, Pasadena, California

The Goldstone radar system was used at a wavelength of 12.6 cm to probe the Martian surface during the 1971 and 1973 oppositions. The surface probed by the radar lay between  $-14^{\circ}$  and  $-22^{\circ}$  latitude. Surface cells isolated by the radar system were 9 Km E-W by 110 Km N-S. Altitudes were calculated from signal time-delays measured relative to a triaxial ellipsoid. The altitudes from both oppositions were combined into a self consistent set and interpolated to form a uniform grid. Contours of constant altitude were calculated at 200 m intervals. The altitudes are presented as maps of grey shades, where each grey shade represents a different altitude. The contours are presented in conjunction with Mars charts derived from Mariner 9 television pictures.

7-5 IMPROVED SURFACE SLOPE PROBABILITIES FROM RADAR DATA: B. J. Lipa and G. L. Tyler, Center for Radar Astronomy, Stanford University, Stanford, California

We describe an improved method of deriving surface slope probabilities from radar frequency spectra. The original method involves the inversion of a linear integral equation. When the data contain noise, the solution for the slope probability as a function of tilt is often poor in the sense that it oscillates, whereas it is believed that it should be smooth. We have included this requirement in the mathematical constraints on the solution and applied the method to radar data from Mars, resulting in slope probabilities which have significantly less scatter than the unconstrained solution. These were fitted with Gaussian and Hagfors laws and the latter found to give the best fit. Because of the theoretical inconsistencies of the Hagfors law due to the assumption of a

non-analytic autocorrelation function, we derive an alternative description of slope probabilities assuming that a filtered version of the surface with a parabolic autocorrelation function interacts with the radar wave. We show that the resulting modified Gaussian law gives an improved fit to the Mars slope probabilities. The analytic technique developed can also be used to predict variations in slope probability density with wavelength.

7-6 NEW RADAR ASTRONOMICAL OBSERVATIONS OF PLANET EARTH AT 13.9 GHz: Nura Itbos, Drahcir Eroom, and Sasnak Ytisrevinu, Remote Sensing Laboratory, The University of Kansas, Lawrence, Kansas

Martian radar astronomers have recently had an unusual opportunity to observe Planet Earth from the Balyks spacecraft placed in orbit of about  $50^{\circ}$  inclination around the distant planet. The radar device used an ICW modulation at 13.9 GHz with a beamwidth (effective) of about  $1.5^{\circ}$  from a height of 435 km. With this instrument measurements were possible at near-vertical incidence from relatively small areas on the planet, so it was possible to distinguish different areas on the planet and use the techniques of radar astronomy heretofore reserved for observations of large parts of the planetary disc. The large blue areas we know as maria were found to have a mean slope of  $4.2^{\circ}$  to  $4.33^{\circ}$ , depending on the model used, and they have a dielectric constant of over 10, indicating the presence of some material not found in quantity on Mars. Because of possible saturation of the instrument, the mare may in fact have even larger dielect constants. The large brown and green areas embedded in the maria seem to have the same roughness as the maria, at least as observed at this short wavelength, but their dielectric constant is much smaller, on the order of 2, indicating the presence of relatively dry soil or rocks. Slopes for different parts of these areas differ more than their dielectric constants. The theory was applied to near-vertical measurements, but it is interesting to note that the returns from the maria drop much more rapidly beyond  $10^{\circ}$  than do those from the brown and green continents. Clearly, use of other frequencies or finer resolutions or both are called for to better define the planetary surface.

WIRE ANTENNAS

URSI COMMISSION VI

Thursday, October 23 1330

URSI Session VI-12, Radio Building Auditorium

Chairman: Chen-To Tai,

University of Michigan

12-1 SUBSURFACE COMMUNICATION BETWEEN DIPOLES IN  
GENERAL MEDIA: DESCRIPTION AND INTERPRETATION  
OF RESULTS: R. W. P. King and B. Sandler,  
Gordon McKay Laboratory, Harvard University,  
Cambridge, Massachusetts

In his book, Dipole Radiation in the Presence of a Conducting Half-Space, Baños provides a detailed analytical study of the problem of communicating between two points in the ocean by means of electric and magnetic dipoles. His general formulas involve complex integrals which are reduced to simple expressions in certain special cases. These correspond to limited ranges of the parameters. A numerical study of the general case for antennas in sea water was made by Siegel and King and compared with Baños' special cases. This numerical approach has now been generalized to apply to other than conducting half-spaces. The three cylindrical components of the electric field maintained by a horizontal electric dipole in sea water, lake water, and earth have been computed and compared as functions of the distance between the source and the receiver. The frequency is one parameter over a wide range that includes lake water ( $\sigma_e = 0.004 \text{ S/m}$ ,  $\epsilon_{er} = 80$ ) as a good conductor at the low frequencies and as a good dielectric at the high frequencies. The applicability of Baños' special formulas to limited ranges is considered. The fields in all three media are interpreted in terms of direct and lateral-wave transmission.

12-2 COUPLED INSULATED ANTENNAS IN A RELATIVELY DENSE MEDIUM: CURRENTS AND ADMITTANCES: R. W. P. King and T. T. Wu, Gordon McKay Laboratory, Harvard University, Cambridge, Massachusetts; and L. C. Shen, Department of Electrical Engineering, University of Houston, Houston, Texas

The analysis of the insulated dipole in a relatively dense medium is extended to coupled, individually insulated elements arranged in a circular array. It is

shown that the transmission-line-like distributions of current are preserved for each phase sequence but with different complex wave numbers that depend not only on the electrical properties of the insulating and ambient media but also on the coupling among the elements. The complex wave numbers, the input admittances, and the current distributions have been calculated and presented in graphical form for a two-element array with symmetrical and antisymmetrical excitations. The parameters chosen in the example correspond approximately to a two-element array insulated by an air column immersed in fresh lake water at 300 MHz.

12-3 THE TERMINATED INSULATED ANTENNA: Kuan-Min Lee and Ronald W. P. King, Gordon McKay Laboratory, Harvard University, Cambridge, Massachusetts

The center-driven insulated antenna end-loaded with a bare quarter-wave section has been investigated theoretically and experimentally. This antenna has been analyzed in terms of the theory of the bare antenna and that of the completely insulated antenna in a relatively dense ambient medium. A simple transmission-line-like solution is obtained. Input admittances computed from the theoretical formula have been shown to agree well with measured results with air-insulated monopoles in both salt water and fresh water. Three different thicknesses of insulation and various lengths were used in the experiment. For a short antenna, the magnitude of the current distributions for a terminated insulated antenna is quite constant, whereas that of the completely insulated antenna has a triangular distribution. This would give a better directivity as far as the field pattern is concerned. By adjusting the radius of the insulation, it is possible to match the characteristic impedance of the insulated antenna to the apparent input admittance of the monopole antenna to obtain a nearly pure traveling wave even for a longer insulated antenna.

12-4 RADIATION CHARACTERISTICS OF STEPPED-DIPOLE ANTENNAS: T. C. K. Rao and M. A. K. Hamid, Department of Electrical Engineering, University of Manitoba, Winnipeg, Manitoba, Canada

The radiation characteristics of a dipole antenna can be significantly improved by varying the diameter along

the length of the radiating cylindrical surface away from the generator. Earlier experimental work on a symmetrical dipole antenna with two symmetrical steps on each arm and analysis using Schelkanoff's concept of average characteristic impedance by Hamid, et al., confirmed the increase in antenna bandwidth and better matching with the feed line. Due to the various reflections at the step-junctions, the resulting current distribution is primarily dictated by the electrical length and diameter of each section. To determine the current distribution, the radiated electric field and the input impedance, the problem is formulated by the boundary value method and later reduced to an integral equation of the Wiener-Hopf type which is solved asymptotically by the method suggested by Hurd for a long uniform antenna. The results for the input impedance, which are also confirmed by numerical solution using the method of moments, are shown graphically to establish the advantages of the multi-stepped dipole. The final objective is to optimize the antenna bandwidth by Rosenbrock's method leading to an optimum design of the electrical length and diameter of each section and to compare with the analogous design of a stepped circular waveguide transformer.

12-5 RADIATION FROM A COAXIAL APERTURE INTO A LOSSY HALF-SPACE: Chalmers M. Butler and Robert D. Nevels, University of Mississippi, University, Mississippi

The results of an investigation are presented for the problem of a coaxial waveguide terminating in a ground screen and radiating into an infinite homogeneous half-space of arbitrary electrical characteristics. The waveguide is excited by a TEM incident wave, and the ground plane is both perfectly conducting and infinite in extent. An integral equation is formulated for the unknown electric field in the aperture, which fully accounts for the higher-order modes in the coaxial guide as well as the coupling between the lossy half-space and the coax. This integral equation is solved numerically and results are presented for various cases of interest. For selected cases, measured input impedance and reflection coefficient in the waveguide are compared with calculated results.

12-6 PROPERTIES OF THE HORIZONTAL WIRE ANTENNA OVER  
 AN IMPERFECT CONDUCTOR WITH SPECIAL APPLICATION  
 TO THE BEVERAGE WAVE ANTENNA: Robert M. Sorbello,  
 Gordon McKay Laboratory, Harvard University,  
 Cambridge, Massachusetts

An experimental investigation of the properties of horizontal wires over an imperfect conductor, including the special case of the Beverage antenna, has been undertaken. Distributions of current and charge as well as input impedance have been measured with antennas that are  $.5\lambda$  to  $1.5\lambda$  in length and are placed at heights ranging from  $.01\lambda$  to  $.25\lambda$  above a variety of media including moist earth, fresh water, and salt water. The effects of the wire height and the different media on the antenna wave number will be discussed along with the observed transmission-line-like distributions of current and charge. Comparisons will be made between measured distributions and the results of a theory recently developed by King, Shen, and Wu. This theory will be extended to include the case of the Beverage antenna, and a comparison with measured results will be presented. Owing to its transmission-line-like characteristics, a novel way of loading the Beverage antenna has been investigated which avoids making physical contact with the medium below the antenna. This method of loading provides a good matched condition, and traveling-wave current distributions have been shown, experimentally, to exist on the wire.

12-7 TRUNCATION OF INFINITE SHEATH SPIRAL ANTENNAS:  
 B.R. Cheo, Polytechnic Institute of New York, Farmingdale, New York

Two solutions of Maxwell's equations on the infinite sheath spiral antennas were published a few years ago. One solution (Cheo, et al., AP 9, 527; '61) corresponds to an excitation of the structure at the center (CE). The second solution (Laxpati and Mittra, Proc. IEE; 114, 3, 352; '67) corresponds to an excitation by a ring of voltage generators (RE) connected in series with the spiral wires  $\rho = K \exp(-a\phi)$  at a radius  $\rho$  from the center. The RE solution, though only given formally in a double integral, revealed a branch singularity, leading to a surface wave. This led to the discovery (Cheo and Rusmey, Rad. Sc., 3, 3, 267; '68) that for the CE solution the input power goes almost entirely to the surface wave when the azimuthal variation of the solution takes the form of  $\exp(-jn\phi)$  ( $n > 0$ ). Since a push-pull type of excitation consists of both  $\exp(\pm jn\phi)$  modes,

the surface wave would cause a gross perturbation when the structure is truncated. This problem is the concern of this paper. We shall consider the case of tightly wound spirals, for which the surface wave is tightly bounded to the structure, and strong reflection would occur when the structure is truncated. We consider that the reflected wave is mainly due to a source distribution at the edge. For this the RE solution is explored in detail. We show that the RE solution approaches the CE solution in the limit  $\rho \rightarrow 0$ , and that the RE solution is uniquely determined only when the termination at the center is specified. We show that by superimposing the CE and RE solutions one can gain the insight of the problem caused by truncation and that the radiation is mainly due to the reflected wave.

#### 12-8 BACKFIRE ZIGZAG ANTENNAS WITH MODULATED PITCH:

Roger Forse and Paul E. Mayes, Electrical Engineering Department, University of Illinois, Urbana, Illinois

A simple nonresonant antenna can be devised using two zig-zag conductors. It was previously shown by Mayes that balanced periodic zigzag antennas will operate in a backfire mode. The antenna current decays with distance from the feedpoint. The rate of decay depends primarily upon the pitch angle and conductor radius being small for large pitch and/or small conductors. Since it is relatively easy to vary the pitch as a function of displacement along the antenna axis, a feasible means of controlling the antenna current distribution results. Achieving high front-to-back ratio depends upon the current being negligibly small at the end opposite the feedpoint. Low sidelobes result when the current decreases in an almost exponential manner. However, for a narrow beam there must be appreciable current over the entire antenna. A computer analysis of bifilar zigzag antennas illustrates some ways in which the current distribution can be controlled to achieve given desired results. Experimental results are presented which show agreement with the computations.

GENERAL BIOLOGICAL EFFECTS  
URSI COMMISSION I (BIOLOGICAL EFFECTS)

Thursday, October 23 1330

URSI Session B-12, UMC East Ballroom

Chairman: S. Michaelson,  
University of Rochester

B12-1 THE EFFECTS OF ENVIRONMENTAL TEMPERATURE ON  
THERMOREGULATORY, SERUM LIPID, CARBOHYDRATE, AND  
GROWTH HORMONE RESPONSES OF RATS EXPOSED TO  
MICROWAVES: William M. Houk, S. M. Michaelson,  
and D. E. Beischer, Naval Aerospace Medical  
Research Laboratory, Pensacola, Florida, and  
University of Rochester, Rochester, New York

Long Evans rats were exposed to 2450 MHz (cw) horizontally polarized microwave radiation at room temperature ( $22.5^{\circ}\text{ C}$ ), at low ( $17.5^{\circ}\text{ C}$ ) as well as higher ( $27.5^{\circ}\text{ C}$ ) environmental temperature. Three different exposure intensities (10.2, 19.6, and  $30.5\text{ mW/cm}^2$ ) ( $\pm 0.8\text{ dB}$ ) were used in a  $1.8 \times 1.8 \times 1.8\text{ m}$  semi-enclosed anechoic environmental control chamber. Sets of four animals were exposed simultaneously to a selected temperature and radiation environment for 150 minutes with a 60-minute post-exposure period following. After exposure the animals were weighed, decapitated, exsanguinated, and colonic temperature measured within 90 seconds after death. This procedure with sets of four animals was repeated with the animal sacrificed at different times during the exposure period. None of the sham-exposed rats demonstrated significant colon temperature alterations in the normal low or high temperature environments. In rats exposed at room temperature to  $10.2\text{ mW/cm}^2$ , there were no differences in colon temperatures compared to the sham-illuminated group. The 19.6 and  $30.5\text{ mW/cm}^2$  exposure groups were observed to have from  $0.7$  to  $1.0^{\circ}\text{ C}$  colon temperature increases in the normal environment. Cooling the room negated the colonic temperature increase in the  $19.6\text{ mW/cm}^2$  exposed group, and suppressed the increase in the  $30.5\text{ mW/cm}^2$  group. Heating the room caused all colon temperature responses seen in all three microwave-exposed animal groups to rise incrementally ( $0.3$ ,  $0.8$ , and  $2.4^{\circ}\text{ C}$ ), with an obvious generalized stress response observed in the  $30.5\text{ mW/cm}^2$  irradiated group. The complex serum parameter interrelationships which correlate with the environmental temperature alterations and the microwave exposures will also be presented.

B12-2 THE EFFECTS OF 19 MEGACYCLE IRRADIATION ON MICE AND RATS: W. B. Stavinotha, M. A. Medina, S. T. Weintraub, D. H. Ross, and A. T. Modak, University of Texas Health Science Center at San Antonio, San Antonio, Texas

Mice and rats were exposed to irradiation of 19 megacycles with a magnetic field of 55 amperes per meter and an electric field of 8000 volts per meter in a "near field synthesizer." After exposure of mice for 40 minutes per day for 5 days a substantially higher death rate was seen in both the irradiated and thermally heated male mice as compared to similarly treated female mice and male control mice. The irradiation and thermal treatments produced an average rise in rectal temperature of approximately 1°C. After irradiation, 28% of the male mice died while only 5% of the female mice died. Thermal exposure produced a death rate of 21% in male mice and 3% in female mice. After one exposure of rats for 40 minutes the average rise in rectal temperature was approximately 1°C. No lethality was observed in either irradiated or thermally heated animals. In rats no remarkable changes were seen in the levels of acetylcholine or catecholamines after RF or thermal exposure. Significant changes were seen, however, in the concentrations of several cations in the brain after exposure. Most notably, the concentration of zinc in the cerebral cortex increased from 0.28  $\mu$ mole/mg to 0.53  $\mu$ mole/mg after irradiation.

B12-3 LONG TERM EXPOSURE STUDIES OF HIGH PEAK POWER (HPP) PULSED ELECTROMAGNETIC RADIATION ON MICE: T. C. O'Grady and Z. R. Glaser, Biomedical Research Laboratory, Naval Surface Weapons Center, Dahlgren, Virginia

Three separate groups of mice were exposed to HPP pulsed radiation over a 6-month period, 1 hour per day, 5 days per week as follows: Group I, exposed from birth to 180 days total exposure, consisting of 59 experimental animals and 29 control animals; Group II, exposed from birth to 180 days also, consisting of 77 experimental animals and 22 controls; Group III, exposed from birth to 60 days of age. At 20-day intervals in Groups I and II (every other day or biweekly in Group III) 6 experimental animals and 3 control animals were sacrificed and analyzed for a variety of biological parameters. These parameters included clinical blood chemistries

(hematocrit, white blood cell count, platelet count, differential counts), serum electrophoresis, liver, heart and skeletal muscle enzyme activities, and gross morphologies. The exposures were made between the plates of a HPP pulser operating at  $\sim$ 27 MHz with a field strength of  $\sim$ 100 kv/m, pulse duration  $\sim$ 200 nsecs, and a repetition rate of 20 pps. The presence of changes in any of the biological parameters mentioned above would be indicative of a stress effect due to the effects of the radiation.

**B12-4 INVESTIGATION OF ELECTROMAGNETIC EFFECTS OF A 1000 FT. TV TOWER ON MIGRATORY BIRDS: D. G. Burks and E. R. Graf, Electrical Engineering Department, Auburn University, Auburn, Alabama**

A high incidence of bird collisions at a 1000 ft. TV tower north of Tallahassee, Florida, has motivated a study of possible electromagnetic effects in bird navigation. Data collected over a 19-year period (1956 to present) concerning daily bird kills, number of birds, species, and position found formed the basis of a correlation study to determine factors responsible for high bird kills. Evidence indicates that bird navigation is a complicated process involving the integration of many sensory inputs including sight, pressure, smell, and magnetic field. Of special interest in our study were bird responses to (1) TV radiation from the tower, (2) disturbances of natural magnetic and electric fields, and (3) lights of the tower. Interference with the bird's navigation process that results in an attraction to the tower is responsible for bird kills not resulting in random incidence. A discussion of the electromagnetic environment of the tower and theories of bird navigation as pertains to this problem will be presented.

**B12-5 SOME DEVELOPMENTAL AND BEHAVIORAL FACTORS OF LOW INTENSITY X-BAND RADIATION: C. W. Kindt, D. M. Bowden, F. A. Spelman, and M. K. Morgan, Regional Primate Research at the University of Washington, Seattle, Washington**

Four pregnant Sprague Dawley rats were exposed to low intensity X-band radiation for the duration of pregnancy (21 days). The offspring were further exposed at the same level for an additional 28 days. Appropriate controls were done. Several developmental, behavioral, and physiological determinations were performed on the

offspring and the mothers. The determinations included weight gain, righting, exploratory behavior, eye opening, ear flap development, internal and external anatomic malformations, tooth eruption, corticosteroid levels and adrenal weight, and maturation of reproductive systems. The rats were used in an attempt to determine possible toxic effects of this type of low level radiation on the developing organism. This experiment precedes the use of infant monkeys in a remote respiration monitoring system using X-band radar.

**B12-6 THE BIOLOGICAL SIGNIFICANCE OF RADIOFREQUENCY RADIATION EMISSION CHARACTERISTICS ON CARDIAC PACEMAKER PERFORMANCE:** John C. Mitchell and William D. Hurt, USAF School of Aerospace Medicine, Radiobiology Division, Brooks AFB, San Antonio, Texas

The effect of radiofrequency (RF) radiation emission on cardiac pacemaker function is a unique bioeffects phenomena. Dependent on the pacemaker type and design, and on the frequency, peak E-field intensity, pulse width, and effective pulse repetition rate of the incident RF signal, the pacemaker may cut off completely, revert to a fixed interference rejection mode of operation, experience intermittent disruption, or be totally unaffected. Experimental evidence is presented for a wide variety of tests conducted under controlled laboratory conditions and in the vicinity of numerous types of RF emitters prevalent in U.S. population centers. These test results are discussed in terms of their clinical significance, technical feasibility of designing pacemakers to avoid electromagnetic interference, and appropriate design goals to achieve overall RF environmental compatibility.

**B12-7 BROADCAST RADIATION: A SECOND LOOK:** R. A. Tell and D. E. Janes, EPA, Washington, D.C.

As part of its program to determine the health and environmental effects of exposure to nonionizing radiation, the Environmental Protection Agency is gathering and analyzing information on sources which produce radiation levels in the environment. The question of broadcast stations as environmental sources of nonionizing radiation exposure has been previously addressed by the authors. This paper extends the results of the previous work. This

investigation is developed around vertical radiation patterns and data supplied by the FCC on the heights of transmitting antennas above ground and above supporting structures such as building roofs. In particular, power densities at roof and ground level are calculated for areas very near FM broadcast installations using recent information on steep depression angle radiation from commonly used FM transmitting antennas. Associated field measurement data are also discussed and the overall implications of this analysis are examined in terms of present RF exposure standards and philosophy.

B12-8 HEALTH HAZARDS IN MICROWAVE FIELDS: K. D. Woolas,  
Medical Officer, MOD, United Kingdom

Few papers are contributed by occupational health physicians having medical care of microwave workers. This is remarkable as their work in preventive medicine is the ultimate object of so much research, conducted by engineers or physicists, into microwave hazards. The use of rats, rabbits, and other small animals for experiments has the advantage of strictly controlled conditions and the great disadvantage that the results of such work do not always clearly extrapolate to human beings. Among populations of work-people exposed to microwave fields there is a wealth of clinical opportunity for research, but the problem is, as always, what to look for. Much work has been concentrated on discovering the threshold of specific macroscopic damage to discrete organs such as the formation of cataracts in eye lenses. It was upon such work that the present 10 m. Watts/cm<sup>2</sup> safety level has been based. The Russian standards, which are not based on such heating effects, cause much heart-searching among occupational health Doctors, as nowadays, in industrial medicine, far from preventing gross damage, it is not even permissible to detract from the quality of life of workers in any industry. Instead of seeking gross pathological changes resulting from microwave exposure therefore, we should be on guard against the occurrence of more subtle effects which detract from industrial comfort or an individual's efficiency. For instance, recent work has shown that protracted exposure to low power microwave fields can cause small vacuole formation and abnormal striation in the eye lens. Whilst this damage is nothing so gross as cataract, causing no discernible opacity, it would cause impairment of the lens elasticity. The focusing capacity is therefore impaired and hence the usual onset of presbyopia in middle life

occurs at an earlier age. Investigations into changes of this degree in human populations are advocated and preventive measures are discussed.

B12-9 CRITICAL ASPECTS OF HUMAN VERSUS TERRESTRIAL ELECTROMAGNETIC SYMBIOSIS: E. Stanton Maxey, Biophysics Consultant, Research Division, Miami Heart Institute, Miami, Florida

Man's terrestrial electrical environment includes four known variables: electrostatic fields, magnetic fields, field modulations, and aerion (positive and negative) concentrations. Nature imposes harmonious variations in these four factors. Laboratory studies often attribute biological changes to variations in a single factor without adequate consideration of the remaining variables. The human organism exhibits revealing electrical characteristics. Brain waves physiologically present at frequencies paralleling the terrestrial Schumann resonance and sferics. States of consciousness and decision making abilities are correlatable to cerebral alpha, beta, and theta frequencies. Can brains be entrained to terrestrial field modulations in the same way that mammalian hearts become synchronized to external rotating magnets? Aerions, positive and negative, affect numerous biological responses including blood pH and serotonin fluctuations, changes in pulmonary oxygen exchange efficiency, and variations in the degree of left/right electroencephalographic synchronization. The travel of all charged particles is influenced by both electrostatic and magnetic field factors. Currents induced into the human organism by earth's electrical forces are subtle but biologically highly significant. Working spaces such as aircraft cockpits, where rapid response and precise decision making are critical, should be conditioned with regard to aerion concentrations, magnetic fields, electrostatic fields, and field modulations. Efficient human function in the man/machine link can thereby be augmented.

SELECTED TOPICS  
URSI COMMISSION I (BIOLOGICAL EFFECTS)

Thursday, October 23 1330

URSI Session B-13, UMC West Ballroom

Chairman: H.M. Altschuler,

National Bureau of Standards

**B13-1 BIOMEDICAL ASPECTS OF RADIOFREQUENCY AND MICROWAVE RADIATION: A REVIEW OF SELECTED SOVIET, EAST EUROPEAN, AND WESTERN REFERENCES:** Zorach R. Glaser, Biomedical Research Detachment, Naval Surface Weapons Center, Dahlgren, Virginia; and Christopher H. Dodge, Congressional Research Service, Science Policy Research Division, Library of Congress, Washington, D.C.

A survey of recent selected Soviet and East European references reveals few new trends in the interpretation of the effects of radiofrequency and microwave fields, at least at the clinical level. Soviet and East European investigators continue to report a variety of reversible changes in nervous and related functions which can occasionally be correlated with changes in animal behavior and organelle shifts under experimental conditions. Western investigators, on the other hand, have been largely unsuccessful in repeating these findings under their own laboratory conditions until somewhat recently. There is now some evidence that some Western investigators are beginning to obtain certain functional and morphological data suggestive of Soviet and East European findings. Recent Soviet, East European, and/or Western experimental findings, coupled with the pressure of public opinion, may have a significant effect on their unique positions with regard to the occupational exposure levels. This report reflects the authors' continuing efforts to comprehensively compile the world literature on the subject, and complements an earlier review of the subject presented in Richmond in 1969. New emphasis has been placed on experimental and theoretical research.

**B13-2 THEORETICAL CALCULATIONS OF POWER ABSORBED BY AN ELLIPSOIDAL MODEL OF MAN AND ANIMALS IN AN ELECTROMAGNETIC PLANE WAVE:** Habib Massoudi, Carl H. Durney, and Curtis C. Johnson, University of Utah, Salt Lake City, Utah; and Stewart Allen, Brooks AFB, Texas

A perturbation technique is used to find internal electric field, the absorbed power distribution, and the average absorbed power density of a tissue ellipsoid irradiated by an electromagnetic plane wave when the wavelength is long compared to dimensions of the ellipsoid,  $a/\lambda \lesssim 0.1$ . Expressions for the average and peak absorbed power inside an ellipsoidal model of man and animals are given. The expressions show that the average and peak power absorption in the ellipsoid are strong functions of frequency, size, and orientation with respect to the incident plane wave field vectors. Six different orientations of the ellipsoid with respect to the incident wave field vectors are considered, and comparisons of calculated data with preliminary experimental data on monkeys are given. A physical explanation for the strong dependence of absorbed power on orientation of the ellipsoid is given. The results for the ellipsoidal model of man are compared with those of the prolate spheroidal model.

B13-3 TIME-COURSE OF ADRENAL RESPONSE IN MICROWAVE-EXPOSED RATS: Ronnie Guillet, W. Gregory Lotz, and Sol M. Michaelson, University of Rochester, Rochester, New York

Adrenal function was studied in unanesthetized young adult male Long Evans rats exposed to microwaves by determining corticosterone levels in sequential blood samples obtained via chronic indwelling jugular catheters. Samples were taken before, during, and following exposure to microwaves (2450 MHz, CW) at power densities of 30, 40, or 60 mW/cm<sup>2</sup> for 15, 30, or 60 minutes. Plasma corticosterone levels rose in all rats (6/6) exposed to 60 mW/cm<sup>2</sup>, regardless of duration of exposure, most within 15 minutes, all within 30 minutes of start of exposure. Plasma corticosterone levels rose in all rats (6/6) exposed to 40 mW/cm<sup>2</sup> for 30 or 60 minutes, but not in those (2/2) exposed for 15 minutes. One of four rats responded with an increase in plasma corticosterone to exposure to 30 mW/cm<sup>2</sup>. Plasma corticosterone levels tend to plateau during exposure and, in general, began to drop sharply following termination of exposure, returning to baseline within 30 minutes in all cases. The data on rats exposed to thermogenic power density-time relationships demonstrate the transient nature of the response.

B13-4 THYROID RESPONSE TO LOCALIZED MICROWAVE EXPOSURE:  
Richard L. Magin, Shin-Tsu Lu, and Sol M.  
Michaelson, University of Rochester, Rochester,  
New York

Previous studies reporting microwave induced changes in thyroid gland function in man and animals have not specified the site of action of the microwaves on a particular part of the hypothalamic-hypophysial-thyroid axis. Localized microwave exposure of the canine thyroid gland was undertaken to determine its thermal sensitivity. The experiments were conducted at 2450 MHz utilizing a small (2" x 1") dielectrically loaded rectangular waveguide applicator. One of the two paired thyroid glands was heated with microwaves while the other was used as a control. Both thyroid glands were surgically exposed and blood collected directly from caudal veins draining each gland so that its thyroxine secretion rate could be determined. The glands were allowed a one hour equilibration period. One gland was then subjected to a two hour exposure to microwaves. The animals were divided into three groups according to the temperature rise in the exposed gland (39°C, 42°C, 45°C) with at least five animals per group. A sham-exposed group (37°C) was also studied. An increase in the exposed gland's thyroxine secretion rate (ng T4/min) was observed in each group with smallest increase occurring during the 39°C exposure and successively larger increases during the 42°C and 45°C heating. These experiments thus show that thyroid gland function can be stimulated by temperature increases at the gland of 2°C or more above normal.

B13-5 THE INFLUENCE OF MICROWAVE EXPOSURE ON NEURO-ENDOCRINE FUNCTION IN THE RAT AND DOG: S. M.  
Michaelson, University of Rochester, Rochester,  
New York

Functional changes in the neuroendocrine system of animals and humans exposed to microwaves or radiofrequency (MW/RF) energies have been reported. It is suggested that these changes are due to 1) direct stimulation of hypothalamic-hypophysial (H-H) activity resulting in changes in production, excretion, or utilization of trophic hormones or other endocrine substances; 2) indirect stimulation via the central nervous system; and 3) stimulation of H-H activity due to thermal interactions at the hypothalamic or immediately adjacent

levels of organization, the hypophysis itself or the particular endocrine gland or end-organ under study. Because of the importance of the neuroendocrine system in physiologic regulation and integration of body function, studies are being performed in rats during various periods of their lifespan (prenatal, postnatal, juvenile, adult, old) to relate hormone levels (adrenal, thyroid, growth hormone) to various regimens of low to high ( $1 \text{ mW/cm}^2$ - $80 \text{ mW/cm}^2$ ) 2450 MHz (CW) microwaves by single acute and repeated or chronic exposures. As these studies are developed, dogs are to be subjected to regional or whole-body microwave exposure for assessment of individual endocrine sensitivity and interspecies comparisons. The first phases of these studies have been initiated and the results will be presented as a series of four interrelated papers. In general these studies show that endocrine perturbation can occur in rats and dogs acutely exposed to certain power density/time durations of 2450 MHz (CW) microwaves. Such perturbation, however, is of a transient nature and is related to increase in temperature of the body or the individual endocrine gland. Chronic exposure at low power density ( $1\text{-}10 \text{ mW/cm}^2$ ) will be required to establish the physiological significance of these neuroendocrine perturbations.

B13-6 PSEUDOSUBSTRATE BINDING TO RIBONUCLEASE DURING EXPOSURE TO MICROWAVE RADIATION AT 1.70 AND 2.45 GHz: John W. Allis and Madeline L. Fromme, Experimental Biology Division, Environmental Protection Agency, Research Triangle Park, North Carolina

The binding between the enzyme ribonuclease and several pseudosubstrates was measured during coincident exposure to 1.70 or 2.45 GHz electromagnetic radiation using a crossed-beam exposure-detection system. This enzyme, isolated from bovine pancreas, hydrolyses ribonucleic acid at the position of the pyrimidine nucleotides. Measurements were made spectrophotometrically between 240 and 300 nm using a difference spectral technique, i.e., in the sample chamber enzyme and binding agent were in the same solution but were kept separate in the reference chamber by use of split compartment cells. The pseudosubstrates, which bind to the enzyme but do not undergo reaction, were 2'-cytidine monophosphate (2'-CMP), 3'-cytidine monophosphate (3'-CMP), and 3'-uridine monophosphate (3'-UMP). Association constants for these agents range from  $9 \times 10^3 \text{ M}^{-1}$  to  $300 \times 10^3 \text{ M}^{-1}$

at pH 5.5, where all experiments were performed. The solutions in the sample chamber were irradiated at a waveguide termination in an apparatus previously described. Measurements were performed immediately after exposure had begun and after exposure for 30 minutes. The absorbed dose rate for the irradiated samples was 40 W/kg. All experiments were carried out at 25°C and the temperature of the sample and reference solutions was monitored continuously. No difference in the binding of ribonuclease in irradiated solutions and unirradiated controls could be detected.

B13-7 CHRONIC LOW-LEVEL EXPOSURE OF RABBITS TO  
MICROWAVES: Esther S. Ferri and Gary J. Hagan,  
U.S. Department of Health, Education and  
Welfare, Food and Drug Administration,  
Bureau of Radiological Health, Division of  
Biological Effects, Winchester, Massachusetts

Few studies have been done to determine whether biological effects do not occur after chronic low-level irradiation at  $10 \text{ mW/cm}^2$ , the level recommended as a safe exposure maximum for the general population. This laboratory studied six rabbits exposed to 2.45 GHz CW radiation in an anechoic chamber to an incident power density of  $10 \pm 1 \text{ mW/cm}^2$  for 8 hours per day, 5 consecutive days a week for periods ranging from 8 to 17 weeks. Monitored daily for possible radiation responses were body weight, food and water consumption, and coat condition. Weekly, counts of total red and white blood cells were made and the lens of the eye was examined by slit lamp for changes. As controls, the same observations were made on six litter mates of the above group, similarly treated and sham-exposed during identical periods of time. Animals were restrained with foamed polystyrene. A slight lowering of food and water consumption was observed in the irradiated group during the first week of exposure. The lowered consumption was not accompanied by a detectable weight loss. No other differences were detected between experimental and control animals. No latent effects were observed up to two months post-irradiation.

B13-8 MICROWAVE FREQUENCY AS A FACTOR IN THE INDUCTION OF LENS OPACITIES IN THE RABBIT EYE:

Gary J. Hagan and Russell L. Carpenter,  
U.S. Department of Health, Education and Welfare,  
Food and Drug Administration, Bureau of  
Radiological Health, Division of Biological  
Effects, Winchester, Massachusetts

The role of microwave frequency in the experimental induction of lens opacities was tested by irradiating the eyes of rabbits for 30 minutes at several power levels of either 2.45 or 10 GHz continuous wave radiation. The aim was to discover whether the lowest incident power density provoking lens changes in at least 50% of the irradiated eyes in each group was the same or different for the two frequencies. In an anechoic chamber, a dielectric lens was employed to focus radiation on the eye region, with distances from the emitting horn to the dielectric lens and from the latter to the eye kept the same in all experiments. Effects were observed by ophthalmoscopy and slit-lamp biomicroscopy. It was found that at 10 GHz, lens changes were induced at a lower power density than at 2.45 GHz. At 10 GHz, the power density causing change in 50% of the subjects was 250 mW/cm<sup>2</sup>. At 2.45 GHz, it was 320 mW/cm<sup>2</sup>.

B13-9 A STUDY OF THE EFFECTS OF MICROWAVE IRRADIATION OF THE RAT TESTES: Gabriel J. Muraca, Jr. and Esther S. Ferri, U.S. Department of Health, Education and Welfare, Food and Drug Administration, Bureau of Radiological Health, Division of Biological Effects, Winchester, Massachusetts

Because of the thermal sensitivity of the mammalian germinal tissues, the testes constitute a critical organ of interest in the study of microwave biological effects. To investigate the possibility that thermal stress by microwave irradiation induces unique biological effects, as opposed to conventional heating, the testes of albino rats of the Sprague-Dawley strain were exposed *in vivo* to 2.45 GHz continuous wave radiation and histologically compared to testes heated by immersion of the scrotum in warm water. Preliminary experiments indicated that an intratesticular temperature rise to 40°C by microwave irradiation, maintained for periods of five to twenty-five minutes, produced degenerative changes in

less than 50% of the animals exposed. Temperature rises to 38°C and 42°C were also investigated for single and repetitive exposures. In both microwave and water bath experiments the intratesticular temperature was continuously monitored and maintained at selected temperatures for chosen periods of time. The testes of one hundred animals were exposed to microwave irradiation and fifty animals had their scrotum immersed in warm water. Similar histological damage was observed in both exposure categories with observations classified in four categories from normal to severely damaged. Results are not inconsistent with a thermal mechanism of microwave injury to the testes.

B13-10 COMPARISON OF THERMAL EFFECTS IN THE RABBIT EYE  
FROM MICROWAVE RADIATION AND FROM EXTERNAL HEATING:  
Russell L. Carpenter and Gary J. Hagan, U.S.  
Department of Health, Education and Welfare, Food  
and Drug Administration, Bureau of Radiological  
Health, Division of Biological Effects, Winchester,  
Massachusetts

If sufficient in power and duration, Microwave radiation causes two demonstrable effects in the rabbit eye: (1) a prompt increase in intraocular temperature and (2) after several days, formation of opacities in the posterior subcapsular cortex of the lens. Whether these two occurrences rest on a cause and effect relationship is a question that has neither been resolved nor satisfactorily addressed experimentally. We therefore have undertaken experiments designed to raise intraocular temperature by the same amount as occurs during a cataractogenic exposure to 2450 MHz microwave radiation and for the same duration but without employing microwaves. This was accomplished by external application of heat to the scleral region overlying the ciliary body, thus heating the blood flowing to it, the iris, and the corneal limbus. The heat source was a thin copper girdle shaped to the contour of this region of the eye. Soldered to its upper surface was a circular brass tube which carried a flow of water from a thermostatically regulated water bath. In an initial series of experiments, water bath temperatures were correlated with temperature measurements made by thermocouple in the vitreous body close behind the lens. We found that this type of heating inflicts more severe damage than does equivalent microwave heating. We observed local venous

stasis as well as hemorrhage in ciliary body and iris vessels, corneal neovascularization, and many instances of extensive hyphemia. The few opacities which developed were in the anterior lens cortex, thereby differing in location from those induced by microwaves.

B13-11 THE USE OF STRIPLINE TO STUDY MICROWAVE BIOLOGICAL EFFECTS: R. L. Seaman and H. Wachtel, Department of Biomedical Engineering, and W. T. Joines, Department of Electrical Engineering, Duke University, Durham, North Carolina

Rectangular coaxial transmission line (stripline) has been found to be especially convenient in studying the effects of microwaves on small biological preparations. Plane wave propagation, as in an antenna far field, along the stripline provides the basis for a straightforward calculation of absorbed power by a preparation placed in the interconductor space. This experimentally verified formulation provides knowledge of absorbed power during irradiation by monitoring input power to the stripline. Only low input powers (1 or 2 watts) are required to produce absorbed powers on the order of 100 milliwatts/cm<sup>3</sup>. Our modified stripline allows observation of and access to the preparation. We have used the stripline technique to irradiate isolated neural tissue while recording electrical activity from the neurons. The confined electromagnetic fields allow essentially artifact-free recording and insure investigator safety. Intracellular recordings from individual neurons of Aplysia indicate effects on neural activity and synaptic efficiency at absorbed power levels of a few milliwatts/cm<sup>3</sup>. Neural output of the optic nerve of Limulus is changed by similar absorbed power levels. Results were obtained at experimental frequencies of 1.5 GHz and 2.45 GHz. Stripline has provided an excellent means of minimizing many of the problems associated with researching microwave effects on neural tissue.

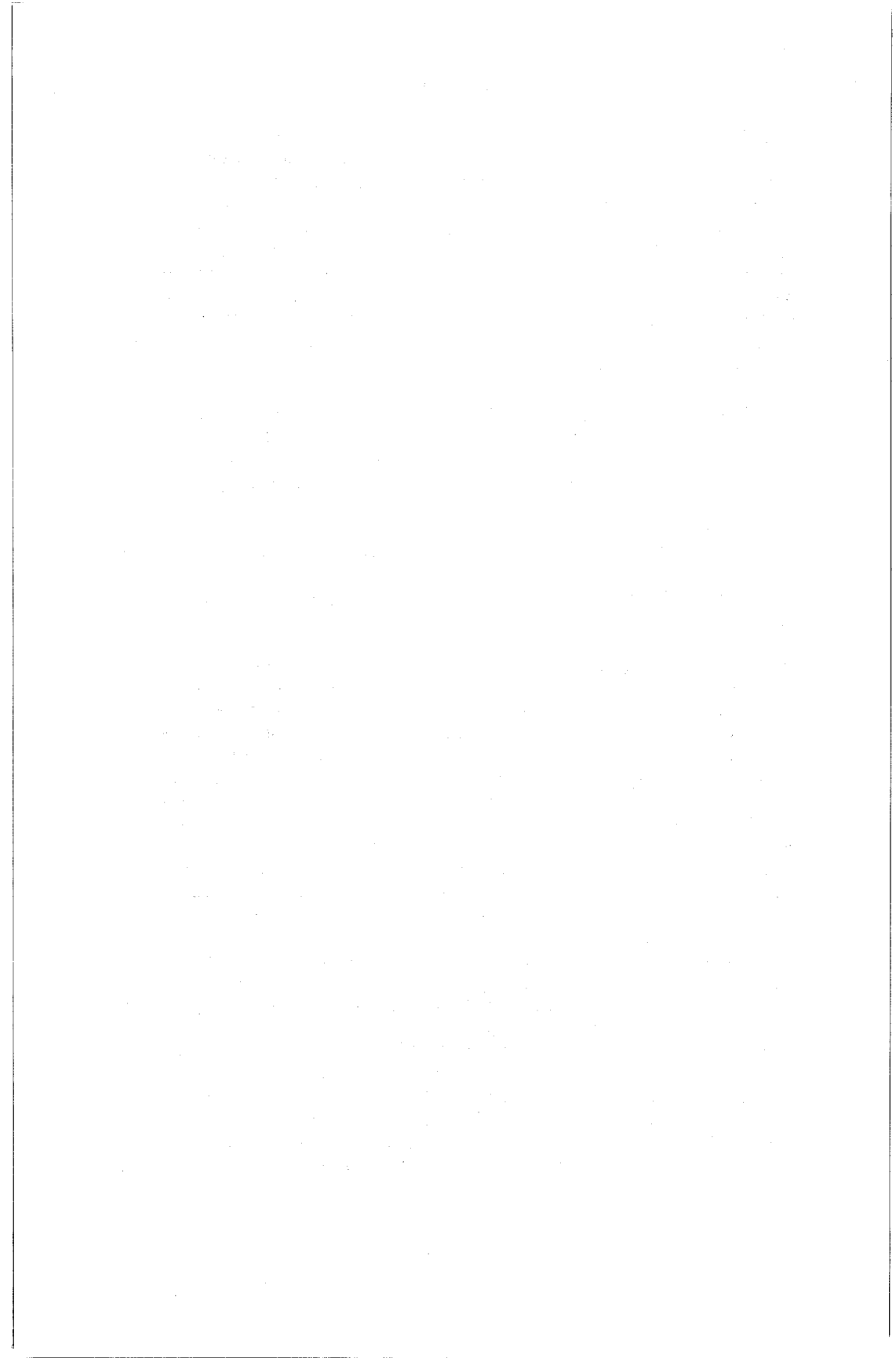
B13-12 ELECTROMAGNETIC FIELD EFFECTS ON ISOLATED NERVE TISSUE: Sheldon S. Sandler, Bioelectromagnetics Laboratory, Department of Electrical Engineering, Northeastern University, Boston, Massachusetts

A technique has been developed in the laboratory for exposing isolated nerve tissue to a known electric field. Freshly dissected frog brains are placed in a coaxial exposure chamber and are subjected to a known electric

field. Both thermal and nonthermal field effects are possible. In previous experiments in our laboratory in which large motor neurons of the spinal cord were exposed to high-voltage sub-nanosecond pulses which produce negligible thermal heating, no gross histological damage to the nerve cells was found. New experiments have been performed to see if there is any field effect that can be seen on the electron microscope level. A series of thermal heating studies have also been initiated to correlate tissue damage to the specific local electric field and the local power density in the tissue.

B13-13 OPTICAL ETALON TEMPERATURE SENSOR FOR MICROWAVE  
TISSUE HEATING APPLICATIONS: D.A. Christensen,  
Departments of Electrical Engineering and Bioen-  
gineering, University of Utah, Salt Lake City,  
Utah

For monitoring tissue temperature changes in the presence of microwave fields in bioeffects, thawing, and hyperthermia applications, we have developed a non-metallic measurement system which uses a small optical etalon as the temperature sensor connected to the display module by an optical path. This avoids the metallic connectors and associated field perturbations normally encountered with thermistor-type systems. When the temperature of the etalon (a small optical flat coated on opposite sides to form a cavity) varies, linear thermal expansion and changes in the index of refraction will cause a shift in the resonant wavelengths, thereby shifting the wavelength positions of nulls in reflectivity from the etalon. One method for tracking the amount of wavelength shift and thus the temperature change, utilizes an external voltage-tunable Fabry-Perot interferometer whose transmitted wavelengths are locked to the etalon's reflectivity nulls by a synchronous detection technique. Theory predicts, and experiments have verified, that the dc tuning voltage to the interferometer is linearly proportional to the temperature variation of the sensor. We have experimentally tested two etalon types with this system. The first etalon, fabricated from 0.145 mm thick crown glass, was tested from  $22^{\circ}\text{C}$  to  $70^{\circ}\text{C}$  over its extrapolated temperature range of  $154^{\circ}\text{C}$ , while the second sample, made from 3.2 mm thick fused silica, gave a range of  $11.1^{\circ}\text{C}$ . Temperature resolution was better than  $0.5^{\circ}\text{C}$  and  $0.05^{\circ}\text{C}$ , respectively, over these temperature ranges.



## INDEX

Aarons, J.	57
Abshire, N.L.	286
Adams, J.W.	33
Adekola, S.A.	238
Adey, W.R.	222, 267
Afarani, M.	147
Agrawal, B.S.	294
Al-Badwaihy, K.A.	39, 90
Albert, E.N.	224
Alexander, J.K.	175, 252
Ali, J.S.	130
Allen, S.J.	199
Allis, J.W.	318
Alspaugh, M.H.	241
Alfschuler, J.M.	315
Alvarez, H.	250
Ament, W.S.	243
Anaya, W.G.	151
Anderson, D.N.	216
Anderson, K.D.	145
Annan, A.P.	284
Apel, J.R.	52
Argo, P.E.	216
Arnold, M.P.	83
Arthur, M.G.	32
Aslan, E.	99
Bahar, E.	243, 294
Ballard, K.A.	168
Bannister, P.R.	215
Bantin, C.C.	159
Barath, F.T.	54, 289
Barber, P.W.	229
Barfield, J.N.	113
Bargellini, P.L.	44
Barnes, F.S.	204
Barnoski, M.K.	120
Barnum, J.R.	148
Baron, M.J.	174, 248
Barrick, D.E.	206
Bassen, H.	91, 100, 101, 278
Batlivala, P.P.	287
Bauer, P.	248
Bawin, S.M.	267
Beard, C.I.	240
Beavjardiere, O.	174
Beck, G.S.	201
Beischer, D.E.	309
Bell, T.F.	11
Benane, S.G.	134

Bender, W.G.	4
Bennett, C.L.	74, 75
Bertharion, G.	192
Berthelot, F.	254
Bhartia, P.	219
Bibl, K.	169
Bickel, G.	81, 82
Bing, J.R.	101
Birenbaum, L.	40, 271
Birnbaum, G.	103
Blackman, C.F.	34
Blanco, M.A.	188
Blasco, A.P.	269
Blattman, D.A.	96
Bleistein, N.	182
Bliss, V.	286
Boerner, W.M.	183, 184
Bogle, R.W.	210
Bojarski, N.N.	181
Borgiotti, G.V.	185, 265
Bostian, C.W.	159
Bottjer, M.F.	70
Bowden, D.M.	96, 34
Bowman, R.P.	98, 277
Braccalente, E.M.	53
Bragg, D.G.	95
Broderick, J.	300
Brooks, L.W.	206
Brotan, N.W.	174
Brown, A.C.	29
Brown, L.W.	301
Brown, W.E.	54
Burch, L.S.	194
Butler, C.M.	76, 127, 230, 306
Burks, D.G.	140, 311
Burrell, G.A.	283
Burrows, M.	49
Bussey, H.E.	181
Bussgang, J.J.	189
Cain, C.A.	35
Caldwell, R.	204
Campbell, D.B.	301
Campbell, W.C.	143
Carlson, F.P.	31
Cardone, V.J.	147
Carpenter, D.L.	10
Carpenter, R.L.	320, 321
Carver, K.R.	104, 207
Cauterman, M.	3, 254

Casey, K.F.	122
Cetas, T.C.	275
Chadhouri, S.K.	183
Chadwick, R.B.	143, 167, 286
Chaio, R.Y.	108
Chamness, F.	226
Chan, H.L.	149
Chan, W.C.	258
Chang, D.C.	32, 120, 123, 221, 256
Chappell, C.R.	112, 248
Chen, C.J.	30
Chen, K.C.	132
Chen, K.M.	278
Cheo, B.R.	307
Cheo, P.K.	120
Cheung, A.Y.	102, 203, 278
Chidsey, I.L.	156
Chilton, C.J.	214
Chou, C.K.	36, 138
Christensen, D.A.	276, 323
Chu, T.M.	292
Chuang, C.W.	257
Claassen, J.H.	107
Claassen, J.P.	147
Clark, T.A.	16, 250
Clark, W.	166
Cleary, S.F.	193, 225
Clifford, S.F.	241
Coates, R.	16
Coffey, T.P.	112
Cohen, J.K.	182
Cohen, M.H.	178
Cole, E.E.	140
Conover, D.L.	101
Counselman, C.C.	13, 16
Cox, D.C.	160
Crain, C.M.	238
Crane, R.K.	7
Crawford, M.L.	32
Croft, T.A.	300
Crombie, D.D.	86, 291
Cornyn, W.M.	175, 251
Crystal, T.L.	111
Cubley, D.	26
Cupp, R.C.	286
Dage, E.L.	134
D'Andrea, J.A.	195
Das, A.	161, 162
Das, Y.	184

Davies, K.	153, 154, 155, 216
Davis, D.T.	238
Davis, J.L.	284
Davis, W.A.	77
Deadrick, F.J.	72, 74
Dean, L.B.	20
Dean, W.A.	156
Deficis, A.	274
Degauque, P.	3, 254
Deitz, J.	87
Demoulin, B.	3, 254
Derr, V.E.	286
Deschamps, G.A.	19
Dethlefsen, L.A.	92
Deide, A.H.	292
Dobroski, H.	1
Dodge, C.H.	315
Dolan, J.L.	119
Dolphin, L.T.	258
Donnelly, R.F.	216
Douley, R.P.	151, 206
Dougherty, H.T.	157
Downs, G.S.	302
Dreher, J.	66
Duff, B.M.	104, 105
Duff, J.E.	101
Dunn, P.J.	13
Dunne, J.A.	52
Durfee, W.K.	269
Durney, C.H.	95, 199, 200, 275, 315
Dutton, E.J.	157
Edgar, B.C.	9
Edrich, J.	69
Eichert, E.S.	38
Einaudi, F.	292
Elachi, C.	123
Elder, J.A.	130
Emery, A.F.	40, 231
Emslie, A.G.	3, 48
Erickson, W.C.	179, 234
Eroom, D.	303
Erskine, F.T.	175, 251
Evans, J.E.	155
Evans, L.G.	251
Fainberg, J.	175, 250
Faller, J.E.	14
Falls, R.A.	285
Farstad, A.J.	1
Fedder, J.A.	112

Fedor, L.S. . . . .	150
Feldman, M.J. . . . .	108
Felson, L.B. . . . .	80
Fenn, A.J. . . . .	27
Ferri, E.S. . . . .	319, 320
Findlay, J. . . . .	115
Fitzenreiter, R.J. . . . .	250, 251
Fitzwater, M. . . . .	243
Fontheim, E.G. . . . .	61
Forster, R. . . . .	66
Forse, R. . . . .	308
Foshee, J.J. . . . .	60
Foster, M.R. . . . .	138
Fradin, D. . . . .	120
Frazer, J.W. . . . .	132, 201, 226, 227
Frazer-Smith, A.C. . . . .	9
Fredricks, R.W. . . . .	63
Frey, A.H. . . . .	35, 38
Frisch, A.S. . . . .	165, 167
Fritz, R.B. . . . .	154, 216
Fromme, M.L. . . . .	318
Fung, A.K. . . . .	149
Furuham, Y. . . . .	245
Gabillard, R. . . . .	3, 254
Gaines, E.E. . . . .	215
Gallawa, R.L. . . . .	79
Gambill, B. . . . .	291
Gandhi, O.P. . . . .	195, 201
Gardner, C.S. . . . .	18
Gay, R.H. . . . .	297
Gillard, J. . . . .	192
Githens, S.H. . . . .	232
Glaser, Z.R. . . . .	192, 310, 315
Gloerson, D. . . . .	52
Goell, J.E. . . . .	79
Goldhirsch, J. . . . .	163
Goldman, S.R. . . . .	8
Gomberg, H. . . . .	218
Goodman, E.M. . . . .	267
Gordon, G.A. . . . .	92
Gordon, M.A. . . . .	66
Gossard, E. . . . .	165, 286
Grantham, W.L. . . . .	53
Graf, E.R. . . . .	140, 311
Gray, T.B. . . . .	154
Green, J.L. . . . .	166
Greenberg, B. . . . .	272
Greenebaum, B. . . . .	267
Greenwood, C. . . . .	147

Griffiths, L.J.	26
Grissett, J.D.	137
LaGrone, A.H.	163
Grossi, M.D.	297
Grubb, R.N.	50, 216, 298
Guillet, R.	316
Guru, B.S.	278
Gustincic, J.J.	71
Guy, A.W.	36, 40, 90, 92, 138, 197, 201, 229, 231, 232
Haddad, J.	221
Haddock, F.T.	250
Hagen, G.J.	319, 320, 321
Hagen, J.P.	118
Hagn, G.H.	219
Hamid, M.A.K.	305
Hammond, O.L.	149
Hansen, R.C.	29
Hanson, D.F.	75
Hanson, W.B.	58
Harker, K.S.	299
Harris, C.	40
Harris, J.H.	45
Hartzell, R.	227
Hasegawa, A.	62
Hartmann, G.K.	153, 154, 155
Hawkins, G.S.	57
Hawkins, T.D.	222, 223, 232, 233
Haydon, G.W.	30, 85
Hayes, J.	147
Hayre, H.S.	26
Heacock, R.R.	173
Heath, H.C.	129
Heiles, C.	180
Helliwell, R.A.	63, 111
Heppner, F.	268
Herman, J.R.	219
Herman, W.A.	101
Hieronymus, R.	74, 75
Hill, D.A.	1, 47, 128, 280
Hill, D.H.	200
Hill, F.S.	188
Hill, J.R.	170, 171
Hinterregger, H.F.	16
Ho, H.S.	131, 138, 197
Hodge, D.B.	158
Hoffman, W.	66
Holzer, R.E.	112
Hong, S.T.	145
Hoover, K.E.	169

Hopper, T.	171
Hopponen, J.	239
Hoshikawa, M.	81
Houk, W.M.	137, 309
Howard, A.Q.	124
Howard, W.E.	116
Hsieh, S.T.	131
Hu, C.L.	204
Hudson, H.G.	72
Hufford, G.	245
Hughes, W.J.	280, 291
Hunsucker, R.D.	173
Hunt, E.L.	192, 195, 201, 223
Hurt, W.D.	200, 312
Hvatum, H.	119
Illgen, J.D.	291
Illinger, K.H.	204
Imhof, W.L.	215
Inan, U.S.	11
Infocino, C.J.	6
Ippolito, L.J.	143
Ishimaru, A.	145
Itbos, N.	303
Itoh, T.	121
Jaggard, D.L.	123
Jain, A.	208
Janes, D.E.	312
Janssen, M.	68
Jennings, R.D.	86
Jensen, D.R.	283, 240
Johnk, C.T.A.	126
Johnson, C.C.	95, 199, 200, 275, 300
Johnson, F.S.	218
Johnson, R.B.	37
Johnson, R.L.	293
Johnston, K.J.	177
Joines, W.T.	322
Jones, W.L.	53
Joshi, R.	134
Juroshek, J.R.	88
Justesen, D.R.	92, 192
Kahn, W.K.	264
Kaiser, M.L.	175, 252
Kajfez, D.	263
Kantor, G.	91
Kao, C.K.	81, 82
Kaplan, I.T.	40
Katsufrakis, J.P.	63
Kellogg, R.B.	200

Kerr, A.B.	70
Kerr, F.J.	119
Kesner, R.P.	195
Kindt, C.W.	96, 311
King, N.W.	192
King, R.W.P.	304, 305
Kisslinger, C.	13
Kivelson, M.G.	112
Klein, L.A.	210
Kleitman, R.E.	19, 125
Klobuchar, J.A.	153
Kokubun, S.	112
Kolenkiewicz, R.	13
Kong, J.A.	255, 258
Konrad, T.G.	165
Koons, H.C.	111
Koopman, D.W.	203
Kozaki, S.	126
Knight, C.	16
Kramer, P.	40
Kraning, K.K.	231
Krishen, K.	107
Kritikos, H.	223
Kropfli, R.A.	164
Krupp, J.H.	200
Ksienski, A.A.	260
Kuester, E.F.	128
Lagace, R.L.	3, 48
Lam, C.	36
Landt, J.A.	96
Langseth, R.E.	260
Lanzerotti, L.J.	110
Larsen, T.R.	215
Larson, T.R.	241
Laviola, M.	213
Lawrence, R.S.	43, 241
Laxpati, S.R.	28
Leader, J.C.	247
Lean, E.G.	120
Leavitt, M.	10
Lee, K.	305
Lee, S.W.	21
Leftin, M.	171
Lehmann, J.F.	90
Leicher-Preka, A.	136
Leighton, R.B.	67
Leinbach, H.	62
Leitinger, R.	153
Levis, C.A.	157

Lewis, G.C. . . . .	127
Liebe, H.J. . . . .	239
Liepa, V.V. . . . .	106
Lin, J.C. . . . .	36, 132, 226
Lin, R.P. . . . .	251
Lipa, B.J. . . . .	302
Lipscomb, T.J. . . . .	196
Liu, C.H. . . . .	6
Liu, T.K. . . . .	74
Livingston, G. . . . .	92
Livingston, G.K. . . . .	275
Lo, K.Y. . . . .	177
Locus, S.S. . . . .	129
Long, M.D. . . . .	130
Longacre, A. . . . .	137
deLorge, J.O. . . . .	140, 195
Lotz, W.G. . . . .	139, 316
Love, A.W. . . . .	43
Lovely, R.H. . . . .	37, 138, 192, 197
Lu, S. . . . .	317
Lyons, L.R. . . . .	61
Lytle, R.J. . . . .	280, 281
Ma, C. . . . .	16
Ma, M.T. . . . .	157, 216
Mack, R.B. . . . .	125
MacDougall, J.A. . . . .	92, 201
MacPhie, R.H. . . . .	264
Magin, R.L. . . . .	317
Mager, R.D. . . . .	182
Mahmoud, S.F. . . . .	48
Maklad, M. . . . .	82
Malaga, A. . . . .	190
Maley, S.W. . . . .	221
Mannan, J.D. . . . .	64
Marouf, E.A. . . . .	22
Manthei, R.C. . . . .	192
Manus, E.A. . . . .	159
Marcuvitz, N. . . . .	218
Maresca, J.W. . . . .	148
Marron, M.T. . . . .	267
Marshall, R.E. . . . .	159
Martin, D.J.R. . . . .	2, 47
Martin, E. . . . .	57
Martin, L.U. . . . .	240
Martin, P. . . . .	269
Massoudi, H. . . . .	199, 315
Matheson, R.J. . . . .	32
Mathewson, N. S. . . . .	269
Matthews, T.A. . . . .	179

May, J.G. . . . .	196
Mayhan, J.T. . . . .	127
Mayes, P.E. . . . .	75, 308
Maxey, E.S. . . . .	314
McAfee, R.D. . . . .	196
McCandless, S.W. . . . .	51
McClellan, W.R. . . . .	287
McClure, J.P. . . . .	58
McColl, M. . . . .	70
McIntosh, R.E. . . . .	190
McNice, G.T. . . . .	286
McRee, D. . . . .	130
Medici, R.G. . . . .	271
Medina, M.A. . . . .	310
Meeks, M.L. . . . .	66
Meijer, P.H.E. . . . .	230
Mendillo, M. . . . .	153
Mennella, R.A. . . . .	149
Merritt, J.H. . . . .	227
Metlay, W. . . . .	40
Michaelson, S.M. . . . .	139, 309, 316, 317
Middleton, D. . . . .	87
Mikołajczyk, H. . . . .	225
Millea, M.F. . . . .	70
Miller, E.K. . . . .	72
Miller, L.J. . . . .	164
Miller, T.R. . . . .	10
Minkoff, J. . . . .	212, 213
Mitchell, J.L. . . . .	53, 312
Mittelman, L. . . . .	285
Mittra, R. . . . .	20, 28, 72
Mitzner, K.M. . . . .	129
Mizuno, K. . . . .	271
Modak, A.T. . . . .	310
Moe, K.E. . . . .	197
Moffatt, D.L. . . . .	257
Moffet, A.T. . . . .	177, 243
Moler, W.F. . . . .	145
Monahan, J.C. . . . .	197
Monson, B. . . . .	19
Moore, C.R. . . . .	119
Moore, R.K. . . . .	147, 210, 288, 289
Moran, J.M. . . . .	17, 174
Moran, K.P. . . . .	143
Moran, W.P. . . . .	233
Morgan, M.G. . . . .	153, 168
Morgan, M.K. . . . .	311
Mozer, F.S. . . . .	248, 296
Muhleman, D.O. . . . .	177

Muller, E.E.	160
Muraca, G.J.	320
Murphy, J.N.	1
Murray, W.E.	101
Muthukrishnan, S.	269
Myers, D.	37
Nakahara, T.	81
Nathanson, F.	206
Negi, J.N.	282
Nemoto, S.	82
Neuder, S.M.	200, 230
Nevels, R.D.	305
Newton, R.W.	287
Niell, A.E.	15
Noonkester, V.R.	145, 238, 240
Nyquist, D.P.	278
Obrenovitch, J.	192
Ochs, G.R.	241
O'Grady, T.C.	310
Oliva, S.A.	269
Olsen, E.T.	68
Olsen, R.L.	142
Oosta, G.M.	269
Orens, J.H.	112
Orswell, P.L.	50
Oscar, K.J.	222
Ossakow, S.L.	8
Ott, R.H.	6
Pan, J.J.	83
Papadopoulos, K.	114
Papierz, A.B.	28
Pappert, R.A.	244
Parr, W.H.	101
Parrish, P.T.	108
Pearson, L.W.	28
Pedersen, P.C.	95
Pedersen, R.J.	70
Perkins, F.W.	296
Perley, R.A.	234
Perrin, J.C.	192
Perry, W.L.	183
Peters, L.	254, 283
Peterson, R.	100
Pettengill, G.H.	301
Philips, R.	267
Phillips, R.D.	192
Pierson, W.J.	147
Plant, W.J.	144
Plante, P.R.	269

Poggio, A.J.	72
Papierz, A.B.	28
Polk, C.	269
Potter, W.J.	250
Pounds, D.J.	107
Powell, R.C.	237
Powers, E.N.	261
Presnell, R.	213
Price, R.M.	117, 187
Probst, S.E.	116
Purcell, G.H.	178
Pyle, S.D.	204
Quincy, E.A.	284
Rabinowitz, J.R.	41
Rahmat-Samii, Y.	20
Rao, N.N.	18, 169
Rao, T.C.K.	305
Ratliff, J.A.	200
Raval, U.	282
Read, E.C.	256
Reagan, J.B.	215
Redman, M.D.	84
Regelson, W.	93
Reichley, P.E.	302
Reid, M.J.	177
Reinisch, B.W.	169
Reinman, R.A.	220
Reno, V.R.	140
Rhine, F.P.	106
Richards, P.L.	107
Richardson, J.M.	43
Richmond, J.H.	77
Richter, J.H.	240
Rino, C.L.	8
Rissman, W.J.	35
Robertson, D.	16
Rogers, A.E.E.	16
Rogers, D.V.	142
Rope, E.L.	185
Rosen, B.R.	17
Rosenthal, S.W.	39, 40
Ross, D.H.	310
Rouse, J.W.	287
Rozzell, T.C.	274, 275
Ruggera, P.S.	98
Rumsey, V.H.	246
Russell, C.T.	112
Rutherford, R.R.	291
Ryan, J.	16
Sackett, G.P.	96

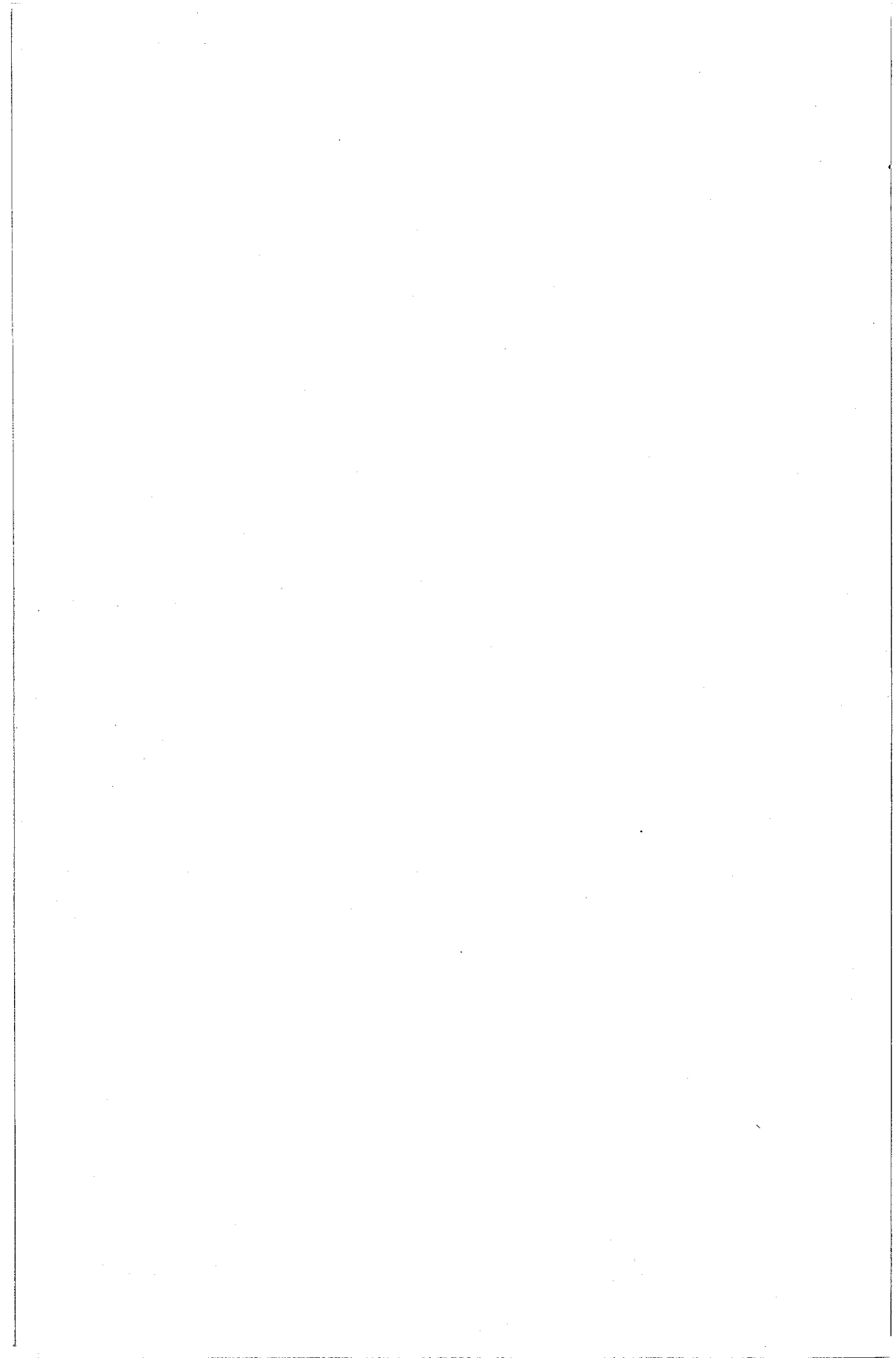
Saffer, J.	203
Salfi, R.	147
Sandler, B.	304
Sandler, S.	322
Sandness, S.	126
Sanzgiri, S.M.	28
Scannapieco, A.J.	8
Schlizzi, R.T.	178
Scholes, H.	226
Schrader, J.H.	53
Schroeder, L.C.	53
Schrot, J.	232, 233
Schuler, D.L.	239
Schulz, M.	110
Schwann, H.	199, 203
Schwartz, P.R.	177
Seaman, R.L.	322
Sears, R.D.	155
Sedigh, K.	201
Senior, T.B.A.	218
Sensintaffer, E.L.	101
Serebreny, S.M.	148
Serrantie, B.	192
Servantie, A.M.	192
Seto, Y.J.	131
Sexauer, S.	226
Shapiro, I.	16
Shawhan, S.D.	9, 175, 251
Shen, L.C.	304
Shephard, N.H.	33
Shimabukuro, F.I.	235
Shin, S.Y.	80
Shore, M.	136
Short, R.	231
Shnitkin, H.	105
Silven, S.	293
Silver, A.H.	70
Silver, S.	218
Simpson, R.A.	301
Singarayar, S.	104, 105
Sinclair, G.	218
Singer, H.	112
Siren, J.C.	173, 249
Slayton, I.B.	83
Sletten, C.J.	218
Smith, D.E.	13
Smith, E.J.	64, 65, 110
Smith, E.K.	115
Smith, J.C.	81

Smith, N.	170
Smith, R.A.	252
Smith, R.S.	103
Smith, T.M.	243
Smyth, J.B.	220
Sobti, A.	288, 289
Soicher, H.	154
Sorbelllo, R.M.	305
Southwood, D.J.	291
Spaulding, A.D.	88, 219
Spelman, F.A.	96, 311
Spencer, R.H.	4
Spiegel, R.J.	230
Spillane, J.E.	96
Spring, W.	147
Stavinoha, W.B.	310
Steele, F.K.	292
Steinberg, B.D.	261
Stenzel, R.L.	63
Stephenson, J.J.	86
Stewart, R.H.	209
Stone, R.G.	175, 219, 250
Stonebridge, J.B.	90
Stoyer, C.H.	254
Straiton, A.W.	142
Strauch, R.G.	143
Struharik, S.J.	157
Stutzman, W.L.	159
Sugiyama, S.	217
Surles, M.C.	134
Suzuki, S.	81
Sweeney, L.E.	142, 260
Swenson, G.W.	235
Swicord, M.L.	91, 101, 102, 138, 203, 278
Swift, C.T.	51, 210
Tai, C.	304
Takashima, S.	223
Taur, Y.	107
Taylor, J.H.	50
Taylor, L.S.	6
Teague, C.C.	207
Tell, R.A.	312
Tesche, F.M.	74
Theobald, D.M.	168
Thiele, G.A.	27
Thomas, J.R.	194
Thome, G.D.	296
Thompson, T.W.	55
Thornton, D.D.	66

Thorne, R.M.	65
Timman, R.	218
Tippet, J.C.	32
Toler, J.E.	103
Tomiyasu, K.	209
Townsend, W.F.	53
Trabculay, E.A.	133
Tricoles, G.	185
Trizna, D.B.	210
Troland, T.H.	179
Trzaska, H.	99
Tsai, L.L.	127, 128
Tsang, L.	255, 258
Tsunoda, R.	213
Tsurutani, B.T.	64, 65
Turner, B.E.	66, 67
Tyler, G.L.	244, 301, 302
Tveten, L.H.	216
Ulaby, F.T.	147, 287, 288
Ulich, B.L.	69
Umeshankar, K.R.	73, 230
Ungrichian, V.	157
Uslenghi, P.L.E.	125
Utlaut, W.F.	57
Vampola, A.L.	110
Van Blaricum, M.L.	72
Van Zandt, T.E.	166, 212
Varma, M.M.	133, 134
Vernon, F.L.	70
Vickers, R.S.	258
Villard, O.G.	45
Vincent, W.R.	219
Viner, M.R.	179
Vogler, L.E.	86
Vondrak, R.R.	173, 174
Wachtel, H.	322
Wacker, P.F.	23
Wade, C.M.	66
Wagner, R.	120
Wait, J.R.	47, 48, 128, 254, 256, 280, 292
Walsh, E.J.	149, 151
Wang, J.C.H.	160, 295
Wang, N.N.	77
Wang, T.	241
Warnock, J.	166
Washburn, T.W.	260
Wasylkiwskyj, W.	24, 264
Waters, J.W.	235
Webb, M.D.	92, 201

Webber, J.C.	235
Weber, R.R.	250
Webster, W.J.	16, 17
Weintraub, S.T.	310
Weissman, P.E.	289
Welch, W.J.	66, 234
West, B.	93
Whitney, A.R.	16
Wieder, B.	214
Wiley, P.H.	159
Williams, D.J.	61, 108
Wilson, K.E.	220
Wilson, L.R.	263
Wilson, W.J.	235
Wilton, D.R.	76
Winkler, R.	166
Wolf, J.K.	187, 189
Wolff, E.A.	85
Woo, R.	25, 59
Woody, J.A.	103
Woolas, K.D.	313
Wright, J.W.	58, 144, 168, 215, 298
Wright, M.C.H.	66, 235
Wu, C.	226
Wu, H.C.	284
Wu, T.K.	127, 128
Wu, T.T.	304
Wyner, A.D.	189
Yang, F.C.	25, 59
Yang, K.S.	235
Yeandle, S.S.	194
Yeh, C.	79, 122
Yeh, K.C.	6
Yeh, Y.S.	260
Yip, G.L.	82, 84
Young, D.T.	108
Young, J.D.	147, 282
Youssef, A.A.	39, 90
Yue, O.	185
Ytisrevinu, S.	303
Yung, E.K.	263
Zaghoul, A.I.	264
Zaret, M.M.	40
Zavoli, W.B.	221
Ziemer, R.E.	190
Zimmerman, B.J.	239





1330-1700	II-8	Radio Oceanography--Wave Spectra, Synthetic Aperture Radars, and Radiometers	UMC F.R.
	III-5	Effects of Natural and Induced Ionospheric Disturbances	UMC 157
	VI-9	Keeve M. Siegel Memorial Session	RB Aud.
	VIII-3	Atmospheric and Man-Made Noise	RB 1107
	B-8a/I	CNS Effects - I	UMC E Blrm
	B-8b/I	CNS Effects - II	UMC E Blrm
	B-9a/I	Assessment of Power Deposition in Tissues by Numerical Methods	UMC W Blrm
	B-9b/I	Polarization Effects	UMC W Blrm
	V-5	Instrumentation and Techniques	UMC 156
		Commission V Business Meeting	UMC 156
1500-1700		Commission I Business Meeting	RB 1103
		Commission IV Business Meeting	UMC 156
		Commission VI Business Meeting	RB Aud.
		Commission VIII Business Meeting	RB 1107
		U.S. National Committee Meeting	Sheraton
<u>Thursday, October 23</u>			

0830-1200	I-2	Workshop on New Needs for Telecommunication Measurements	UMC 159
	II-9	Atmospheric Effects	UMC F.R.
	II-10	Theoretical Development of Electromagnetic Problems	UMC 158
	IV-5/III	Feasibility of Scatter Radars on the Space Shuttle - I	UMC 157
	V-6	Solar and Planetary Observations - I	UMC 156
	VI-10/I	Sub-Surface Probing	RB 1107
	VI-11	Arrays	RB Aud.
	B-10a/I	Effect of ELF Fields on Biological Systems - I	UMC E Blrm
	B-10b/I	Effect of ELF Fields on Biological Systems - II	UMC E Blrm
	B-11	Measurement of Power Deposition in Biological Tissues	UMC W Blrm
	II-11	EM Probing and Sub-Surface Propagation	UMC 159
	II-12	Remote Sensing	UMC F.R.
	III-6	ELF-HF Propagation	UMC 158
	IV-6/III	Feasibility of Scatter Radars on the Space Shuttle - II	UMC 157
<hr/>			
1300-1700	V-7	Solar and Planetary Observations - II	UMC 156
	VI-12	Wire Antennas	RB Aud.
	B-12/I	General Biological Effects	UMC E Blrm
	B-13/I	Selected Topics	UMC W Blrm

1976 International IEEE/APS Symposium  
and USNC/URSI Meeting

October 10-15, 1976

University of Massachusetts  
Amherst, Massachusetts

This will be the principle U.S. National Meeting of URSI in 1976. For information contact:

Robert E. McIntosh  
Department of Electrical Engineering  
University of Massachusetts  
Amherst, Massachusetts 01002

